SYNTHESIS, CHARACTERIZATION, BIOCIDAL AND VIRUCIDAL PROPERTIES OF METAL OXIDE NANOPARTICLES

by

JOHANNA A. HÄGGSTRÖM

B.S., Mälardalen University, Sweden, 2002

AN ABSTRACT OF A DISSERTATION

submitted in partial fulfillment of the requirements for the degree

DOCTOR OF PHILOSOPHY

Department of Chemistry
College of Arts and Sciences

KANSAS STATE UNIVERSITY
Manhattan, Kansas

2007

Abstract

Non-polar halogens (Cl_2, Br_2 and I_2) and polar interhalogen molecules (ICl, IBr and ICl_3) have been adsorbed on the surface of several high surface area materials, including three different nanosized metal oxides (NanoActive® (NA) Al_2O_3 Plus, NA-TiO_2 and NA-CeO_2). The prepared halogen and interhalogen adducts have been characterized in detail by thermogravimetric analysis (TGA), UV-Vis, Raman and X-ray photoelectron spectroscopies (XPS) and the results are discussed herein. The different metal oxides lead to varying strength of adsorption of the halogen/interhalogen in the prepared adducts and adsorption is stronger in the nanosized metal oxides as compared to their macrocrystalline available counterparts.

Nanosized metal oxide halogen adducts possess high surface reactivities due to their unique surface morphologies. These adducts have been used as reactive materials against vegetative cells, such as *Escherichia coli* and *Bacillus megaterium*, as well as spores, including *Bacillus subtilis* and *Bacillus anthracis* (Δ Sterne strain). High biocidal activities against both Gram-positive and Gram-negative bacteria, as well as spores have been obtained. Bactericidal test procedures include a water suspension method and a dry membrane method and the results illustrate that good results are obtained using both procedures. Transmission electron micrographs have been used to illustrate the treated and untreated cells and spores, giving insight into the mechanism. It is proposed that the abrasive character of the particles, along with the oxidative power of the halogens/interhalogens as well as the electrostatic attraction between some of the metal oxides and the biological material are main reasons for the high biocidal activities.

Three different bacteriophages (MS2, φX174 and PRD1) have also been studied and initial results indicate that there is big potential for the use of metal oxide halogen and interhalogen adducts for the destruction of viruses. Other potential uses for them also include halogenating agents in organic and inorganic synthesis as well as a safe way to store intact halogens.

SYNTHESIS, CHARACTERIZATION, BIOCIDAL AND VIRUCIDAL PROPERTIES OF METAL OXIDE NANOPARTICLES

by

JOHANNA A. HÄGGSTRÖM

B.S., Mälardalen University, Sweden, 2002

A DISSERTATION

submitted in partial fulfillment of the requirements for the degree

DOCTOR OF PHILOSOPHY

Department of Chemistry
College of Arts and Sciences

KANSAS STATE UNIVERSITY
Manhattan, Kansas

2007

Approved by:

Major Professor
Kenneth J. Klabunde

Copyright

Abstract

Non-polar halogens (Cl_2, Br_2 and I_2) and polar interhalogen molecules (ICl, IBr and ICl_3) have been adsorbed on the surface of several high surface area materials, including three different nanosized metal oxides (NanoActive® (NA) Al_2O_3 Plus, NA-TiO_2 and NA-CeO_2). The prepared halogen and interhalogen adducts have been characterized in detail by thermogravimetric analysis (TGA), UV-Vis, Raman and X-ray photoelectron spectroscopies (XPS) and the results are discussed herein. The different metal oxides lead to varying strength of adsorption of the halogen/interhalogen in the prepared adducts and adsorption is stronger in the nanosized metal oxides as compared to their macrocrystalline available counterparts.

Nanosized metal oxide halogen adducts possess high surface reactivities due to their unique surface morphologies. These adducts have been used as reactive materials against vegetative cells, such as *Escherichia coli* and *Bacillus megaterium*, as well as spores, including *Bacillus subtilis* and *Bacillus anthracis* (Δ Sterne strain). High biocidal activities against both Gram-positive and Gram-negative bacteria, as well as spores have been obtained. Bactericidal test procedures include a water suspension method and a dry membrane method and the results illustrate that good results are obtained using both procedures. Transmission electron micrographs have been used to illustrate the treated and untreated cells and spores, giving insight into the mechanism. It is proposed that the abrasive character of the particles, along with the oxidative power of the halogens/interhalogens as well as the electrostatic attraction between some of the metal oxides and the biological material are main reasons for the high biocidal activities.

Three different bacteriophages (MS2, φX174 and PRD1) have also been studied and initial results indicate that there is big potential for the use of metal oxide halogen and interhalogen adducts for the destruction of viruses. Other potential uses for them also include halogenating agents in organic and inorganic synthesis as well as a safe way to store intact halogens.

Table of Contents

List of Figures

List of Tables

Acknowledgements

First of all, I would like to thank my doctorate advisor at Kansas State University, Professor Kenneth J. Klabunde, for the honor to work under his guidance. I greatly appreciate the freedom he gave me and the opportunity to pursue my research in my own way. I also would like to thank him for the opportunities to travel to conferences such a great amount. I tremendously enjoyed all the trips taken in the past few years, including the trips to Australia, Bulgaria, Wyoming, Montana, Washington DC, Philadelphia and Colorado, to name a few. The people I have met during these trips have made my life richer and my research better.

Secondly, I would like to thank my undergraduate professor, Dr. Simon J. Dunne. He guided my undergraduate research as well as taught me in several classes. Simon really opened my eyes for chemistry and the possibility for further studies. Along those lines I would also like to thank Per Lohikoski and Professor Christer Aakeroy for the opportunity to come to K-State and attend graduate school. A special thanks to Christer also for all the help he gave us prior to coming here through many e-mails and once we had arrived. I will never forget the look on his face when we had been at Wal-Mart for three hours and still were not done…Thank you Dr. Yasmin Patell for picking us up when we arrived and were so lost!

I also want to thank Göran Wennerberg, Anita Lazar and Azadeh Lalehzari for making my first semester here easier. It was nice with Swedish folks around me. A special thanks, of course, goes to Azi for being my good friend for the past five years. Without her, the five years here would have been so much more difficult.

I would like to thank my committee members: Dr. Kenneth J. Klabunde, Dr. Eric A. Maatta, Dr. Christopher T. Culbertson, Dr. George L. Marchin and Dr. Michael R. Kanost. Thank you for your time and valuable suggestions and discussions. I really appreciate Dr. Kanost accepting the role as the chair of my committee, especially as it was very last minute.

A special thanks to all the present and former group members of the KJK group during my time there: Dr. Shalini Rodrigues, Dr. Uma Sitharaman, Dr. Jeevanandam Pethaiyan, Dr. Ranjit Koodali, Dr. Igor Martyanov, Dr. Alexander Bedilo, Dr. Aldo Ponce, Dr. Peter Stoimenov, Dr. Savka Stoeva, Dr. Gavin Medine, Dr. David Heroux, Dr. Alexander Smetana, Dr. Dmytro Demydov, Aaron Yang, Dambar Hamal, Xiangxin Yang, Erin Beavers, Sreeram Cingarapu, Luther Mahoney, Yen-Ting Kuo, Denitza Balyozova, Benny Mwale and Kevin Quinn. The Russian crew, Dr. Ilya Mishakov, Dr. Vladimir Zaikovskii, Dr. Alexander Volodin, Dr. Maxim Melgunov and Dr. Elena Melgunova, is also acknowledged with gratitude. Dr. Shalini Rodrigues and Dr. Ranjit Koodali are especially acknowledged for sharing a difficult time with me after the fire accident.

Thank you Richard Bachamp, Tobe Eggers and Jim Hodgson for fixing my equipment whenever needed! Thank you, Earline Dikeman for the introduction to the teaching experience and thank you to all the ladies in the office for helping with all kinds of things!

I would like to thank Dr. George Marchin at the Division of Biology for all his help in teaching me microbiology. Thank you for answering all my questions! I would also like to thank Mr. Adam Henry, research assistant in the Division of Biology, for his endless help and answers to all my microbiology questions. In addition, I would like to thank Dr. Dan Boyle and the Division of Biology for the assistance and use of the Transmission Electron Microscope.

Stephen Lee also deserves a special thanks for his funding through the Army Research Office grant, and especially for paying for my trip to Australia.

I would like to express my sincere appreciation to my husband, Thom Murphy. He certainly has made the time here much easier and I will always be thankful for that!

Lastly, I would like to thank my friends and family back home for all their support and for making it easier being so far away from home. Without you this dissertation would not have been written.

Dedication

To my parents:

Boel and Staffan Häggström

And

To my brother:

Johan Häggström

For their endless love and support.

Preface

Size matters. One nanometer is 10^{-9} m.

CHAPTER 1 - Introduction

1.1 Importance of Nanomaterials

To be considered a 'nanomaterial' one dimension needs to be in the nanometer range (1-100 nm). The interest and use of nanomaterials has increased tremendously in the past ten years. If the periodic table of elements is considered "a puzzle that has been given to us by God",[1] imagine the possibilities that could arise from the use of nanoparticles. While chemistry is the study of atoms and molecules and condensed matter physics involves the study of solid materials containing arrays of large atoms or molecules much larger than 100 nm, a significant gap exists between these two phases.[2] It is in this gap that nanoparticles in the size range of 1 to 100 nm are placed and each one of these particles contain about 10 to 10^6 atoms or molecules.[3,4] The interesting aspect of this regime is that here, neither quantum chemistry, nor classical laws of physics hold and we start to see structural changes with change in size.[2] This in turn leads to chemical and physical properties that can be fine-tuned through a change in size of the particles. Examples of changed properties are melting points, specific heats, surface reactivity, magnetic and optical properties. With these changed properties, the possibilities are endless. Many applications arising from nanostructures have already arisen and the use of TiO_2 in sunscreens, self-cleaning windows, antibacterial textiles and remediation are examples of that. Several usage areas will in the near future become possible, such as better batteries, improved ceramics and metals, information storage and catalysts, to mention a few.

The main reason for the increased interest in improved nanostructured materials lately has been the development of methods of characterization and analysis of these new materials. Before these new techniques were developed there was really no good way to fully characterize nanomaterials. Now, a combination of several different techniques is often used, including microscopy techniques (Tranmission Electron Microscopy and High Resolution TEM, Scanning Electron Microscopy, and Atomic Force Microscopy), Brunauer-Emmet-Teller Gas Adsorption Surface Area and Pore Structure Analysis (BET Method) and Powder X-Ray Diffraction (XRD), to name a few. Without these techniques and others, a full understanding of these materials is impossible and applications are hard to find. Especially TEM and HRTEM have proven necessary for many types of nanostructured materials, as these techniques can give essential information about morphology, crystallographic details and chemical composition.[5]

The number of scientific journals published each year involving nanoscience and technology is growing exponentially with more and more research groups devoting their time to this new class of materials. Several novel methods of fabrication to prepare these materials are constantly discovered. The various kinds of nanostructures formed are many, including nanoparticles, nanocrystals and clusters (quantum dots), nanowires and rods, nanotubes, thin films and superlattices.[6] In order to take nanotechnology to the next step, the immediate objectives of nanotechnology include (1) to master the synthesis of nanostructures with the desired properties (this includes the ability to prepare monodisperse nanoparticles), (2) to form new classes of high performance nanomaterials, (3) to connect nanotechnology with other sciences to its full extent, and (4) to improve current methods of characterization. A crucial aspect of the synthesis involves the control of size, shape and structure.[7] With controllable size, shape and structure comes controllable properties and new applications arise. Both physical and

chemical methods have been used to prepare nanosized ceramic materials, whereas colloid chemical methods have been utilized in order to prepare nanocrystals of metals, semiconductors and magnetic materials.

One important concern of nanostructured materials recently has been safety. Critics are afraid that nanoparticles could become the 'asbestos' of the 21st century.[8] In regards to the materials in this dissertation, nanosized metal oxides, there is little need for concern. So far the nanomaterials we have made have been proven to be close to harmless. Animal studies have shown that inhalation exposure to high levels of nanostructured metal oxides – magnesium oxide (MgO) and titanium dioxide (TiO_2) – cause no adverse clinical signs, weight loss or increased mortality.[9] Animal exposures to eyes, to wounds and oral exposure support this data. Most data show no toxicity, or at worst an irritant dust response. Inhalation exposure of several NanoActive® metal oxides and subsequent animal observations concluded that these nanostructured materials should be categorized as EPA category IV, practically non-toxic.

Nanotechnology has been considered "the biggest engineering innovation since the Industrial Revolution".[8] Nanoscience is a very interdisciplinary science, covering chemistry, physics, biology, materials and engineering.[6,7] Interaction between the different groups of scientists is very important and will ultimately lead to new discoveries with novel technological possibilities. Nanoscience and technology will benefit various industrial sectors, including industries as well as manufacturing. The future of nanoscience will depend on the development of new technologies.

1.2 Biocidal Properties of Nanomaterials

Several researchers have investigated the use of different nanomaterials as biocides in the last few years. Most of the work has involved the use of nanosized TiO_2, ZnO and silver, but other materials have been studied as well. Several products with incorporated nano-silver are already on the market, including antibacterial clothes that will kill bacteria and prevent odor.

Li et al.[10] reported the use of ZnO in fabrics and its resistance to sweat. The use of nanoparticles to kill bacteria to prevent odor in clothes/textiles is one of the most researched biocidal areas. The authors found that ZnO in fabrics has a durable antibacterial function. Further, Brayner, et al.[11] reported on the toxicological impact of nano-ZnO on *E. coli*. It was found that ZnO is toxic to *E. coli*, but only above certain concentrations. These results indicate that ZnO might be useful in textiles to kill small amounts of bacteria such as *E. coli*, but that the preparation is most likely not powerful enough to tackle the more resistant forms of bacteria, the dormant spores. The search for a powerful biocide/sporicide continues, and there is much promise in the use of nanomaterials. Nano-TiO_2 and silver particles, or a combination of the two (e.g. silver-doped TiO_2), are other promising biocides with potential to be used as a first response against chemical and biological threats (bioterrorism). Much of the research performed has included the use of UV light; however, it would be desirable to find a material that works without the use of UV light. Vohra et al.[12] have reported on the use of silver ion-doped TiO_2 for the destruction of *B. cereus* spores under UV light and in the dark. They found that the UV light further increased the activity but that some activity was present even in the dark. The main problem with these materials has been the lack of fast kinetics in the inactivation of spores and the need for UV light in many cases.

Along the same lines, Sambhy and co-workers[13] have investigated the use of silver bromide nanoparticles as part of a polymer composite material. The material was active against both Gram-negative and Gram-positive bacteria and had the ability to slowly release active silver ions into aqueous LB (Luria Broth) media, leading to biocidal activity over a period of several days. In addition, they were able to fine-tune the activity of the composite by changing the size of the silver bromide nanoparticles. Interestingly, the smaller the particles were the more active the composite material became. The potential usage areas for such a material include antimicrobial coatings for general and biomedical uses to prevent the formation of biofilms. These composite materials however, are probably not aggressive enough for future use in bioterrorism.

The advantages of finding nanosized biocides are many. For example, since the properties change on the nanoscale, it is possible that there are many elements that are non-biocidal when they are micron-sized that may be biocidal once they are nanosized. It is also possible and very likely that micron-sized materials that are biocidal become even more biocidal on the nanoscale. One example of that is MgO, which is more biocidal in the nanosized form than in its micron-sized counterpart. Nanoparticles can also be prepared in a variety of forms, such as powders, slurries and pellet form, which makes the use of them much more convenient and widely applicable. Nanoparticles are also very easily stored and transported, further utilizing their flexibility of use.

Currently used biocides include hydrogen peroxide (vaporous or liquid), chlorine dioxide and liquid bleach. The current problem with these is that they are very corrosive and damaging to the surfaces they come in contact with. Second, it is very difficult to clean up the biocide after its use. Liquid biocides are easy to apply, but not very easy to clean up. Liquid disinfectants are also

prone to aging, which further increases the difficulty of their use. The main disadvantage with solid disinfectants is that it is harder for them to contact the cell or spore, as compared to liquid or gaseous disinfectants. However, by using nanosized materials, this problem could be minimized as the nanoparticles are much smaller and have much better penetration ability than micron-sized solid disinfectants. Further, the nanoparticles could be biocidal by themselves, or they could carry an active disinfectant. The solid disinfectants could also be removed easily by vacuum cleaning. Depending of what kind of nanomaterials, some of them could even be safe enough to use on sensitive equipment, such as electronics. Another advantage as compared to the corrosive gaseous and liquid disinfectants is that solid nanoparticles could be applied not only in closed spaces but also in open atmospheres.

1.3 Systems of Interest

The main focus of this study was to investigate nanosized metal oxides, their halogen and interhalogen adducts and their use as biocides and virucides. Several metal oxides were studied throughout this research, but the main focus was set on NanoActive® (NA) Al_2O_3 Plus, NA-TiO_2 and NA-CeO_2.

Nanosized Aerogel-prepared (AP) MgO, its halogen and interhalogen adducts, as well as their use as biocides have been studied in the past[14-16] with very promising results, leading us to believe that there was much potential for similar materials. It was found that AP-MgO had a considerably higher activity against a variety of compounds including warfare mimics[2,17-19] and real warfare agents,[20-22] as compared to micron-sized magnesium oxide.

Nanosized metal oxides are very easy to handle and they are considerably more environmentally friendly as compared to many other currently used biocides. They can all easily be prepared with high surface areas (up to almost 600 m^2/g) and in large quantities. NA-Al_2O_3 Plus has a surface area of 550 m^2/g and has a fibrous structure and large pore volume, as seen in Figure 1.1. NA-TiO_2 (Figure 1.2) has a surface area of 500 m^2/g with a structure consisting of a large number of spheres/squares that agglomerate together to form a porous structure. Similarly, NA-CeO_2 consists of spheres/squares (Figure 1.3), but has a lower surface area of 50 m^2/g. Cerium oxide is also a heavy metal oxide and less environmentally friendly as well as worse to inhale than aluminum oxide an titanium oxide are.

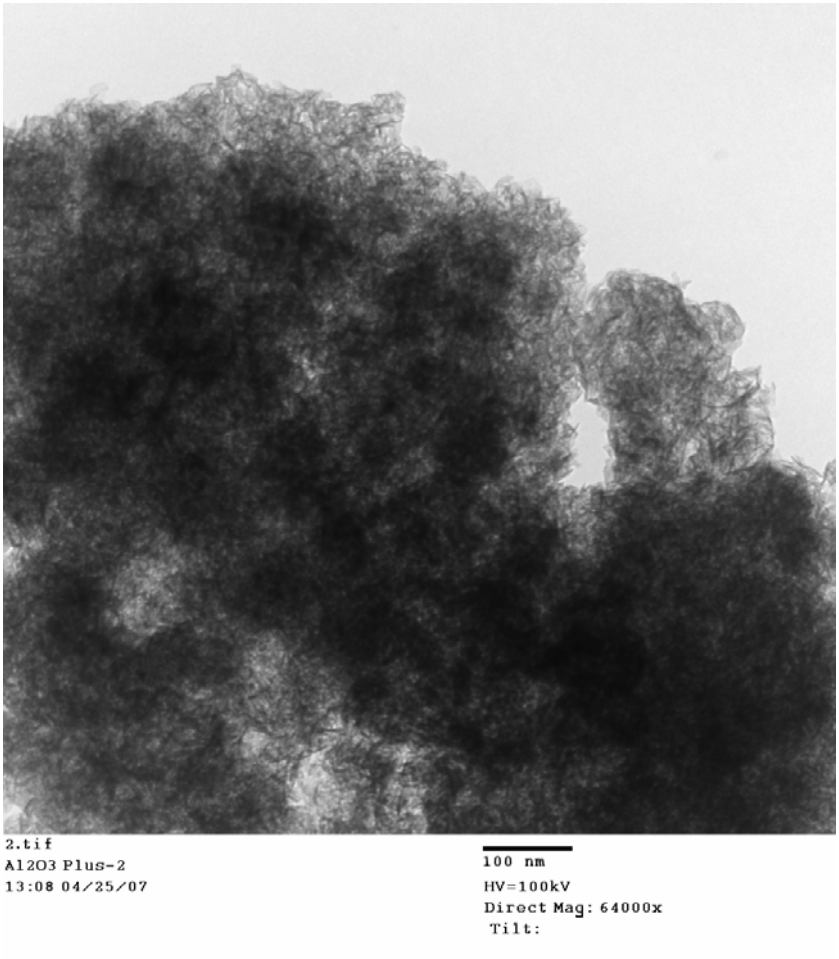

Figure 1.1 TEM image of NA-Al_2O_3 Plus.

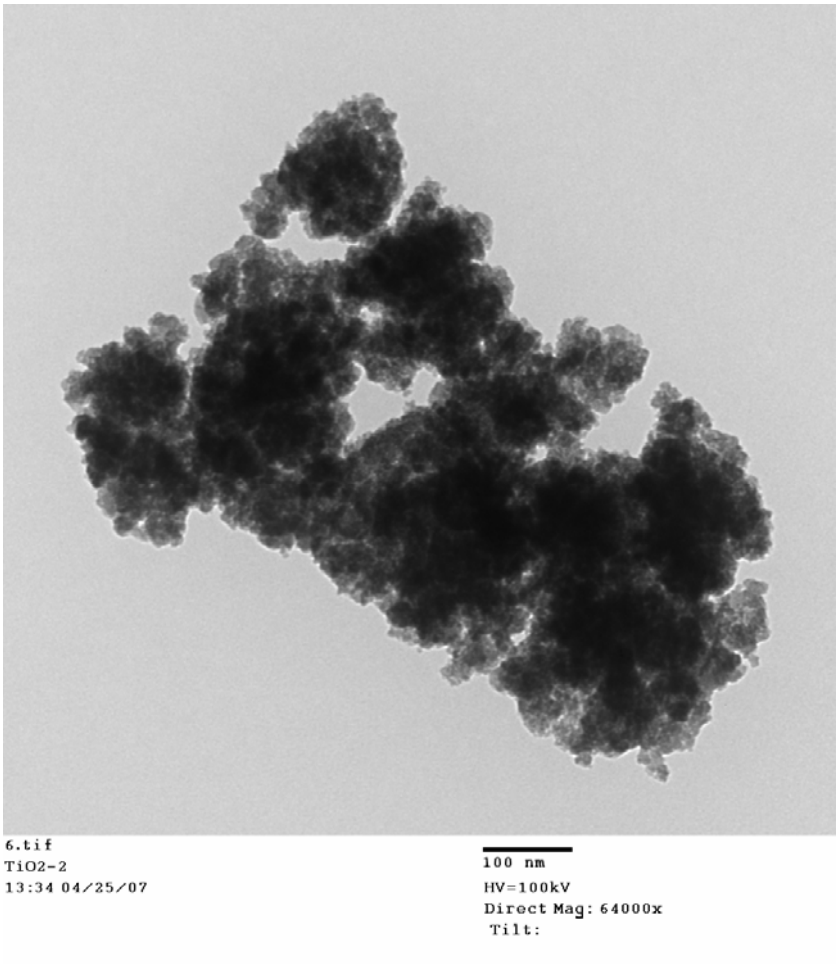

Figure 1.2 TEM image of NA-TiO_2.

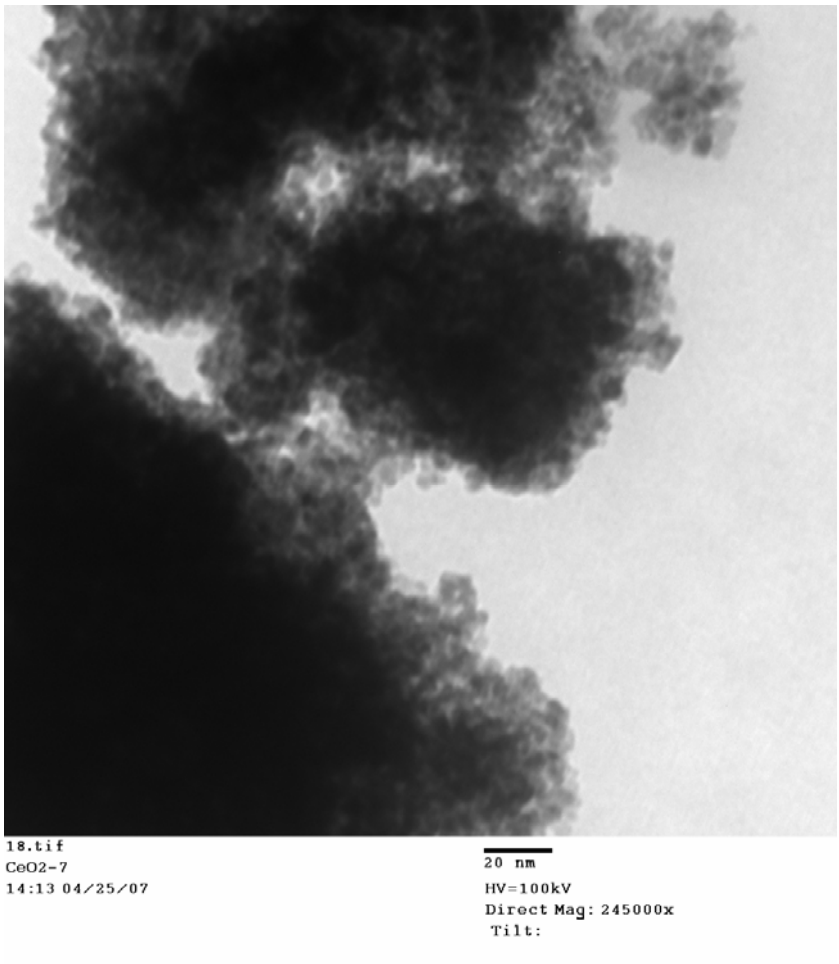

Figure 1.3 TEM image of NA-CeO_2.

Many halogen and interhalogen adducts of NA-Al_2O_3 Plus, NA-TiO_2 and NA-CeO_2 have been prepared and characterized. Their distinct structure as well as their use in biocidal and virucidal applications has been studied. The halogens used in this study include chlorine, bromine and iodine. The interhalogens used consist of iodine monochloride, iodine monobromide and iodine trichloride. Especially the interhalogens are very corrosive, which is expected to result in some very potent biocides and virucides. They are also expected to interact rather strongly with the ionic metal oxide surfaces due to their dipole moment, which the non-polar halogens lack. In addition to studying their biological applications it was also of interest to study the change of the halogens/interhalogens upon adsorption on the metal oxide surfaces.

Many different techniques have been used to study the prepared halogen/interhalogen adducts – Thermogravimetric Analysis (TGA), Raman Spectroscopy, UV-Vis Spectroscopy and X-Ray Photoelectron Spectroscopy (XPS). The interaction between the nanoparticles and bacterial cells/spores and viruses has been investigated using Transmission Electron Microscopy (TEM).

1.4 References

(1) Amato, I., *Science*, **1991**, *252*, 644.

(2) Klabunde, K. J., Nanoscale Materials in Chemistry, Wiley, Interscience, New York, NY, **2001**.

(3) Klabunde, K. J., *Free Atoms, Clusters, and Nanoscale Particles*, Academic Press, San Diego, **1994**, pp. 2, 36.

(4) Klabunde, K. J., Mohs, C., in *Chemistry of Advanced Materials: An Overview*, Interrante, L. V., Hampden-Smith, M. J. (Editors), Wiley-VCH, New York, **1998**, p. 271.

(5) Neogy, S.; Savalia, R. T.; Tewari, R.; Srivastava, D.; Dey, G. K. *Indian Journal of Pure & Applied Physics*, **2006**, *44*, 119-124.

(6) Rao, C. N. R.; Mueller, A.; Cheetham, A. K. *Nanomaterials – An Introduction*, **2004**, *1*, 1-11.

(7) Rao, C. N. R.; Cheetham, A. K., Nanomaterials Handbook, CRC Press LLC, Boca Raton, **2006**.

(8) Gwinn, M. R.; Vallyathan, V., *Environmental Health Perspectives*, **2006**, *114*, 1818-1825.

(9) Koper, O. B.; Bergmann, J.; Klabunde, K. J.; Wilson, C. M.; Pickrell, J. A., submitted.

(10) Li Q.; Chen, S-L.; Jiang, W-C., *J. Appl. Polym. Sci.* **2006**, *103*, 412-416.

(11) Brayner, R.; Ferrari-Iliou, R.; Brivois, N.; Djediat, S.; Benedetti, M. F.; Fievet, F., *Nano Lett.* **2006**, *6*, 866-870.

(12) Vohra, A.; Goswami, D. Y.; Deshpande, D. A.; Block, S. S., *Appl. Catal. B,* **2006**, *65*, 57-65.

(13) Sambhy, V.; MacBride, M. M.; Peterson, B. R.; Sen, A., *J. Am. Chem. Soc.* **2006**, *128*, 9798-9808.

(14) Stoimenov, P. K.; Zaikovski, V.; Klabunde, K. J. *J. Am. Chem. Soc.* **2003**, *125*, 12907-12913.

(15) Stoimenov, P. K.; Klinger, R. L.; Marchin, G. L.; Klabunde, K. J., *Langmuir*, **2002**, *18*, 6679-6686.

(16) Koper, O. B.; Klabunde, J. S.; Marchin, G. L.; Klabunde, K. J.; Stoimenov, P. K.; Bohra, L., *Curr. Microbiol.* **2002**, *44*, 49-55.

(17) Rajagopalan, S.; Koper, O.; Decker, S.; Klabunde, K. J. *Chem. Eur. J.* **2002**, *8*, 2602-2607.

(18) Narske, R. M.; Klabunde, K. J.; Fultz, S. *Langmuir*, **2002**, *18*, 4819-4825.

(19) Lucas, E. M.; Klabunde, K. J., *Nanostruct. Mater.* **1999**, *12*, 179-182.

(20) Wagner, G. W.; Bartram, P. W.; Koper, O.; Klabunde, K. J., *J. Phys. Chem. B.* **1999**, *103*, 3225-3228.

(21) Wagner, G. W.; Procell, L. R.; O'Connor, R. J.; Munavalli, S.; Carnes, C. L.; Kapoor, P. N.; Klabunde, K. J., *J. Am. Chem. Soc.* **2001**, *123*, 1636-1644.

(22) Wagner, G. W.; Koper, O. B.; Lucas, E.; Decker, S.; Klabunde, K. J., *J. Phys. Chem. B.* **2000**, *104*, 5118-5123.

CHAPTER 2 - Synthesis and Characterization of Nanosized Halogenated and Interhalogenated Metal Oxide Adducts

2.1 Introduction

The intriguing properties of nanoparticles arise from the presence of numerous corners, edges and defect sites, which lead to unique surface morphologies and reactive surface ions or atoms. The characteristic morphology of nanosized materials becomes very important in solid state interactions, where the morphology of the surface decides the reactivity of the material. Nanosized metal oxides have been extensively studied in the past,[1-7] mainly for their use as destructive adsorbents,[1,3,4,6] but also for their role in catalysis.[2,7] One of the most recent interests has involved using nanoparticles for decontamination of vegetative cells and spores[4,8-10] and to increase the biocidal activity of the nanosized metal oxide, halogen has been adsorbed on the surface,[8,11] which also leads to a safe and efficient method to store intact halogen.[11] Halogen species adsorbed on various high surface area solids, such as zeolites,[12-16] silicas[17] and Vycor glass[18] have been described in the literature in detail. It has been found that when halogen molecules are adsorbed on a surface their properties can significantly change and the reactivity of the halogen can significantly increase.[18] Risbood et al.[12] reported selective bromination of a side-chain double bond by bromine preadsorbed on a zeolite, more efficiently than by bromine itself. It has also been reported that bromine adsorbed on zeolites is more chemically reactive than gas phase bromine as a result of reduced molecular force constants.[13,14]

The advantage of using different nanosized metal oxides for adsorption of halogen and interhalogen is the varying strength of adsorption capability of the metal oxides. This could lead to the ability to fine tune the final product to display the properties necessary for the desired application. For example, using these adducts as a safe way to store halogen and interhalogens would require a metal oxide with the capability to hold on to the halogen/interhalogen tightly for long periods of times, whereas in the use of these adducts as biocides, one might imagine using a metal oxide that only temporarily retains the halogen and then can release it to act as an oxidizer during contact with the bacterial cell. Stoimenov et al. have previously reported the use of nanosized halogen magnesium oxide adducts as biocides,[9,10] but also state that they are stable for several months.[8]

2.2 Experimental Section

2.2.1 Synthesis

The preparation of halogenated and interhalogenated metal oxide adducts has been reported previously.[8] The metal oxide used then was Aerogel-Prepared (AP) MgO and the adducts were well characterized. Prior to then, only chlorine and bromine adducts had been reported.[11,19]

The methods used for synthesis herein are similar to those reported by Stoimenov et al.[8]

2.2.1.1 Synthesis of Chlorine, Bromine and Iodine Monochloride Adducts of Nanosized Metal Oxides

In order to remove any undesired water and carbon dioxide adsorbed on the surface of the metal oxide, an activation step was applied prior to adsorption of halogen/interhalogen. The activation step consisted of gradual heating of the material in a 150 mL Schlenk tube to 400ºC over 2 hours and then maintaining this temperature for another 4 hours, either under O_2 atmosphere (TiO_2) or under dynamic vacuum (other materials). Before adsorption of halogen/interhalogen the samples were allowed to cool to room temperature.

The procedure was carried out as described in the literature[8] and is described in short below.

About 10 grams of freshly activated powder contained in a 150 mL Schlenk tube was allowed contact with chlorine gas, or in case of Br_2 and ICl, connected to a Schlenk tube containing liquid Br_2 or ICl. Normally two doses of halogen/interhalogen were transferred initially. The difference in pressure between the atmosphere above the metal oxide and in the halogen source allowed the transfer of Cl_2 gas or Br_2 and ICl vapors to the Schlenk tube containing the metal oxide. During this step, the outlet to the vacuum line was closed. As the color of the atmosphere above the powder changed to green-yellow (chlorine) or brown-red (bromine or iodine monochloride), the connection was disengaged and the powder was well shaken to encourage maximum contact. Another dose of halogen was transferred when the atmosphere above the powder had cleared up. Halogen dosage continued until the atmosphere above the powder did not clear up and halogen remained. The halogen container was then disconnected and the powder was again connected to the vacuum line and maintained until the

pressure reached 50 x 10^{-3} torr or below. This step took approximately 20 minutes and ensured the removal of excess halogen The freshly prepared halogen adduct was transferred to a Teflon® sealed glass vial.

2.2.1.2 Synthesis of Iodine, Iodine Monobromide and Iodine Trichloride Adducts of Nanosized Metal Oxides

In order to remove any undesired water and carbon dioxide adsorbed on the surface of the metal oxide, an activation step was applied prior to adsorption of halogen/interhalogen. The activation step consisted of gradual heating of the material in a 150 mL Schlenk tube to 400ºC over 2 hours and then maintaining this temperature for another 4 hours, either under O_2 atmosphere (TiO_2) or under dynamic vacuum (other materials). Before adsorption of halogen/interhalogen the samples were allowed to cool to room temperature.

Iodine, iodine monobromide and iodine trichloride are all solids and not volatile enough to be transferred as vapors or gas as in the procedure described previously. Instead, solid material (about a quarter of a spatula) was added directly to about 10 grams of activated powder contained in a 150 mL Schlenk tube and the powder was well shaken. Upon adsorption, the powder changed color. Another dose of solid halogen particles was added to ensure complete adsorption, if no solid halogen/interhalogen particles remained. Persistence of halogen particles was considered the saturation point, and once reached; the powder was connected to the vacuum line and maintained until the pressure reached 50 x 10^{-3} torr or below. The iodine sample was further heated to 125°C for about 20 minutes to ensure enough volatility to remove excess iodine. The freshly prepared halogen adduct was then transferred to a Teflon® sealed glass vial.

2.2.1.3 Synthesis of Bromine adducts of other Materials of interest

In order to remove any undesired water and carbon dioxide adsorbed on the surface of the metal oxide, an activation step was applied prior to adsorption of bromine. The activation step consisted of gradual heating of the material in a 150 mL Schlenk tube to 400ºC over 2 hours and then maintaining this temperature for another 4 hours under dynamic vacuum or under O_2 atmosphere (anatase and rutile TiO_2). Before adsorption of halogen/interhalogen the samples were allowed to cool to room temperature.

Freshly activated powder, about 2 grams, contained in a 150 mL Schlenk tube was connected to a Schlenk tube containing liquid Br_2. During this step, the outlet to the vacuum line was closed. As the color of the atmosphere above the powder changed to brown-red, the connection was disengaged and the powder was well shaken to encourage maximum contact. Another dose of halogen was transferred when the atmosphere above the powder had cleared up. Halogen dosage continued until the atmosphere above the powder did not clear up and halogen remained. The bromine container was then disconnected and the powder was again connected to the vacuum line and maintained until the pressure reached 50×10^{-3} torr or below. This step took approximately 20 minutes and ensured the removal of excess bromine. The freshly prepared bromine adduct was transferred to a Teflon® sealed glass vial.

2.2.2 Experimental Techniques

Several different experimental techniques were used to characterize the prepared halogen and interhalogen adducts and they are described in separate sections below.

2.2.2.1 Specific Surface Area

Quantachrome NOVA-1200 was used to determine the surface area of the materials. The BET method using nitrogen adsorption was utilized.

2.2.2.2 Thermogravimetric Analysis (TGA)

Thermogravimetric Analysis (TGA) was recorded on a Shimadzu TGA model TGA-50, using He atmosphere. A gas flow of around 25 mL per minute was used with a heating rate of either 5 or 10°C/min.

2.2.2.3 Raman Spectroscopy

FT-Raman spectra were collected on a Nicolet Nexus 670 with a Raman module using a continuous Nd-YAG laser (1064 nm). Either a liquid nitrogen cooled germanium or InGaAs detector within the range of 4000-100 cm^{-1} was used. The sample holder consists of a static glass cylindrical Raman cuvette and the laser power used was between 0.2-0.65 W.

2.2.2.4 UV-Vis Spectra Analysis

A Varian UV-Vis-NIR spectrophotometer Cary 500 Scan instrument was used to record diffuse reflectance and UV-Vis spectra. Teflon® powder (polytetrafluoroethylene) was used as

the diffuse reflectance reference. The spectra of solutions were recorded using the corresponding solvent as a reference.

2.2.2.5 Transmission Electron Microscopy (TEM)

TEM images were recorded on a Philips CM 100, operating at 100kV. The nanosized metal oxides were dissolved in ethanol and sonicated for 5-10 minutes. One drop of the supernatant was then put on a 300 mesh copper Formvar/carbon grid, allowed to air-dry and then imaged under the microscope.

2.2.2.6 X-Ray Photoelectron Spectroscopy (XPS)

XPS spectra were recorded on a Kratos Axis Ultra Spectrometer. Monochromatic Al radiation was used with 50 meV energy step increments and 1200 ms dwell time. The samples were pressed flat on double sticky tape and imaged in a vacuum of $1x10^{-8}$ Torr or better.

2.3 Results and Discussion

Each method of characterization is described in separate sections below.

2.3.1 NA-Al_2O_3 Plus and its Adducts

2.3.1.1 Specific Surface Area

The BET method was used to find the specific surface area of the NA-Al_2O_3 Plus, before and after the activation step. Since no difference is seen in the appearance of the powder, even when varying temperatures were used during the activation step, this is a very critical method to find out exactly what temperature is appropriate for the activation of the starting metal oxide.

Initially, the metal oxide has a specific surface area of ~550 m^2/g. During an increase of the temperature from room temperature up to 400 °C over a period of two hours and then keeping this temperature for another four hours (six hours total) the surface area remains close to the same, which indicates that the porous structure of NA-Al_2O_3 Plus is not very sensitive to collapse during heat-treatment.

2.3.1.2 Thermogravimetric Analysis (TGA)

Thermogravimetric Analysis is an easy and straightforward method to use for determination of total volatile content in solids, such as metal oxides. The samples were heated at a rate of either 5 or 10 °C per minute up to 600 °C in a helium atmosphere. The first derivative is a tool that can be useful to determine the temperature at which maximum weight loss occurs.

The halogen/interhalogen content based on thermogravimetric data, as well as the calculated surface concentration for the prepared adducts, can be seen in Table 2.1.

Table 2.1 Halogen/Interhalogen content as determined by TGA and the calculated Surface Concentration.

Material	Halogen Content wt % (TGA)	Surface Concn molecules/nm^2
NA-Al_2O_3/Cl_2 Plus	14	2.5
NA-Al_2O_3/Br_2 Plus	15	1.2
NA-Al_2O_3/I_2 Plus	18	1.0
NA-Al_2O_3/ICl Plus	35	3.6
NA-Al_2O_3/IBr Plus	28	2.1
NA-Al_2O_3/ICl_3 Plus	37	2.8

It can be seen that the values obtained from TGA vary from 14 wt % (Cl_2 adduct) up to 37 wt % (ICl_3 adduct). The adducts are very stable and can be safely stored in a vial for several months and then used. If the adducts are completely exposed to the atmosphere, i.e. put on a weighing paper on a bench top, they will lose halogen over time. The iodinated adduct has shown to be the most stable, taking more than 30 hours for the iodine on the surface to dissipate. The interhalogen adducts are also very stable, as expected since they are polar molecules and will interact strongly with the ionic metal oxide surface, whereas the brominated adduct is less stable. This coincides well with the thermogravimetric analysis data that shows that iodine is lost at a higher temperature than the interhalogen molecules (Appendix A). The brominated adduct has lost much of its bromine already at 40 °C and is much less stable. Among the interhalogen adducts, NA-Al_2O_3/ICl Plus is the most stable, most likely due to the strong dipole moment of the iodine monochloride molecule, leading to a very strong interaction with the ionic oxide surface.

The surface concentration for the NA-Al_2O_3 Plus adducts are in the range 1.0-3.6 molecules/nm^2. These are slightly higher values than those reported for MgO adducts by

Stoimenov et al,[8] which can be explained by the slightly higher surface area of the Aerogel Prepared (AP)-MgO.

2.3.1.3 Raman Spectroscopy

The halogens and interhalogens have been extensively studied and their Raman spectra recorded both in the gas and the condensed phase.[20-32] Both Raman and Infrared spectroscopies have been used frequently in the past to study the formation and strength of the interaction between different donors and acceptors. Several of the halogens and interhalogens have been investigated,[33-37] but other molecules have been of interest as well.[38,39] Raman and Infrared spectroscopies are very useful in the detection of small changes in many molecules and Raman spectroscopy is suitable for the study of these halogen and interhalogen changes, especially as even the non-polar halogens are Raman active, whereas in the infrared light region, they are not.

The nature of the interaction that takes place between the halogen/interhalogen with the metal oxide surface is of considerable interest. Stoimenov et al.[8] reported halogen/interhalogen adsorbed on nanosized magnesium oxide and concluded that a strained halogen-halogen bond existed, causing a frequency shift of the halogen vibration to a lower wavenumber in the Raman spectrum. The two different possibilities of adsorption have been explained[8] and are described below:

Case 1: Chemisorption without polarization or bond breakage of the halogen/interhalogen. This would cause a lengthening and weakening of the halogen/interhalogen bond and hence a lowering of the frequency shift of the halogen itself in the Raman spectrum. One should expect to see the vibration of the halogen/interhalogen moiety

as well as the metal oxide lattice vibration in the Raman spectrum if this occurs. Klaboe[35] has described a possible intensity variation of the lattice vibrations in the Raman spectrum during the interaction with halogens and Cooney et al.[40] have reported that the shift of the halogen vibration can vary significantly depending upon the strength of adsorption.

Case 2: The polarization of the halogen/interhalogen molecule is stabilized by the dipoles of the metal oxide surface (metal cations and oxygen anions), leading to bond breakage and further formation of new bonds causing disproportionation of the surface. This would cause new species on the surface, such as M -X(Y) and/or O-X(Y), where M is the metal and X, Y=Cl, Br, I. These new species would then lead to new bands that are allowed in the Raman spectrum.

The Raman spectrum of activated NA-Al_2O_3 Plus shows a broad peak with a peak position at 376 cm^{-1} (Figure 2.1). The chlorinated adduct shows a similar spectrum (not shown), with no distinct peak for the chlorine stretch. The absence of this peak in the Raman spectrum could possibly be explained by the fact that the Raman Intensity is directly related to the polarizability of the molecule. Since chlorine is a small non-polar molecule it is likely that an absence of the peak would occur. In addition, the chlorine amount on the surface is pretty low. The frequency for chlorine in the gas phase has been determined to 557 cm^{-1}.[22]

NA-Al_2O_3/Br_2 Plus, however, shows an intense peak at 286 cm^{-1}, which can be compared to Br_2 itself in the gas phase with a peak position at 313.9 cm^{-1}(Figure 2.2).[8,24] This shift of 28 wavenumbers can be attributed to significant weakening of the Br-Br bond, leading to a lowering of the shift. There is no spectral evidence indicating formation of Br_3^-, which has a frequency value reported between 160-170 cm^{-1}, [35,37,41-44] or of Br_5^- with a Raman band at 250 cm^{-1}.[45] Several oxygen containing bromine compounds, such as BrO_x^- have been discussed in the literature.[43,45-47] The reported frequency values for BrO^-, BrO_2^-, BrO_3^- and BrO_4^- are all higher

than 400 cm^{-1} and hence much higher than the observed Raman peak in the spectrum of NA-Al_2O_3/Br_2 Plus. We therefore exclude bond breakage and formation of new surface species, or at least assume that they are formed to a very small extent. Beattie et al.[48] have reported Raman values for aluminum trihalides in the gas phase at different temperatures. The observed Raman band of the NA-Al_2O_3/Br_2 Plus adduct at 286 cm^{-1} does not coincide with the reported frequency bands arising from $AlBr_3$ at 360, 228 and 93 cm^{-1}.

I_2 itself has a Raman peak at 213 cm^{-1} [22,24,29] and the iodinated adduct has a peak at 192 cm^{-1}, giving a shift of 21 cm^{-1}(Figure 2.3). Reported frequency values for I_3^- are in the range of 110-120 cm^{-1} [22,41,42,49] and there is no evidence for such a species in the Raman spectrum of the I_2 adduct. Kiefer et al. reported the Raman band for I_5^- [49] of 160 cm^{-1} which is also lower than the observed frequency of our adduct. Oxygen containing species, such as IO_3^-, IO_4^- and IO_6^-,[45,46] all have Raman bands much higher than the observed frequency shift and the formation of such compounds is excluded or it is assumed that it occurs only to a small extent. AlI_3 has been investigated using Raman spectroscopy by Beattie et al.[48] and two bands at 64 and 156 cm^{-1} are reported, neither of which evidence is found for in NA-Al_2O_3/I_2 Plus.

ICl in the gas phase has an intense Raman peak at 381.5 cm^{-1},[22,24,31,32] whereas NA-Al_2O_3/ICl Plus has two Raman peaks, one at 200 cm^{-1} and one broader peak at 325 cm^{-1}, leading to downshifts of 181.5 and 56.5 cm^{-1}, respectively (Figure 2.4). A couple of works in the literature[8,22] have reported large frequency shifts of the ICl stretch during interaction with other surfaces. ICl is a polar molecule, causing a strong interaction with the ionic metal oxide surface, leading to a possible large Raman shift. Isotopic splitting of the halogen peak has been discussed in the literature frequently as a cause for several peaks,[22-24,26-29,33] but these two peaks do not arise from an isotope effect since the frequency difference is much too large. Several works in

the literature have reported Raman bands for ICl_2^- and ICl_4^- as 254-278 cm^{-1} [22,35,44,50] and 288 cm^{-1},[51] respectively, in which range we do not see any peaks in the Raman spectrum of the ICl adduct. One possible and probably the most reasonable explanation for the two values would be that the value at 200 cm^{-1} is due to I_2 on NA-Al_2O_3 Plus and the value at 325 cm^{-1} is due to ICl on the surface of NA-Al_2O_3 Plus. Nagasao et al. has reported that during adsorption of ICl on silica,[17] the Raman spectrum shows decomposition of ICl at the silica surface resulting in iodine on the surface. Partial decomposition upon adsorption has also been speculated by McCarthy et al., where IBr on the surface of MgO results in I_2 and Br_2 on the surface.[52] It is also known that solid ICl contains ICl, I_2 and Cl_2 in its vapor, which means that all three species could have been directly adsorbed onto the surface.

The Raman peak for IBr in the gas phase has been reported at 267 cm^{-1},[29] while NA-Al_2O_3/IBr Plus has one peak at 194 cm^{-1}, and one shoulder at 218 cm^{-1} (Figure 2.5). The peak at 194 cm^{-1} lies very close to the one resulting from NA-Al_2O_3/I_2 Plus and is most likely due to partial decomposition of IBr to I_2. The frequency downshift of 49 cm^{-1} of the IBr molecule seems reasonable in comparison to the previously discussed ICl shift. IBr is slightly less polar than ICl and should hence theoretically interact less strongly with the ionic surface of the metal oxide, leading to a smaller downshift.

The Raman spectrum of solid ICl_3 consists of several Raman peaks:[8,30] two intense peaks at 343.2 and 312.3 cm^{-1}, followed by several very small peaks of values 198.6, 142.6 and 117.6 cm^{-1}. The Raman spectrum of NA-Al_2O_3/ICl_3 Plus however, is slightly different and it displays one peak at 334 cm^{-1} and one shoulder at 280 cm^{-1} (Figure 2.6). It is possible that the three small peaks of ICl_3 are lost in the broad background spectra of NA-Al_2O_3 Plus or that some chemical reaction has taken place.

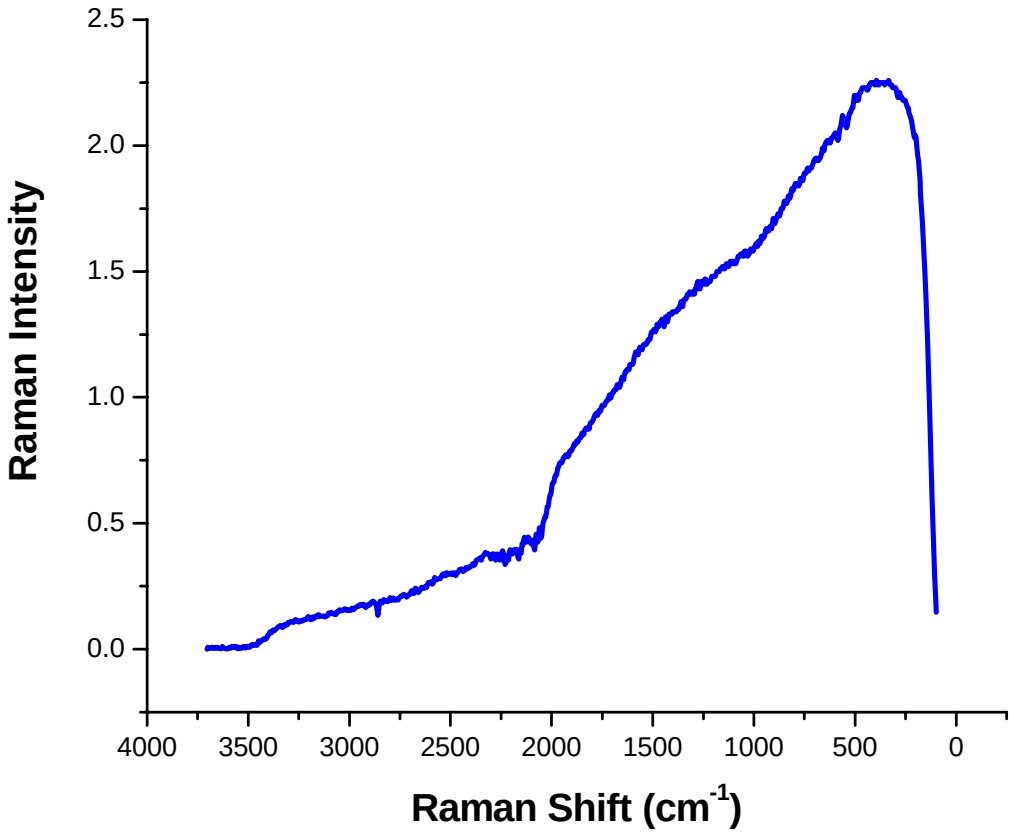

Figure 2.1 Raman spectrum of act. NA-Al_2O_3 Plus.

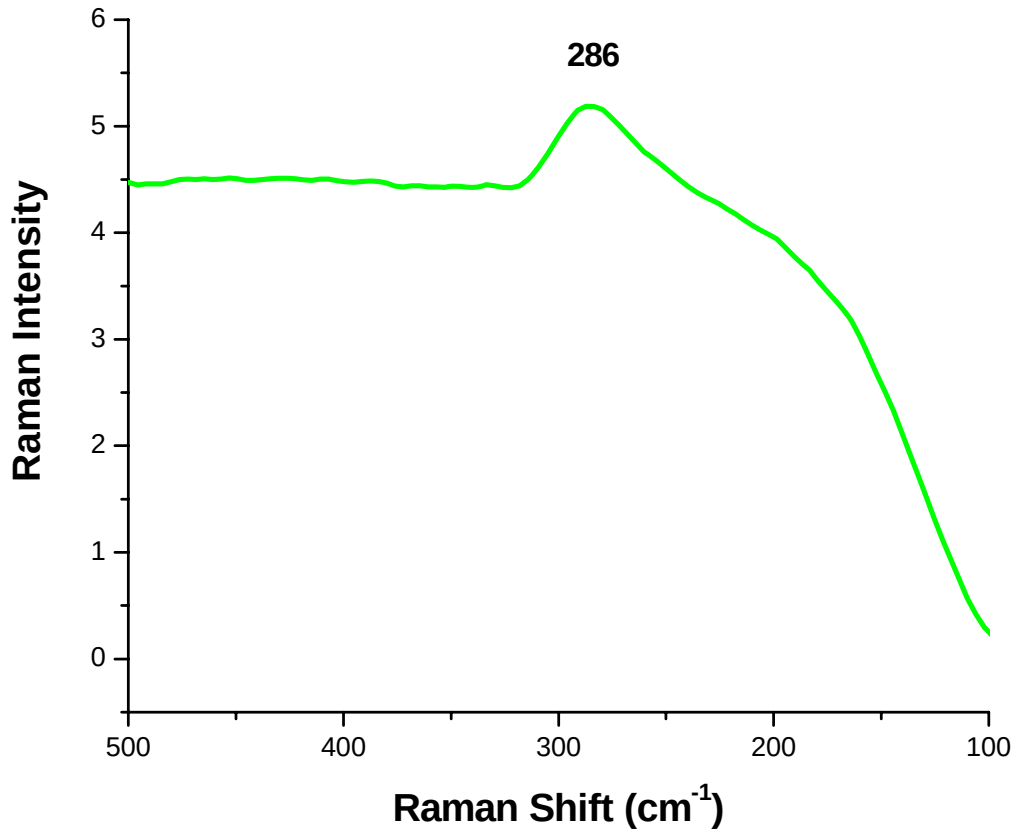

Figure 2.2 Raman spectrum of NA-Al_2O_3/Br_2 Plus.

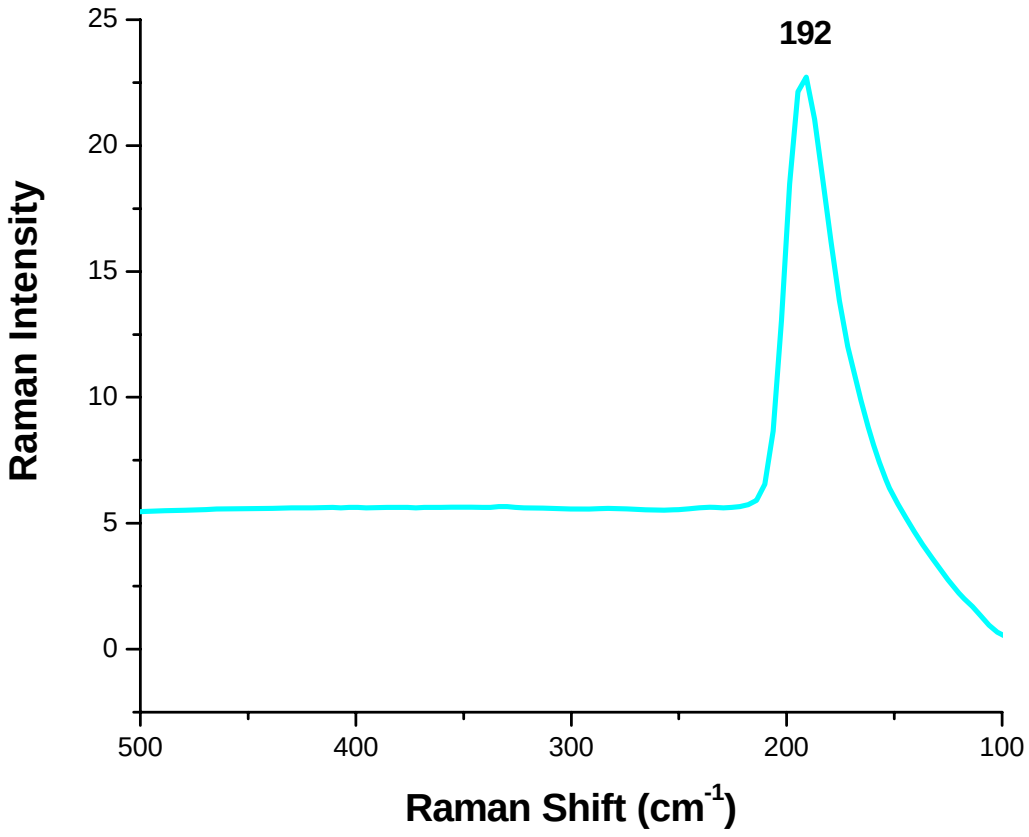

Figure 2.3 Raman spectrum of NA-Al_2O_3/I_2 Plus.

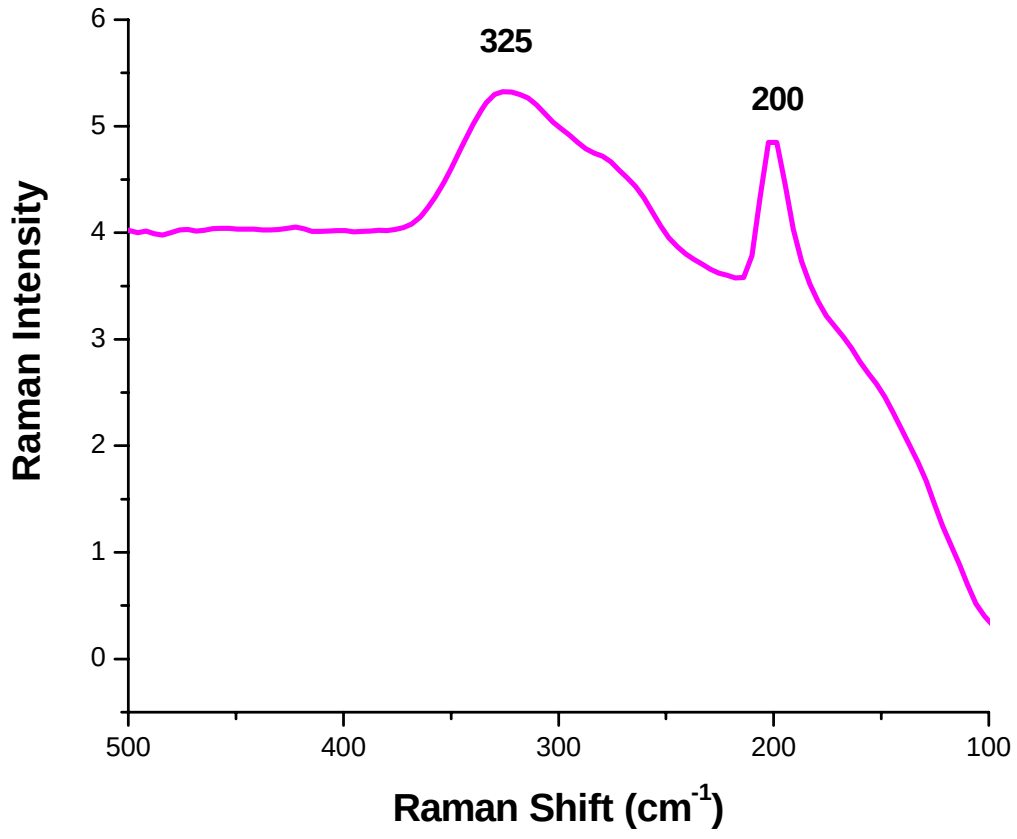

Figure 2.4 Raman spectrum of NA-Al_2O_3/ICl Plus.

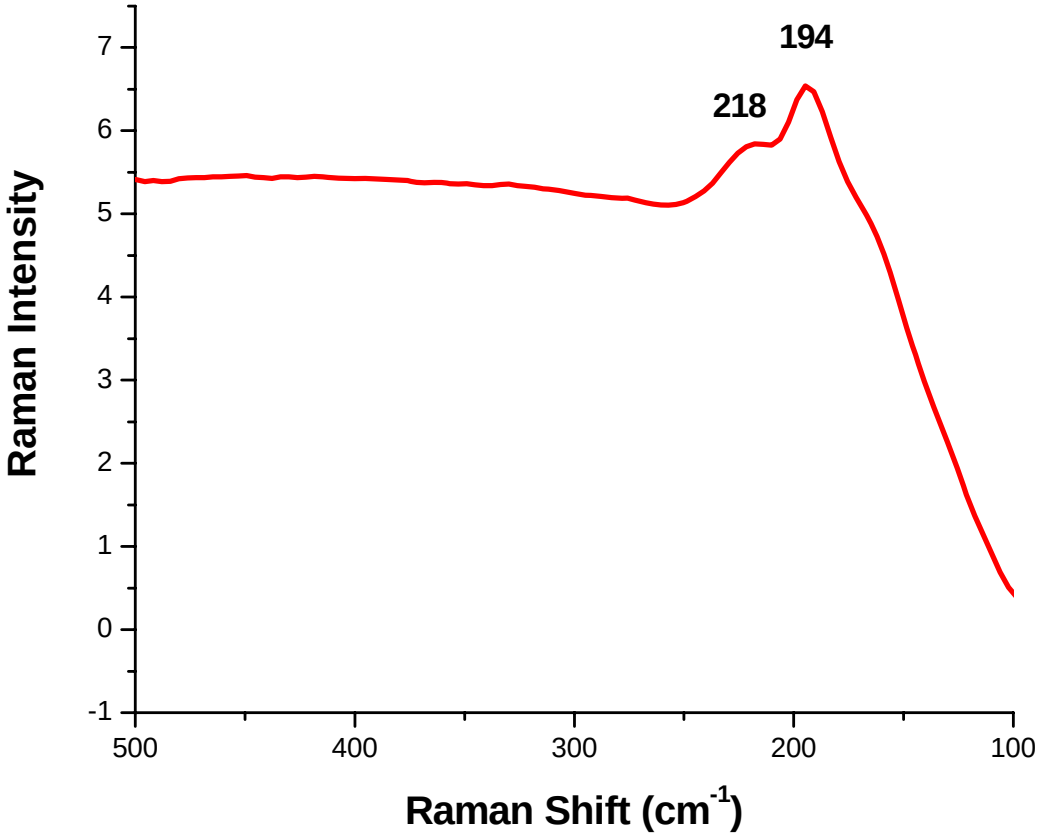

Figure 2.5 Raman spectrum of NA-Al_2O_3/IBr Plus.

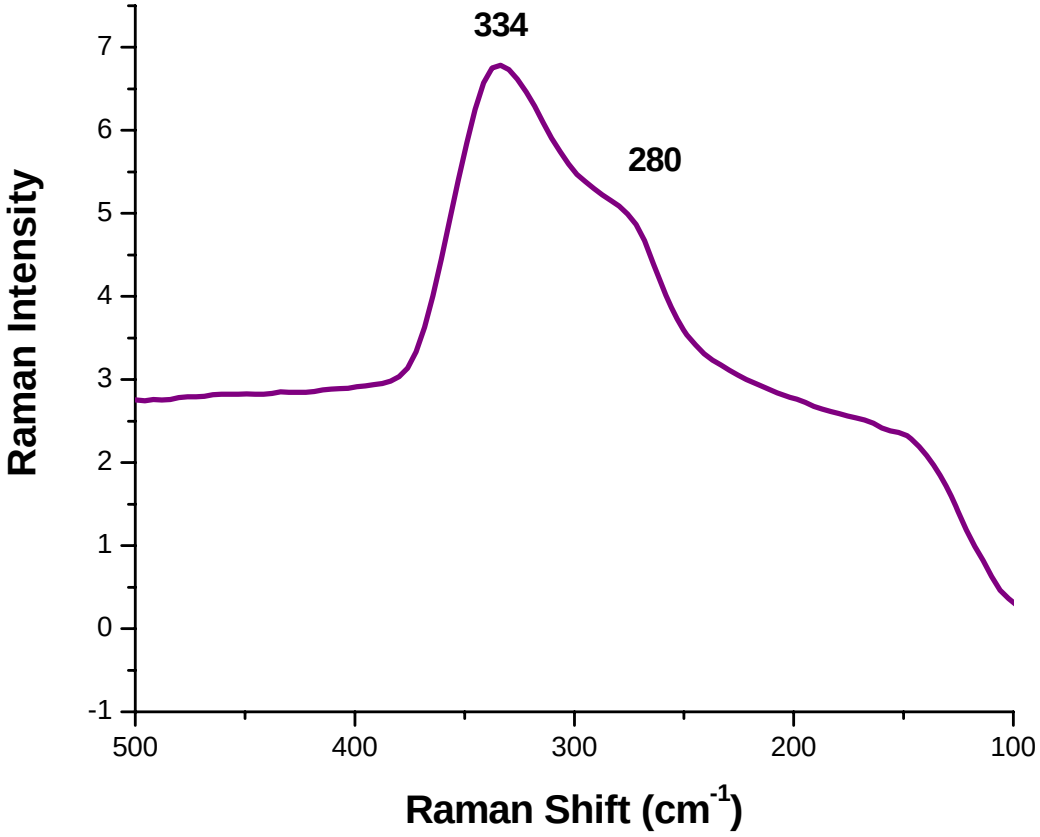

Figure 2.6 Raman spectrum of NA-Al_2O_3/ICl_3 Plus.

2.3.1.4 UV-Vis Spectra Analysis

The non-polar halogens and the polar interhalogen compounds investigated in this study all exhibit significant absorption in the UV-Visible light range. Many of them have been explored in the gas phase and in different solvents, both polar and non-polar.[53-61] During absorption of light, the halogen and interhalogen molecules undergo several electronic transitions from the ground state to one or more of the excited electronic states, which leads to a number of broad bands in the UV-Vis spectrum.[54,55,60] Several works in the literature have described theoretically and experimentally how different halogen and interhalogens, such as I_2, ICl and IBr, interact with various surfaces, for example with magnesium oxide, at different temperatures.[52,62-65] Very large molecule-surface energy transfer has been observed in the case of I_2 collision with the MgO surface.[64,65] Further, theoretical simulations indicate a change in orientation of the interhalogen molecule ICl at the surface, at temperatures ranging from below 150 K and above 350 K.[63] In addition, Jiang et al.[62] have developed a model for computing the absorption spectrum of diatomic molecules adsorbed on a nonzero temperature surface in hope that it will yield valuable information about molecule-surface interactions. Several works indicate that the electronic structure of the molecule and hence their absorption spectra, can be changed significantly upon adsorption.[52,62,63]

A photograph of the prepared adducts can be seen in Figure 2.7. NA-Al_2O_3 Plus is a white powder with essentially no absorbance in the 200-800 nm range. Similarly, NA-Al_2O_3/Cl_2 Plus is a nearly white powder with a diffuse reflectance spectrum coinciding with that of NA-Al_2O_3 Plus. However, this is not the case with NA-Al_2O_3/Br_2 Plus, which has a yellow color and shows significant absorption with a peak position at 275 nm and a shoulder at 390 nm (Figure

2.8). These values can be compared with Br_2 dissolved in CCl_4 with peak positions at 255 nm and 440 nm. Iodine dissolved in CCl_4 has two distinct peaks at 260 and 516 nm, whereas NA-Al_2O_3/I_2 Plus has a broader absorption spectrum with peak positions at 294 and 373 nm (Figure 2.9). Similarly, ICl in CCl_4 has two intense peaks at 250 and 460 nm while NA-Al_2O_3/ICl Plus has a wider band with peak positions at 229 and 475 nm and a shoulder at approximately 345 nm (Figure 2.10). The diffuse reflectance spectra of NA-Al_2O_3/IBr and NA-Al_2O_3/ICl_3 Plus are both less distinct than their corresponding halogens dissolved in CCl_4, with a peak position at 306 nm and a broad shoulder around 500 nm for IBr, and 238 and 345 nm for ICl_3. (Figure 2.11 and 2.12).

Figure 2.7 Photograph of NA-Al_2O_3 Plus Adducts.

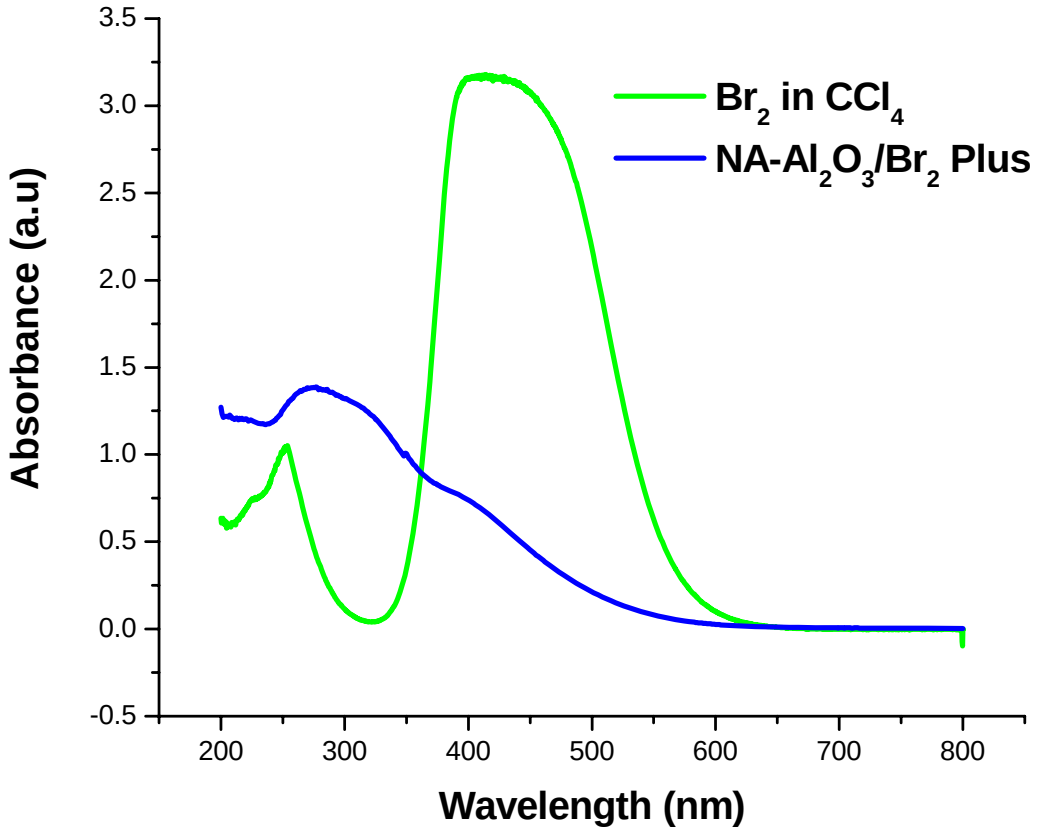

Figure 2.8 UV-Vis spectrum of bromine in CCl_4 and Diffuse reflectance spectrum of NA-Al_2O_3/Br_2 Plus.

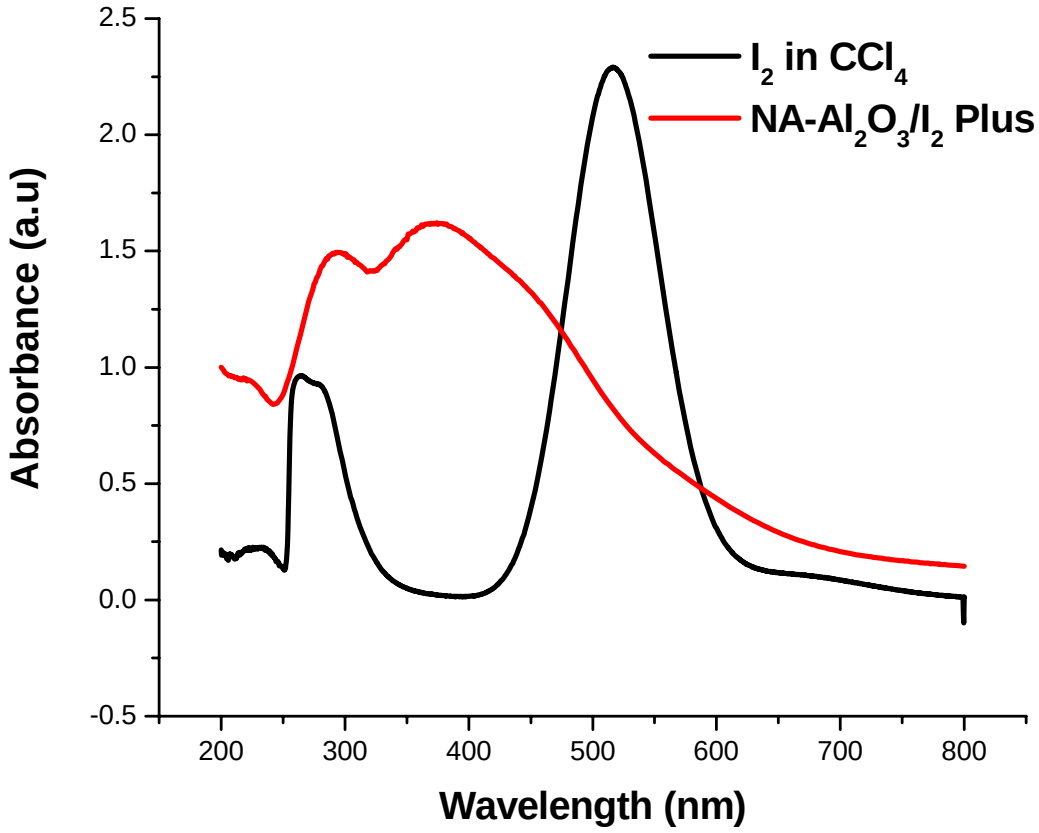

Figure 2.9 UV-Vis spectrum of iodine in CCl_4 and Diffuse reflectance spectrum of NA-Al_2O_3/I_2 Plus.

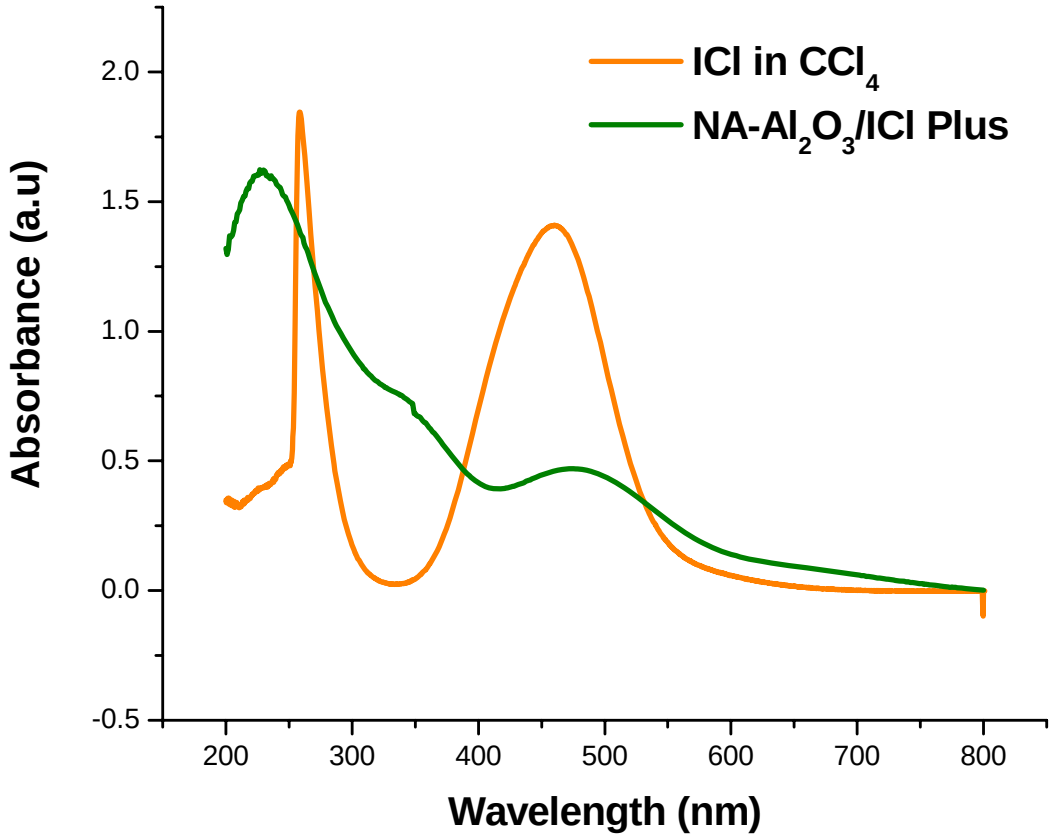

Figure 2.10 UV-Vis spectrum of iodine monochloride in CCl_4 and Diffuse reflectance spectrum of NA-Al_2O_3/ICl Plus.

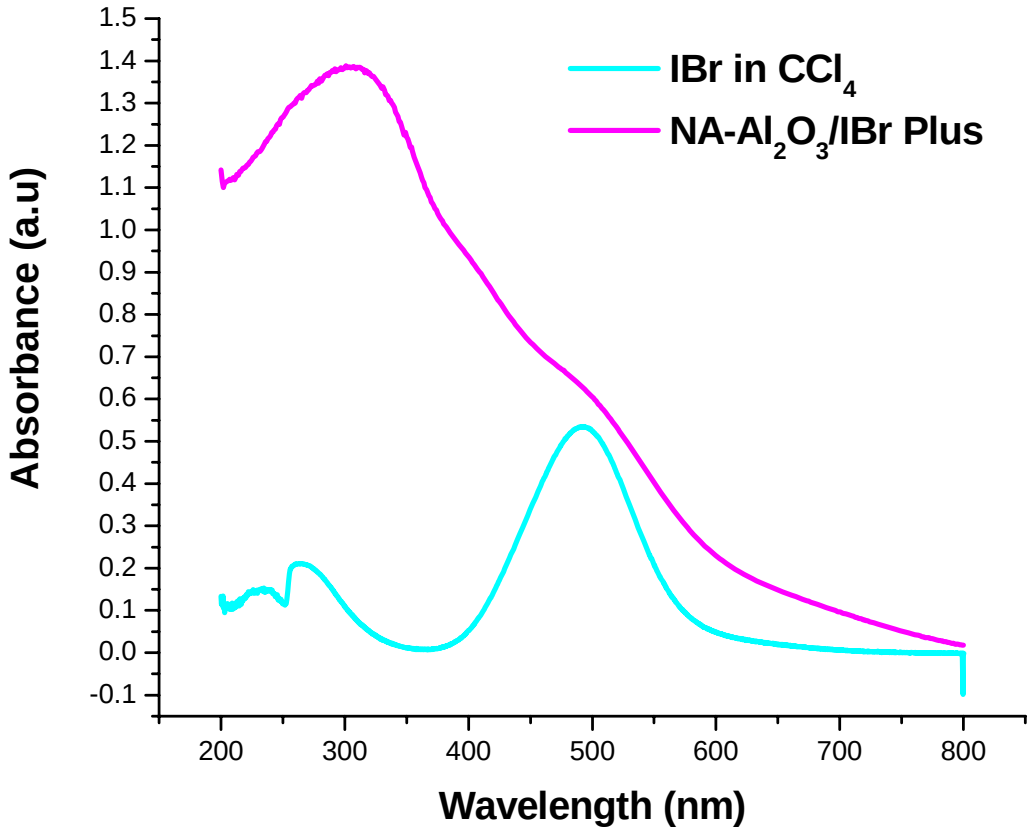

Figure 2.11 UV-Vis spectrum of iodine monobromide in CCl_4 and Diffuse reflectance spectrum of NA-Al_2O_3/IBr Plus.

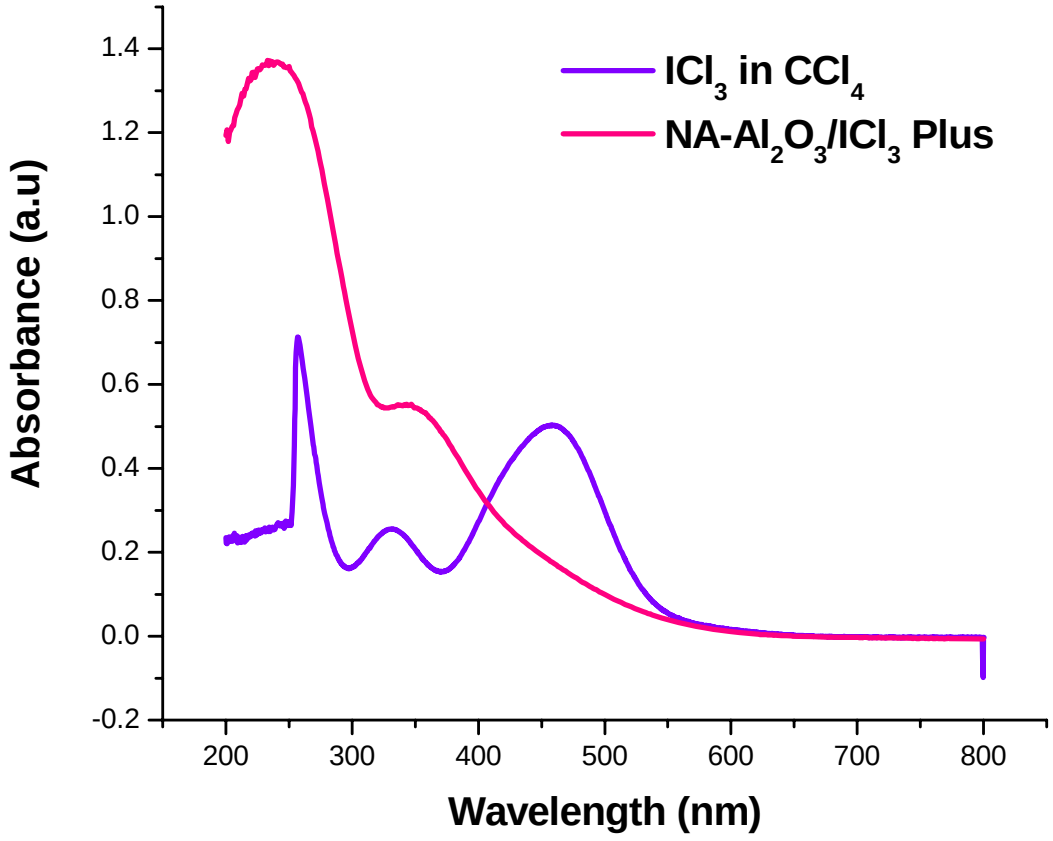

Figure 2.12 UV-Vis spectrum of iodine trichloride in CCl_4 and Diffuse reflectance spectrum of NA-Al_2O_3/ICl_3 Plus.

2.3.1.5 Transmission Electron Microscopy (TEM)

Transmission electron microscopy (TEM) is a very useful tool to characterize nanostructured materials as it is possible to see details even on the nanoscale. Nanoparticles consist of small nanocrystals that tend to aggregate together, forming larger aggregates. The structure of the nanocrystals varies. Some of them consist of small cubes or spheres, whereas others have a more fibrous structure, all of which are possible to identify using TEM. High Resolution TEM (HRTEM) can give further information about the way the atoms are arranged since it is possible to see the rows of atoms. This is sometimes possible using TEM at high magnification, but very unusual and somewhat difficult.

TEM images of NA-Al_2O_3 Plus, as received when purchased can be seen in Figure 2.13-2.14. It can be seen that NA-Al_2O_3 Plus possesses a very fibrous structure. To find out if the structure of the material changes after heat-treatment, several images were recorded of the sample after the activation step (400°C, ramp 2 hrs, soak 4 hrs). The images can be seen in Figure 2.15 and 2.16. It can be observed that the structure of the sample is nearly identical to the metal oxide before the heat-treatment step, very fibrous. Further images were recorded of the halogenated samples and two examples are seen in Figure 2.17 and 2.18 of NA-Al_2O_3/IBr Plus. No morphological change in the structure has been observed.

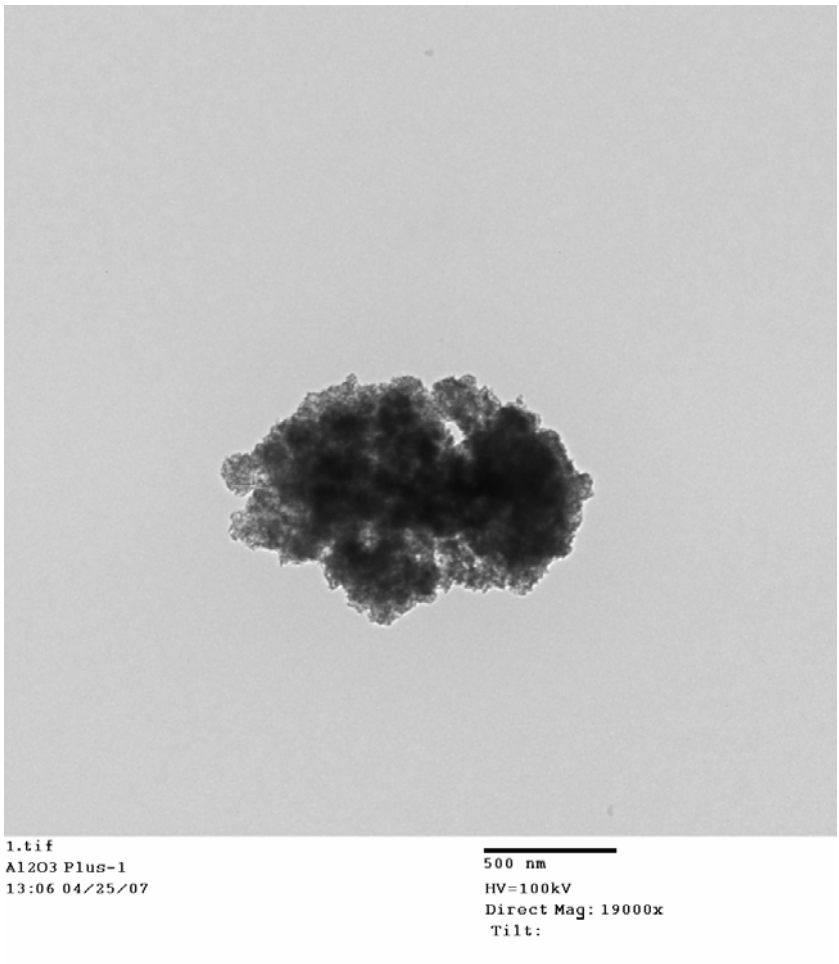

Figure 2.13 TEM image of NA-Al_2O_3 Plus (1).

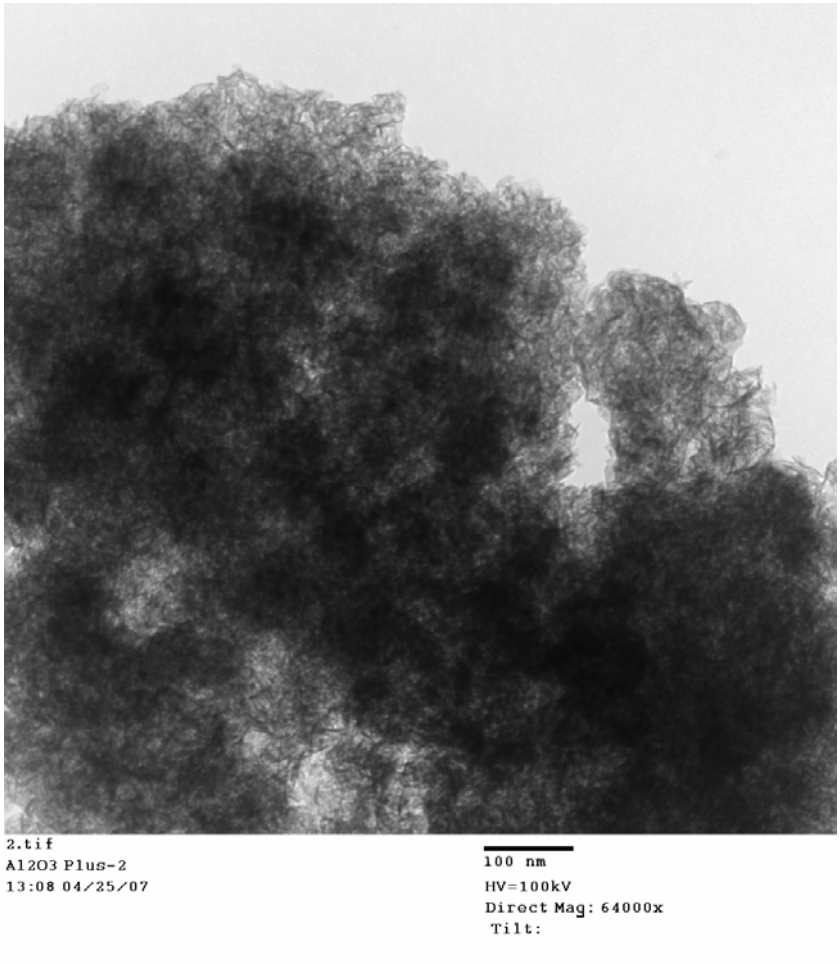

Figure 2.14 TEM image of NA-Al_2O_3 Plus (2).

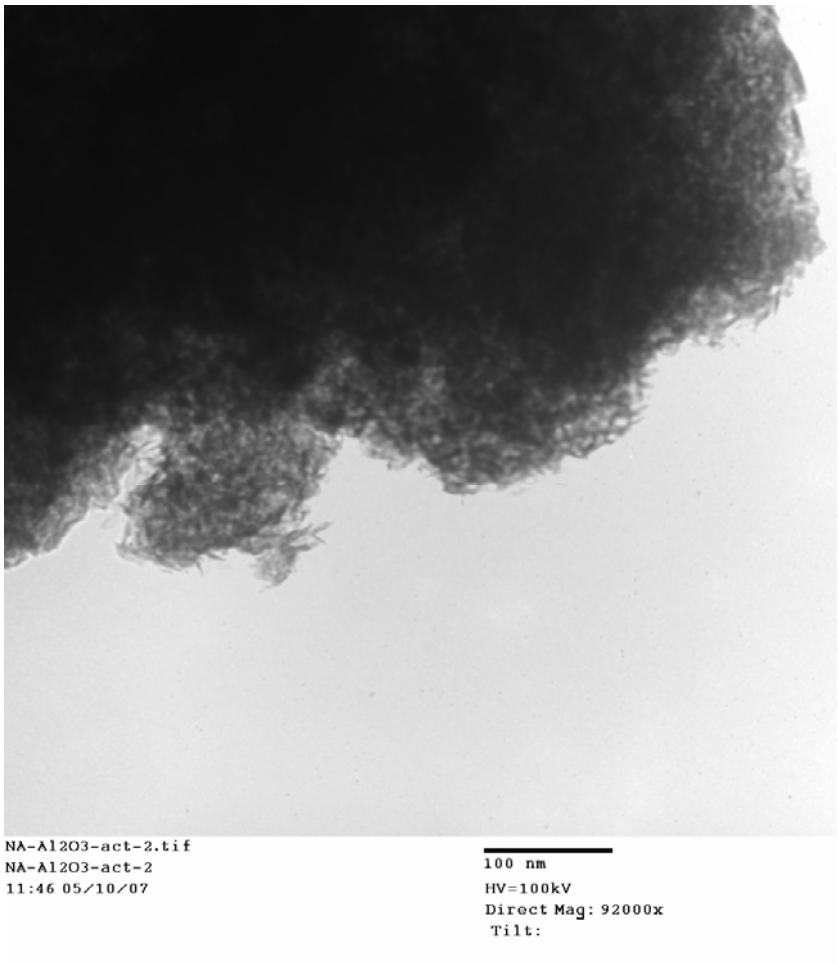

Figure 2.15 TEM image of NA-Al_2O_3 Plus (act.) (1).

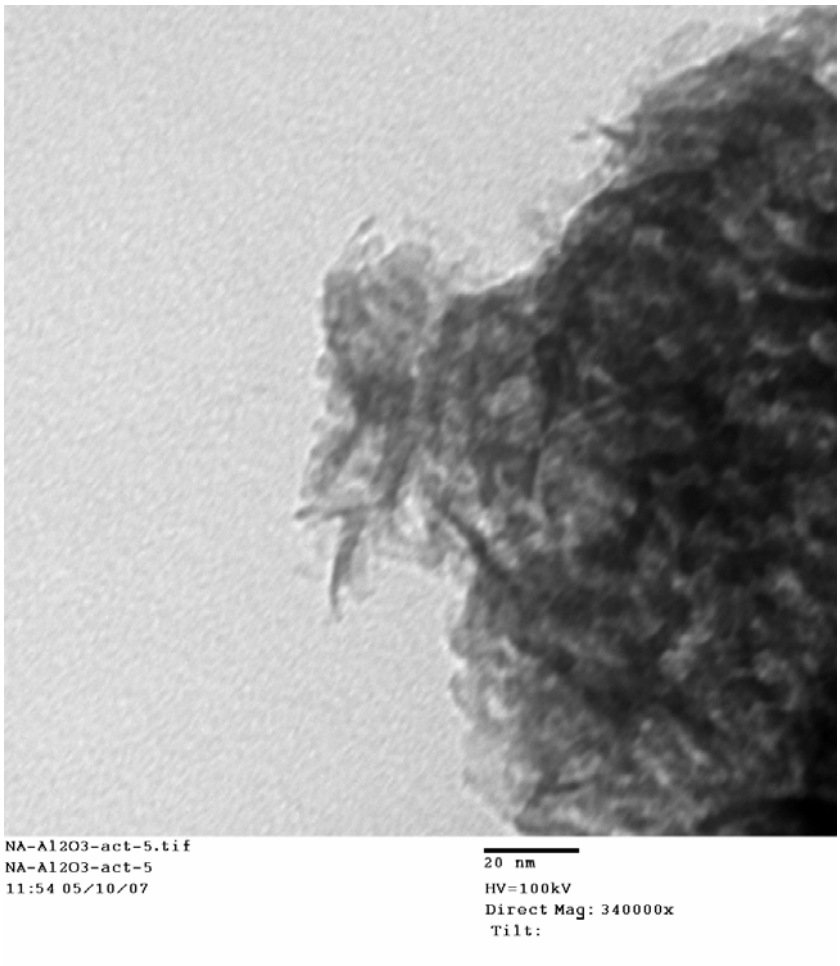

Figure 2.16 TEM image of NA-Al_2O_3 Plus (act.) (2).

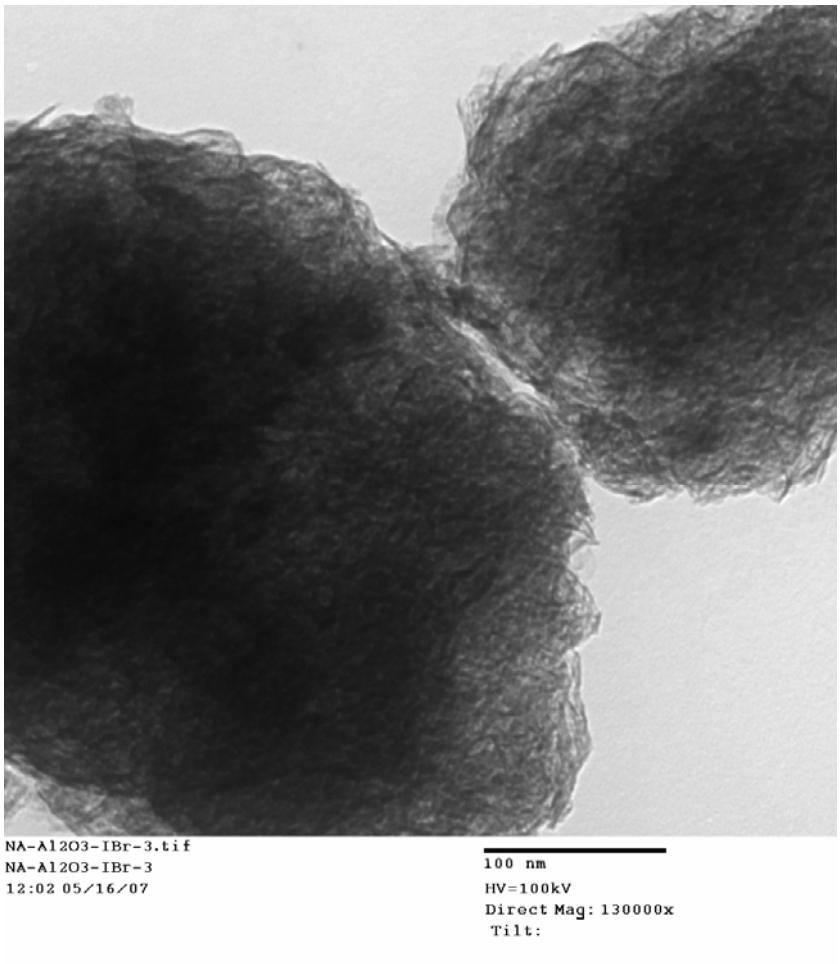

Figure 2.17 TEM image of NA-Al_2O_3/IBr Plus (1).

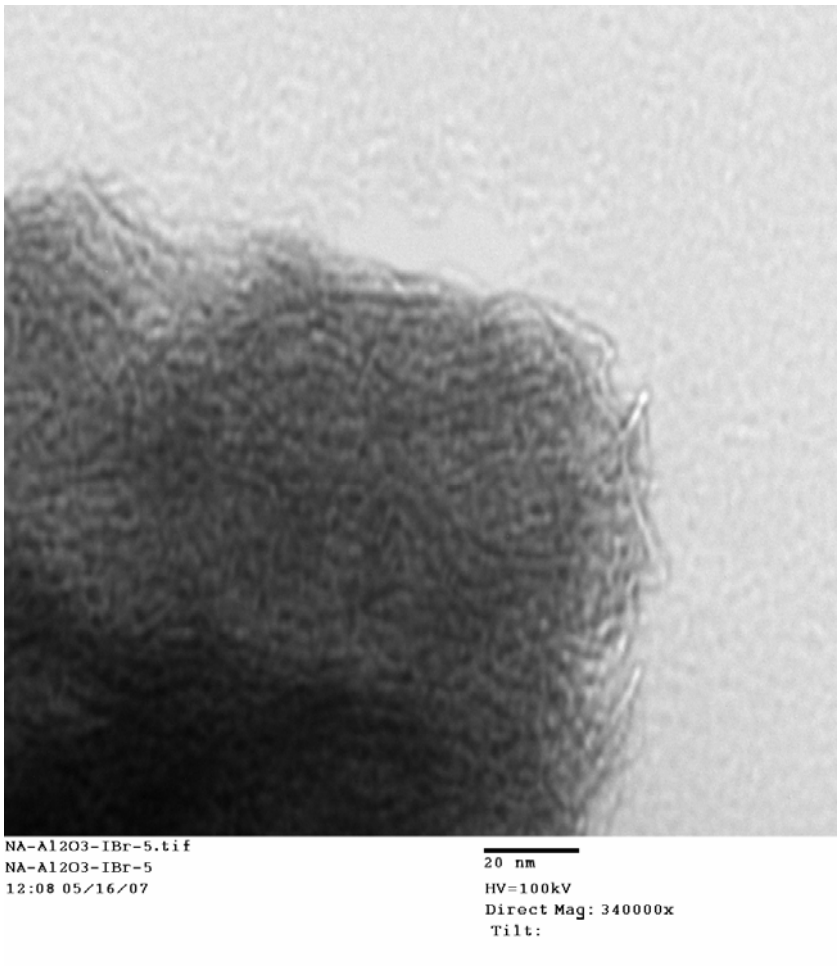

Figure 2.18 TEM image of NA-Al_2O_3/IBr Plus(2).

2.3.1.6 X-Ray Photoelectron Spectroscopy (XPS)

The XPS analysis was conducted to confirm the presence of halogen on the surface of the materials and their chemical state. Halogens/interhalogens were observed in all cases except the NA-Al_2O_3/Cl_2 Plus adduct, when the observed spectrum was identical to that of pure NA-Al_2O_3 Plus (data not shown). However, this observation is attributed to the volatility induced by the local heating by the intensive X-ray beam. This hypothesis is supported by the fact that a similar effect was induced with the bromine adduct when long acquisition time was used. Thus, relatively short acquisition times were used for all samples to avoid X-ray induced desorption and decomposition of the fairly unstable halogen and interhalogen compounds. The bromine and iodine samples have peak locations as expected for free elements (Figure 2.19-1 and 2.19-3), each one displaying one set of two peaks. Peaks confirming salt formation such as $AlCl_3$, $AlBr_3$ or AlI_3, were not observed for any of the adducts. For all interhalogens two sets of peaks were observed in the iodine region: one of the sets has higher binding energy, corresponding to the adsorbed interhalogen iodine (ICl, IBr and ICl_3), while the lower binding energy set of peaks coincide with that of the free adsorbed iodine, I_2 on the metal oxide surface, which is due to partial decomposition of the interhalogen or presence of I_2 in the interhalogen at the time of adsorption (Figure 2.19-2 and 2.19-5). In the case of NA-Al_2O_3/IBr Plus, a set of peaks corresponding to adsorbed Br_2 was also observed (Figure 2.19-4), again possibly caused by partial decomposition of the interhalogen into I_2 and Br_2 or presence of I_2 and Br_2 in the interhalogen. These results are supported by the literature,[52] where it has been reported that IBr adsorbed on MgO decomposes forming I_2 and Br_2. In addition, Nagasao and co-workers reported decomposition of ICl adsorbed on silica into I_2 and release of the lighter halogen, Cl_2, from the

surface.[17] This finding also helps explain why we did not observe any peak corresponding to Cl_2 in either the ICl or ICl_3 adduct, since the light Cl_2 has apparently been released from the surface. The origin of the free halogen, I_2, is probably caused by several processes: it was formed due to partial spontaneous decomposition of the interhalogen upon adsorption or under the influence of the X-ray radiation, leading to a larger fraction of free I_2 on the surface, or both. It is also known that solid interhalogens such as ICl and IBr contain ICl (or IBr), I_2 and Cl_2 (or Br_2) in its vapor, which means that all three species could have been directly adsorbed onto the surface. Since XPS is a technique which analyzes only the top several nanometers of the sample and can change the sample due to the measurement, these data are not to be considered representative for the quantitative content of the halogens and their state in the samples. Thus the interhalogen vs. halogen content was not analyzed and reported.

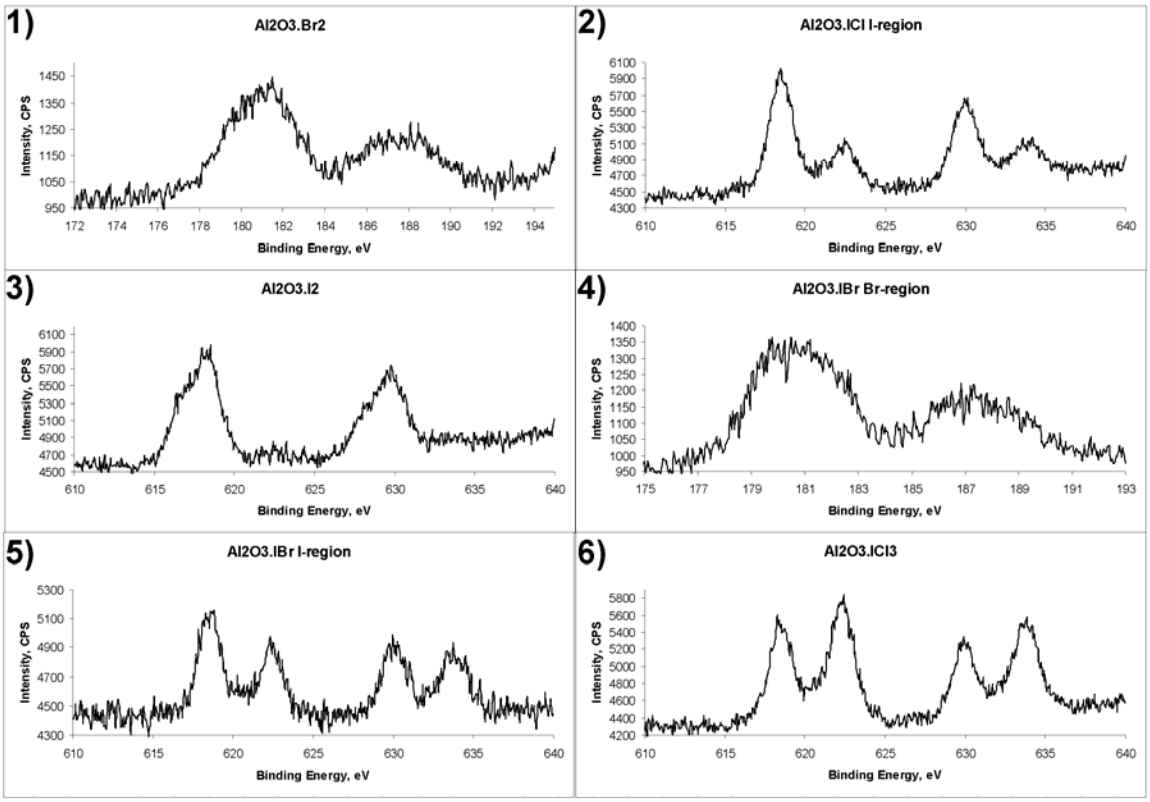

Figure 2.19 XPS spectra of NA-Al_2O_3 Plus halogen and interhalogen adsorbates. 1) $Al_2O_3.Br_2$ ($3p^{3/2}$ and $3p^{1/2}$); 2) $Al_2O_3.ICl$ (iodine region, $3d^{5/2}$ and $3d^{3/2}$); 3) $Al_2O_3.I_2$ ($3d^{5/2}$ and $3d^{3/2}$); 4) $Al_2O_3.IBr$ (Br-region, $3p^{3/2}$ and $3p^{1/2}$); 5) $Al_2O_3.IBr$ (iodine region, $3d^{5/2}$ and $3d^{3/2}$); 6) $Al_2O_3.ICl_3$ (iodine region, $3d^{5/2}$ and $3d^{3/2}$).

2.3.2 NA-TiO_2 and its Adducts

2.3.2.1 Specific Surface Area

The BET method was used to find the specific surface area of NA-TiO_2, before and after the activation step.

Initially, the metal oxide has a specific surface area of ~500 m^2/g. During an increase of the temperature from room temperature up to 400 °C over a period of two hours and then keeping this temperature for another four hours (six hours total) the surface area decreases significantly to about 100 m^2/g. Initially, higher temperatures during heat-treatment were conducted; however, the surface area then decreased to much less than 100 m^2/g so the temperature was decreased. To preserve the high surface area, a lower activation temperature than 400 °C was also tried, but it was not successful. TGA data showed that there were many surface species remaining so the material would not be suitable for adsorption of halogen/interhalogen.

2.3.2.2 Thermogravimetric Analysis (TGA)

The samples were heated at a rate of either 5 or 10 °C per minute up to 600 °C in a helium atmosphere. The first derivative is a tool that can be useful to determine the temperature at which maximum weight loss occurs.

The halogen/interhalogen content, based on thermogravimetric data can be seen in Table 2.2, as well as the calculated surface concentrations for the prepared adducts.

Table 2.2 Halogen/Interhalogen content as determined by TGA and the calculated Surface Concentration.

Material	Halogen Content wt % (TGA)	Surface Concn molecules/nm^2
NA-TiO_2/Cl_2	3	2.6
NA-TiO_2/Br_2	5	2.0
NA-TiO_2/I_2	13	3.6
NA-TiO_2/ICl	19	8.7
NA-TiO_2/IBr	15	5.1
NA-TiO_2/ICl_3	12	3.5

Table 2.2 shows the wt % adsorbed halogen for the NA-TiO_2 adducts and values as high as 19 percent by weight were obtained. The weight percent adsorbed halogen on the surface is in general lower for the NA-TiO_2 adducts than for those of NA-Al_2O_3 Plus. This can be explained in part by the significantly lower surface area of NA-TiO_2 compared to that of NA-Al_2O_3 Plus. The lower molecular weight of TiO_2 (79.9 g/mol) compared to Al_2O_3 (102.0 g/mol), as well as the lower wt % of halogen adsorbed on the metal oxide surface concludes that NA-TiO_2 is not as good of an adsorbant as compared to NA-Al_2O_3 Plus. It was also observed that the NA-TiO_2 halogen adducts were not stable for as long as those of NA-Al_2O_3 Plus. Thermogravimetric analysis (not shown) indicates that the iodinated adduct undergoes significant weight loss at higher temperatures than do the other adducts, coinciding well with its observed higher stability that the other adducts. Thermogravimetric analysis data for the iodinated adducts of NA-Al_2O_3 Plus and NA-TiO_2 are very similar, both with maximum weight loss at high temperature.

The calculated surface concentration of the adducts is in the range 2.0 to 8.7 molecules/nm^2 which is significantly higher than those obtained from the NA-Al_2O_3 Plus adducts. This can be explained by the much lower surface area of the TiO_2.

As with the NA-Al_2O_3 Plus adducts, these adducts did not release any noticeable heat upon adsorption, which indicates that they may not be as stable as the previously reported adducts of nanosized MgO.[8]

2.3.2.3 Raman Spectroscopy

The Raman spectrum of activated NA-TiO_2 clearly indicates that the metal oxide is in the anatase phase, as supported by the literature,[66-68] with peaks at 640.9, 517.3, 398.2 and 146.1 cm^{-1} (Figure 2.20). The chlorinated adduct shows no additional chlorine peak, as was the case for NA-Al_2O_3/Cl_2 Plus.

However, the brominated adduct shows a peak in the Raman spectrum at 307 cm^{-1}, which gives a small downshift of 7 cm^{-1}, compared to bromine itself at 313.9 cm^{-1} [24] (Figure 2.21). Again, there is no spectral evidence indicating formation of Br_3^-, which has a frequency value between 160-170 cm^{-1},[35,37,41-44] or of Br_5^-, with a Raman band of 250 cm^{-1}.[45] The frequency values for BrO^-, BrO_2^-, BrO_3^- and BrO_4^- [43,45-47] are all above 400 cm^{-1} and much higher than those observed in the Raman spectrum of NA-TiO_2/Br_2. The liquid and vapor-phase Raman spectra of titanium tetrabromide have been reported by Clark et al.[69] The strongest frequency band appears at 231.5 cm^{-1} (vapor-phase) or 229.5 cm^{-1} (liquid phase), neither of which appear present in the Raman spectrum of NA-TiO_2/Br_2, reported here.

In addition, the iodinated adduct of NA-TiO_2 has a small downshift of 17 cm^{-1} with NA-TiO_2/I_2 displaying a Raman peak at 196 cm^{-1}, compared to 213 cm^{-1} for I_2 itself (Figure 2.22).[22,24,29] I_3^- has a Raman band of 110-120 cm^{-1}, as reported in the literature,[22,41,42,49] whereas Kiefer et al.[49] reported the Raman band for I_5^- at 160 cm^{-1}, neither of which appear to be present

in our iodinated adduct. Oxygen containing species, such as IO_3^-, IO_4^- and IO_6^-,[45,46] all have Raman bands much higher than the observed frequency value. Several works in the literature have reported the Raman spectrum of titanium tetraiodide.[69-71] Its spectrum has been obtained as a solid[70] or from TiI_4 dissolved in cyclohexane[69-71] with the most intense peak appearing around 160-162 cm^{-1}. We therefore exclude the formation of this specie as well.

NA-TiO_2/ICl has two peaks, one at 340 and one at 196 cm^{-1} (Figure 2.23), similar to the NA-Al_2O_3/ICl Plus adducts. We explain the peak at 196 cm^{-1} to I_2 adsorbed on the surface and this can be explained by partial decomposition of the ICl into I_2 and Cl_2 upon adsorption.[17] Cl_2, however, is a light halogen and appears to have been released from the surface. ICl itself has a Raman band of 381.5 cm^{-1},[22,24,31,32] which would mean a downshift of 41.5 cm^{-1} for the peak at 340 cm^{-1}. Reported Raman values of ICl_2^- [22,35,44,50] and ICl_4^- [51] do not coincide with our obtained bands and do not seem likely to have been formed.

The IBr adduct also displays two peaks, one at 241 and one at 199 cm^{-1} (Figure 2.24). Compared to IBr in the gas phase at 267 cm^{-1} [29] this is a downshift of 26 cm^{-1} for the observed 241 cm^{-1} value. The second peak at 199 cm^{-1} can be explained by partial decomposition of IBr into I_2 and Br_2, leaving the heavier halogen behind and leading to a peak in the Raman spectrum for the adsorbed I_2, in addition to the adsorbed IBr.[52]

NA-TiO_2/ICl_3 displays one peak at 342 cm^{-1}, almost completely coinciding with the most intense peak of ICl_3 itself at 343.2 cm^{-1} (Figure 2.25). It is possible that the three less intense peaks of ICl_3 (198.6, 142.6 and 117.6 cm^{-1}) are hidden by the metal oxide background moiety, including the very intense anatase peak at 146.1 cm^{-1} and the shoulder at slightly higher wavenumber. The very small downshift of 1.2 cm^{-1} most likely means that the halogen is retained in the pore structure or adsorbed on the surface very weakly. It does not seem likely that

either $TiCl_4$ or TiI_4 has formed; their Raman bands have been reported in the literature as 389 cm^{-1} and 162 cm^{-1}, respectively.[70]

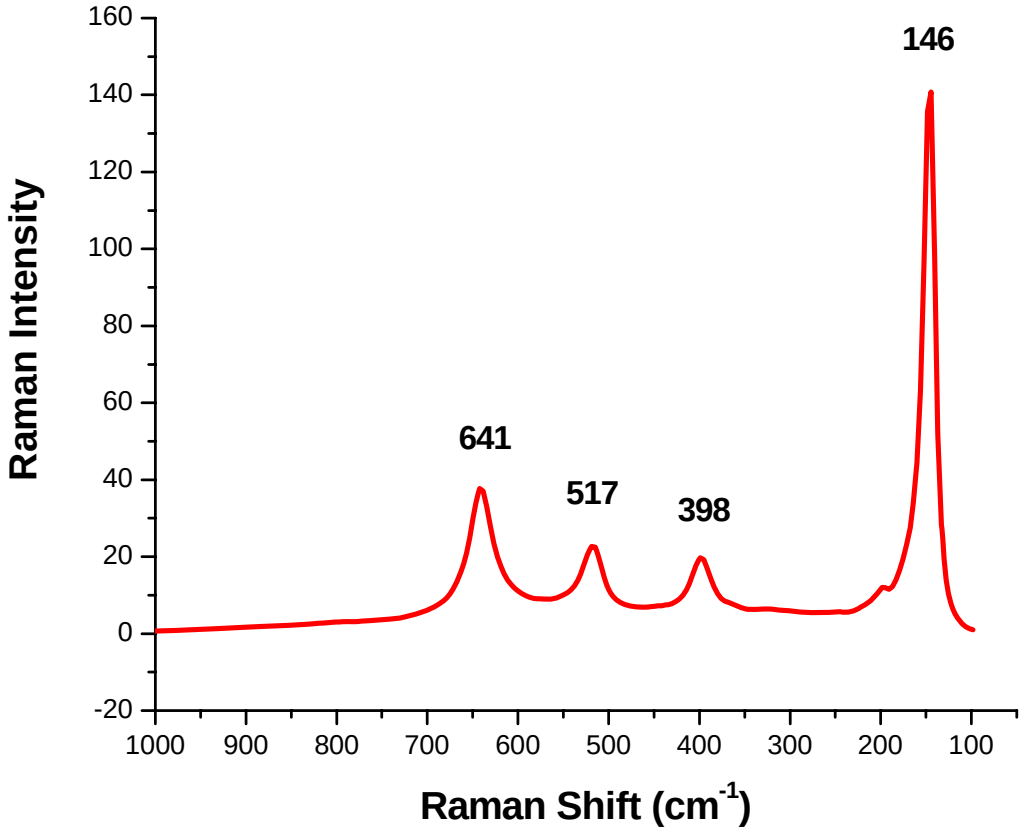

Figure 2.20 Raman spectrum of NA-TiO_2.

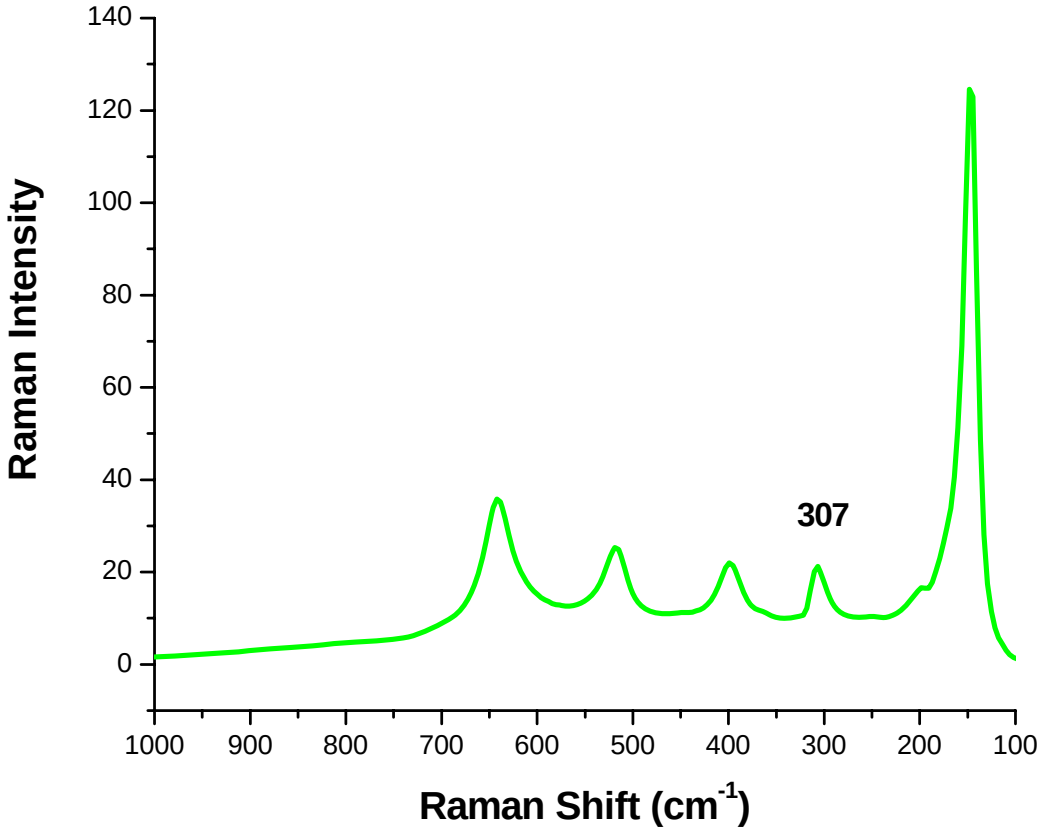

Figure 2.21 Raman spectrum of NA-TiO_2/Br_2.

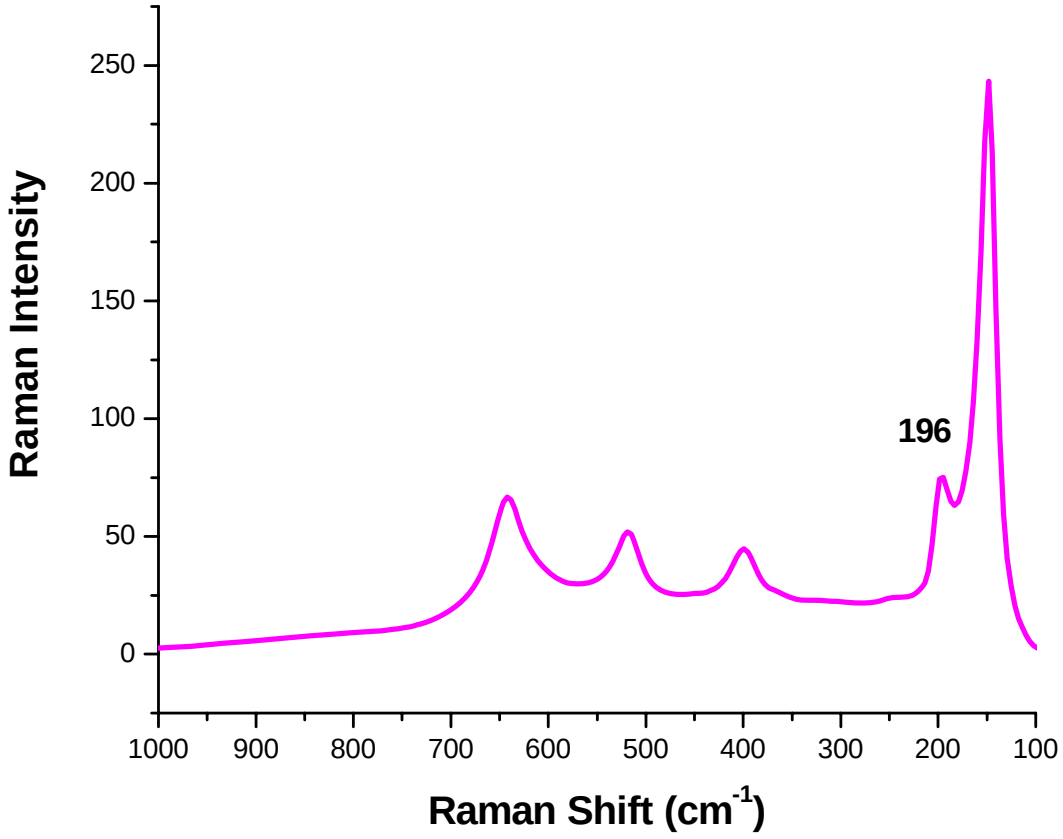

Figure 2.22 Raman spectrum of NA-TiO_2/I_2.

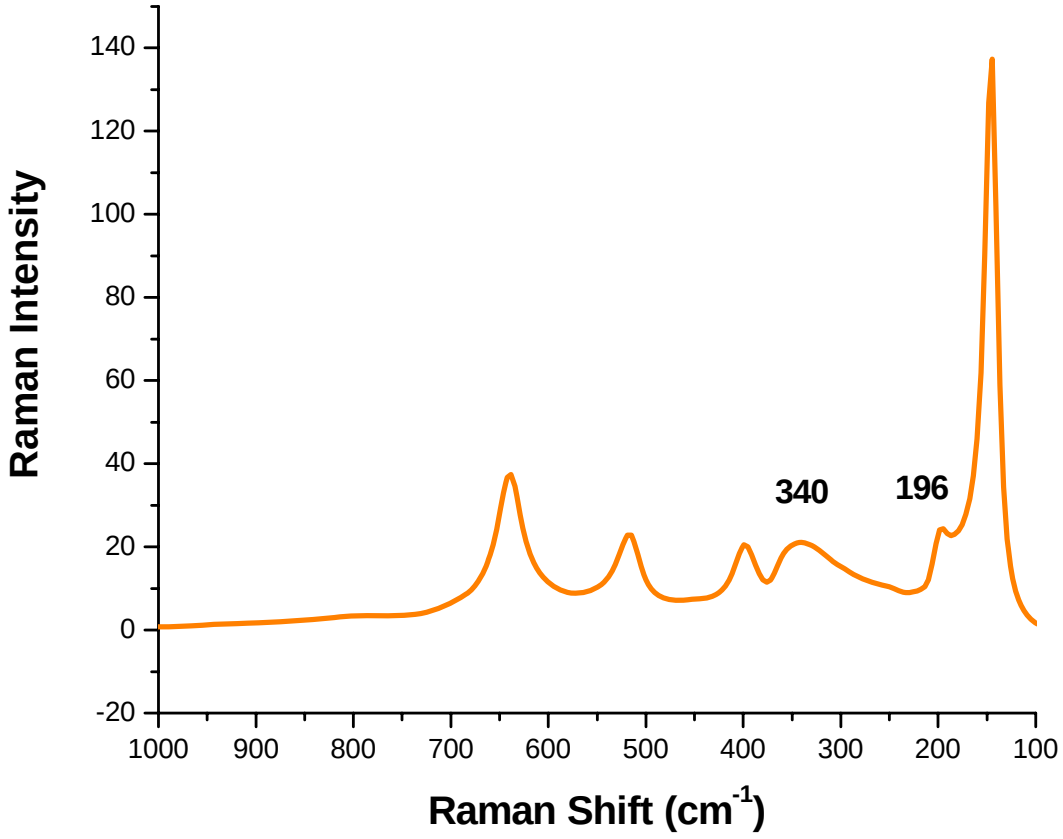

Figure 2.23 Raman spectrum of NA-TiO_2/ICl.

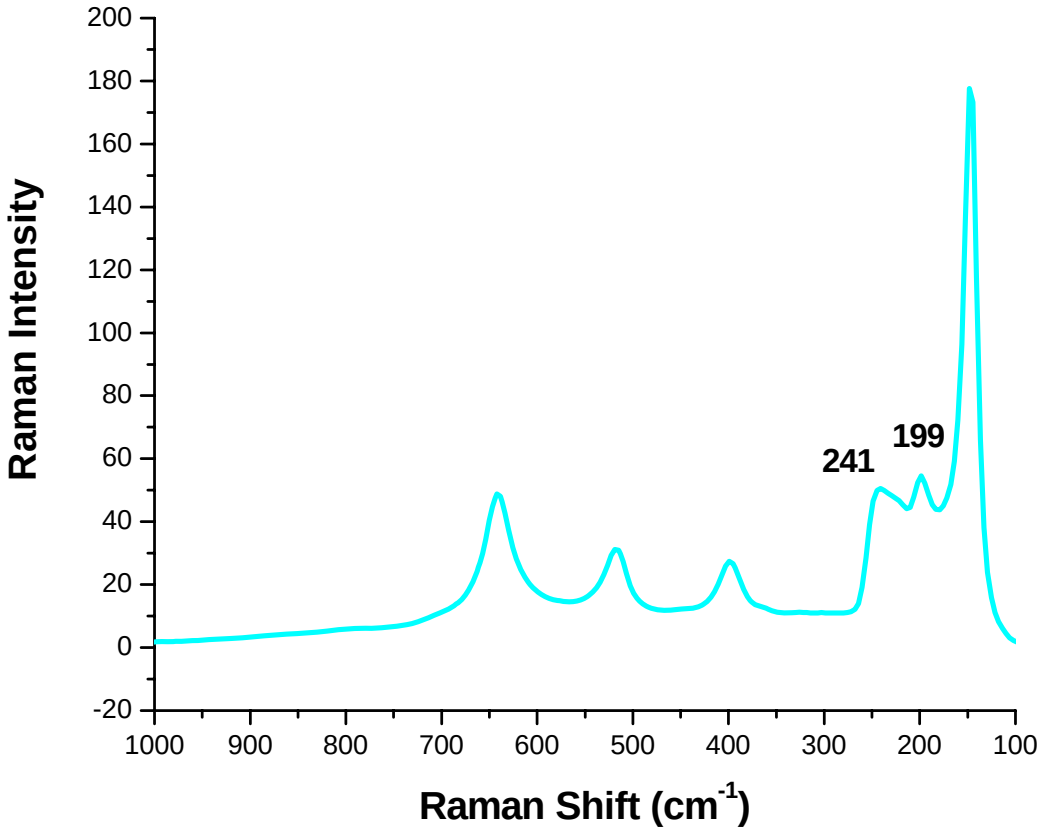

Figure 2.24 Raman spectrum of NA-TiO_2/IBr.

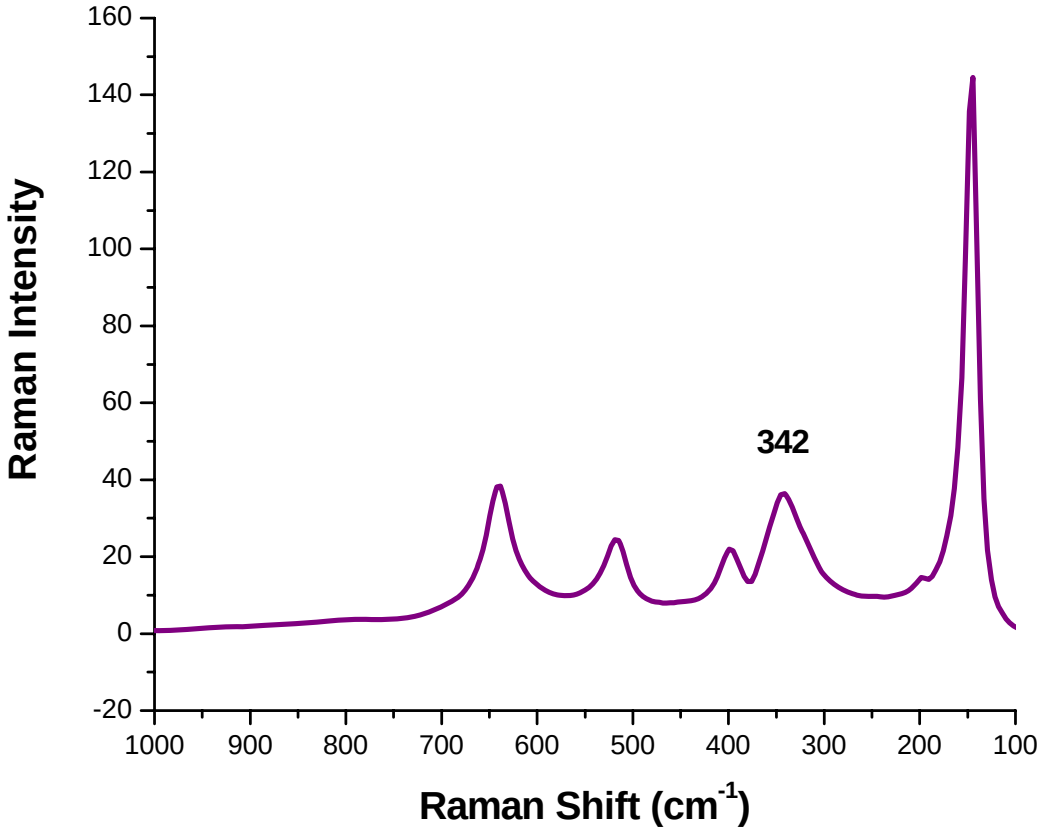

Figure 2.25 Raman spectrum of NA-TiO_2/ICl_3.

2.3.2.4 UV-Vis Spectra Analysis

A photograph of the prepared adducts can be seen in Figure 2.26. NA-TiO_2 is a white powder with absorbance in the 200-400 nm range, but no absorbance in the 400-800 nm range. Similarly, NA-TiO_2/Cl_2 is a nearly white powder with a diffuse reflectance spectrum coinciding well with that of NA-TiO_2. Further, in the case of NA-TiO_2/Br_2, a yellow colored powder, the absorbance spectrum shows a shoulder around 340 nm (Figure 2.27). Br_2 in CCl_4 has two peaks at 255 nm and 440 nm. Iodine dissolved in CCl_4 has two distinct peaks at 260 and 516 nm, whereas NA-TiO_2/I_2 has a broader absorption spectrum with a peak position at 500 nm (Figure 2.28). Similarly, ICl in CCl_4 has two sharp peaks at 270 and 465 nm while NA-TiO_2/ICl has a wider band with peak positions at 330 and 470 nm (Figure 2.29). The diffuse reflectance spectrum of NA-TiO_2/IBr is broad with a decreasing intensity with increasing wavelength. Its shoulder at 500 nm coincides well with the peak of IBr itself (Figure 2.30). The diffuse reflectance spectrum of NA-TiO_2/ICl_3 is similar in appearance to that of NA-TiO_2/IBr, but with a slightly weaker absorbance in the range 400-800 nm (Figure 2.31).

Figure 2.26 Photograph of NA-TiO_2 Adducts.

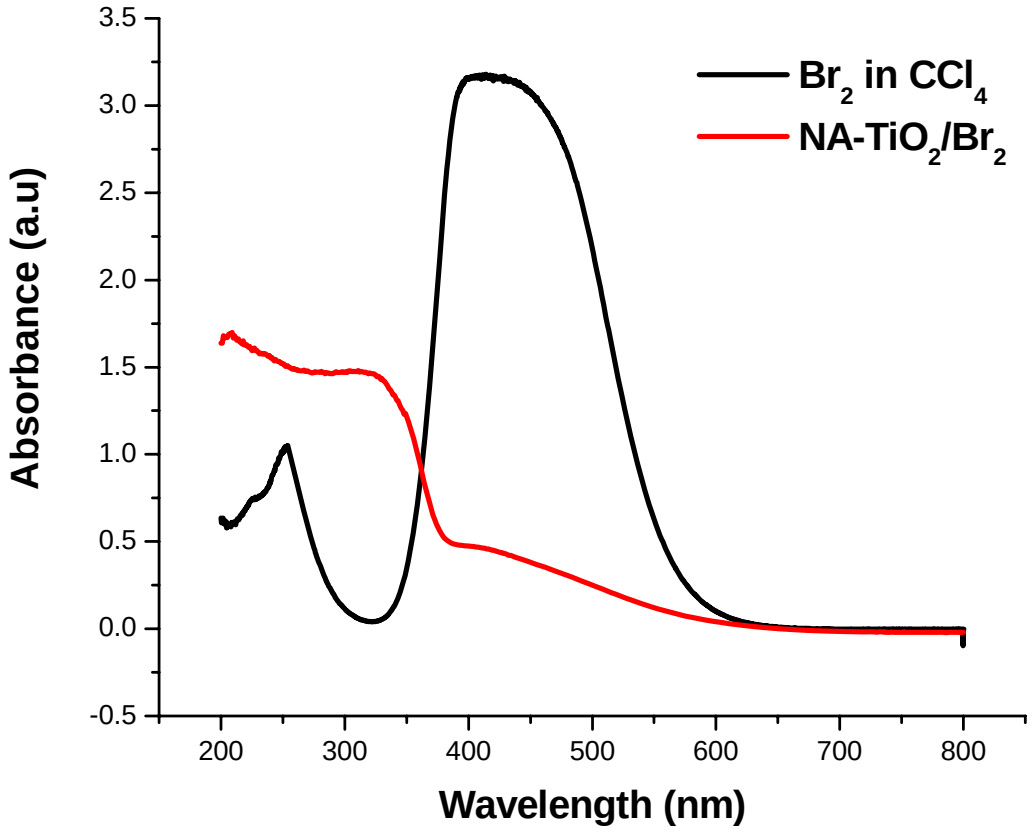

Figure 2.27 UV-Vis spectrum of bromine in CCl_4 and Diffuse reflectance spectrum of NA-TiO_2/Br_2.

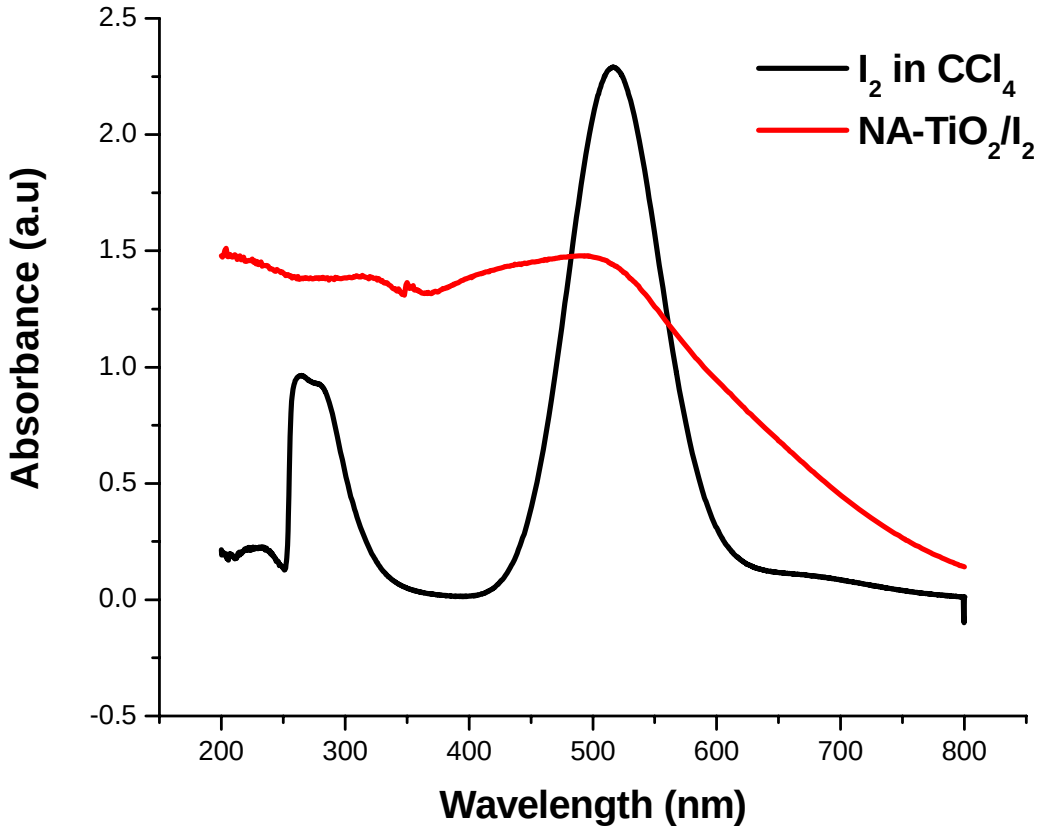

Figure 2.28 UV-Vis spectrum of bromine in CCl_4 and Diffuse reflectance spectrum of NA-TiO_2/I_2.

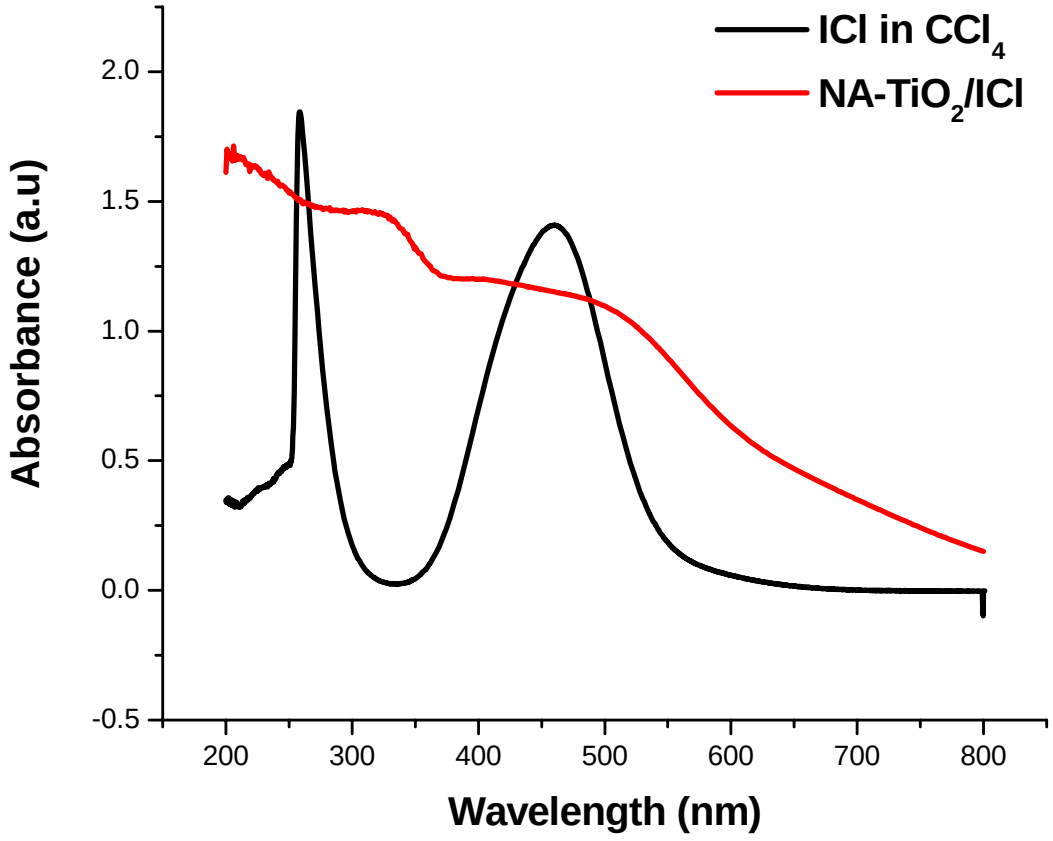

Figure 2.29 UV-Vis spectrum of bromine in CCl_4 and Diffuse reflectance spectrum of NA-TiO_2/ICl.

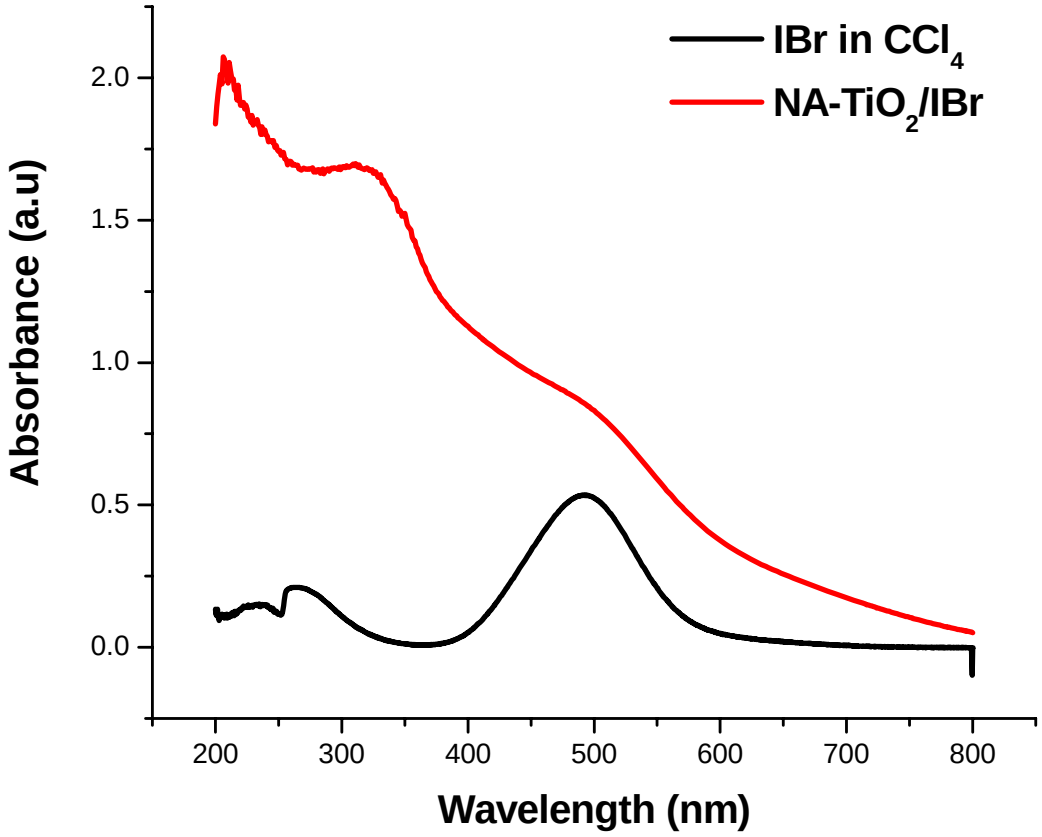

Figure 2.30 UV-Vis spectrum of bromine in CCl_4 and Diffuse reflectance spectrum of NA-TiO_2/IBr.

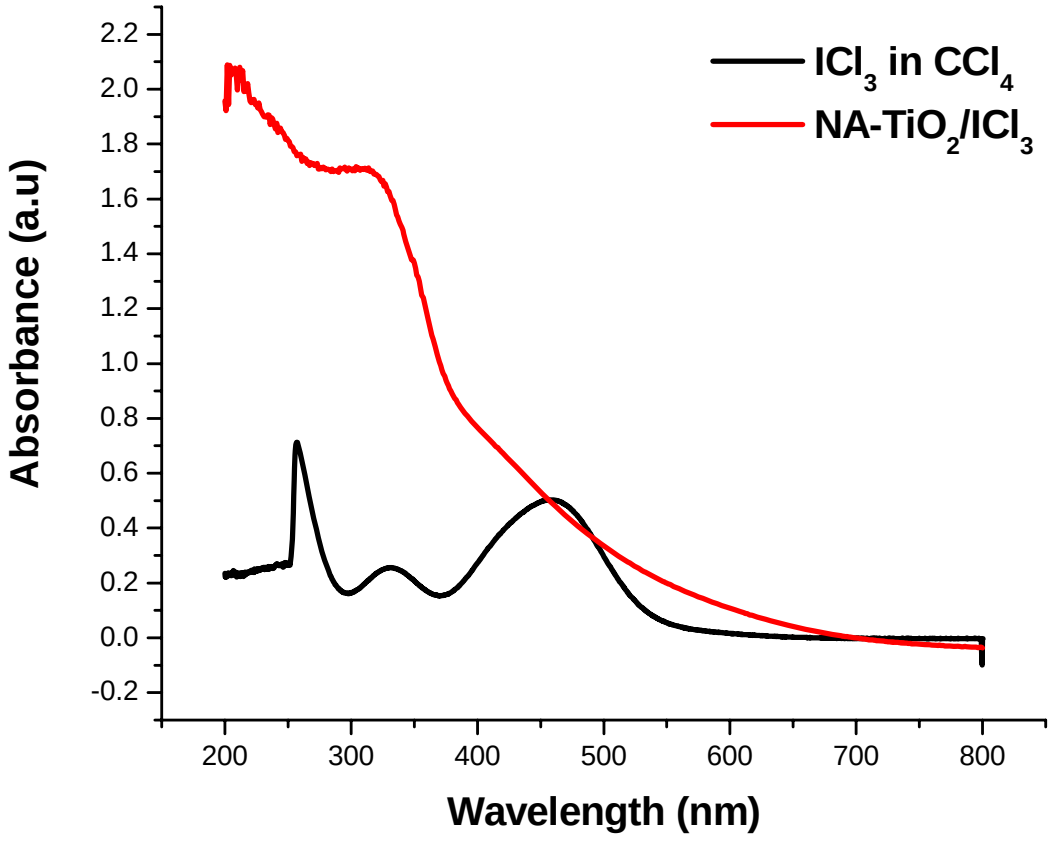

Figure 2.31 UV-Vis spectrum of bromine in CCl_4 and Diffuse reflectance spectrum of NA-TiO_2/ICl_3.

2.3.2.5 Transmission Electron Microscopy (TEM)

Images of NA-TiO_2 as received can be seen in Figure 2.32 and 2.33. It can be noticed that the morphology of this metal oxide is very different from NA-Al_2O_3 Plus, in which that it is not fibrous, but rather consists of spheres or squares that aggregate together to form a porous network. Upon heat-treatment the NA-TiO_2 transforms into the well-known anatase form and in the images it can be observed that the morphology is very porous and consists of many individual spheres/squares (Figure 2.34 and 2.35). Upon halogenation the morphology looks very similar. It appears however, that the carbon on the grid has interacted with the particles, forming a white frame around them (Figure 2.36 and 2.37).

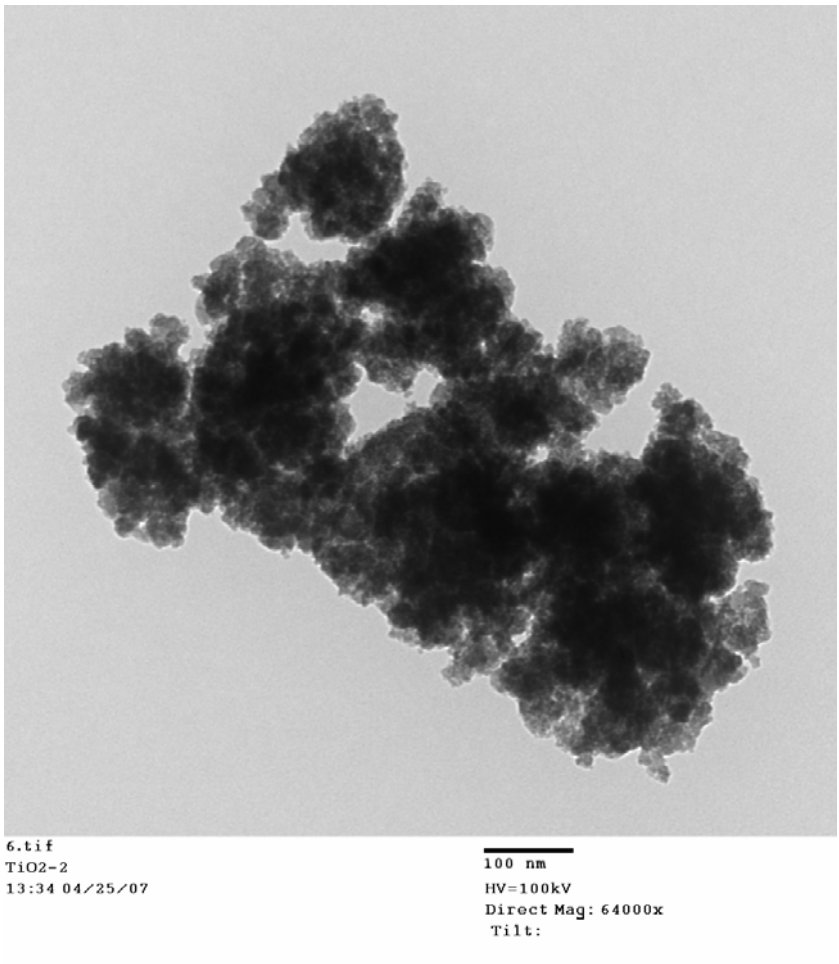

Figure 2.32 TEM image of NA-TiO_2 (1).

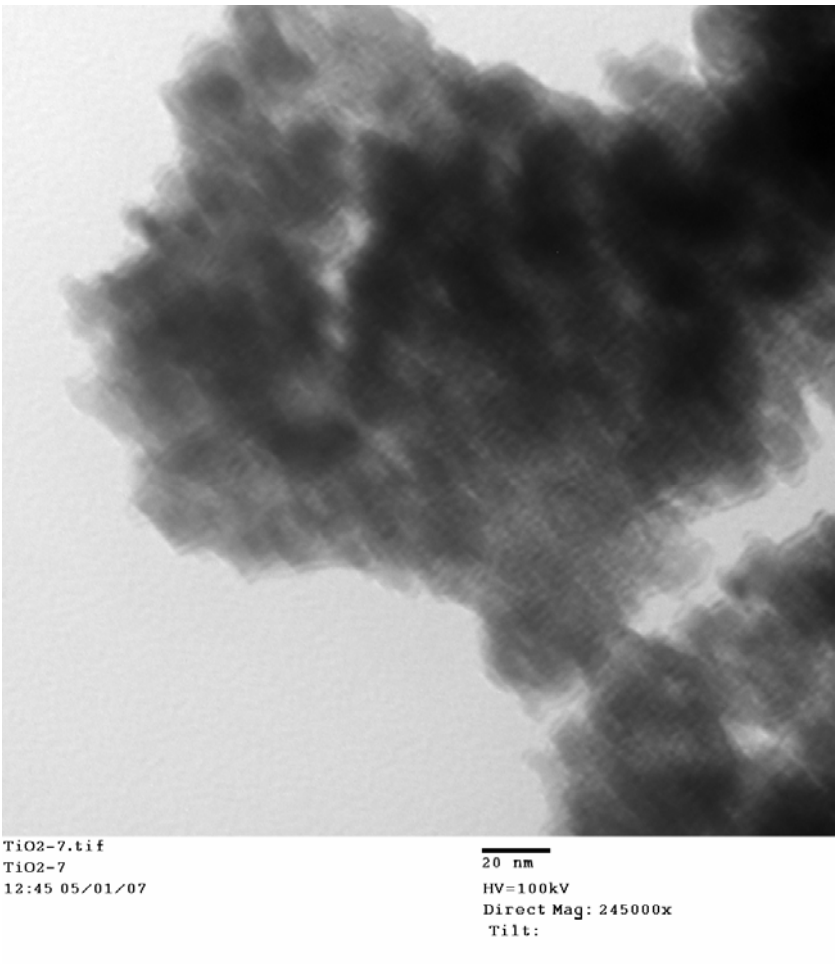

Figure 2.33 TEM image of NA-TiO_2 (2).

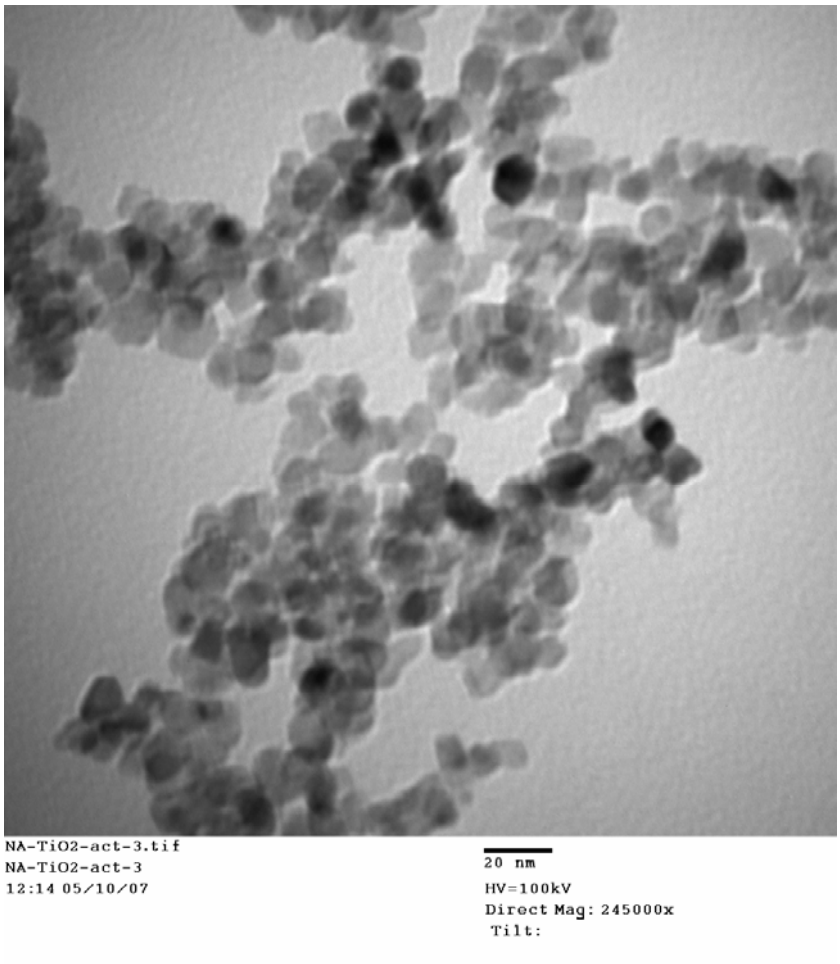

Figure 2.34 TEM image of NA-TiO_2 (act.) (1).

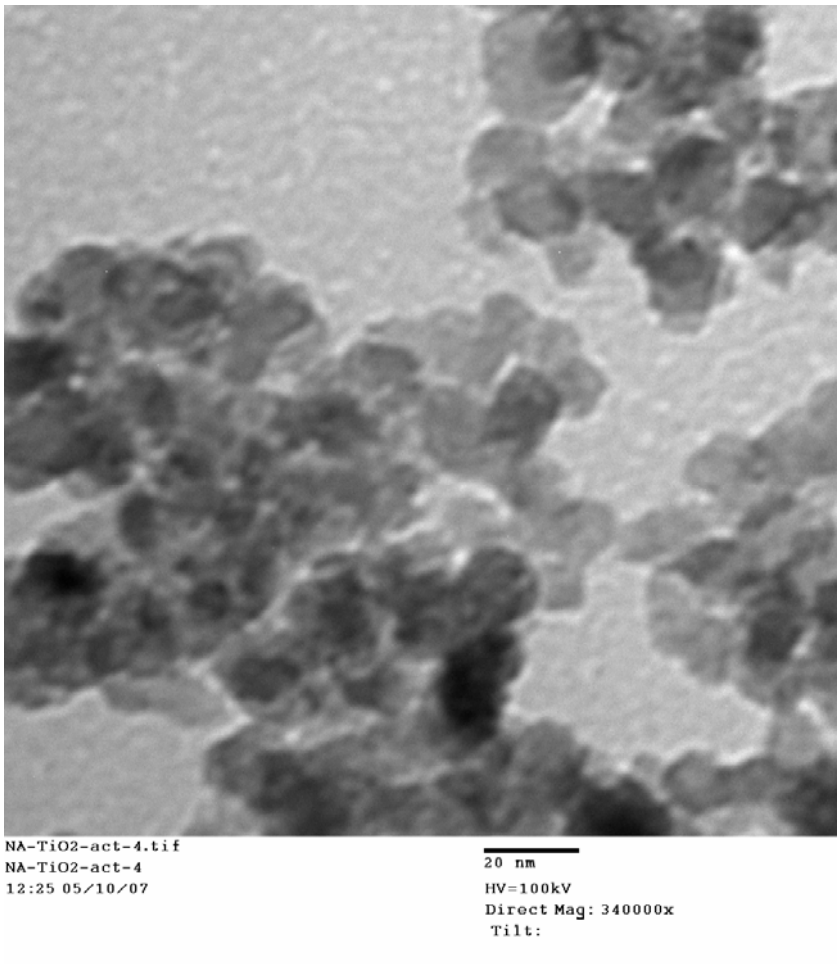

Figure 2.35 TEM image of NA-TiO_2 (act.) (2).

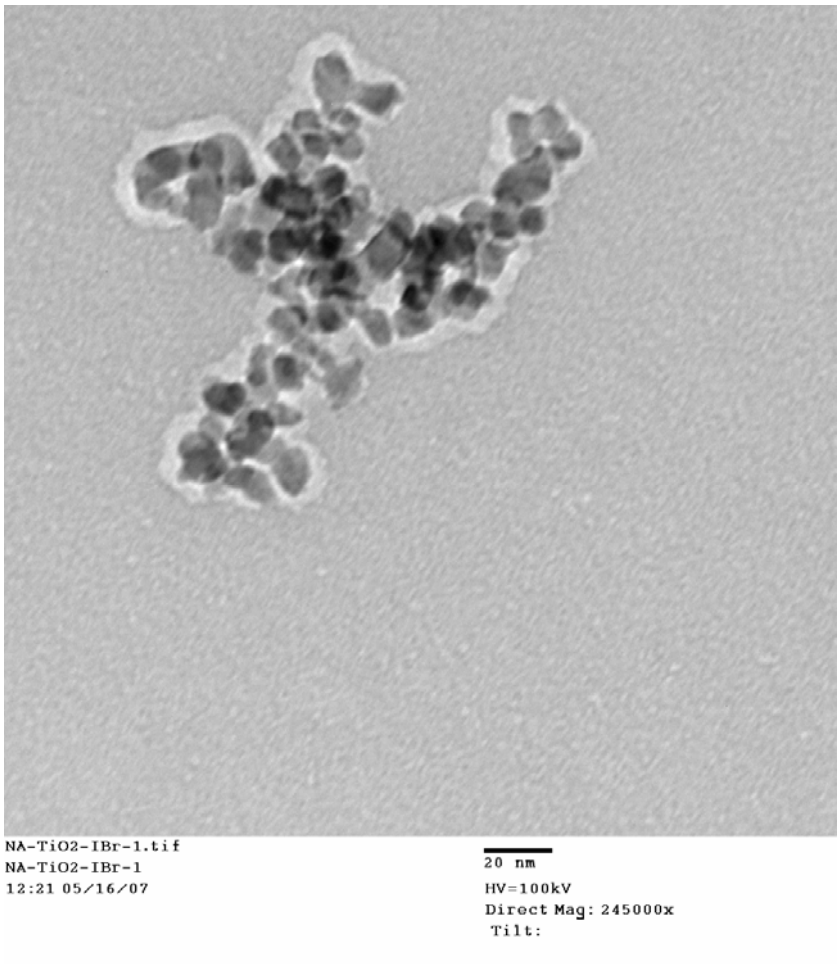

Figure 2.36 TEM image of NA-TiO_2/IBr (1).

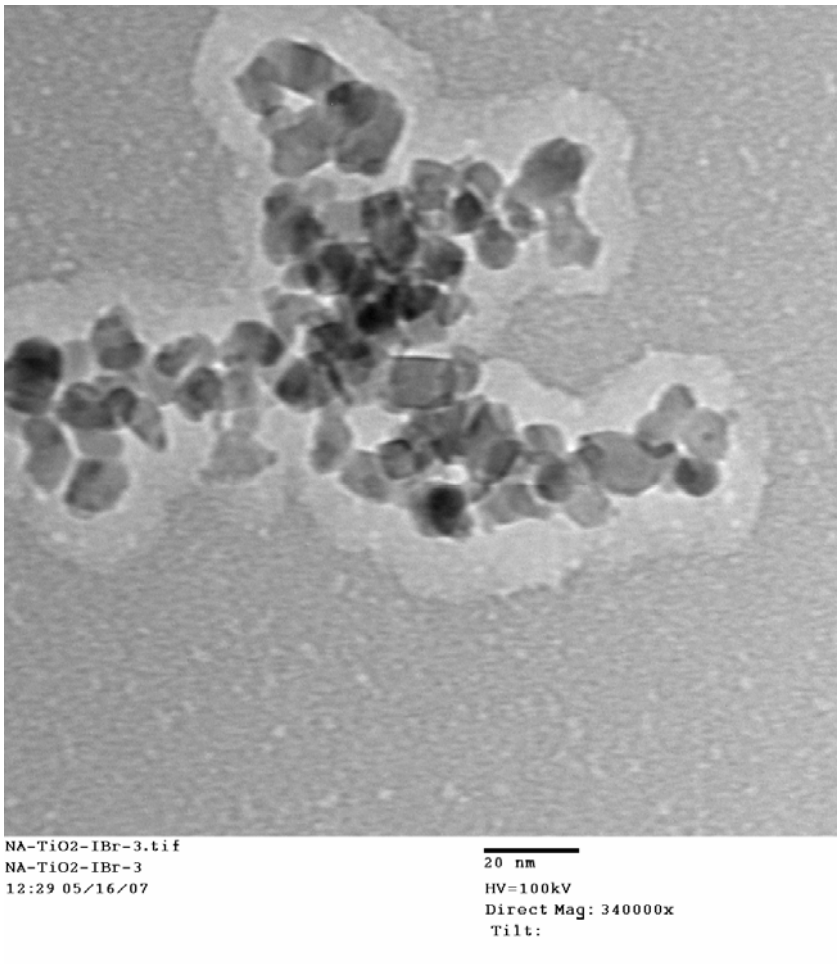

Figure 2.37 TEM image of NA-TiO_2/IBr (2).

2.3.3 NA-CeO_2 and its Adducts

2.3.3.1 Specific Surface Area

The BET method is used to find the specific surface area of the NA-CeO_2, before and after the activation step.

Initially, the metal oxide has a specific surface area of ~50 m^2/g. This surface area is very low compared to those of NA-Al_2O_3 Plus and NA-TiO_2; however, CeO_2 is a much heavier metal oxide, leading to a lower surface area. During an increase of the temperature from room temperature up to 400 °C over a period of two hours and then retaining this temperature for another four hours (six hours total) the surface area remained close to the same, which indicates that the porous structure of NA-CeO_2 is not very sensitive to collapse during heat-treatment.

2.3.3.2 Thermogravimetric Analysis (TGA)

The samples were heated at a rate of either 5 or 10 °C per minute up to 600 °C in a helium atmosphere.

The halogen/interhalogen content, based on thermogravimetric data can be seen in Table 2.3, as well as the calculated surface concentrations for the prepared adducts.

Table 2.3 Halogen/Interhalogen content as determined by TGA and the calculated Surface Concentration.

Material	Halogen Content wt % (TGA)	Surface Concn molecules/nm^2
NA-CeO_2/Cl_2	2	3.5
NA-CeO_2/Br_2	3	2.3
NA-CeO_2/I_2	5	2.5
NA-CeO_2/ICl	4	3.1
NA-CeO_2/IBr	4	2.4
NA-CeO_2/ICl_3	4	2.2

Table 2.3 shows the wt % adsorbed halogen for the NA-CeO_2 adducts and values up to 5 percent by weight have been obtained. These values are significantly lower than the respective values for both the NA-Al_2O_3 Plus and NA-TiO_2 adducts, as discussed earlier in this paper, due to the much higher molar mass of the NA-CeO_2 (172.1 g/mol) as compared to the two other metal oxides. In addition, the much lower surface area of this material also contributes to the decreased adsorption. During the adsorption process, it can be observed that the halogen is adsorbed very quickly on the cerium oxide surface and the stabilities of the prepared halogen adducts are very good, especially compared to the NA-TiO_2 adducts. NA-CeO_2/I_2 was the most stable in the series of NA-CeO_2 adducts, followed by the iodine monochloride adduct. No heat was evolved during the adsorption of halogen/interhalogen on the NA-CeO_2 surface, however, which suggests a rather weak strength of adsorption as compared to the nanosized MgO adducts.[8]

The surface concentration for the NA-CeO_2 adducts have been calculated and are between 2.2 and 3.5 molecules/nm^2.

2.3.3.3 Raman Spectroscopy

The Raman spectrum of activated NA-CeO_2 shows one strong peak at 463.7 cm^{-1} and one smaller peak at 256.2 cm^{-1} (Figure 2.38). The obtained peak values match up well to the findings of Shyu et al.[72] with reported values of a strong peak at 465 cm^{-1}, corresponding to the F_{2g} Raman active mode that is characteristic of fluorite structured materials, as well as a smaller, weaker band at 265 cm^{-1}. The small crystallite sizes of the NA-CeO_2 might be the explanation for the slightly lower wavenumbers, as compared to the literature values.[72] As with the chlorinated adducts of NA-Al_2O_3 Plus and NA-TiO_2, the chlorinated adduct of NA-CeO_2 does not have a Raman spectrum different than that of the metal oxide itself.

The brominated adduct has a Raman peak corresponding to Br_2 at 279 cm^{-1} (Figure 2.39), which gives a 35 cm^{-1} lowering of the Br_2 peak from 313.9 cm^{-1}.[8,24] No spectral evidence is found for either Br_3^- [35,37,41-44] or Br_5^- [45] with Raman bands in the range of 160-170 cm^{-1} and 250 cm^{-1}, respectively. The same is true for oxygen containing compounds such as BrO_x^-, with frequency values well over 400 cm^{-1}.[43,45-47] To our knowledge, there are no reports in the literature of Raman bands for cerium tetrabromide and since there is no evidence of the formation of oxygen containing species, we assume no formation of $CeBr_4$, or it occurs to a very small extent.

A slightly stronger peak, at 177 cm^{-1}, was observed for the iodinated adduct, giving a downshift of 37 cm^{-1}, compared to I_2 itself at 213 cm^{-1} (Figure 2.40).[22,24,29] The Raman spectrum shows no presence of I_3^- with a Raman frequency in the range between 110-120 cm^{-1}.[22,41,42,49] I_5^- has been observed at 160 cm^{-1} by Kiefer et al.,[49] but this value is slightly lower than what we observe here. No oxygen containing species, such as IO_3^-, IO_4^- and IO_6^-, were observed,[45,46] and

to the best of our knowledge, no reports exist containing the Raman spectrum of cerium tetraiodide.

NA-CeO_2/ICl has a strong peak at 196 cm^{-1} and one very small peak at 320 cm^{-1} (Figure 2.41). With ICl itself at 381.5 cm^{-1} [22,24,31,32] downshifts of 185.5 cm^{-1} and 61.5 cm^{-1} are obtained. Formation of ICl_2^- and ICl_4^-, displaying bands at 254-278 cm^{-1} [22,35,44,50] and 288 cm^{-1},[51] respectively, are excluded as no peaks in the 250-290 cm^{-1} range were observed. Isotopic splitting is excluded as the two Raman peaks are too far apart. However, the peak at 196 cm^{-1} is most likely due to iodine on the surface, caused by partial decomposition of the interhalogen upon adsorption. The downshift of 61.5 cm^{-1} for the peak at 320 cm^{-1} is realistic, as ICl is a polar molecule, leading to a strong interaction with the ionic surface of the metal oxide.

NA-CeO_2/IBr has two peaks; one larger at 196 cm^{-1} and one smaller at 233 cm^{-1} (Figure 2.42). The large peak at 196 cm^{-1} could be caused by I_2 on the surface, arising from partial decomposition of IBr upon adsorption. The downshift of 34 cm^{-1} for the peak at 233 cm^{-1} of the IBr moiety is reasonable compared to the larger ICl shift of 61.5 cm^{-1}. It is slightly larger than the shift of the non-polar halogens, but smaller than that of the more polar ICl molecule.

NA-CeO_2/ICl_3 has a peak that almost completely coincides with the strongest peak of ICl_3 itself, at 343 cm^{-1} (Figure 2.43), indicating that the interhalogen might be retained in the pore structure of the metal oxide, or very weakly adsorbed on the surface. There is no evidence of the other peaks corresponding to ICl_3 itself so it can not be completely ruled out that some chemical reaction might have taken place.

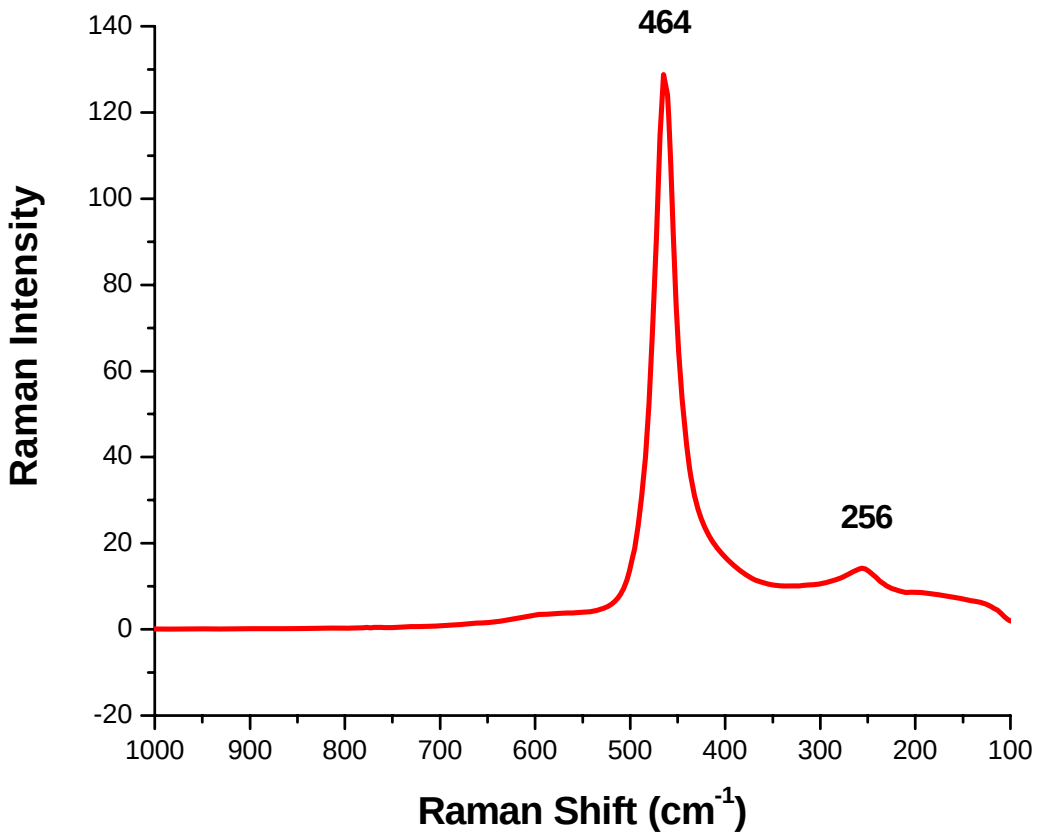

Figure 2.38 Raman spectrum of act. NA-CeO_2.

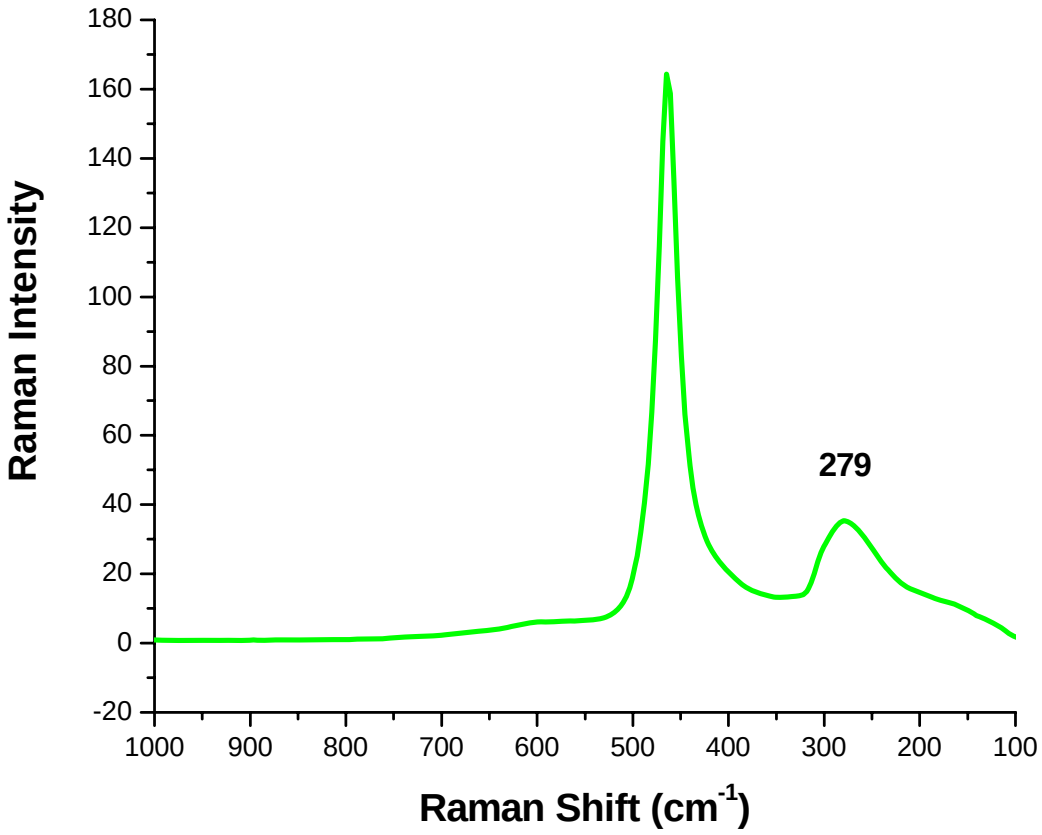

Figure 2.39 Raman spectrum of act. NA-CeO_2/Br_2.

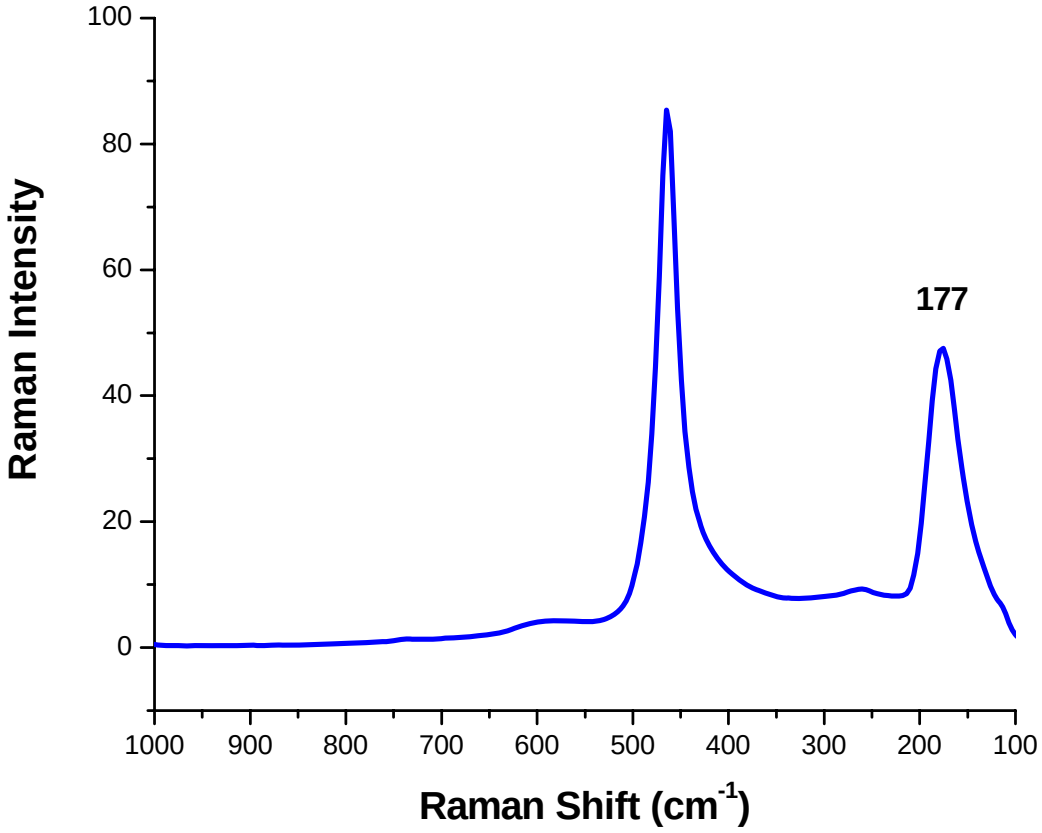

Figure 2.40 Raman spectrum of act. NA-CeO_2/I_2.

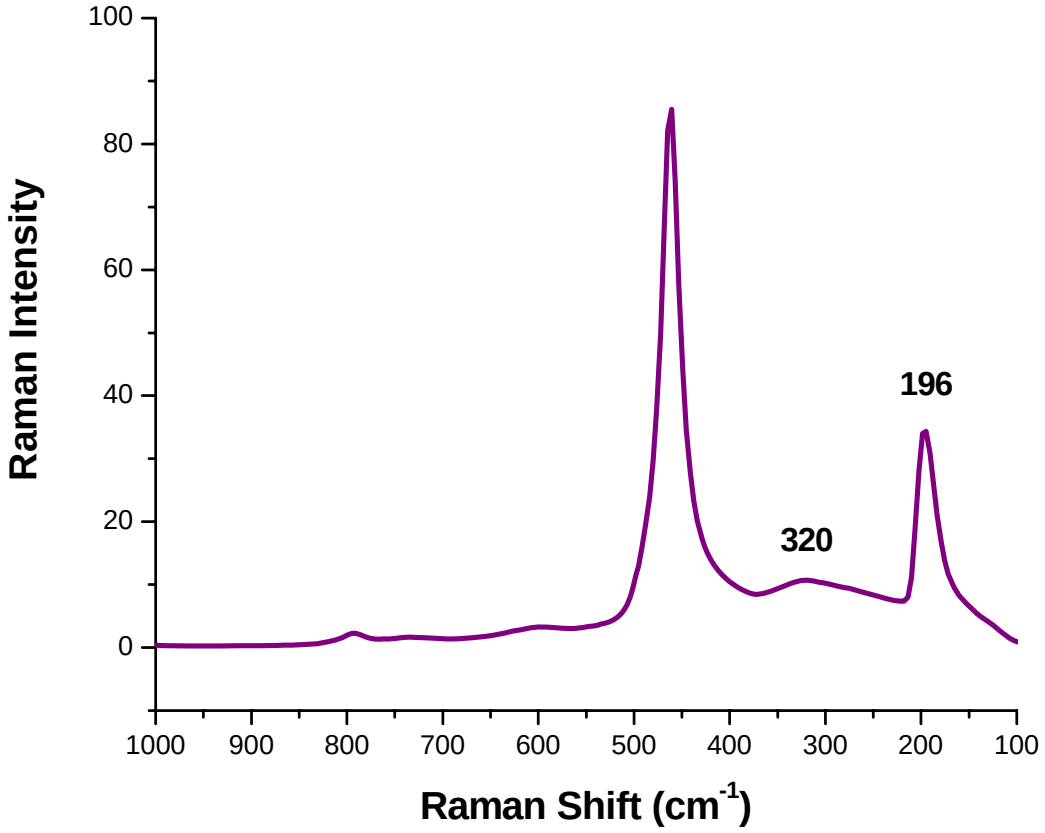

Figure 2.41 Raman spectrum of act. NA-CeO_2/ICl.

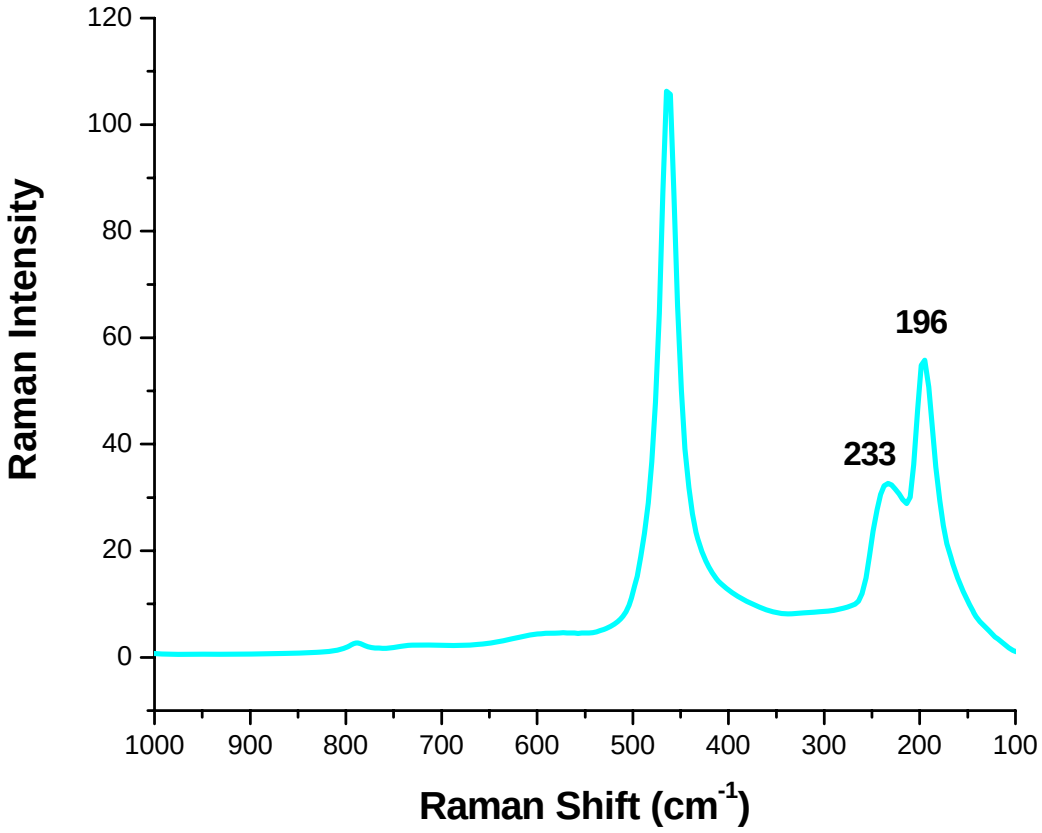

Figure 2.42 Raman spectrum of act. NA-CeO_2/IBr.

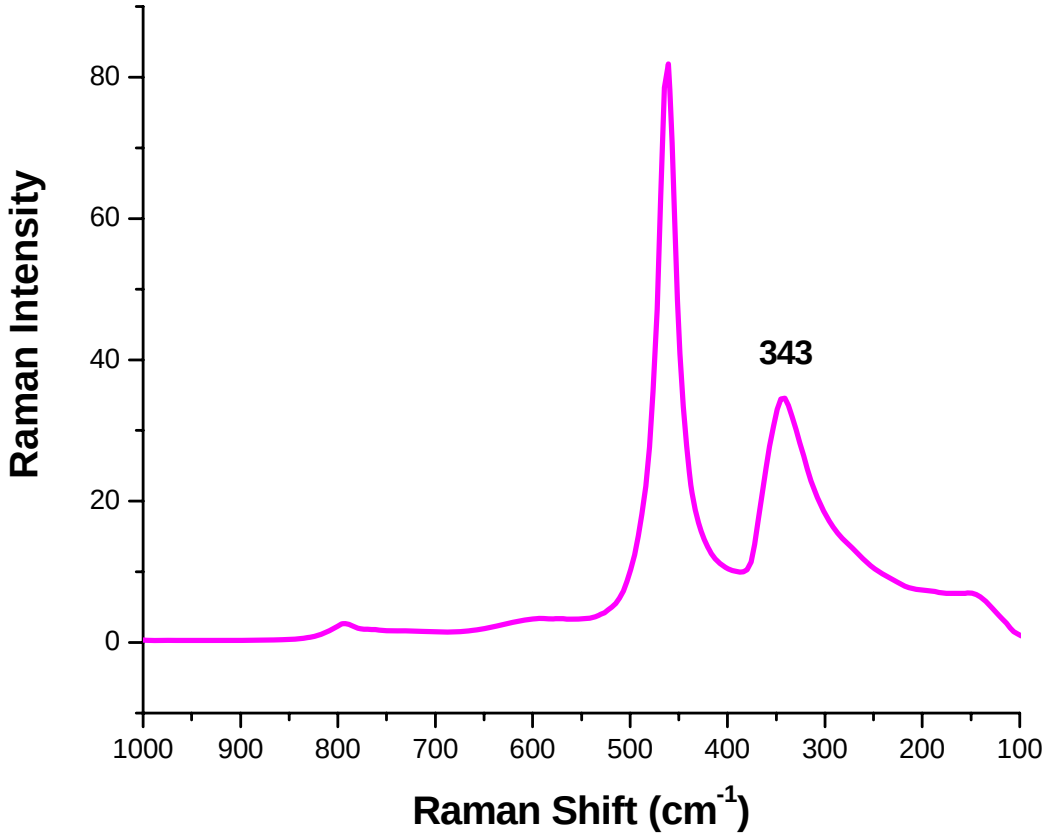

Figure 2.43 Raman spectrum of act. NA-CeO_2/ICl_3.

2.3.3.4 UV-Vis Spectra Analysis

A photograph of the prepared adducts can be seen in Figure 2.44. NA-CeO_2 is a pale yellow powder with absorbance in the 200-500 nm range, as reported in the literature,[73-75] with a peak position at ~350 nm. Similarly, NA-CeO_2/Cl_2 is a pale yellow powder with a diffuse reflectance spectrum coinciding with NA-CeO_2. NA-CeO_2/Br_2 however, with a stronger yellow color, has an absorbance spectrum that is similar but with a slightly wider absorption range that that of NA-CeO_2 (Figure 2.45). The spectrum is very different from that of Br_2 dissolved in CCl_4 which gives rise to two peaks at 255 nm and 440 nm. Similarly, iodine dissolved in CCl_4 has two distinct peaks at 260 and 516 nm, whereas NA-CeO_2/I_2 has a very broad absorption spectrum with no specific features (Figure 2.46). Similarly, ICl in CCl_4 has two sharp peaks at 250 and 460 nm while NA-CeO_2/ICl has a wider band with peak positions at 350 and 520 nm (Figure 2.47). The diffuse reflectance spectrum of NA-CeO_2/IBr displays a decreasing intensity with increasing wavelength with a peak position at 350 nm and a shoulder at 475 nm. Its shoulder coincides well with the peak of IBr itself (Figure 2.48). The diffuse reflectance spectrum of NA-CeO_2/ICl_3 is similar in appearance to that of NA-CeO_2/IBr, with a peak position at 350 nm, but with the shoulder at a higher wavelength (Figure 2.49).

Figure 2.44 Photograph of NA-CeO_2 Adducts.

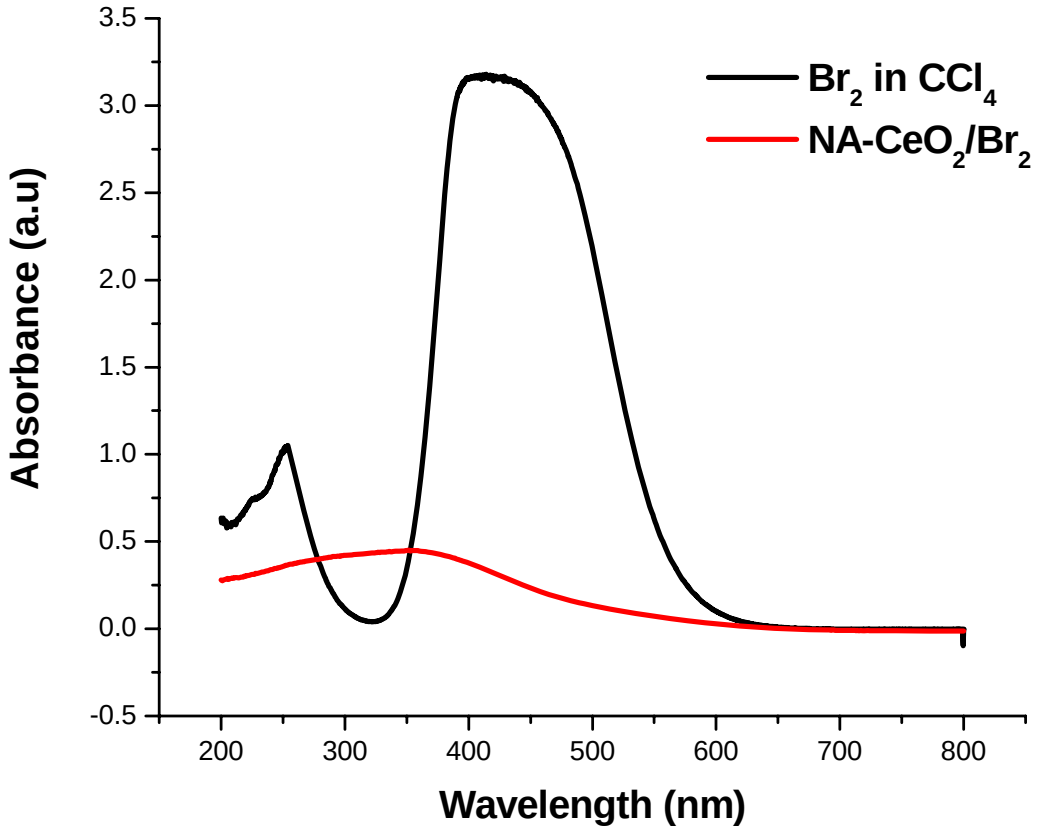

Figure 2.45 UV-Vis spectrum of bromine in CCl_4 and Diffuse reflectance spectrum of NA-CeO_2/Br_2.

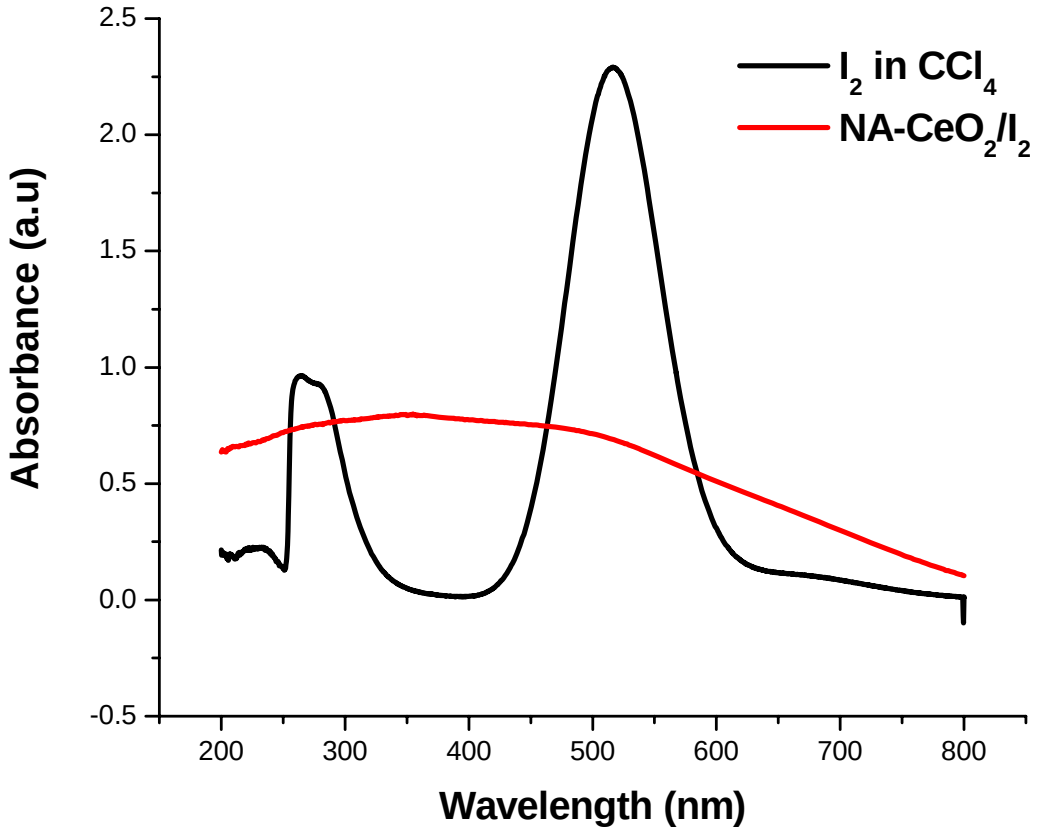

Figure 2.46 UV-Vis spectrum of iodine in CCl_4 and Diffuse reflectance spectrum of NA-CeO_2/I_2.

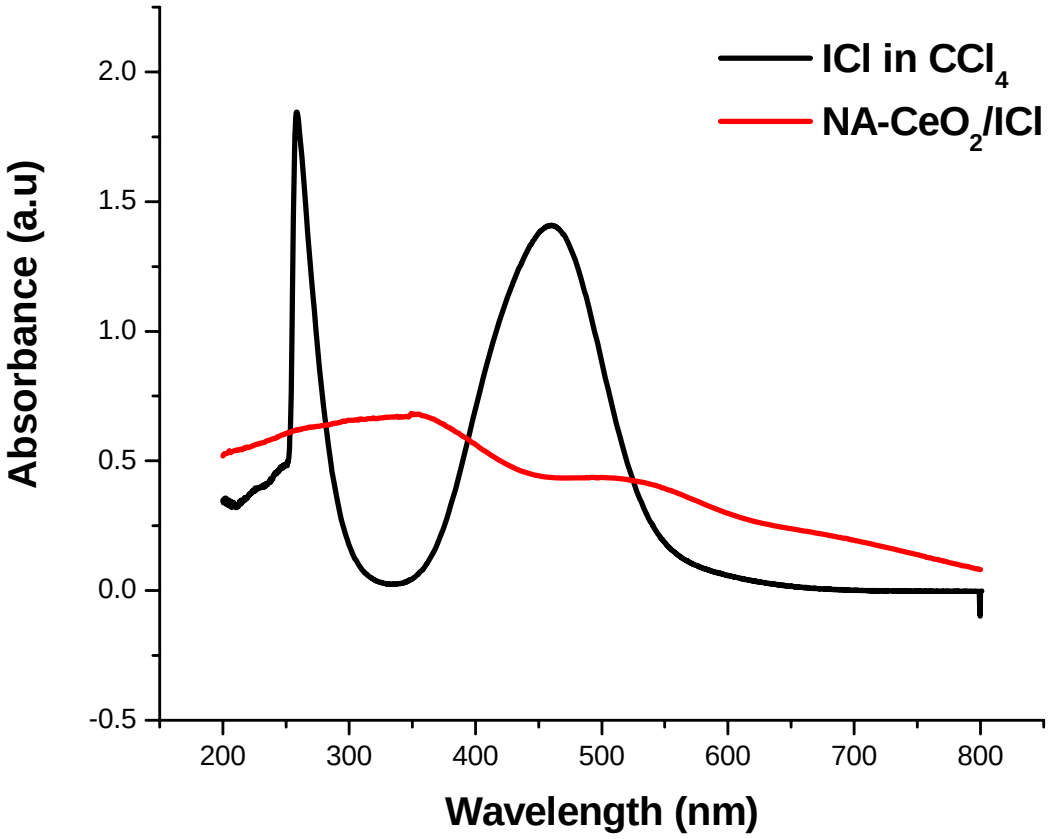

Figure 2.47 UV-Vis spectrum of iodine monochloride in CCl_4 and Diffuse reflectance spectrum of NA-CeO_2/ICl.

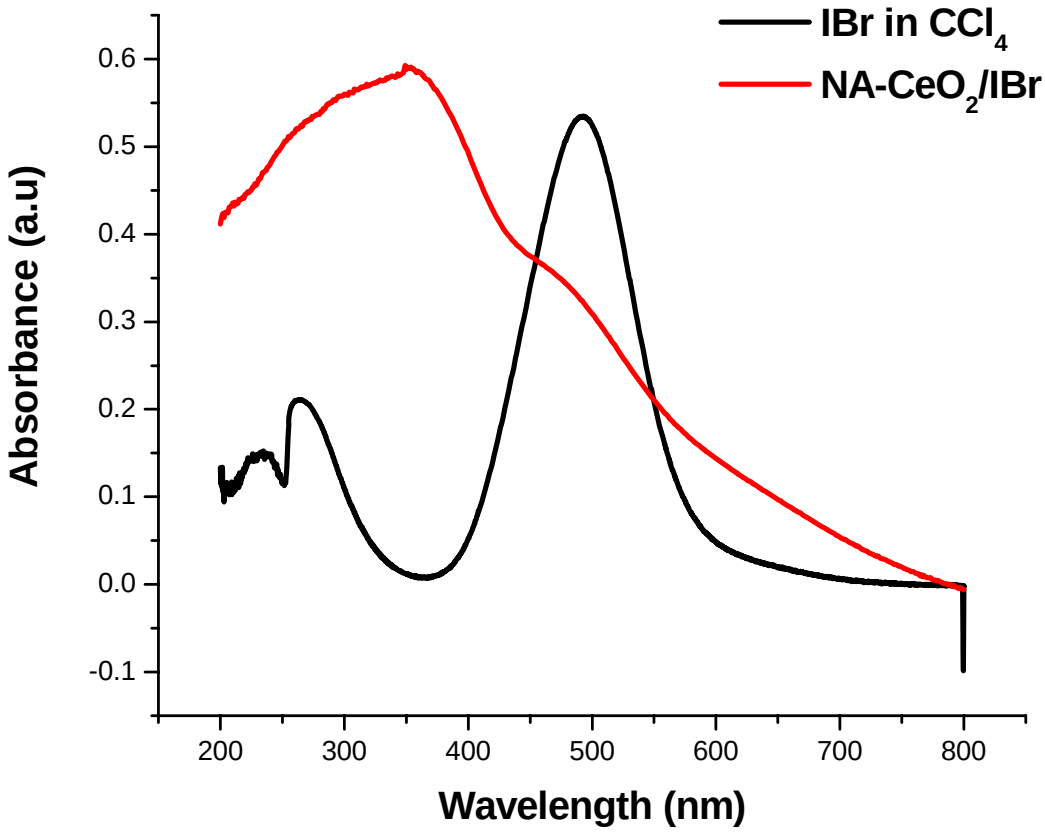

Figure 2.48 UV-Vis spectrum of iodine monobromide in CCl_4 and Diffuse reflectance spectrum of NA-CeO_2/IBr.

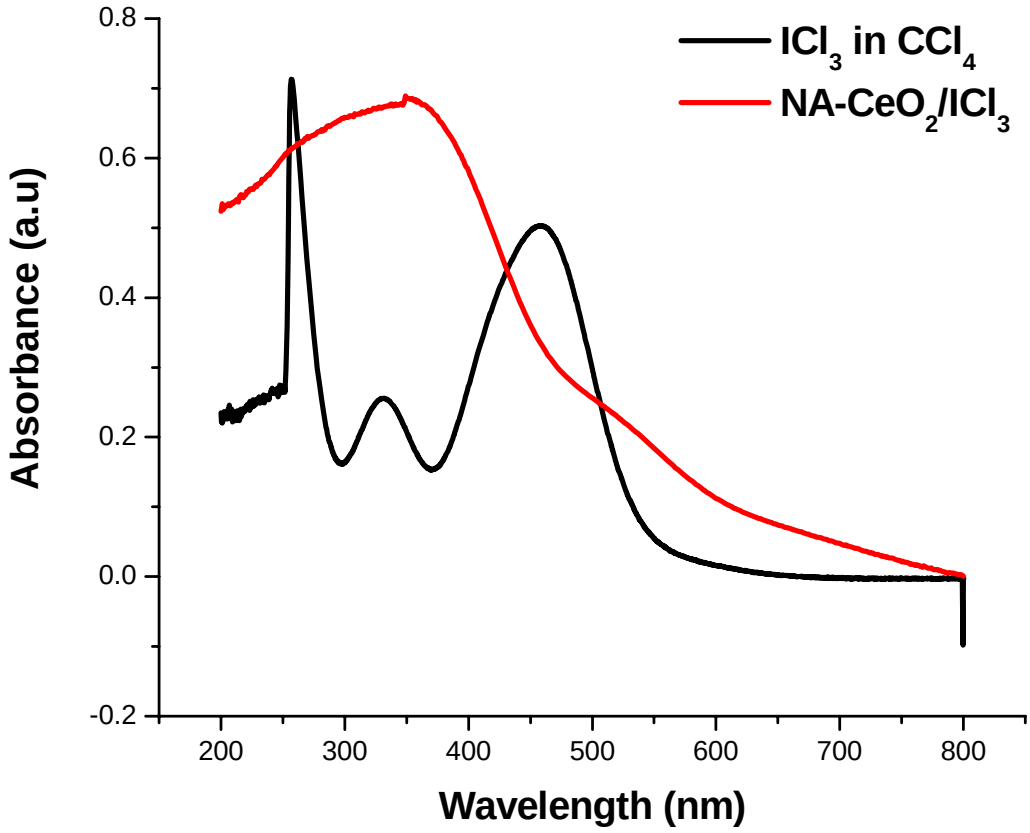

Figure 2.49 UV-Vis spectrum of iodine trichloride in CCl_4 and Diffuse reflectance spectrum of NA-CeO_2/ICl_3.

2.3.3.5 Transmission Electron Microscopy (TEM)

As NA-TiO_2, NA-CeO_2 does not have a fibrous morphology like NA-Al_2O_3 Plus. NA-CeO_2 consists of small spheres/squares of only a few nanometers in size (Figure 2.50 and 2.51). Once the metal oxide is activated (400 °C) the structure appears very similar (Figure 2.52 and 2.53). The halogenated samples also possess a similar morphology, as shown in the images of NA-CeO_2/IBr (Figure 2.54 and 2.55).

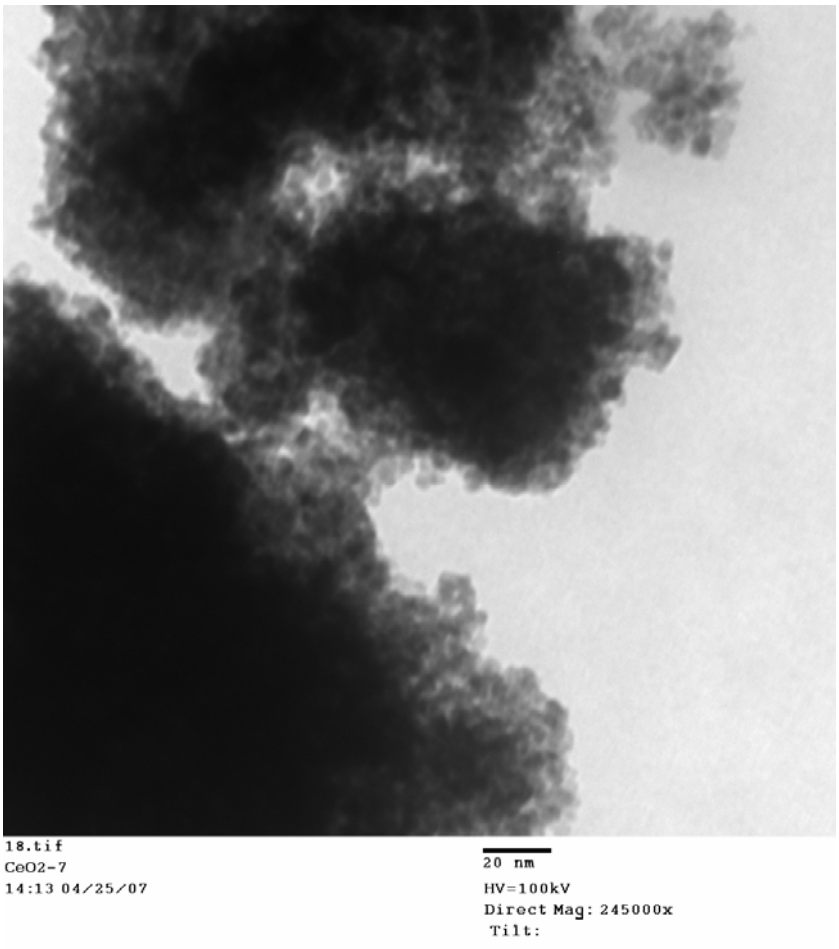

Figure 2.50 TEM image of NA-CeO_2 (1).

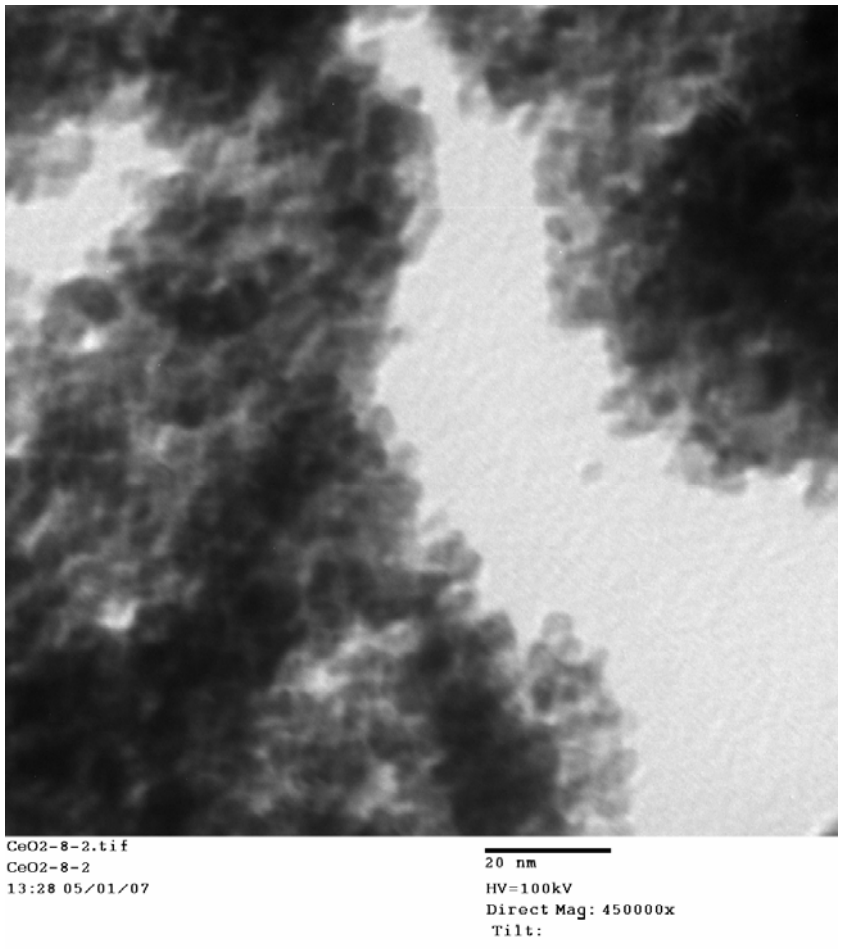

Figure 2.51 TEM image of NA-CeO_2 (2).

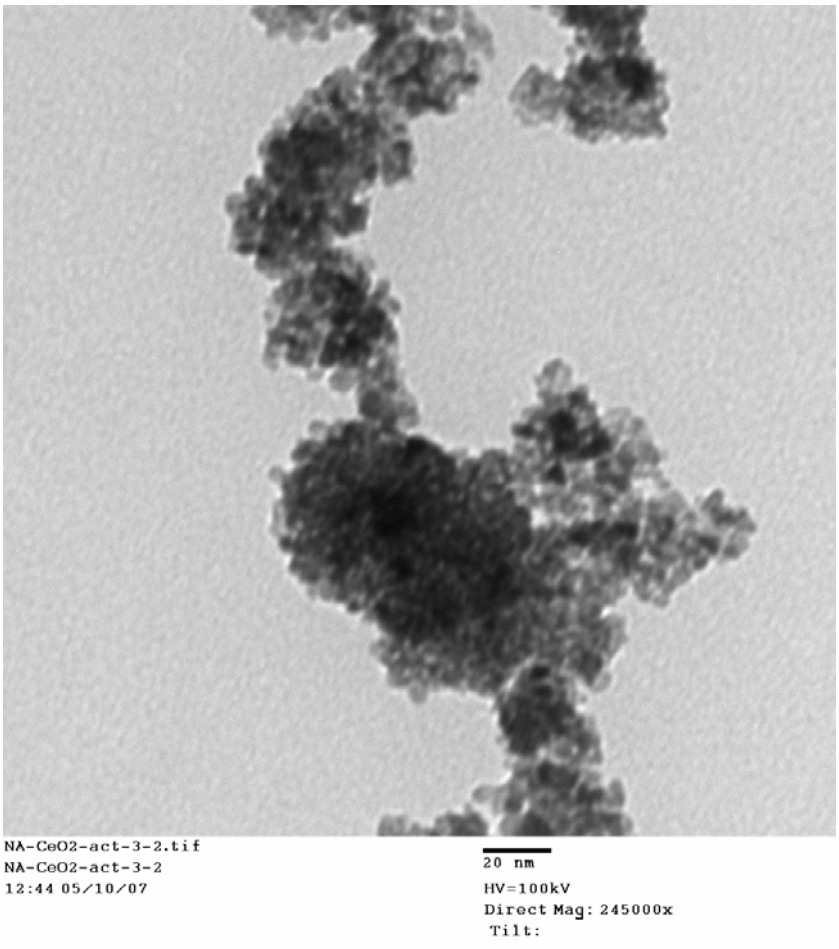

Figure 2.52 TEM image of NA-CeO_2 (act.) (1).

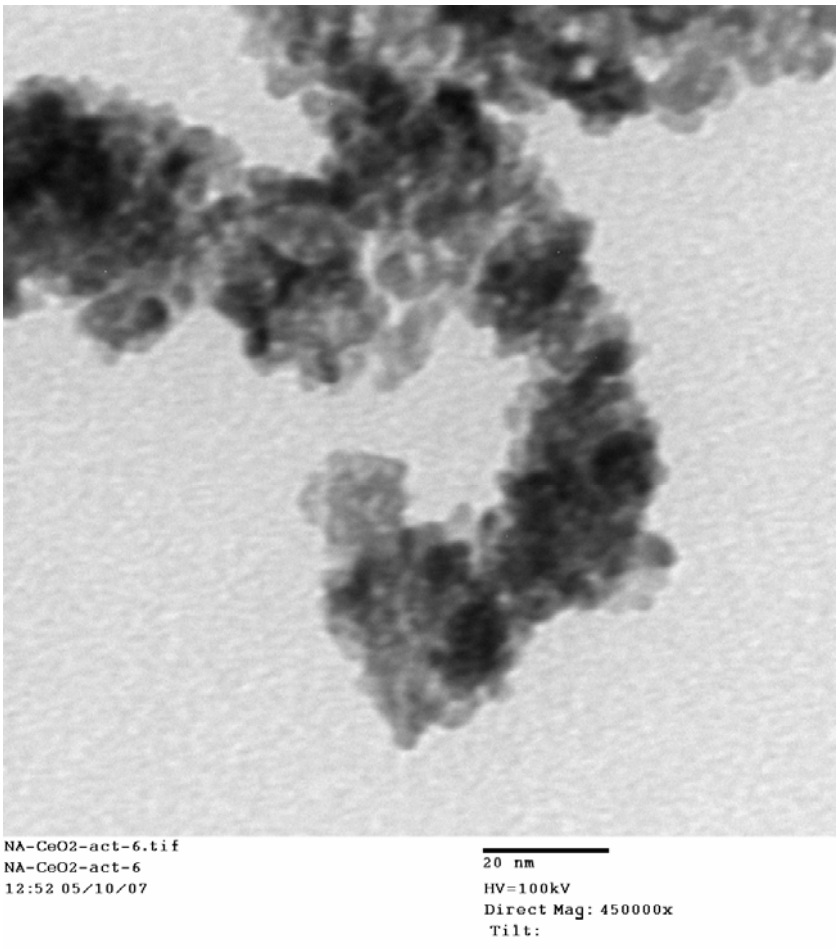

Figure 2.53 TEM image of NA-CeO_2 (act.) (2).

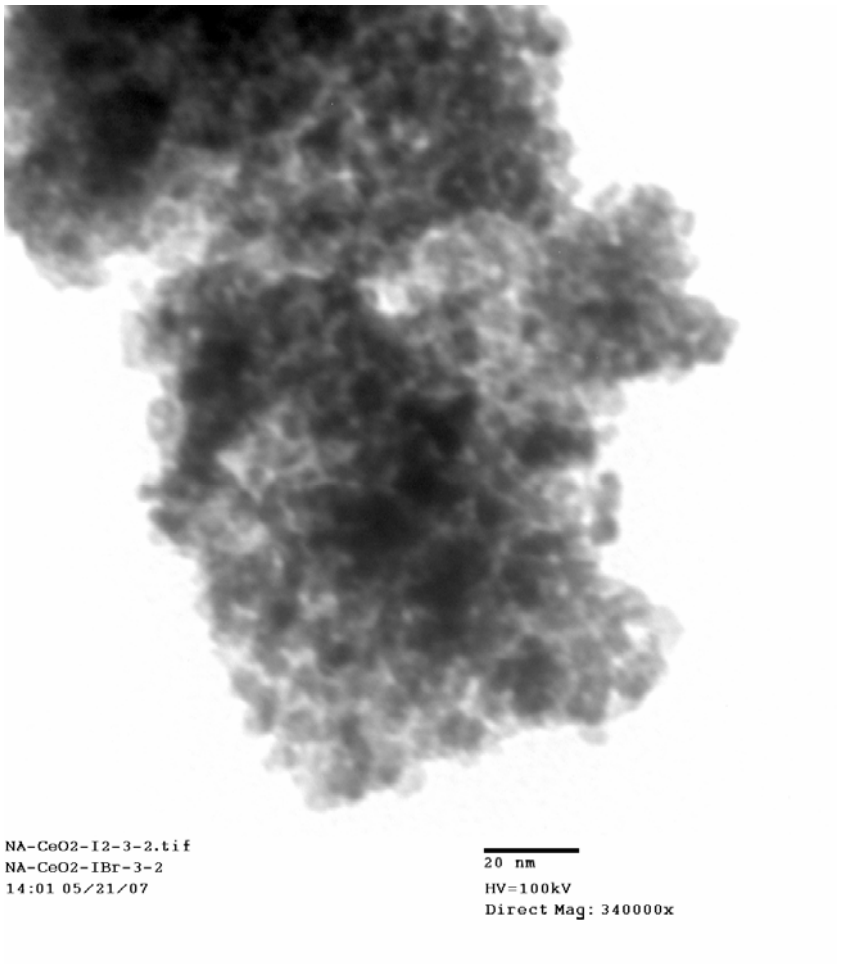

Figure 2.54 TEM image of NA-CeO_2/IBr (1).

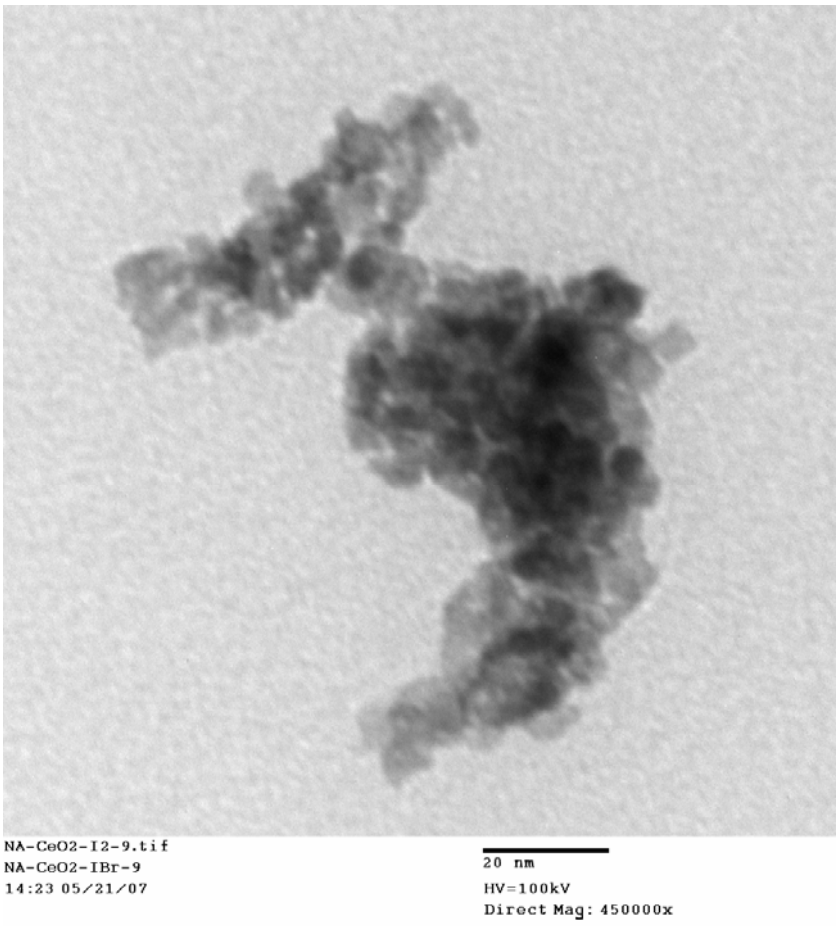

Figure 2.55 TEM image of NA-CeO_2/IBr (2).

2.3.4 Other Materials and their Adducts

One of the purposes of this study has been to identify what kind of materials (metal oxides, mesoporous materials and so on) are capable of adsorption of halogens/interhalogens and to what extent they will retain them. The above discussed metal oxides (NA-Al_2O_3 Plus, NA-TiO_2 and NA-CeO_2) are only a few of the materials tested for adsorption. The factors which influence the adsorption capability have been of interest and hence a wide range of materials have been tested.

Bromine was chosen as the 'test halogen', as it is the most practical and safe halogen to work with.

2.3.4.1 Specific Surface Area

The surface area of the material is believed to play a large role in the adsorption process. This has been confirmed in previous research conducted in our laboratory in which commercially available (CM) micron-sized MgO (low surface area) was compared to aerogel-prepared (AP) nanosized MgO (high surface area).[8] It was found that the CM-MgO adsorbed much lower amounts of halogen than did AP-MgO. It was also found that the prepared adducts from AP-MgO were much more stable, with weaker smells of halogens.

Table 2.4 shows some of the materials tested for adsorption of bromine, in addition to the previously discussed nanosized metal oxides, as well as their specific surface areas. AP-MgO was one of the first metal oxides tested for adsorption and has been reported in the literature.[8] In

the column 'Adsorption of Bromine', **Y** means Yes, the material did adsorb bromine and **N** means No, the material did not adsorb bromine.

Table 2.4 Compounds tested for bromine adsorption.

Compound	Surface Area (m^2/g)	Adsorption of Bromine
AP-MgO	600	Y
AP-MgO/Al_2O_3	640	Y
AP-CaO/Al_2O_3	520	Y
AP-SrO	20	N
AP-ZrO_2	94	Y
NA-ZnO	70	N
NA-CaO plus	90	Y
NA-Al_2O_3	275	Y
NA-CuO	65	N
ETS-10	235	Y
ETS-4	235	N
Al-MCM-41	1200	N
NiO	50-80	N
AP-$SrTiO_3$	93	Y
AP-$BaTiO_3$	45	Y
Gd_2O_3	<10	N
Sm_2O_3	<10	N
Y_2O_3	6	N
Eu_2O_3	<10	N
CeO_2	<10	N
MgO/SiO_2	>500	N
TiO_2/SiO_2	>500	N
$25TiO_2:75SiO_2$	>500	N
AP-SiO_2	N/A	N

It can be seen that some high surface area materials adsorb bromine, but not all of them. For example, the highest surface area material tested, Al-MCM-41, did not adsorb bromine. This might be explained by the one dimensional pore structure of the material that might lead to the bromine just passing right through it. It can also be seen that none of the very low surface area materials (<10 m^2/g) adsorb bromine at all.

A comparison of two similar materials (NA-Al_2O_3 and NA-Al_2O_3 Plus, previously discussed), both nanosized and with relatively high surface areas, showed that they both adsorbed bromine; however, the higher surface area material (NA-Al_2O_3 Plus) adsorbed a higher

amount and retained the halogen for a longer time. This result concludes that surface area of the material is of importance, but it is not the only important factor. In addition to the above mentioned materials, two different forms of commercially available Al_2O_3: γ-Al_2O_3 and α-Al_2O_3, as well as commercially available anatase and rutile-TiO_2, were also tested for adsorption. None of the materials adsorbed and retained bromine on the surface, which further emphasizes the importance of the surface morphology of the material in order to adsorb halogen.

2.3.4.2 Thermogravimetric Analysis (TGA)

In general, the color of the prepared bromine adducts of the above materials was much weaker than the bromine adducts of the previously discussed NA-Al_2O_3 Plus, NA-TiO_2 and NA-CeO_2. In addition, the bromine did not stay on the surface of these materials for very long; some of the materials lost the bromine in just a few days. If the powders are exposed directly to air, for example, put on a weighing paper, many of the adducts lose the adsorbed bromine within minutes. The bromine content, based on TGA measurements is presented below in Table 2.5, and it can be seen that the values are slightly lower for most of these materials than for the earlier mentioned materials, discussed in detail. The value for AP-CaO/Al_2O_3/Br_2 could not be measured as the adduct was very unstable and the bromine disappeared very quickly when the vial was opened. It can also be seen that the bromine content of NA-Al_2O_3/Br_2 is slightly lower than that of NA-Al_2O_3/Br_2 Plus, at 12 wt% compared to 15 wt%. This lower bromine content of NA-Al_2O_3/Br_2 can be explained by the slightly lower surface area (275 versus 550 m^2/g). As previously mentioned, the main problem with most of these prepared adducts consisted in their

instability. Although adduct formation occurred, they remained their characteristic yellow/orange adduct color only for short times, making them impractical for any uses.

Table 2.5 Bromine content as determined by TGA.

Compound	Br_2 content wt% (TGA)
AP-MgO	16
AP-MgO/Al_2O_3	14
AP-CaO/Al_2O_3	N/A
AP-ZrO_2	3
AP-CaO	8
NA-Al_2O_3	12
ETS-10	18
AP-$SrTiO_3$	3
AP-$BaTiO_3$	3

2.3.4.3 Raman Spectroscopy

The Raman spectra of the prepared brominated adducts are shown below (Figures 2.56-2.62). Of the seven materials that changed color upon adsorption of bromine, only two of them showed a Br-Br stretch in the Raman spectrum. Br_2 itself has a peak in the Raman spectrum at 313.9 cm^{-1},[8,24] and upon adsorption to the surface, there should be a slight downshift of the stretch. ETS-10/Br_2 has a peak at 312 cm^{-1}, which would lead to a downshift of only 1.9 cm^{-1} (Figure 2.60). This small shift might indicate that the halogen is retained in the pore structure of ETS-10, or adsorbed very weakly on the surface. However, this material proved to be one of the most stable one, out of the seven materials studied here. The lack of a bromine peak in the other bromine adducts might be caused by the fact that these adducts were very unstable and retained only small amounts of bromine. Bromine is not extremely polarizable and if only small amounts

are present it is likely that an absence of peak would occur. In addition, during exposure to the laser beam during the Raman collection, the halogen might leave the surface, leading to a lack of the bromine peak in the Raman spectrum.

NA-Al_2O_3 showed a Br_2 peak at 276 cm^{-1}, which gives a downshift of 37.9 cm^{-1} (Figure 2.61). This is similar to the shift present for NA-Al_2O_3/Br_2 Plus and corresponds to a strained halogen-halogen bond.

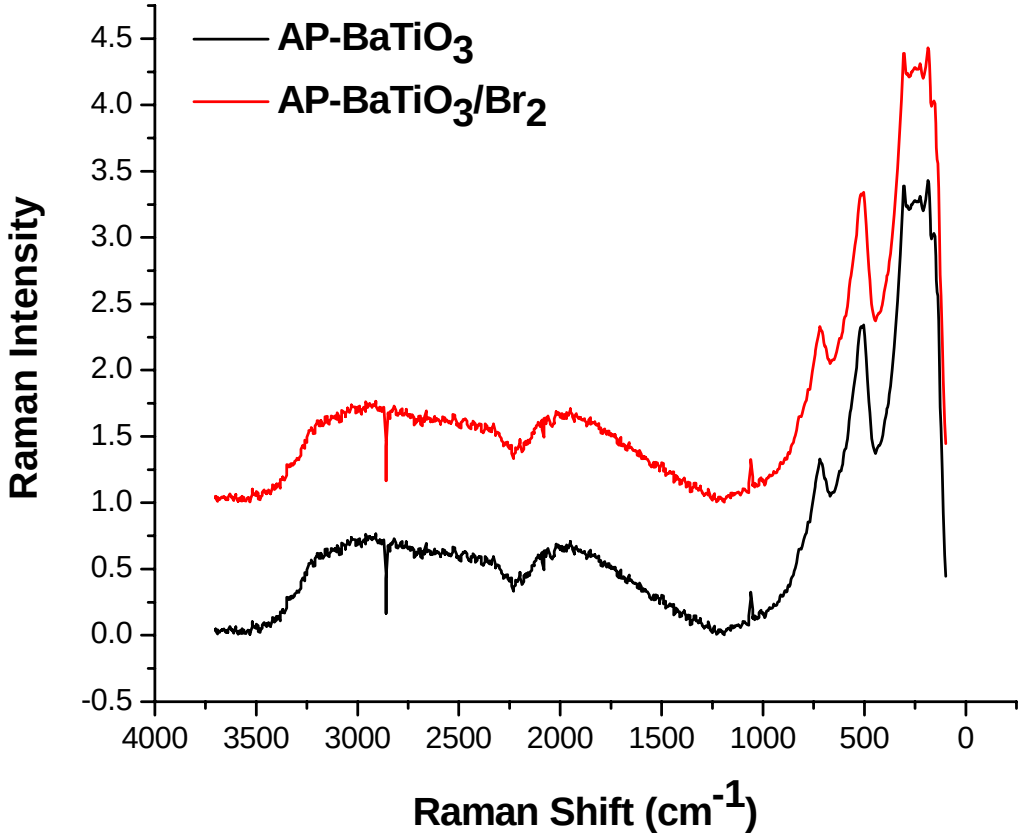

Figure 2.56 Raman spectra of AP-$BaTiO_3$ and AP-$BaTiO_3/Br_2$.

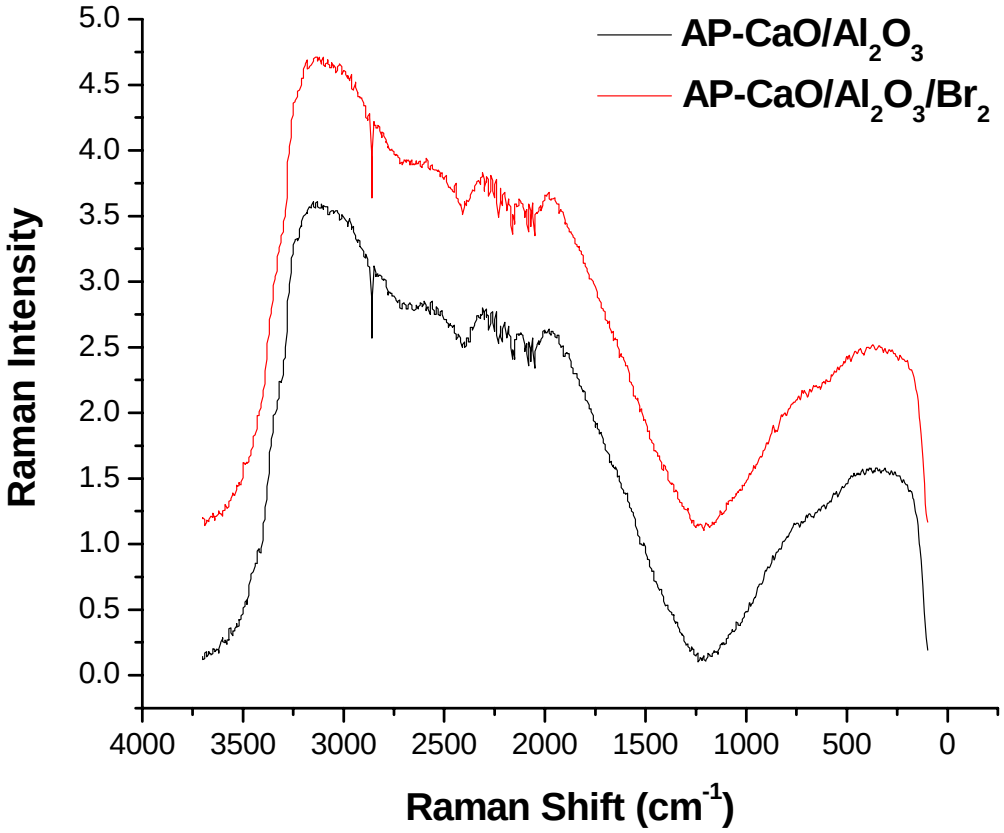

Figure 2.57 Raman spectra of AP-CaO/Al_2O_3 and AP-CaO/Al_2O_3/Br_2.

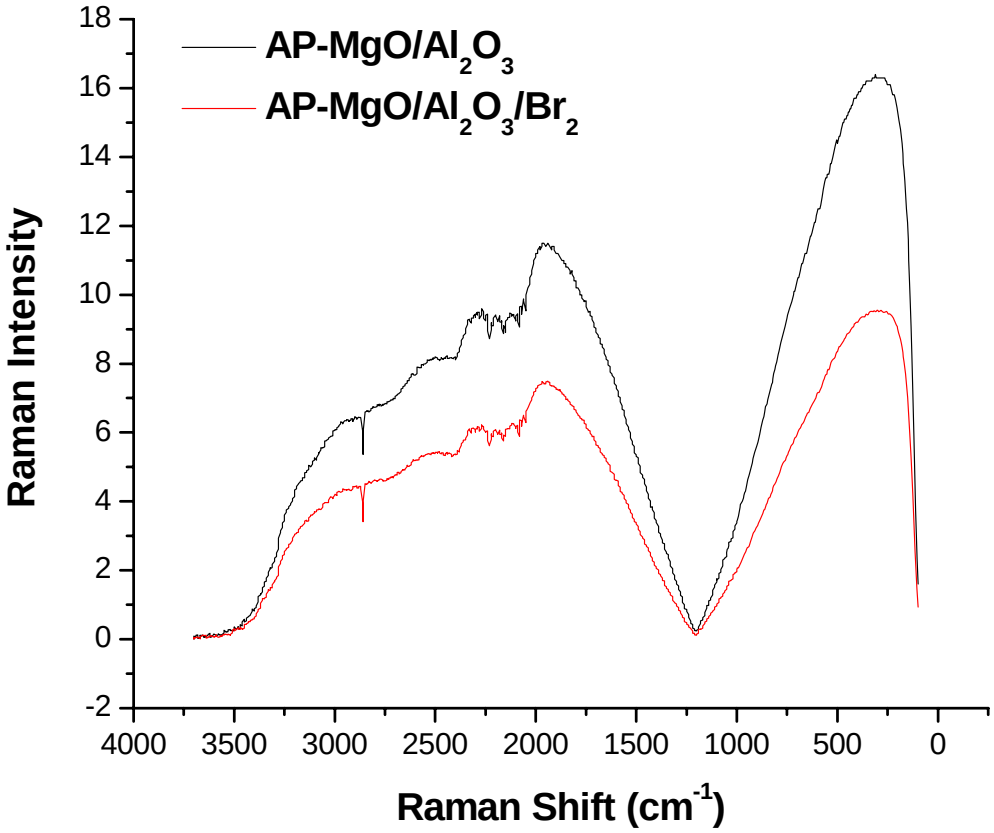

Figure 2.58 Raman spectra of AP-MgO/Al_2O_3 and AP-MgO/Al_2O_3/Br_2.

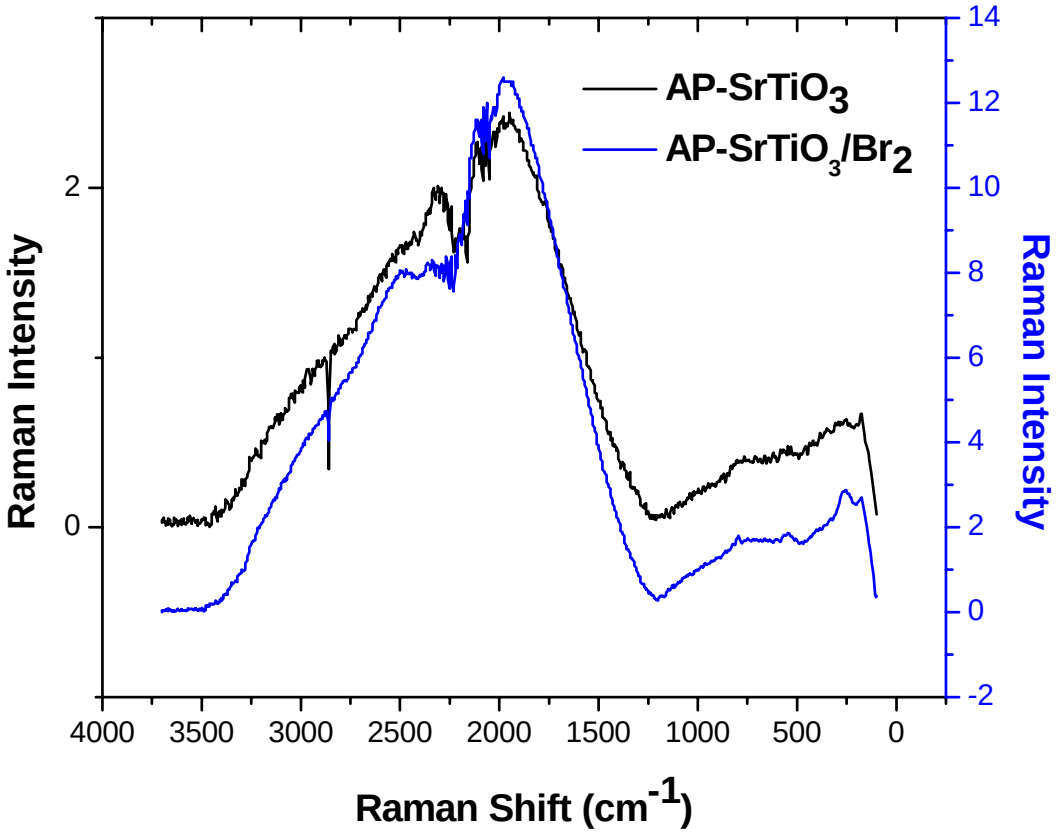

Figure 2.59 Raman spectra of AP-$SrTiO_3$ and AP-$SrTiO_3/Br_2$.

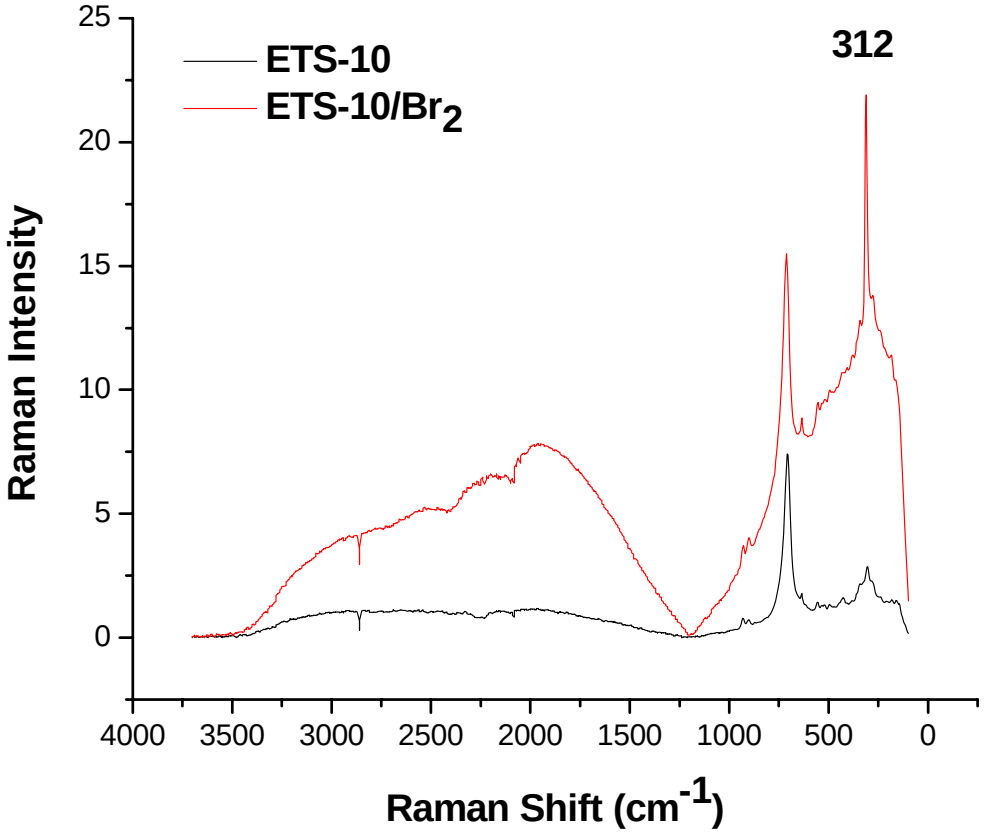

Figure 2.60 Raman spectra of ETS-10 and ETS-10/Br_2.

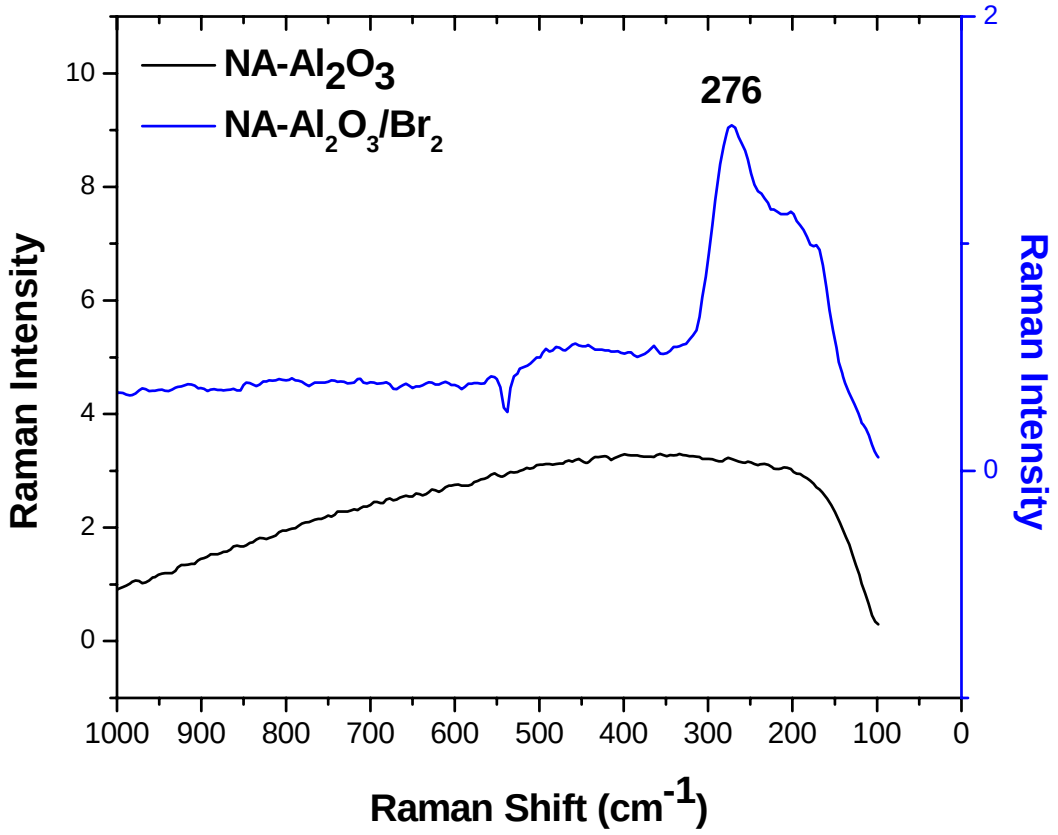

Figure 2.61 Raman spectra of NA-Al_2O_3 and NA-Al_2O_3/Br_2.

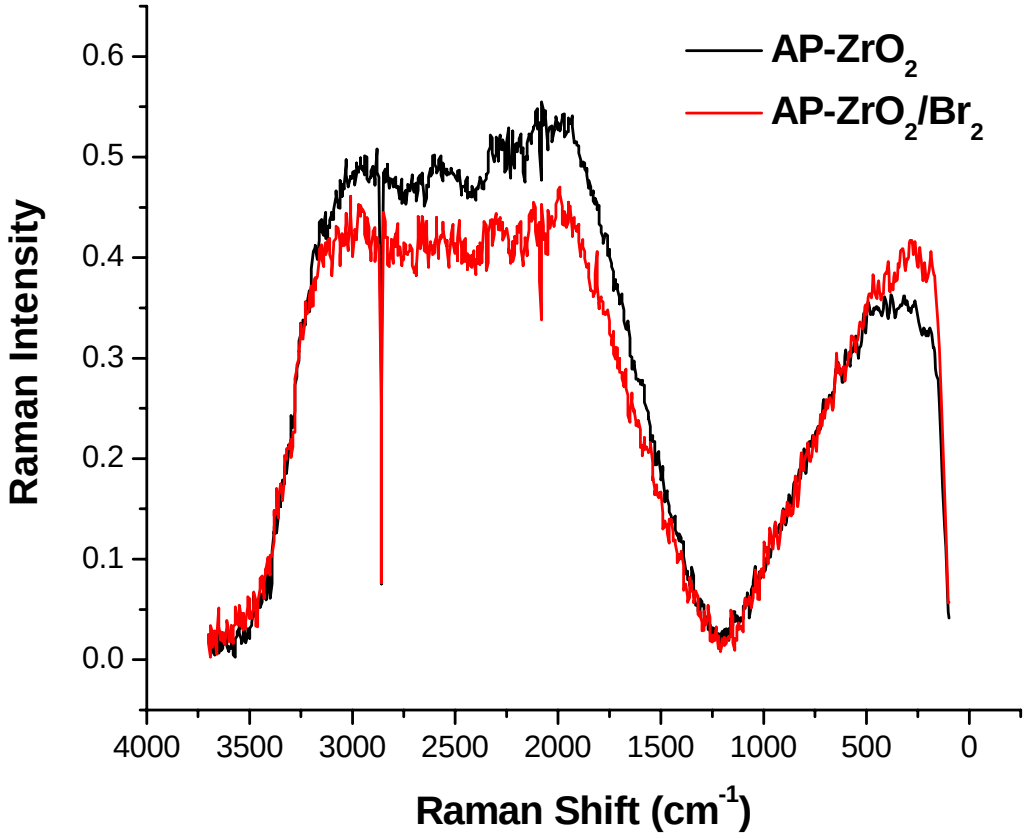

Figure 2.62 Raman spectra of AP-ZrO_2 and AP-ZrO_2/Br_2.

2.4 Conclusions

In this chapter it has been described the straightforward synthesis of halogen (Cl_2, Br_2 and I_2) and interhalogen (ICl, IBr and ICl_3) adducts of mainly three different nanosized metal oxides (NA-Al_2O_3 Plus, NA-TiO_2 and NA-CeO_2), as well as their characterization utilizing several different techniques, including UV-Vis, Raman and X-Ray Photoelectron spectroscopies and Thermogravimetric Analysis. The synthetic procedure can be scaled up and large quantities produced for possible applications such as a safe way to store intact halogen/interhalogen, for use as halogenating agents in organic/inorganic synthetic reactions or in the use as agents against vegetative cells, spores and viruses (discussed more in Chapter 3 and 4).

We conclude that different nanosized metal oxides interact with various adsorbing strengths with the halogen/interhalogens used in our experiments and this can be used to an advantage in the design of an adduct with specific characteristics, such as with a very strong interaction between the ionic metal oxide surface and the halogen/interhalogen, which could be used as a safe way to store intact halogen/interhalogen for longer periods of time. As a contrast, it may be useful to have a weaker interaction between the metal oxide and the halogen/interhalogen to give a potent biocide with a strong oxidizing power of the released halogen/interhalogen. There are many possibilities to fine-tune the adducts and thus for the use of such prepared compounds in various applications.

The prepared adducts show significant differences in their electronic transitions, which along with their altered vibrational frequency values indicate changes in the chemical properties of the prepared adducts, giving rise to new possible applications.

The interaction between the ionic metal oxide surface and the halogen/interhalogen is concluded to be that of a strained halogen/interhalogen bond and with no formation of new

surface species, such as halogen salts. This leads to a weakened halogen/interhalogen bond, causing a lowering of the Raman band for the halogen/interhalogen moiety, which is easily detected. In addition, Raman spectroscopy and XPS also confirm that in some cases, the interhalogen molecules partially decompose upon adsorption on the metal oxide surface, leading to the formation of I_2 and Cl_2 (ICl and ICl_3) or Br_2 (IBr), with the lighter halogen being released from the surface, in the case of ICl and ICl_3.

No evidence of lowering of the Cl_2 stretch is observed for any of the three metal oxide chlorinated adducts investigated. The Cl_2 stretch is not detected at all in the Raman spectrum but rather, the evidence of formation of such chlorinated adducts lie in TGA, smell, increased biocidal activity and EDX analysis (not shown), all indicating that chlorine is present in the adducts, although no Raman peak is observed. The absence of the chlorine peak could possibly be explained by the low polarizability of the chlorine molecule and its low content on the metal oxide surfaces.

Overall, when NA-Al_2O_3 Plus, NA-TiO_2 and NA-CeO_2 are compared, the stability of the prepared halogen/interhalogen adducts varies significantly. When exposed to air, the adducts of NA-TiO_2 are the least stable, whereas the stability of the adducts based on NA-Al_2O_3 Plus and NA-CeO_2 is similar.

Also, in general the strength of interaction with the oxides lies in the order of I_2>ICl>IBr~Br_2>ICl_3. The strength of interaction in the chlorinated adducts is difficult to quantify as these adducts have no significant color change from the starting materials and no halogen peak present in the Raman spectrum.

Furthermore, it was found that not all nanosized materials adsorb and retain halogens onto the surface. The surface area was found to be one important aspect for adsorption; however,

a high surface area did not guarantee halogen adsorption. Other important factors may include pH of the material, acidity and basicity, as well as structure of the surface of the material. The defect sites as well as numerous corners and edges on the studied nanomaterials are believed to be of importance for the adsorption process.

2.5 References

(1) Ranjit, K. T.; Medine, G.; Jeevanandam. P.; Martyanov, I. N.; Klabunde, K. J. *Environ. Catal*. **2005**, 391-420.

(2) Demydov, D.; Klabunde, K. J. NATO *Science Series, II: Mathematics, Physics and Chemistry*. **2005**, *204*, 237-330.

(3) Martin, M. E.; Narske, R. M.; Klabunde, K. J. *Microporous and Mesoporous Materials*. **2005**, *83*, 47-50.

(4) Klabunde, K. J.; Medine, G.; Bedilo, A; Stoimenov, P. Heroux, D. *ACS Symposium Series*. **2005**, *890*, 272-276.

(5) Jeevanandam, P.; Klabunde, K. J.; Tetzler, S. H. *Microporous Mesoporous Mater*. **2005**, *79*, 101-110.

(6) Medine, G. M.; Zaikovski, V.; Klabunde. K. J. *J. Mater. Chem*. **2004**, *14*, 757-763.

(7) Carnes, C. L.; Klabunde, K. J. *J. Mol. Catal. A: Chemical*. **2003**, *194*, 227-236.

(8) Stoimenov, P. K.; Zaikovski, V.; Klabunde, K. J. *J. Am. Chem. Soc*. **2003**, *125*, 12907-12913.

(9) Stoimenov, P. K.; Klinger, R. L.; Marchin, G. L.; Klabunde, K. J. *Langmuir*. **2002**, *18*, 6679-6686.

(10) Koper, O. B.; Klabunde, J. S.; Marchin, G. L.; Klabunde, K. J.; Stoimenov, P. K.; Bohra, L. *Curr. Microbiol*. **2002**, *44*, 49-55.

(11) Sun, N.; Klabunde, K. J. *J. Am. Chem. Soc*. **1999**, *121*, 5587-5588.

(12) Risbood, P. A.; Ruthven, D. M. *J. Am. Chem. Soc*. **1978**, *100*, 4919-4921.

(13) Cooney, R. P.; Tsai, P. *J. Raman Spectrosc*. **1979**, *8*, 195-198.

(14) Tsai, P.; Cooney, R. P. *J. Raman Spectrosc*. **1979**, *8*, 236-238.

(15) Rubim, J. C.; Sala, O. *J. Raman Spectrosc*. **1980**, *9*, 155-156.

(16) Rubim, J. C.; Sala, O. *J. Raman Spectrosc*. **1981**, *11*, 320-321.

(17) Nagasao, T.; Yamada, H. *J. Raman Spectrosc*. **1975**, *3*, 153-160.

(18) Favre, P.; Jayasooriya, U. A.; Powell, D. B. *J. Raman Spectrosc*. **1987**, *18*, 133-135.

(19) Sun, N. Ph.D Thesis in Chemistry; Kansas State University: Manhattan, **1999**.

(20) Stammreich, H. *Physical Review*. **1950**, *78*, 79-80.

(21) Stammreich, H.; Forneris, R. *J. Chem. Phys*. **1954**, *22*, 1624.

(22) Stammreich, H.; Forneris, R.; Tavares, Y. *Spectrochim. Acta*. **1961**, *17*, 1173-1184.

(23) Anderson, A.; Sun, T. S. *Chem. Phys. Lett*. **1970**, *6*, 611-616.

(24) Holzer, W.; Murphy, W. F.; Bernstein, H. J. *J Chem. Phys*. **1970**, *52*, 399-407.

(25) Cahill, J. E.; Leroi, G. E. *J Chem. Phys*. **1969**, *51*, 4514-4519.

(26) Melveger, A. J.; Brasch, J. M.; Lippincott, E. R. *Materials Research Bulletin*. **1969**, *4*, 515-523.

(27) Suzuki, M.; Yokoyama, T.; Ito, M. *J Chem. Phys*. **1969**, *51*, 1929-1931.

(28) Suzuki, M.; Yokoyama, T.; Ito, M. *J Chem. Phys*. **1969**, *50*, 3392-3398.

(29) Anthonsen, J. W. *Spectrochim. Acta*. **1976**, *32A*, 963-970.

(30) Stammreich, H.; Kawano, Y. *Spectrochim. Acta*. **1968**, *24A*, 899-904.

(31) Brooks, W. V. F.; Crawford, B., Jr. *J Chem. Phys*. **1955**, *23*, 363-365.

(32) Herzberg, G. Spectra of Diatomic Molecules, 2nd ed.; D. Van Nostrand, Company, Inc.: New York, **1950**.

(33) Person, W. B.; Humphrey, R. E.; Deskin, W. A.; Popov, A. I. *J. Am. Chem. Soc*. **1958**, *80*, 2049-2053.

(34) Person, W. B.; Erickson, R. E.; Buckles, R. E. *J. Am. Chem. Soc*. **1960**, *82*, 29-34.

(35) Klaboe, P. *J. Am. Chem. Soc*. **1967**, *89*, 3667-3676.

(36) Kimel'fel'd, Ja. M.; Mostovoy, A. B.; Mostovaja, L. M. *Chem. Phys. Lett*. **1975**, *33*, 114-117.

(37) Loo, B. H.; Lee, Y. G. *J. Phys. Chem*. **1984**, *88*, 706-709.

(38) Person, W. B.; Humphrey, R. E.; Popov, A. I. *J. Am. Chem. Soc*. **1959**, *81*, 273-277.

(39) Heaviside, J.; Hendra, P. J.; Tsai, P.; Cooney, R. P. *J. Chem. Soc., Faraday Transactions 1*. **1978**, *74*, 2542-2549.

(40) Cooney, R. P.; Tsai, P. *J. Raman Spectrosc*. **1979**, *8*, 195-198.

(41) Rubim, J. C.; Sala, O. *J. Raman Spectrosc*. **1981**, *11*, 320-321.

(42) Favre, P.; Jayasooriya, U. A.; Powell, D. B. *J. Raman Spectrosc*. **1987**, *18*, 133-135.

(43) Evans, J. C.; Lo, G. Y-S. *Inorg. Chem*. **1967**, *6*, 1483-1486.

(44) Person, W. B.; Anderson, G. R.; Fordemwalt, J. N.; Stammreich, H.; Forneris, R. *J. Chem. Phys.* **1961**, *35*, 908-914.

(45) Brown, L. C.; Begun, G. M.; Boyd, G. E. *J. Am. Chem. Soc*. **1969**, *91*, 2250-2254.

(46) Chantry, G. W.; Plane, R. A. *J. Chem. Phys*. **1961**, *34*, 1268-1271.

(47) Levason, W.; Ogden, J. S.; Spicer, M. D.; Young, N. A. *J. Chem. Soc., Dalton Transactions: Inorg. Chem*. **1990**, *1*, 349-353.

(48) Beattie, I. R.; Horder, J. R. *J. Chem. Soc*. **1969**, *17*, 2655-2659.

(49) Kiefer, W.; Bernstein, H. J. *Chem. Phys. Lett*. **1972**, *16*, 5-9.

(50) Maki, A. G.; Forneris, R. *Spectrochim. Acta*. **1967**, *23A*, 867-880.

(51) Stammreich, H.; Forneris, R. *Spectrochim. Acta*. **1960**, *16*, 363-367.

(52) McCarthy, M. I.; Gerber, R. B.; Shapiro, M. *J. Chem. Phys.* **1990**, *92*, 7708-7715.

(53) Gillam, A. E.; Morton, R. A.; *Proceedings of the Royal Society of London*. **1929**, *A124*, 604-616.

(54) Acton, A. P.; Aickin, R. G.; Bayliss, N. S. *J. Chem. Phys.* **1936**, *4*, 474-479.

(55) Gray, R. I.; Luckett, K. M.; Tellinghuisen, J. *J. Phys. Chem A.* **2001**, 105, 11183-11191.

(56) Seery, D. J.; Britton, D. *J. Phys. Chem.* **1964**, *68*, 2263-2266.

(57) Wren, J. C.; Paquette, J.; Sunder, S.; Ford, B. L. *Can. J. Chem.* **1986**, *64*, 2284-2296.

(58) Gibson, G. E.; Ramsperger, H. C. *Phys. Rev*. **1927**, *30*, 598-607.

(59) Binder, J. L. *Phys. Rev*. **1938**, *54*, 114-117.

(60) Nebeker, E. B.; Pings, C. J. *J. Phys. Chem.* **1965**, *69*, 2483-2484.

(61) Rogers, L. J.; Ashfold, M. N. R.; Matsumi, Y.; Kawasaki, M.; Whitaker, B. J. *Chem. Phys. Lett.* 1996, 258, 159-163.

(62) Jiang, X-P.; Shapiro, M.; Brumer, P. *J. Chem. Phys.* **1996**, *105*, 3479-3485.

(63) McCarthy, M. I.; Gerber, R. B. *J. Chem. Phys.* **1990**, *93*, 887-893.

(64) Kolodney, E.; Amirav, A.; Elber, R.; Gerber, R. B. *Chem. Phys. Lett.* **1984**, *111*, 366-371.

(65) Gerber, R. B.; Amirav, A. *J. Phys. Chem*. **1986**, *90*, 4483-4491.

(66) Iida, Y.; Furukawa, M.; Aoki, T.; Sakai, S. *Appl. Spectrosc*. **1998**, *52*, 673-678.

(67) Niilisk, A.; Moopel, M.; Pärs, M.; Sildos, I.; Jantson, T.; Avarmaa, T.; Jaaniso, R.; Aarik, J. *Central European Science Journals of Physics*. **2006**, *4*, 105-116.

(68) Domae, M.; Tani, J-I.; Fujiwara, K.; Katsumura, Y. *J. Nucl. Sci. Technol*. **2006**, *43*, 675-680.

(69) Clark, R. J. H.; Hunter, B. K.; Rippon, D. M. *Inorg. Chem*. **1972**, *11*, 56-61.

(70) Clark, R. J. H.; Mitchell, P. D. *J. Am. Chem. Soc*. **1973**, *95*, 8300-8304.

(71) Clark, R. J. H.; Willis, C. J. *J. Chem. Soc. [section] A: Inorganic, Physical, Theoretical*. **1971**, *6*, 838-840.

(72) Shyu, J. Z.; Weber, W. H.; Gandhi, H. S. *J. Phys. Chem*. **1988**, *92*, 4964-4970.

(73) Sathyamurthy, S.; Leonard, K. J.; Dabestani, R. T.; Paranthaman, M. P. *Nanotechnology*. **2005**, *16*, 1960-1964.

(74) Ho, C.; Yu, J. C.; Kwong, T.; Mak, A. C.; Lai, S. *Chem. Mater*. **2005**, *17*, 4514-4522.

(75) Yan, B.; Zhao, W. *J. Adv. Mater*. **2006**, *Special Issue 1*, 44-47.

CHAPTER 3 - Biocidal Properties of Metal Oxide Nanoparticles and their Adducts

3.1 Introduction

In Chapter 2, it was demonstrated that halogen (Cl_2, Br_2 and I_2) and interhalogen (ICl, IBr and ICl_3) adducts of nanosized metal oxides, such as NA-Al_2O_3 Plus, NA-TiO_2 and NA-CeO_2, have been successfully prepared and characterized. These adducts showed various strengths of adsorption and in this chapter it will be described how the strength of adsorption affects the biocidal activity of these prepared adducts.

Two different methods have been used to test the bactericidal activity: 1) a water-suspension method, and 2) a membrane method. In especially the latter one the surface of the material used will be a very important factor, which gives nanomaterials a significant advantage with their high surface area, many defect sites like corners and edges, and in general abrasive character. A solid interaction depends mainly on the surface morphology and the more of the surface exposed, the more interaction, leading to a hopefully better biocidal activity.

There are many types of microorganisms of interest that could be studied, such as bacteria, spores, viruses, fungi and so on. Our attention was focused on mimics of biological warfare agents and also of common bacteria that represents different bacteria classes. In the next chapter the interaction of these prepared adducts with viruses will be discussed as well.

The organisms studied in this chapter include *Escherichia coli* (*E. coli*), a Gram-negative rod-shaped bacterium, *Bacillus megaterium* (*B. megaterium*), a Gram-positive rod-shaped

bacterium, *Bacillus subtilis* (*B. subtilis*), an endospore forming Gram-positive bacterium and the Δ sterne strain of *Bacillus anthracis* (*B. anthracis*), an endospore forming bacterium and the cause of the terrorist attack agent anthrax.

Different groups of bacteria were chosen to see if the interaction with the nanoparticles were the same for the two different groups of bacteria. The main difference between the two bacteria groups lies in the structure of the cell wall. It was believed that this slight difference might lead to a differentiation in the biocidal results as the interaction takes place first at the surface of the cell. No such difference was found, but a higher concentration of bacteria might need to be studied in order to find such results.

As expected, the spores were much more resistant against nanoparticle treatment than the different bacteria were. The structural difference between a bacteria and a spore is that the spore has a very thick and chemically resistant spore coat, composed of a variety of proteins, which protects the spore from harsh environments.

3.2 Bacterial Structure and Properties

This section will cover a detailed discussion of the structures of Gram-negative and Gram-positive bacteria, as well as of endospores. It is very important to know what their structures consist of as that is related to the bactericidal activity of the organisms.

Many researchers have paid special attention to the mechanism in which bacteria and spores die, however, there are very many possible mechanisms and especially with spores, it is most often unknown what the mechanism is. Sometimes very specific actions of the bactericide occur but other times there is a very general action that can affect many systems of the cell,

eventually leading to death. One example of a bactericide with a specific action is one where the process of building the cell envelope is completely blocked or significantly slowed down, which leads to alterations of the cell membrane and hindering the reproduction.[1] Halogens that have oxidizing powers however, have a more general activity that is not limited to only the cell membrane, but that rather affects all systems in the cell.[2-5]

Most bactericides interact with major chemical pathways of the cell. Many antibiotics, for example, suppress the protein synthesis, whereas heavy metal ions bind to the sulfhydryl groups of important enzymes, eventually leading to cell death. Another major example of cell death cause is damage to the cell membrane, which then could lead to cell leakage of the internal content. However, depending on the severity of the damage, the cell might not die if the environment is favorable. On the other hand, the cell could easily be killed by other factors now when the membrane is already slightly damaged. This process where a cell or spore is damaged and more susceptible to death is called sensitization. This concept becomes very important in the case of spores, where a combination of two agents is often much more efficient than one agent alone, and very often necessary.[6-19]

Nanoparticles have, as discussed previously, very different surface morphology as compared to their micron-sized counterparts. This leads to an expectation that the nanoparticle surface-cell membrane interaction would be the major one that will determine the activity of the nanoparticles. In addition, the active halogen/interhalogen on the surface of the particles will carry an oxidizing power with them, further increasing the activity of the material. The size of the nanoparticles themselves however, is much too large to directly penetrate a healthy cell membrane.

3.2.1 Gram-Negative Bacterial Cells

The main difference in Gram-positive and Gram-negative cells lies in their cell wall (see Figure 3.1 and 3.2). Gram-negative bacteria have a composition very different from that of Gram-positive bacteria in that they have an outer membrane.[20] This outer membrane is part of the cell wall and it contains lipopolysaccharide and lipids. The outer membrane also contains porins, which act like pores for particular molecules (very small ones). Inside this outer membrane the cell wall has only a few layers of peptidoglycan and little cross-linking between them (as compared to Gram-positive bacteria that has a much thicker layer). Inside the peptidoglycan layer there is a small space that separates the layer from the secondary cell membrane, also called the periplasmic space. The surface of Gram-negative cells is very hydrophobic, which prevents many biocides to get enough contact with the cells. Most Gram-negative bacteria do not form endospores, although exceptions do exist.

The name Gram-negative arose from a staining technique (Gram-staining) that distinguishes between the two classes of bacteria, namely Gram-negative and Gram-positive. Gram-negative bacteria do not retain the crystal violet dye stain that binds to all negatively charged groups after washing with ethanol, because of the limited thickness and chemical composition of the cell wall. However, Gram-negative bacteria interact with the counterstain (normally safranin), since they still have a lot of available negative groups and then pick up a red or pink color. Gram-positive bacteria however, already have their negative charges interacting with the crystal violet and hence remain violet.

Examples of Gram-negative bacteria are *Escherichia coli* and species from the *Salmonella* family. *E. coli* was chosen as the representative for this class of organisms as it has

been widely studied in microbiology and is probably the most common bug that chemists work with. There are many research works available for comparisons. The strain investigated was C3000, but there are a variety of strains available. We did not attempt to study any other strains in this work.

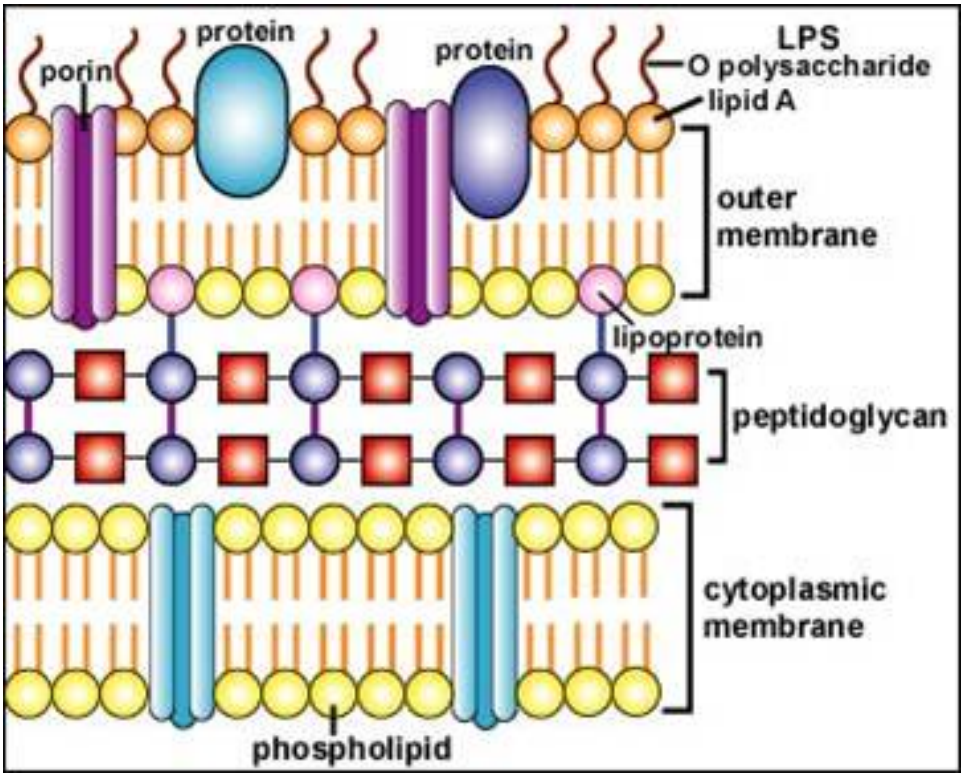

Figure 3.1 Scheme of the Gram-negative cell wall.[21]

3.2.2 Gram-Positive Bacterial Cells

The cell wall of Gram-positive bacteria is slightly different,[20] mainly due to the lack of an outer cell membrane. However, the cell wall is still very thick, in fact much thicker than that of a Gram-negative cell wall, because of its extremely dense and severely cross-linked peptidoglycan layer. Inside the peptidoglycan layer is a thin cytoplasmic membrane.

Examples of Gram-positive bacteria are those belonging to the *Bacillus*, *Staphylococcus* and *Chlostridium* families. Out of these we have studied some of the species belonging to the aerobic *Bacillus* family, namely *B. megaterium*, *B. subtilis* and a benign strain of *B. anthracis*. *B. subtilis* is an important model organism that has been studied widely, often because of its similarity in composition to *B. anthracis*. *B. anthracis* is of interest because of its ability to cause anthrax, the very dangerous food, air and water born biological warfare agent.

Many Gram-positive organisms have the ability to convert into endospores (spores), during exposure to restricted conditions such as heat, drying, freezing, or lack of nutrients. The organisms in the *Bacillus* family are examples of spore-forming bacteria. Once converted into spores, the organisms are much more resistant to harsh environments such as chemical and physical treatments, as will be discussed later.

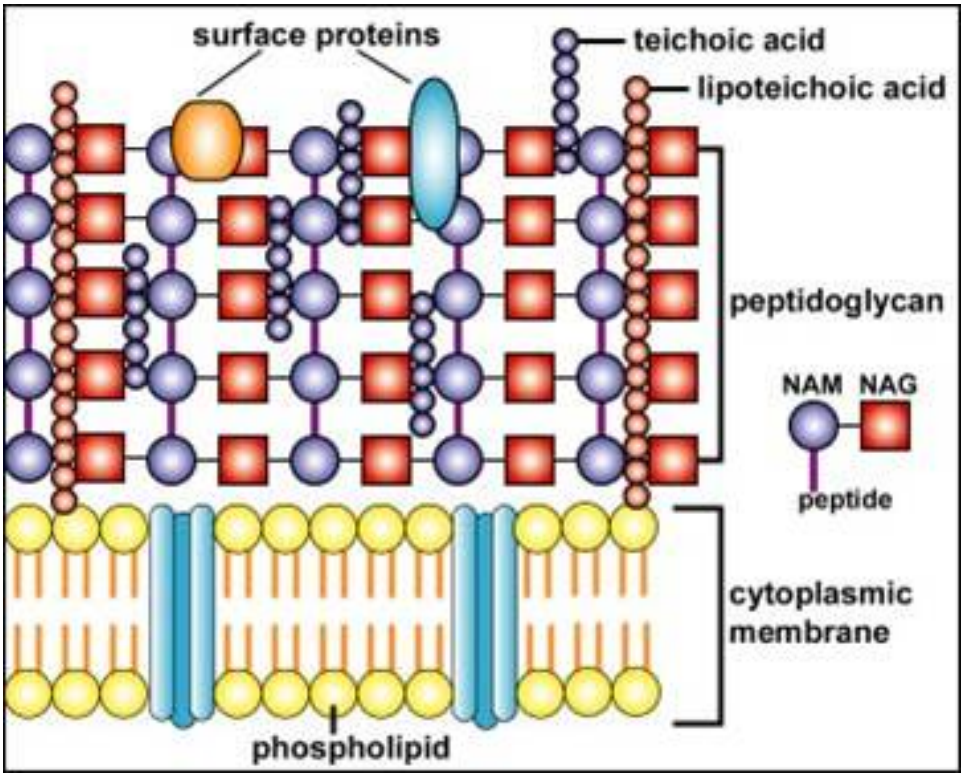

Figure 3.2 Scheme of the Gram-positive cell wall.[21]

3.2.3 Bacterial Endospores

The purpose of endospore formation is to enable the cell to survive harsh environmental conditions.[20] Unlike vegetative cells (Gram-positive and Gram-negative cells), endospores are not associated with growth, metabolism and reproduction. Under nutrient-limiting conditions (such as lack of nutrient media), some types of bacteria have the ability to form a resistant, dormant cell type, called an endospore. The name originates from the fact that the spore is formed within the cell.

The main difference between a spore and a cell is that the spore contains only about 15% water, whereas a cell contains about 70%. This low water content leads to a lack of reproduction in spores. Another major difference between a cell and a spore lies in the outer protection, which is in the cell wall versus the spore wall. The spore wall consists of several layers making it very difficult for a disinfectant to penetrate into the actual spore (Figure 3.3). Every layer has a different composition and hence different properties. In order to kill the spore, the disinfectant needs to be able to reach the genetic material in the core structure, which requires the need to penetrate all the different layers of the spore wall. These layers are often resistant to different kinds of treatments, leading to the need for a combination of more than one disinfectant, or a disinfectant with more than one penetrative property. The various layers in the spore wall include the exosporium, which overlies the spore coat (absent in some spores). The spore coat is the main barrier for many toxic molecules as they can not penetrate through it. Beneath the spore coat lies the cortex, which consists of peptidoglycan. Beneath the cortex lies the core wall, which surrounds the protoplast or core of the endospore.

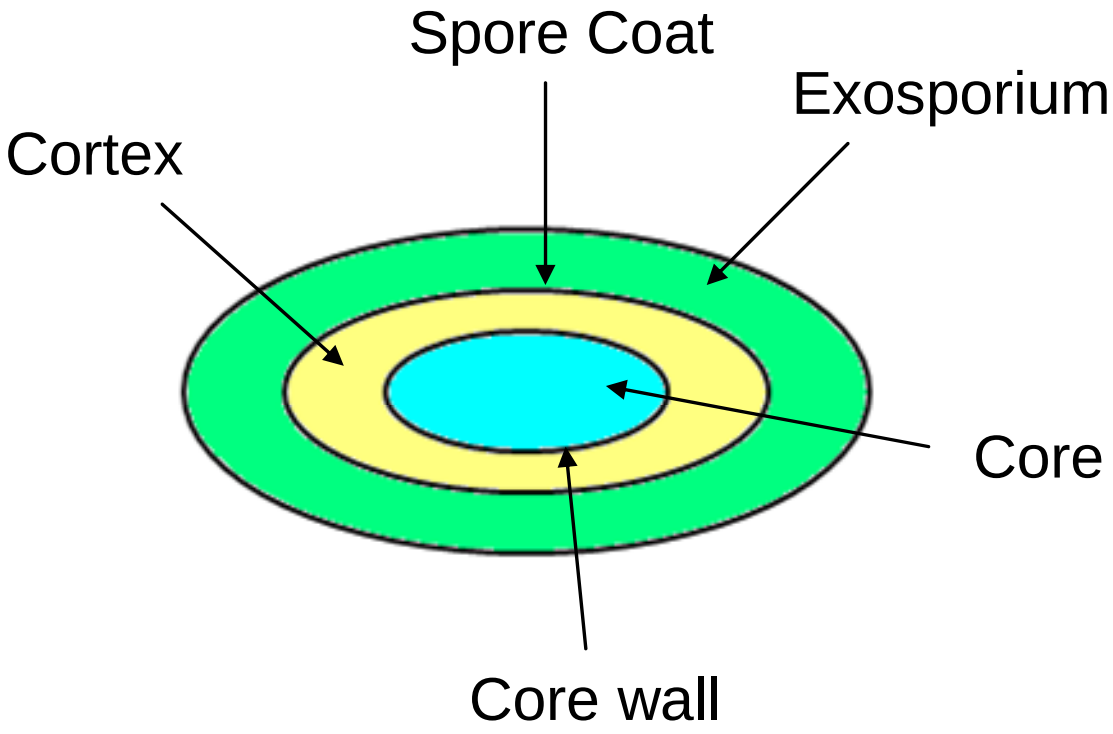

Figure 3.3 Schematic presentation of a typical spore.

The procedure in which a cell converts into a spore is a complex process that contains several steps.[20] The first step involves replication of nucleic acid to form two complete sets of DNA. The second step consists of invagination of the plasma membrane to form the spore septum that separates the two sets of DNA. Thirdly, the forespore is developed and in step four, it is engulfed, which means that the core is surrounded by the spore cell wall and the cortex. Then the spore coat is formed and in some cases, an exosporium around the spore. Lastly, the endospore is released through lysis of the sporangium.

The survival of spores against drying, heating and UV-radiation is poorly understood. Bacterial endospores are however about 10,000 times more resistant to heat and 100 times more resistant to UV radiation than vegetative cells.

3.3 Experimental Methods

3.3.1 Optical Microscopy

Optical microscopy was used as the first tool to check if spores were formed. A Nikon Eclipse TE200 microscope with a Nikon Coolpix 995 attached camera was used. Further, the spores were identified using Transmission Electron Microscopy (TEM).

3.3.2 Preparation of a Bacterial Culture

Escherichia coli strain C3000 and *Bacillus megaterium*, ATCC 14581, were obtained from ATCC. *Bacillus subtilis* spores ATCC 6633 were purchased from Raven Biological Labs.

E. coli and *B. megaterium* (either a small amount of previously prepared liquid bacterial culture or a single colony from a Petri dish) were added to a sterile flask, containing 25-100 mL Luria Broth (LB) nutrient. The solution was typically agitated under aerobic conditions for 12-24 hrs. on a shaker-thermostat at 37°C. At that moment the flask contained a turbid suspension of bacteria cells with a concentration between 10^6-10^9 Colony Forming Units (CFU)/mL. For some of the experiments a more precise concentration was desired, in order to use the same concentration for several experiments. Further, this attempt included the use of the cells in their log phase, versus stationary phase. At those times, 100 μL of previously prepared culture was inoculated in 100 mL LB broth and left over night. At 8 am the following morning, 50 μL of the previously grown overnight culture (ON culture) was extracted and added to 50 mL of fresh LB broth and agitated at 37°C on a shaker thermostat. At certain time intervals, samples were extracted, and their optical density (OD) was measured at 420 nm. During these time intervals, aliquots were also plated to determine CFU/mL at each time interval. Graphs were prepared, including an OD versus Time (hrs) graph and CFUs versus Time (hrs).

B. subtilis spore suspension was used as received with the concentration already determined by Raven Biological Labs.

B. anthracis, Δ Sterne strain, vegetative cells were prepared in a similar manner as *E. coli* cells, described above.

B. anthracis spores, Δ Sterne strain, were prepared using two different techniques. To prepare small amounts for testing procedures, 100 μL of *B. anthracis* culture was added to a nutrient agar plate and incubated for 5-15 days (depending on how thick the agar on the plate was), until no nutrients remained and sporulation had occurred. The spores were then suspended in 3 mL PBS buffer and centrifuged at 2500 rpm to obtain a pellet. The supernatant was

discarded and the pellet was resuspended in 10 mL of PBS buffer, vortexed and centrifuged again. This washing procedure was repeated three times and finally the spores were stored at room temperature in PBS buffer until used. In order to prepare larger amounts of highly concentrated spore suspensions for TEM imaging, 100 μL of *B. anthracis* culture was added to 50 mL LB broth and the solution was agitated under aerobic conditions over night on a shaker-thermostat at 37°C. The next day 3 mL of the ON culture was inoculated in 300 mL LB broth and this new solution was agitated under aerobic conditions for three-four days on a shaker-thermostat at 37°C. To kill any remaining vegetative cells, the solution was heated at 80°C for 30 minutes. The solution was then poured into pre-sterilized centrifuge tubes and stored at room temperature until use. To minimize cross-contamination, the tubes were sprayed frequently with ethanol, especially before handling of the spore solutions.

Throughout all culture preparations and handling, special care was taken to make sure no contamination occurred. This included using sterile glass ware, needles and syringes throughout all the experiments. The used glassware was autoclaved before use at 121 °C for 20 minutes to ensure that all microorganisms were dead. Syringes and needles were purchases pre-sterilized and used as received.

3.3.3 Bacteriological Test Procedure

Several different test procedures were used to determine the biocidal and sporicidal activity during this study. The most widely used ones include the water suspension method and the membrane method, both described below.

3.3.3.1 Water Suspension Method

Vegetative cells or spores were diluted in Millipore water to a concentration between 10^2 and 10^4 CFU/mL. 50 mg each of the metal oxide sample was added to 1 mL of bacteria or spore solution in a sterile test tube, vortexed and left to sit for 5 minutes. The samples were then centrifuged at 2500 rpm at 4°C for about 2 minutes and three aliquots of 100 µL were extracted from each supernatant and plated on Petri dishes, containing nutrient agar. The agar plates were incubated for 24 hrs at 37°C, the colonies formed were counted and percent kill or log reduction values calculated (Log Reduction = Log_{10} (c_0/c), where c_0 = initial concentration of cells/spores used for the experiment, and c = concentration of cells/spores after treatment with metal oxides at measured time). The counts on the three plates were averaged and the experiment was performed at least two different times. An average value was calculated and reported.

3.3.3.2 Membrane Method

Vegetative cells or spores were diluted to desirable concentration (normally in the order of 10^3-10^9 CFU/mL, depending on organism and nanoparticles used). This was very easy with the *B. subtilis* spore solution as its concentration already had been determined by Raven Biological Labs. An approximate concentration was predictable of *E. coli* and *B. anthracis* through measuring the UV absorbance of the cells (as described in **3.3.2**).

For each experiment, sterile individually wrapped nitrocellulose water membranes (Millipore) with a pore diameter of 0.45 µm (*E. coli*) or 0.22 µm (*B. subtilis* and *B. anthracis*

spores) were used to retain the bacteria cells or spores. Different pore diameters were needed since the standard pore diameter of 0.45 μm was found to be too large to retain the spores.

Before the experiments, the Fisher Scientific filtering system, including removable funnels, were washed with 70% ethanol to avoid contamination from other organisms. Everything was then rinsed with Distilled water several times, to ensure complete removal of ethanol. Each filter used was moistened before use by submerging it into a beaker containing Distilled water. The filter was then positioned in the filtering system and approximately 30 mL Distilled water was added. With the filtering system still off, the desired amount of bacteria or spores was added (normally 100 μL). The filtering system was started and the bacteria or spores retained on the filter paper. The filter paper was then carefully removed using special tweezers and allowed to partially dry on a clean paper towel with the inoculated side of the filter upwards. The filtering system contained three funnels so this step was repeated until the desired amounts of filter papers were obtained.

To avoid sticking of the nanoparticles to the filter membranes, the filters needed to be partially or completely dried. However, it was found that if the filter membranes with *E. coli* completely dried, then the cells died. In the case of vegetative cells, the filters were only partially dried (15 minutes) because of this. In the case of spores the filter membranes were completely dried (45 minutes), as spores are not sensitive to drying. To make sure that no false results were obtained, a control filter membrane that underwent the exact same treatment as the nanoparticle-treated ones, except for the addition of nanoparticles was always used. After drying, nanoparticles were added directly on the filters, completely covering the inoculated area. The particles were left for 30 minutes, and then carefully tapped off. To get rid of the possible remaining halogens/interhalogens, the filter was put in the filtering system and washed with a

small amount of 5 wt. % sodium thiosulfate solution. Without this step, false good results could arise from the remaining halogen suppressing the growth of survived bacterial cells or spores. The filter membranes were then deposited directly onto agar plates and incubated for 24 hrs. The nutrients from the agar penetrate easily due to capillary forces and bacteria form colonies even if they are not in direct contact with the nutrient surface. The colonies that were formed were then counted and the results averaged, since each nanoparticle formulation was tested in duplicate or triplicate. The experiment was later repeated at least one more time and the results averaged. The results were compared to the control plates and percent kill or log reduction values were calculated. The log kill values have standard deviation values less than one and most of them have a standard deviation less than ±0.5.

3.3.4 Malachite Green Stain

The malachite green stain,[22] or more commonly called spore stain, is a fast way to determine if spores have been formed. It is a very fast procedure in which the culture is air-dried and heat-fixed using a flame on a glass slide. A beaker containing water is prepared and put on a hot plate to boil so that water steam is coming up from the water. The heat is then reduced to a slightly boil. A wire stain rack is placed over the steaming water. A small piece of paper covering the glass slide is put on top of the slide that is on the wire stain rack. The paper towel will keep the dye from evaporating too quickly, thereby increasing the contact time between the cells/spores and the dye. Add the malachite green dye to the paper towel; keeping the towel moist at all times with the dye (keep adding dye) and leave for 5 minutes. The paper towel is then discarded and the smear is washed very thoroughly with water. If desired, a counterstain can

be applied (normally safranin) for one minute and then the smear is washed again. The spores will appear green if viewed under the microscope. If a counterstain is applied, the vegetative cells will be pink. A schematic of the procedure can be seen in Figure 3.4, where a) shows a heat-fixed culture on a glass slide, covered by a paper towel; b) addition of malachite green stain to the paper towel; c) water steam helping the dye penetrate the spore walls and d) washing of slide with water and if necessary pat dry the slide using blot-free paper.

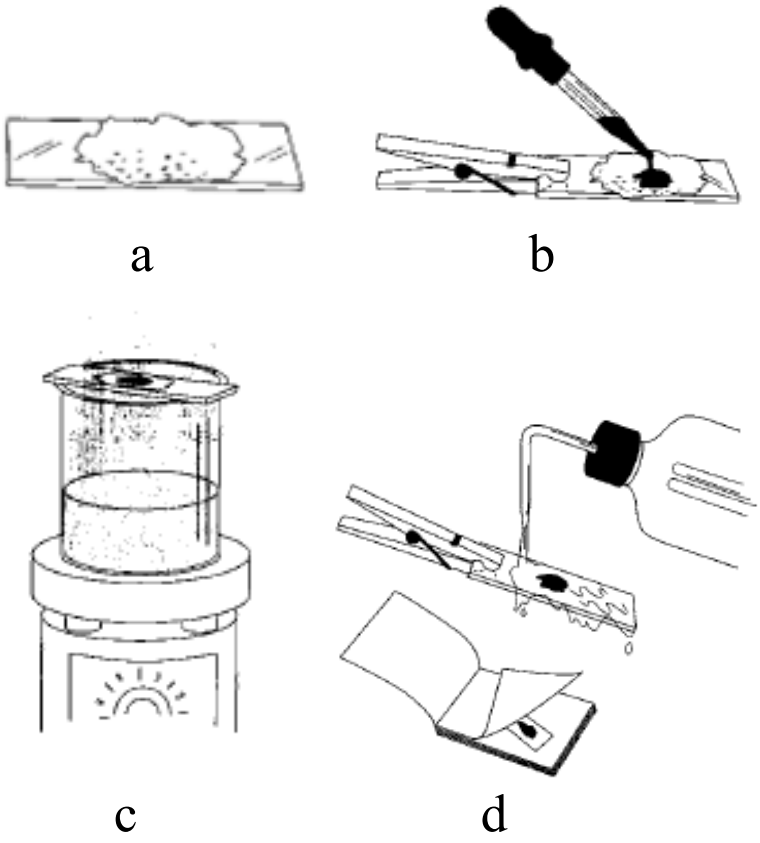

Figure 3.4 Schematic of the Malachite Green Staining Procedure.[22]

3.3.5 Transmission Electron Microscopy (TEM)

TEM images were recorded on a Philips CM 100, operating at 100kV.

In order to obtain 'good' control images of *E. coli* and *B. anthracis* cells, it was very important to catch the cells in their log phase growth and not in their stationary growth phase, where cells are weaker and many even dead. The best TEM images of *E. coli* cells were found to be obtained after the following procedure: 100 μL of an old *E. coli* suspension was inoculated in 50 mL LB broth in a shaker at 37°C for 6 hours. The entire fresh culture was centrifuged and re-suspended in PBS buffer and kept for further treatments. The best TEM images of *B. anthracis*, Δ Sterne strain cells, were found to be obtained after the following procedure: one single colony from agar plate, containing *B. anthracis* cells, was inoculated in 50 mL LB broth in a shaker at 37°C for 11 hours. 35 mL of this overnight culture was centrifuged and re-suspended in PBS buffer.

After re-suspension of the different cells (*E. coli* and *B. anthracis*) and spores (*B. subtilis* and *B. anthracis*) in PBS buffer, each one of the obtained pellets was dissolved in 2 mL DI water, vortexed and divided into two equal parts in eppendorf tubes. One of the tubes served as the control sample and the other one was used for nanoparticle treatment. NA-Al_2O_3/ICl_3 Plus was added to one of the tubes, vortexed and left to interact for 60 minutes. Both tubes were then centrifuged, decanted and washed five times with 0.1 M freshly prepared (less than 2 hours old) ascorbic acid solution. The pellets were then washed with DI water, centrifuged and decanted. The control and nanoparticle-treated pellet cells/spores were then immersion fixed with 2 % glutaraldehyde and left over night with constant rotation. The samples were then washed with sodium cacodylate buffer a total of three times, each time for five minutes and with constant

rotation in order to remove all the glutaraldehyde. During each washing, the pellet was resuspended in the buffer. The pellets were resuspended and post-fixed with 0.1 mL of 1 % osmium tetraoxide solution, under constant rotation for 1.5 hrs. The pellets were then washed three times for five minutes each with sodium cacodylate buffer under constant rotation, each time the pellets were resuspended. At this time, the resin was removed from the freezer to soften for later use. The samples were then gradually dehydrated with increasing concentrations of acetone, each concentration for five minutes. 0.5 mL each of 50, 60, 70, 80, 90, 95 and 100 % acetone was used to resuspend the pellet and this step was also done under constant rotation. If needed, the resin was put in an oven to soften even more for easy handling. Further, the pellets were gradually embedded in resin: firstly a 1:1 resin: acetone mixture was used and secondly a 1:2 acetone: resin mixture was used, each for about 10-15 minutes. Finally, approximately 250 μL pure resin was added to each pellet and the eppendorf tube was sealed and put in an oven, upright, to polymerize. The samples were later cut with a microtome diamond knife and viewed in the electron microscope.

3.4 Results and Discussion

3.4.1 Optical Microscopy

As a quick indicator that spores were formed, the malachite green stain was performed on *B. subtilis* and *B. anthracis*, Δ Sterne strain spores, before TEM preparation and imaging and before experiments were performed. Figure 3.5 shows *B. anthracis*, Δ Sterne strain, spores after staining with Malachite Green dye. It can be clearly seen that spores have been formed.

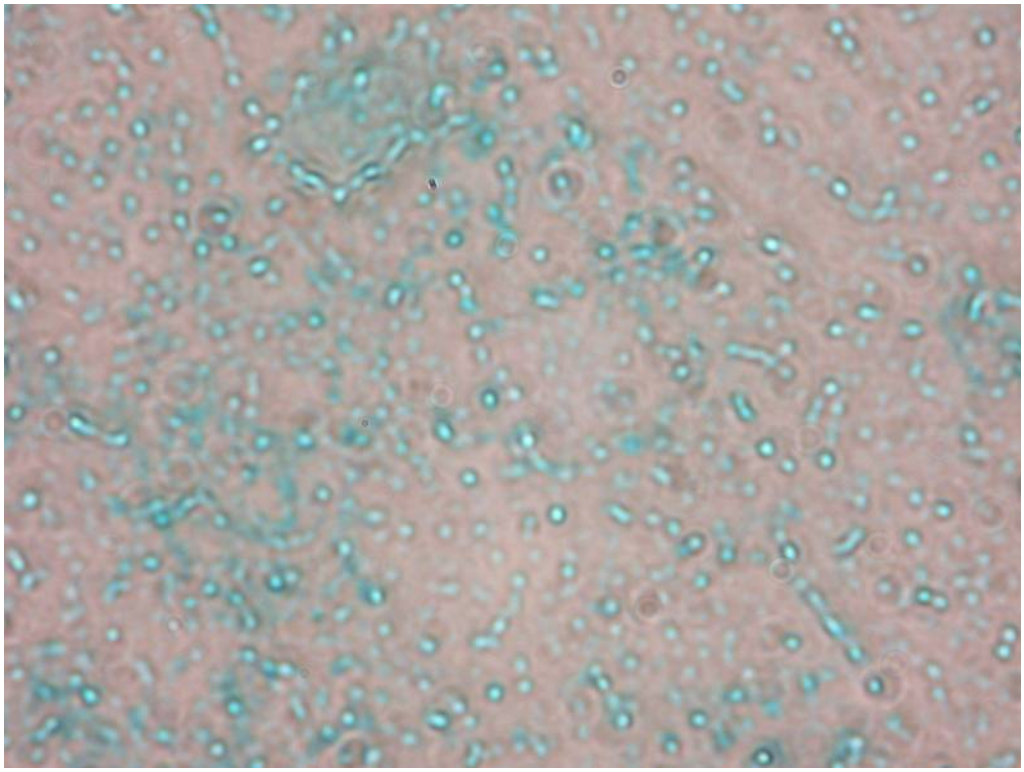

Figure 3.5 Malachite Green stain of *B. anthracis*, Δ Sterne strain, spores.

3.4.2 *B. megaterium* - vegetative cells

One of the first organisms investigated was *Bacillus megaterium*. *B. megaterium* is an aerobic, rod-shaped, Gram-positive bacterium with the ability to form endospores. The name originated from the fact that the bacterium is very big, hence 'mega'. It is commonly found in the soil.

First, one set of water suspension experiment involving the use of NA-TiO_2 adducts was performed. Fairly low concentrations of the culture were used and the efficiency of the adducts seemed promising. All the halogenated and interhalogenated adducts had a 100% kill of the cells, whereas the non-halogenated TiO_2 nanoparticles had a slightly lower kill. The control solution had a concentration of a low 884 CFU/mL, which corresponds to a $\log_{10}$ kill slightly lower than 3. However, since the control solution was low, but all of the cells were killed, there is potential that the materials are indeed even more effective.

Secondly, to mimic a real-life situation, where no water would be added, an attempt to use solid membranes was performed. Solid nanoparticles were added to membranes containing *B. megaterium* cells. This time, since promising results were already obtained with the NA-TiO_2 adducts, the adducts prepared from NA-Al_2O_3 Plus and NA-CeO_2 were also tested. Still fairly low concentrations were used and percentage kill was reported. Table 3.1 contains the results and it can be seen that most of the adducts are very efficient displaying a complete kill of the cells present, whereas some of the 'naked' metal oxides are not. The experiment was repeated with the same results obtained.

Table 3.1 Percent kill of *B. megaterium* cells.

Halogen	TiO_2	Al_2O_3	CeO_2
None	100	0	0
Cl_2	100	100	100
Br_2	100	100	100
I_2	100	100	100
ICl	100	100	100
IBr	100	100	100
ICl_3	100	100	100

Again, very promising results were obtained in the killing of *B. megaterium* cells, even with the membrane method. However, the difficulty in obtaining reproducible data (control counts of stock solutions) with the microorganism lead to that we did not attempt to kill any higher concentrations. The problem consisted in colonies forming on top of each other, so called clumping, which is not completely unusual with *B. megaterium*, as the cells have sticky polysaccharides on the cell wall. After ordering a brand new culture to see if the results improved with no positive results, we decided to explore other organisms instead.

3.4.3 *E. coli* – vegetative cells

Escherichia coli is a Gram-negative, rod shaped bacterium. It is one of the most common bacteria found in the gut of mammals. It is a fairly large bacterium with a size of approximately 1-1.5 μm x 2-5 μm, depending on the strain. Many strains cause illness to humans and *E. coli* infections are widely discussed in the media. Like most other Gram-negative bacteria, *E. coli* can

not sporulate, but exists only in the vegetative form. Because of this, most treatments that kill active bacteria in general will also kill *E. coli*. *E. coli* is responsible for many different infections in humans, including urinary tract infection and gastrointestinal problems.

The experiments performed on *E. coli* all utilized the membrane method. Solid nanoparticles were added to membranes containing *E. coli* cells. Adducts prepared from NA-Al_2O_3 Plus, NA-TiO_2 and NA-CeO_2 were all tested. Fairly low concentrations were used initially and percentage kills were reported. No standard deviations were calculated since most of the formulations displayed a 100 % kill using this low concentration. Table 3.2 contains the results and it can be seen that most of the adducts were very efficient, whereas the activities of the 'naked' metal oxides vary slightly.

Table 3.2 Percent kill of *E. coli* cells.

Halogen	TiO_2	Al_2O_3	CeO_2
None	71	12	57
Cl_2	100	100	100
Br_2	100	100	100
I_2	100	100	100
ICl	100	100	100
IBr	100	100	100
ICl_3	100	100	100

Since very promising data were obtained using these low concentrations of *E. coli* cells, further attempts using higher concentrations in hope to obtain high log kills, were performed.

In order to perform several comparable experiments, it was very important to make sure that the culture suspensions used during each experiment were of similar concentrations. As

described in the experimental section, we developed a method that gave us very consistent concentrations during the various times that we performed the experiments. This procedure included preparing an overnight culture of *E. coli*, then inoculating 50 µL of this ON culture in 50 mL LB broth and measure optical density at different time intervals.

Figure 3.6 shows the polynomial fit of the Optical Density (OD) versus Time, whereas Figure 3.7 shows the growth curve of *E. coli* over time.

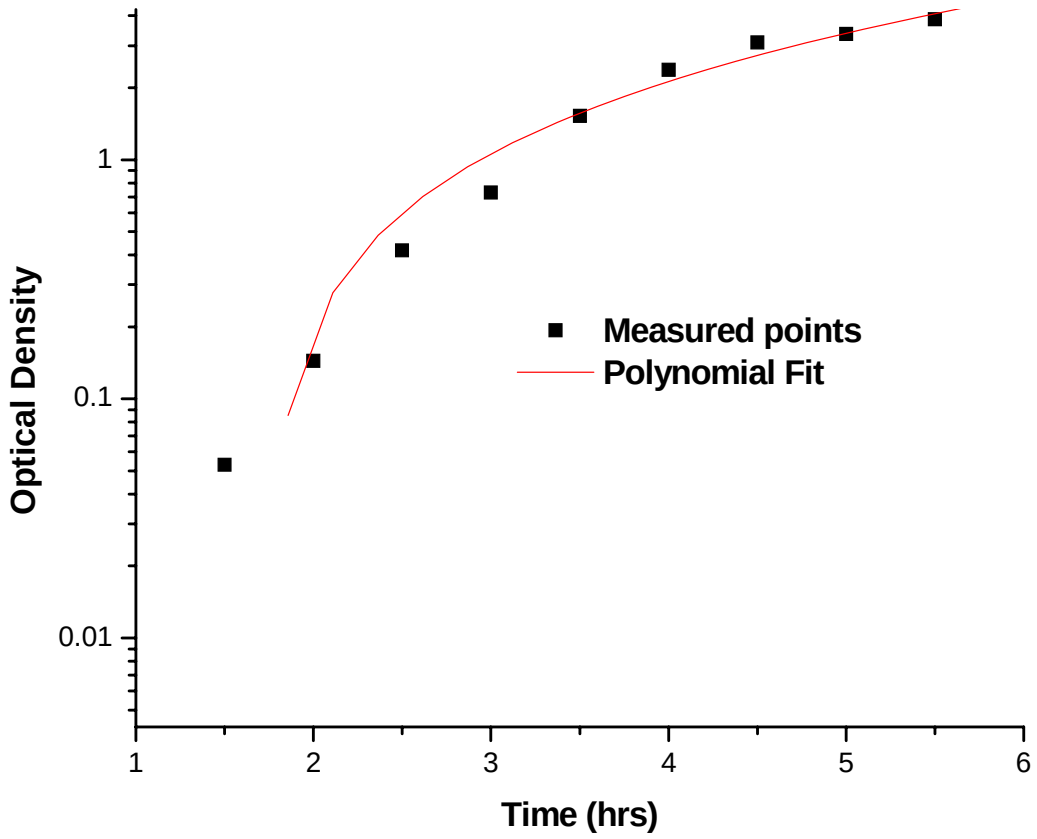

Figure 3.6 OD versus Time (hrs) of *E. coli* growth.

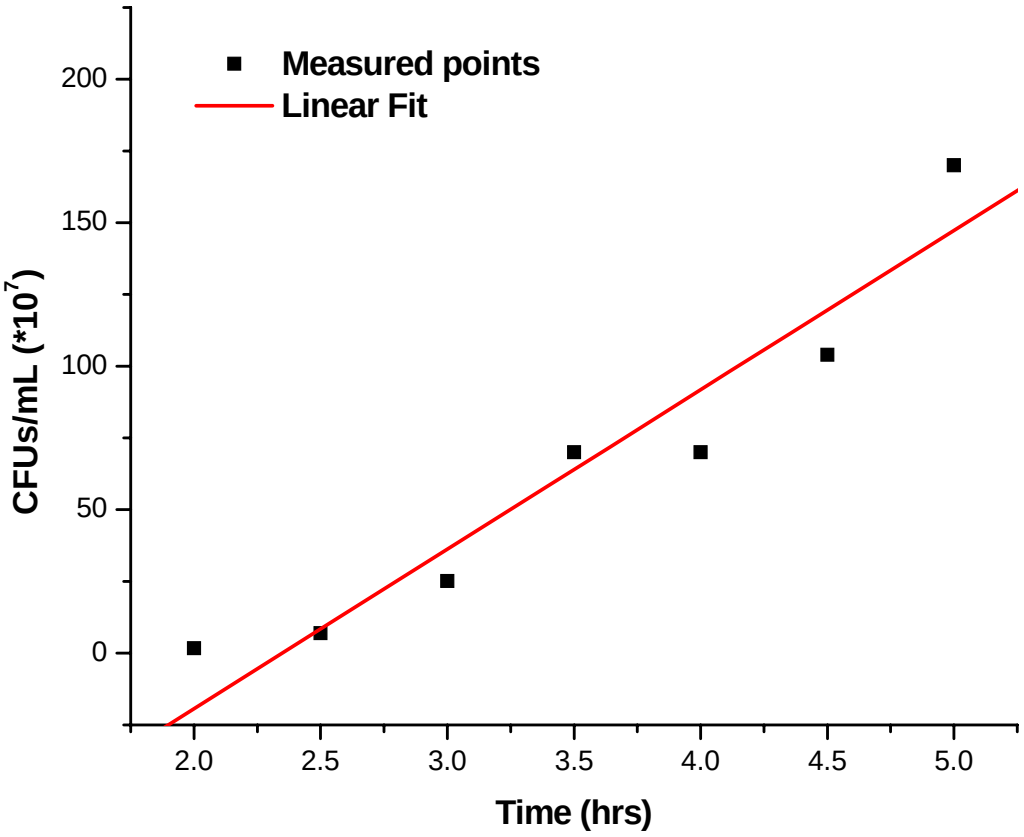

Figure 3.7 CFUs versus Time (hrs) of *E. coli* growth.

Using these graphs it was possible to follow the same procedure each time, measure the OD at a certain time and know approximately what the concentration of the culture was. Similar concentrations could then be used for every experiment. The results obtained were very reproducible.

The goal of using *E. coli* as a test organism was to obtain as high log reduction values as possible, using all the different halogenated and interhalogenated adducts. Higher concentrations of the *E. coli* cultures were used and log reduction values were calculated. Transmission Electron Microscope images were also obtained to prove that the cells were in fact destroyed, rather than just prevented from reproduction. For future application in decontamination and as possible first-response weapons against terrorist attacks it is very important that the materials are bactericidal and not just bacteristatic.

Table 3.3 shows the log reduction values of the NA-Al_2O_3 Plus adducts. The highest concentration used leads to a log kill of 8.6, so all the halogen/interhalogen adducts have a complete kill of *E. coli* cells. Since all the adducts displayed a complete kill of all the cells present at each repeated experiment, no standard deviation calculations were possible. The standard deviation for the heat-activated NA-Al_2O_3 Plus was less than ±0.5.

Table 3.3 Log kills of *E. coli* by NA-Al_2O_3 Plus adducts.

Nanoparticle Formulation	Log Reduction *E. coli*
NA-Al_2O_3-act.	5.8
NA-Al_2O_3/Cl_2	8.6
NA-Al_2O_3/Br_2	8.6
NA-Al_2O_3/I_2	8.6
NA-Al_2O_3/ICl	8.6
NA-Al_2O_3/IBr	8.6
NA-Al_2O_3/ICl_3	8.6

It can be seen that even the 'naked' metal oxide displays quite high activity, although not as high as the prepared adducts. *E. coli* is not extremely difficult to kill and the cells are very responsive to various kinds of treatments, hence it is not very surprising that the halogen/interhalogen adducts are extremely efficient.

Table 3.4 shows the log reduction values for the NA-TiO_2 adducts. Again, it can be seen that the halogenated/interhalogenated adducts are performing very well, most of them having a complete kill of the concentration tested. However, the chlorinated and brominated adducts are not as efficient as the other halogen adducts. The reason for this could be the stability of those adducts; it is very likely that the halogens (Cl_2 and Br_2) have escaped from the TiO_2 surface early during the 30 minutes interaction, since the solid membrane method was used, leading to lower kills. It should also be noted that the standard deviation for the 'naked' TiO_2 was slightly larger (in the order of ±0.9) than for the chlorine and bromine adducts (both less than ±0.5) due to unknown reasons. It was difficult obtaining reproducible data and since the average value is reported and the standard deviation was quite large, it is possible that with more experiments done, the average value could have been lower, which is more likely, as the chlorinated and

brominated adducts should have a higher activity due to the oxidative power of the halogens. The high value obtained for the NA-TiO_2 could have been an outlier, which is a value that is numerically distant from the rest of the values. The standard deviation values were again not possible to calculate for the remaining adducts since they all displayed a complete kill of all the cells present at every experiment performed.

Table 3.4 Log kills of *E. coli* by NA-TiO_2 adducts.

Nanoparticle Formulation	**Log Reduction *E. coli***
NA-TiO_2-act.	7.6
NA-TiO_2/Cl_2	7.6
NA-TiO_2/Br_2	7.6
NA-TiO_2/I_2	8.6
NA-TiO_2/ICl	8.6
NA-TiO_2/IBr	8.6
NA-TiO_2/ICl_3	8.6

The adducts prepared from NA-CeO_2 were also tested using the membrane method and the results can be seen in Table 3.5. Again, it can be seen that the chlorinated adduct is not quite as efficient as the other adducts and that the 'naked' CeO_2 is slightly less active than the ones containing halogen/interhalogen. The standard deviation values for the activated NA-CeO_2 and the chlorinated adduct were both less than ±0.5 and the remaining adducts all displayed a complete kill of the cells present. However, it should be noted that all the 'naked' metal oxides are quite active, considering that they contained no halogens or other corrosive chemicals. The reason for this unusual activity of the nanoparticles is most likely due to their abrasive character and high surface area leading to a very close contact with the cells.

Table 3.5 Log kills of *E. coli* by NA-CeO_2 adducts.

Nanoparticle Formulation	Log Reduction *E. coli*
NA-CeO_2-act.	6.9
NA-CeO_2/Cl_2	7.6
NA-CeO_2/Br_2	8.6
NA-CeO_2/I_2	8.6
NA-CeO_2/ICl	8.6
NA-CeO_2/IBr	8.6
NA-CeO_2/ICl_3	8.6

To summarize, the activities of all of the prepared halogen/interhalogen adducts are very high, most of them displaying a complete kill of all *E. coli* cells present, even at high concentrations of bacteria. It seems that the NA-Al_2O_3 Plus adducts have the highest activity against *E. coli* cells, so they most likely have the highest potential in performing well against other microorganisms such as spores and viruses (Chapter 4). Interestingly, even the non-halogenated metal oxides performed very well, with log kills of over 5. This is very impressive for materials that are relatively environmentally friendly, containing no harsh chemicals that could potentially destroy sensitive equipment.

To further visualize the action of the nanoparticles and to show that the cells are indeed dead and not just hindered to reproduce, transmission electron microscopy was used. The images were recorded using fresh *E. coli* cultures and the treated cells were treated with NA-Al_2O_3/ICl_3 Plus for one hour. The goal of the study was not to quantify the ratio of dead versus alive cells, but rather to see if the cells in fact were dead from the treatment.

Control images of healthy *E coli* cells can be seen in Figures 3.8 and 3.9. It can be observed that they are indeed in the healthy log phase and not in the stationary phase. The cells

are uniformly dense, indicating that they are healthy. Since the cells have been sliced during the preparation, the shapes of them vary, depending on orientation when cut.

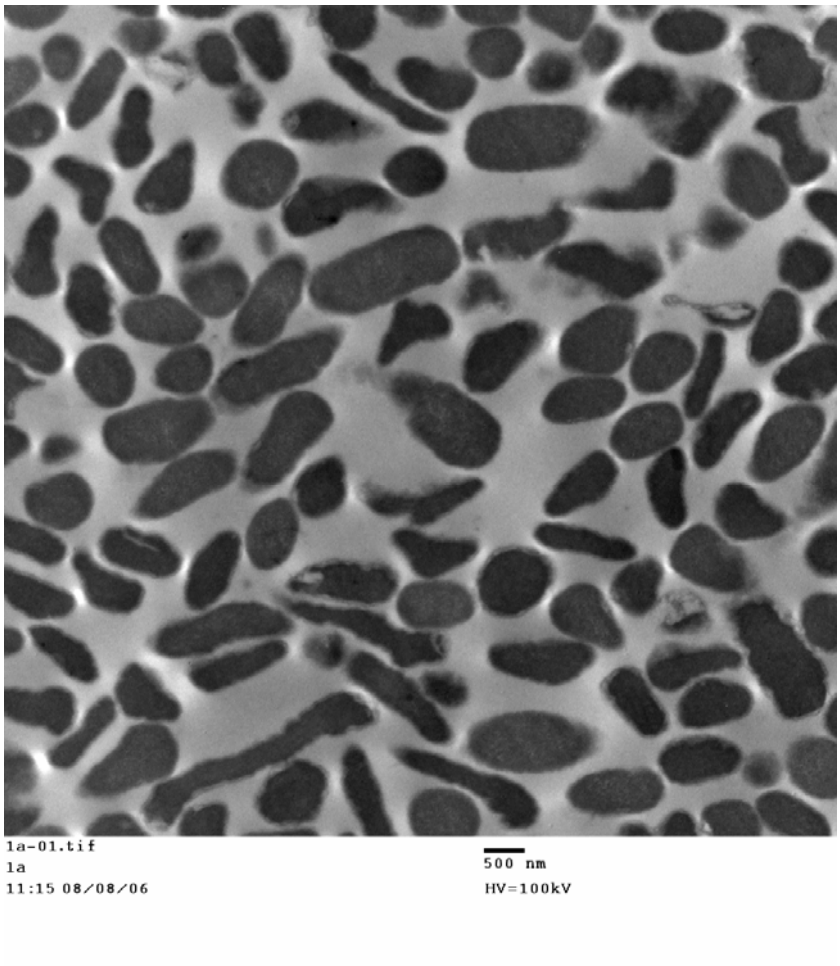

Figure 3.8 TEM micrograph of untreated *E. coli* cells – low magnification.

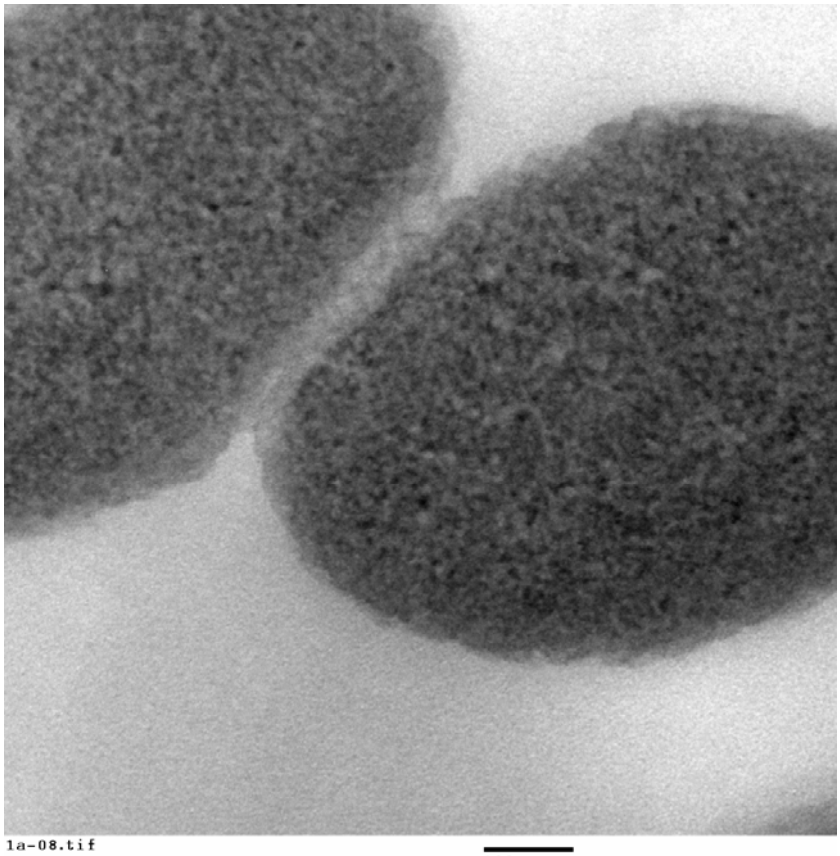

Figure 3.9 TEM micrograph of untreated *E. coli* cells - displaying cell wall.

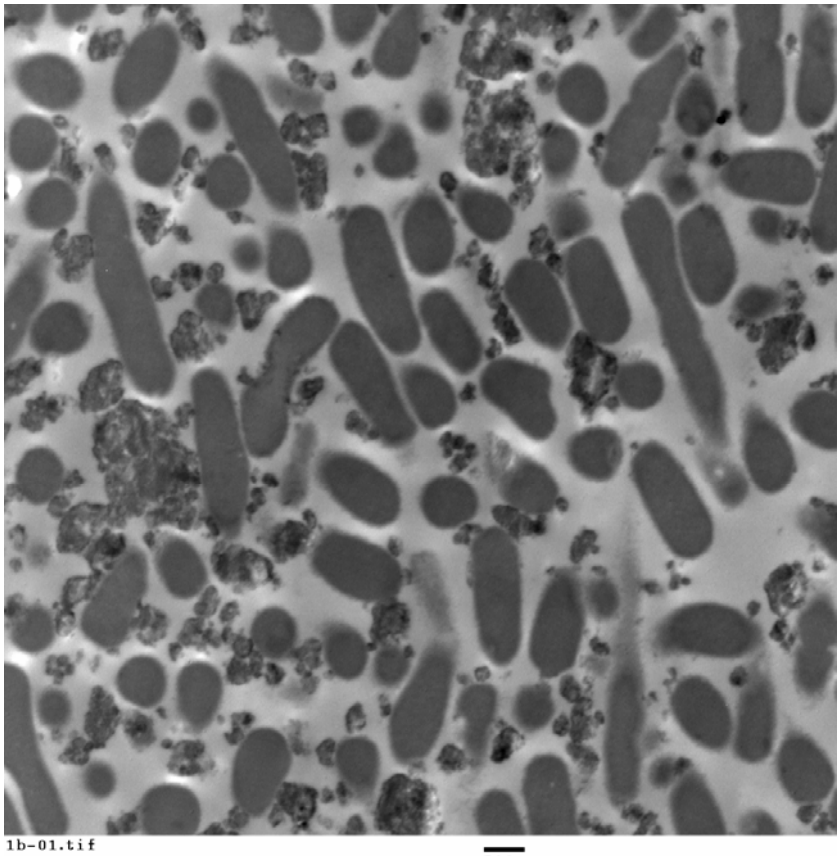

Figure 3.10 TEM micrograph of treated *E. coli* cells – low magnification.

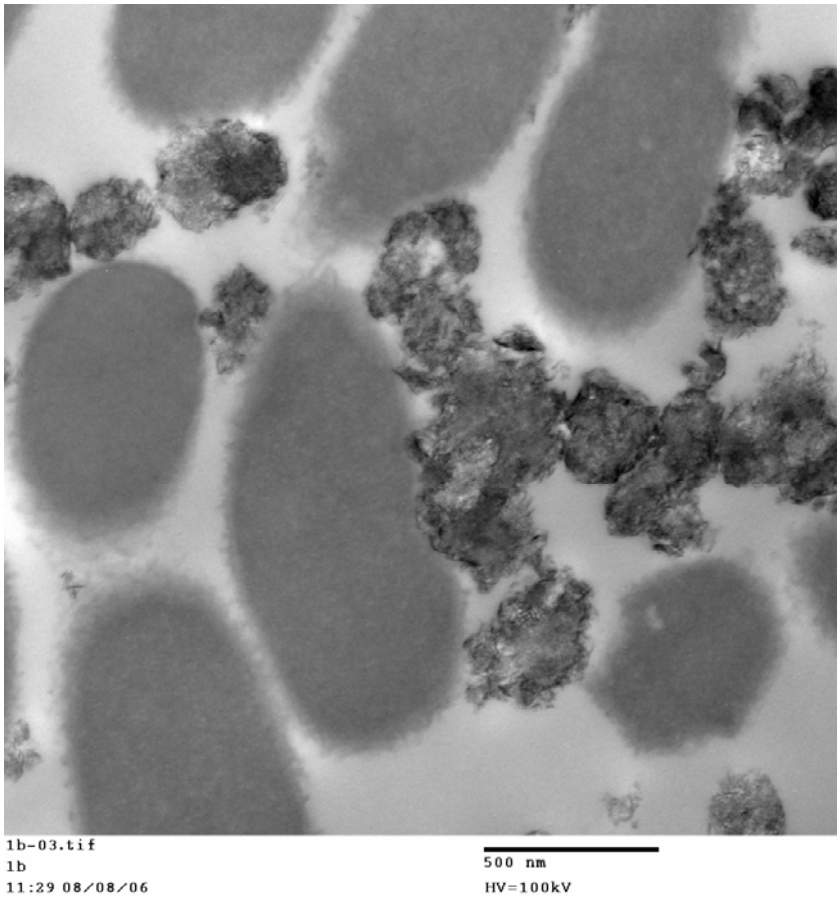

Figure 3.11 TEM micrograph of treated *E. coli* cells – medium magnification.

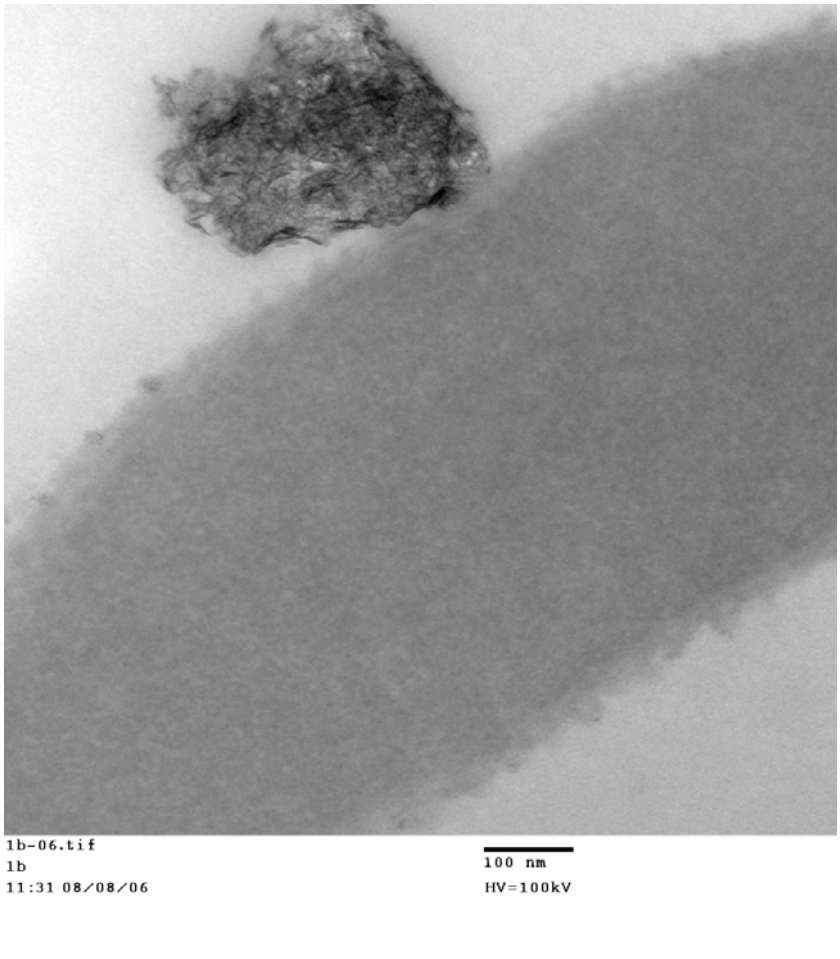

Figure 3.12 TEM micrograph of treated *E. coli* cells – high magnification.

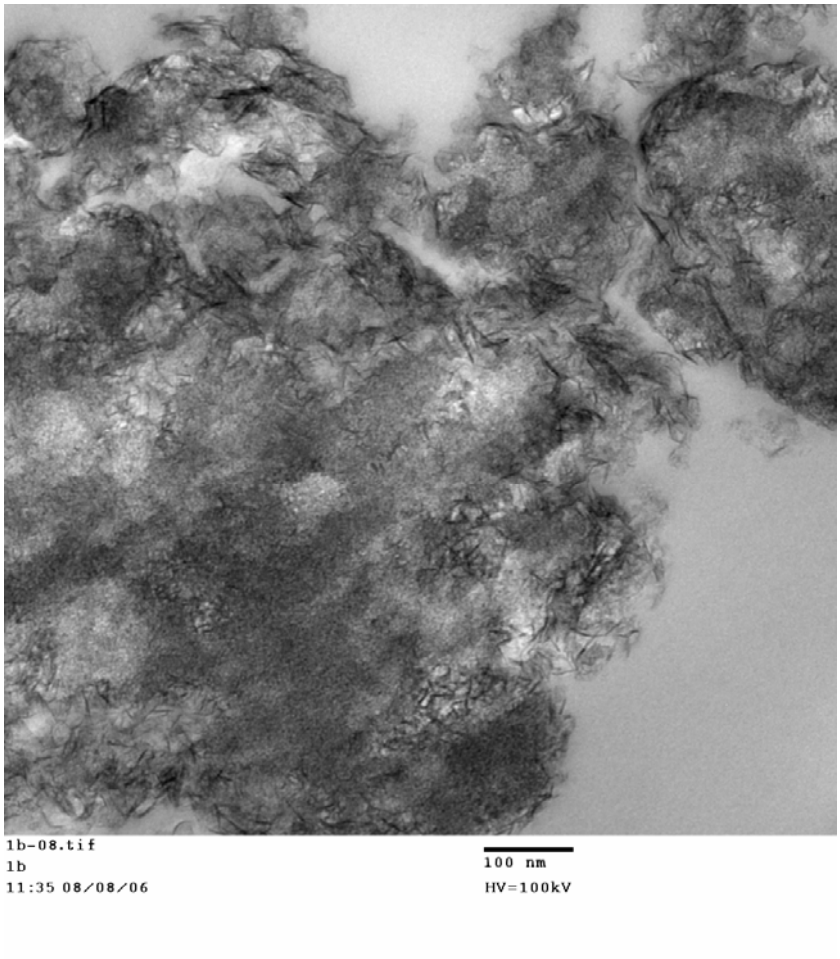

Figure 3.13 TEM micrograph of treated *E. coli* cells – displaying dead cell parts.

The treated cells in Figures 3.10-3.13 clearly show the difference between treated and untreated cells. Crystallinity can be observed in some of the images containing dead cell parts, DNA parts and proteins, indicating the mechanism in which the cells have died. The metal oxide has an affinity for the cells, the abrasive character increases biocidal effect, and the oxidative power of the halogen kills the cell.

3.4.4 *B. subtilis* – endospores

Bacillus subtilis is a Gram-positive bacterium with the ability to form endospores. Although capable of contaminating food, it rarely causes food poisoning. As an endospore, it is very resistant to chemical and physical treatments, such as heat, acid and drying. *B. subtilis* is probably the most commonly studied Gram-positive organism, just as *E. coli* is probably the most commonly studied Gram-negative organism. The endospore form is often used as a simulant for the biowarfare agent *B. anthracis*, which has significantly increased its interest in the last several years.

The experiments performed on *B. subtilis* spores utilized the membrane method. Solid nanoparticles were added to membranes containing *B. subtilis* spores. Adducts prepared from NA-Al_2O_3 Plus, NA-TiO_2 and NA-CeO_2 were all tested. Very low concentrations were used initially and percentage kills were reported. The reason for the initially used low concentrations was due to cost of spores and the fact that spores are very resistant to chemical treatments, including oxidizing materials. Due to this difference between vegetative cells and endospores, the efficiency of the prepared adducts was expected to be somewhat or significantly lower than those of *E. coli* cells. Table 3.6 contains the results using a low concentration of spores and it can

be seen that several of the adducts had a complete kill, whereas the iodinated adducts of all the metal oxides were not 100% efficient. The chlorinated adducts of NA-CeO_2 had an even lower efficiency and it was very difficult to determine the activity of the 'naked' metal oxide nanoparticles. The small activity that was observed was difficult to reproduce and could very well have been within the experimental error.

Table 3.6 Percent kill of *B. subtilis* spores.

Halogen	TiO_2	Al_2O_3	CeO_2
None	N/A	N/A	N/A
Cl_2	100	100	~50
Br_2	100	100	100
I_2	91	90	95
ICl	100	100	100
IBr	100	100	100
ICl_3	100	100	100

To further determine the exact efficiency of the adducts, and to notice possible distinctions between them, higher concentrations were utilized. It was also desirable to determine the highest possible log kills for these materials. Since the spores of *B. subtilis* were available for purchase in many concentrations, these experiments were very easy to perform as the solutions were used as received and the concentration was already pre-determined. In order to keep the costs down, experiments with increasing concentrations were performed, with lower concentrations performed first. Each adduct that was successful at the lower concentration was again tested using a higher concentration. This method requires several more experiments than if

you were to start at the highest concentration available and directly calculate log kills; however this method was cheaper.

Table 3.7 displays the calculated log kill values of the NA-Al_2O_3 Plus adducts using the membrane method. It can be observed that the 'naked' metal oxide is not active against the spores, as expected. The iodinated adduct has a low log kill of one, which can be explained by iodine's inability to completely kill large concentrations of spores.[23,24] The other adducts, however, performed very well. The iodine trichloride adduct, especially, had a very high log kill. In fact, all the interhalogen adducts performed very well against the spores. This is not surprising as they all have strong oxidizing powers and most likely interact strongly with the spores. The standard deviation values for the adducts are all less than ±0.5 and most of them even lower than that.

Table 3.7 Log kills of *B. subtilis* spores by NA-Al_2O_3 Plus adducts.

Nanoparticle Formulation	**Log Reduction *B. subtilis***
NA-Al_2O_3-act.	0
NA-Al_2O_3/Cl_2	4.4
NA-Al_2O_3/Br_2	5.2
NA-Al_2O_3/I_2	1
NA-Al_2O_3/ICl	4.3
NA-Al_2O_3/IBr	5.2
NA-Al_2O_3/ICl_3	6

Table 3.8 shows the log reduction values for the NA-TiO_2 adducts using the membrane method. As expected the iodinated adduct had a low log kill, as did the 'naked' NA-TiO_2. Again, the interhalogenated adducts performed very well with results of up to a log 6 kill for the ICl_3

adduct. The chlorinated and brominated adducts had an intermediate activity. Several of the TiO_2 adducts are very unstable, meaning that the halogen leaves the surface quickly, possibly leading to this lower activity of the Cl_2 and Br_2 adducts. Again, the interhalogens have a very strong oxidizing power leading to very high log kills. The standard deviation values for the adducts are all less than ±0.5.

Table 3.8 Log kills of *B. subtilis* spores by NA-TiO_2 adducts.

Nanoparticle Formulation	Log Reduction *B. subtilis*
NA-TiO_2-act.	0
NA-TiO_2/Cl_2	3.6
NA-TiO_2/Br_2	3.6
NA-TiO_2/I_2	1
NA-TiO_2/ICl	6
NA-TiO_2/IBr	4.3
NA-TiO_2/ICl_3	6

The adducts prepared from NA-CeO_2 were also tested using the membrane method and the results can be seen in Table 3.9. Worth to notice is that the performance of the chlorinated adduct is very low, in fact even lower than the iodinated adduct. Within the series, there is also no adduct that has a log kill of 6 or higher, as there was in both the NA-Al_2O_3 Plus and NA-TiO_2 series. Again, the bare NA-CeO_2 was inefficient, as expected. The amounts of halogens/interhalogens adsorbed on the NA-CeO_2 are low, possibly leading to some of these lower log kill values. Especially the chlorinated adduct contains a low amount of halogen, as determined by TGA, explaining the low activity of the adduct. The standard deviation values for the adducts are all less than ±0.5 and smaller than that for the chlorinated adduct. The activity of

the chlorinated adduct was noticeably higher than for the activated NA-CeO_2; however, at such low activity the log kill number should not be the main focus, especially not considered the experimental error present. This number listed purely represents the average value obtained during a set of several experiments and should mainly state that the adduct is in fact more active than the non-halogenated cerium oxide.

Table 3.9 Log kills of *B. subtilis* spores by NA-CeO_2 adducts.

Nanoparticle Formulation	**Log Reduction *B. subtilis***
NA-CeO_2-act.	0
NA-CeO_2/Cl_2	0.3
NA-CeO_2/Br_2	3.6
NA-CeO_2/I_2	1.3
NA-CeO_2/ICl	3.6
NA-CeO_2/IBr	5
NA-CeO_2/ICl_3	5

To further visualize the action of the nanoparticles and to show that the spores are indeed dead and not just hindered to reproduce, transmission electron microscopy was used. The treated spores were treated with NA-Al_2O_3/ICl_3 Plus for one hour. The spores used for the imaging were not the ones purchased as this would have been extremely expensive. Instead, spores were prepared according to the same procedure described in **3.3.2** utilized to prepare *B. anthracis* spores. The goal of the study was not to quantify the ratio of dead versus alive spores, but rather see if the spores in fact were dead from the treatment.

Control images of healthy *B. subtilis* spores can be seen in Figures 3.14-3.16. The thick spore coat is easily seen in Figure 3.15 and 3.16. The spores are uniformly dense, indicating that

they are healthy. The spores have a diameter of approximately 400 nm, which is much smaller than the *E. coli* cells we investigated previously. The few rod-shaped organisms in Figure 3.14 are most likely stressed cells, as they are not as large as normal cells, but not round like spores. The white specs in the images are due to bubbles in the resin or other artifacts. Figures 3.17 and 3.18 show the treated spores and they no longer have any characteristic shape to them, but are rather remaining spore parts, DNA and proteins. Again, it appears that the metal oxide is attracted to the spores, as can be seen in both Figure 3.17 and 3.18, where it appears that the Al_2O_3 remains on the dead spore remains.

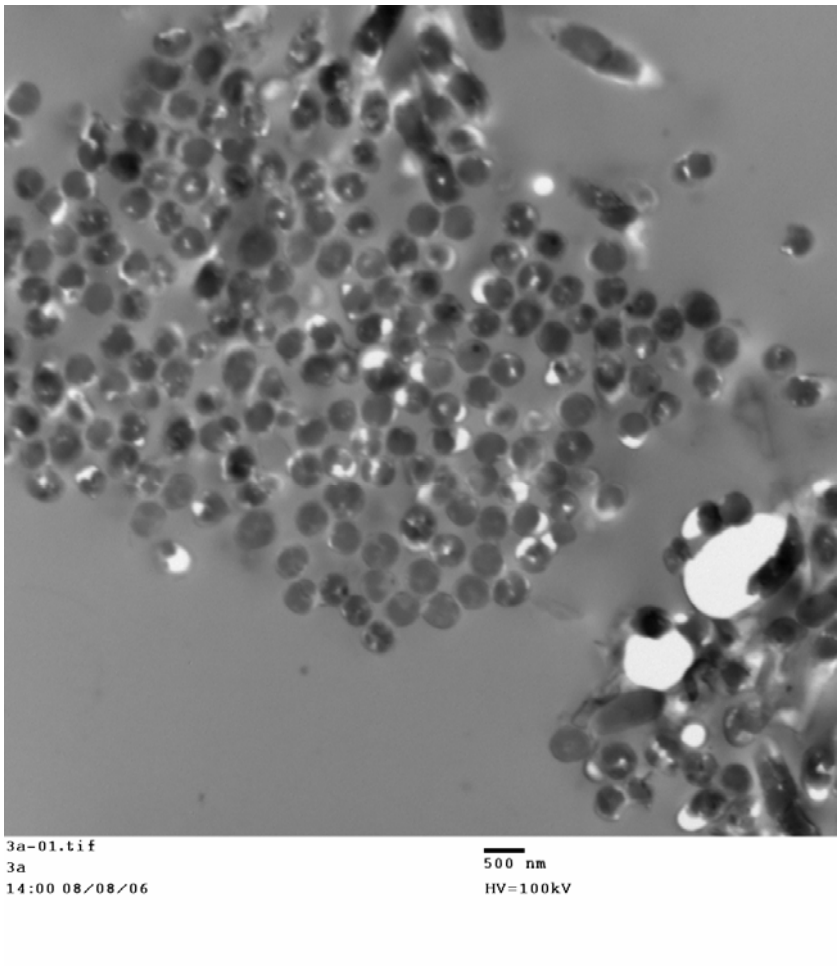

Figure 3.14 TEM micrograph of untreated *B. subtilis* spores – low magnification.

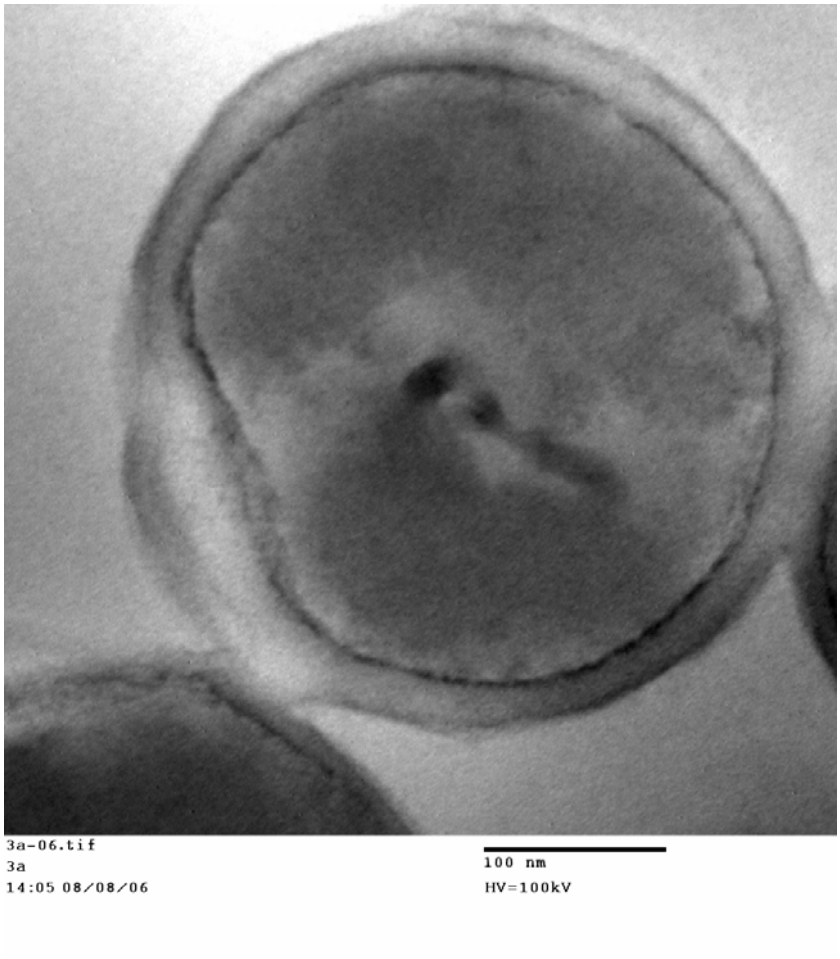

Figure 3.15 TEM micrograph of untreated *B. subtilis* spores – one single spore.

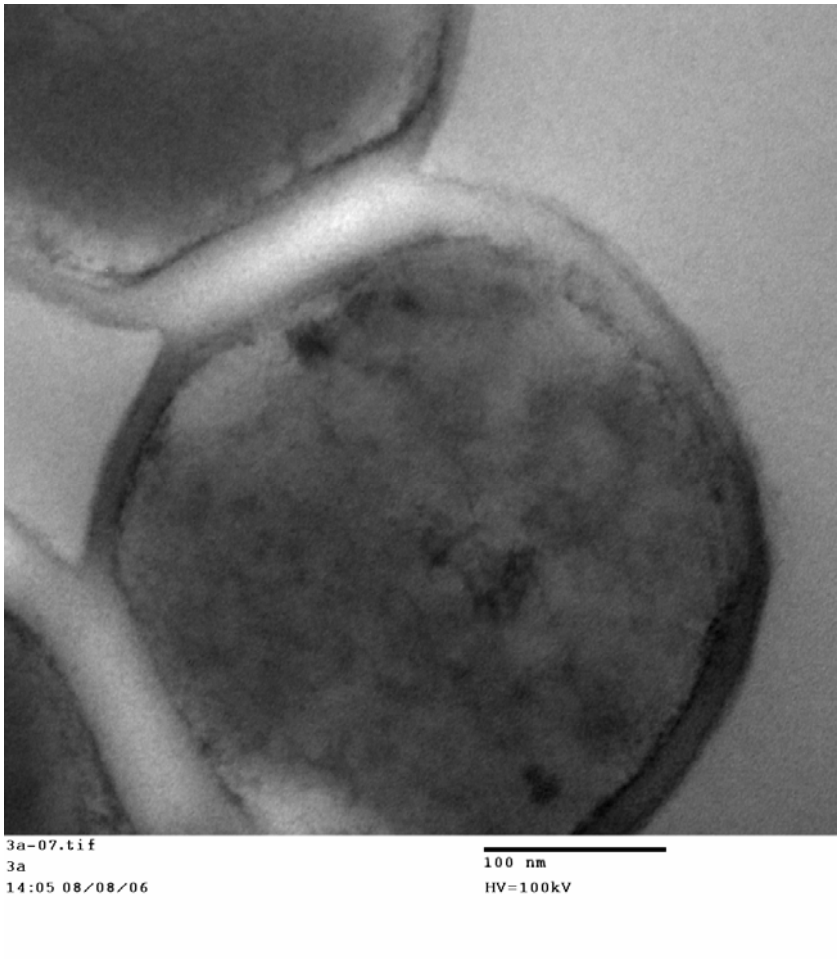

Figure 3.16 TEM micrograph of untreated *B. subtilis* spores – high magnification.

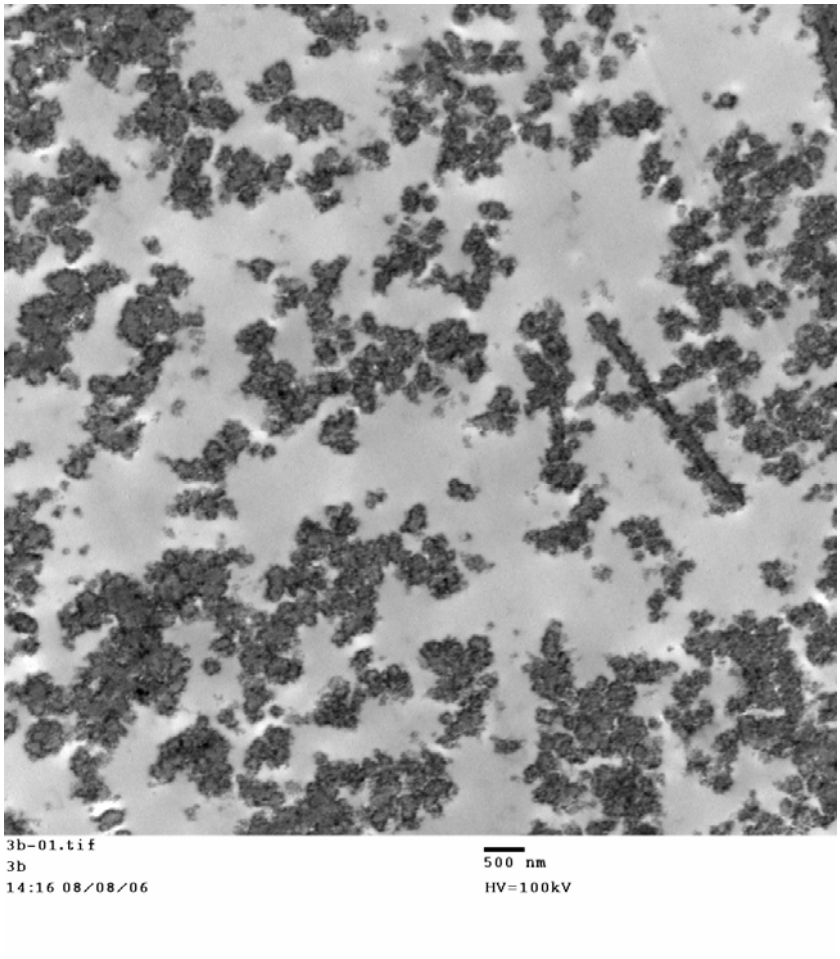

Figure 3.17 TEM micrograph of treated *B. subtilis* spores – low magnification.

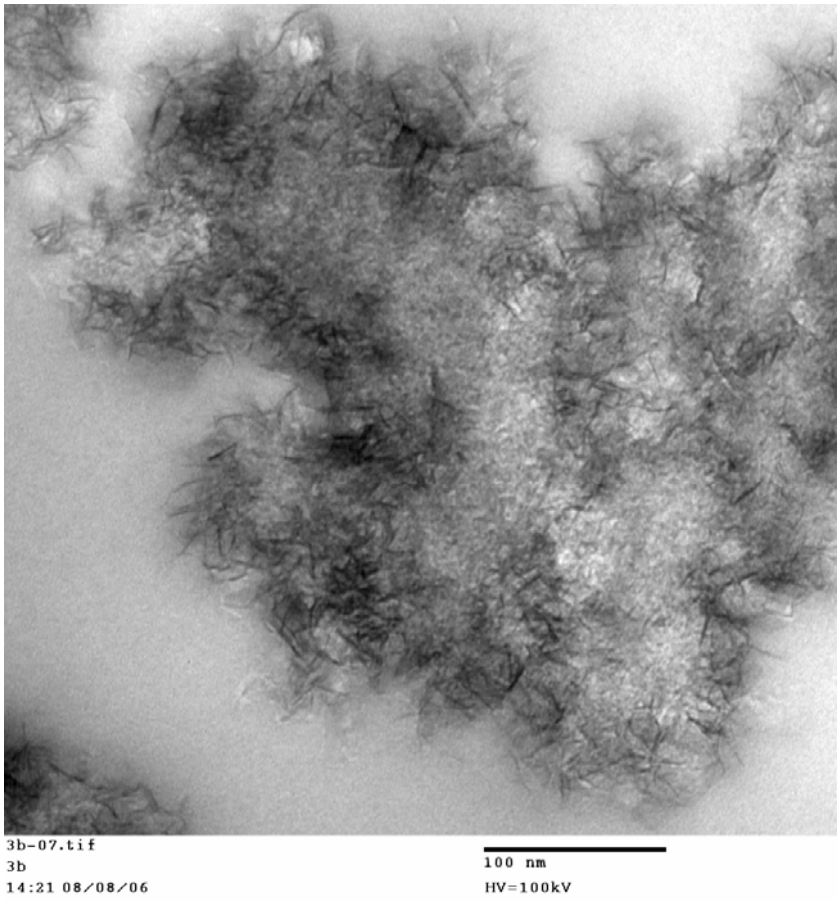

Figure 3.18 TEM micrograph of treated *B. subtilis* spores – high magnification.

To summarize, the activities of many of the prepared halogen/interhalogen adducts are very high, some of them displaying log 6 kills of *B. subtilis* spores. It seems like the NA-Al_2O_3 Plus adducts are the most promising against *B. subtilis* spores, but they are closely followed by the NA-TiO_2 adducts. Some of the NA-CeO_2 adducts were also good, but no adduct reached a log 6 kill value. The non-halogenated metal oxides did not appear to have any deadly effect on the spores.

3.4.5 *B. anthracis*, Δ Sterne strain- vegetative cells and endospores

Bacillus anthracis is a Gram-positive bacterium, with the ability to form endospores. The vegetative cell is rod-shaped with a size of approximately 1 x 3 to 6 μm. During environmental stress *B. anthracis* form spores that can then survive in the soil for a very long time. *B. anthracis* is the cause of the infectious disease anthrax. Depending on which form of contact with anthrax, the survival rate varies. The most critical conditions occur after ingestion and will most often lead to death. As other bacteria, many strains of *B. anthracis* exist, some of them extremely virulent. The Δ Sterne strain is a benign strain, often used in experiments such as these discussed herein. The different strains differ in the genes present and their activity. This in turn determines the toxins produced by the certain strain.

In order to perform several comparable experiments, it was very important to make sure that the culture suspensions used during each experiment were of similar concentrations. As described in the experimental section, we developed a method that gave us very consistent concentrations during the various times that we performed the experiments, just like with the use of *E. coli* cells. This procedure included preparing an overnight culture of *B. anthracis*, then

inoculating 50 µL of this ON culture in 50 mL LB broth and measure optical density at different time intervals.

Figure 3.19 shows the polynomial fit of the Optical Density versus Time, whereas Figure 3.20 shows the growth curve of *B. anthracis* over time.

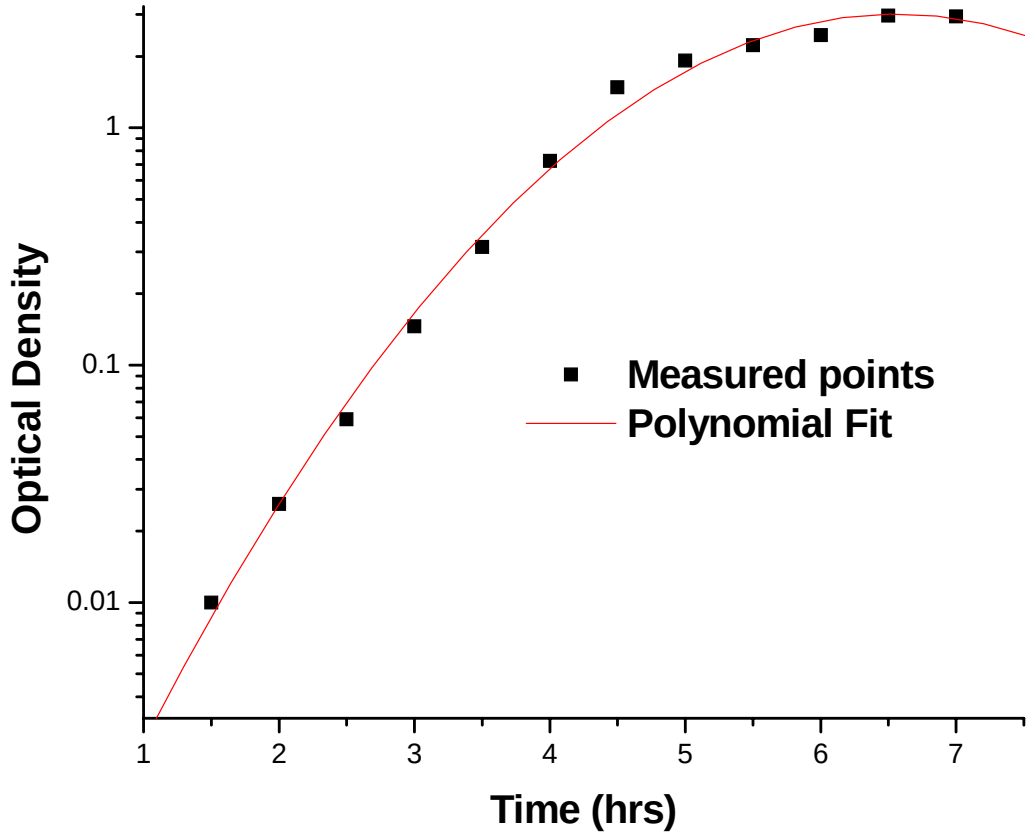

Figure 3.19 OD versus Time (hrs) of *B. anthracis* growth.

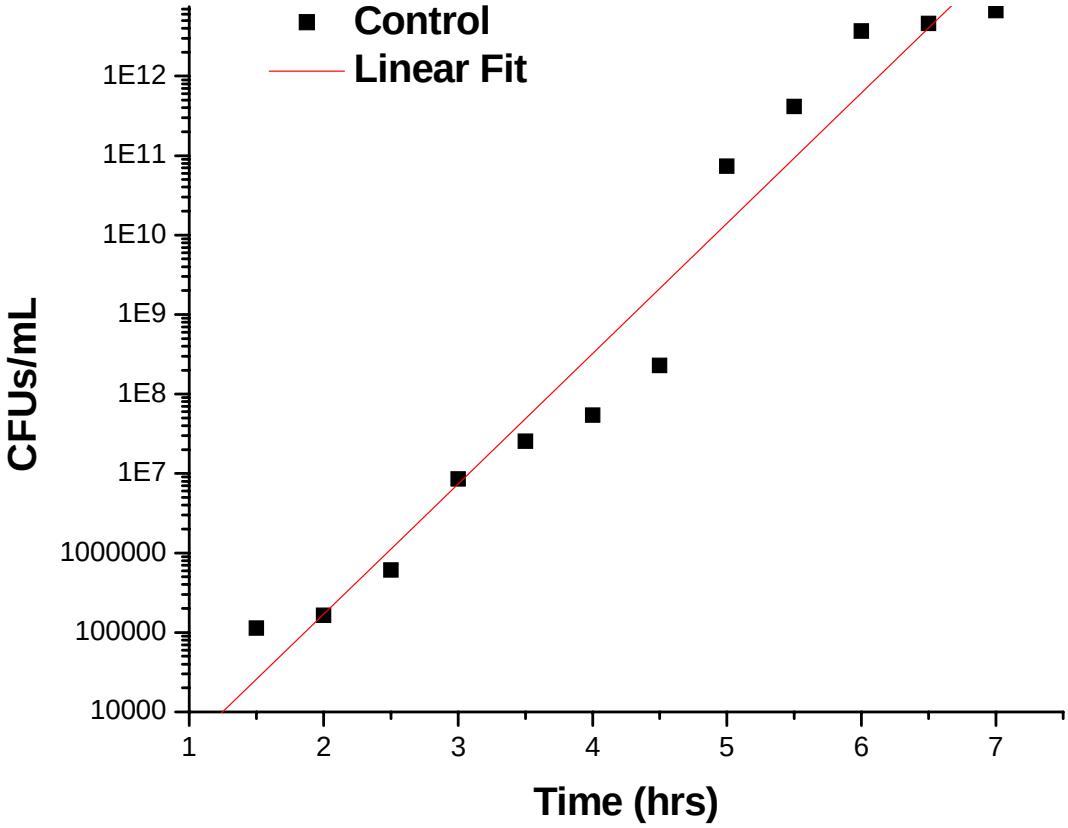

Figure 3.20 CFUs versus Time (hrs) of *B. anthracis* growth.

Using these graphs, it was possible to follow the same procedure each time, measure the OD at a certain time and know approximately what the concentration of the culture was. The results obtained were very reproducible.

Since preparation and testing of all the prepared adducts simultaneously was extremely time consumable, only the most promising adducts were chosen to be part of the study of *B. anthracis* Δ Sterne strain vegetative cells and spores. The adducts chosen included NA-Al_2O_3/Cl_2 Plus, NA-Al_2O_3/Br_2 Plus, NA-Al_2O_3/ICl Plus, NA-Al_2O_3/IBr Plus and NA-Al_2O_3/ICl_3 Plus, as well as NA-TiO_2/ICl, NA-TiO_2/IBr and NA-TiO_2/ICl_3. Although there were some of the NA-CeO_2 adducts that were indeed very efficient, they were excluded due to the facts that NA-CeO_2 is a heavier metal oxide and hence less environmentally friendly, it is more expensive and more dusty, leading to higher risks of inhalation issues.

B. anthracis vegetative cells were not expected to be very difficult to kill, since it is a bacteria rather than a spore. The results of the adducts using the membrane method can be seen in Table 3.10. The highest concentration tested corresponds to a log 8 kill, which means that all adducts displayed a complete kill of *B. anthracis* vegetative cells. This was not surprising considering that all of the tested adducts were also lethal towards *E. coli* cells of high concentrations. The standard deviation values were not calculated since all the tested adducts displayed a complete kill of all the cells present.

Table 3.10 Log kills of *B. anthracis* cells.

Nanoparticle Formulation	Log Reduction *B.anthracis*
NA-Al_2O_3/Cl_2	8
NA-Al_2O_3/Br_2	8
NA-Al_2O_3/ICl	8
NA-Al_2O_3/IBr	8
NA-Al_2O_3/ICl_3	8
NA-TiO_2/ICl	8
NA-TiO_2/IBr	8
NA-TiO_2/ICl_3	8

For the experiments involving *B. anthracis* spores using the membrane method, the spores used were prepared as described in **3.3.2**. The same spores were also imaged using TEM.

Assuming a 70% conversion of cells to spores (assumption based on counting stressed cells versus spores on several TEM images taken from different parts of the grid), the log kills are seen in Table 3.11. All the studied materials displayed a complete kill of the spores used. However, it is very likely that at even higher concentrations this will not be the case. These experiments were slightly harder to perform than previous experiments including the use of *E. coli* cells and *B. anthracis* cells. It appeared that the nutrient agar had difficulties penetrating through the 0.22 μm membrane to utilize growth of colonies. The plates were incubated longer times with improved results. Several experiments were performed to study the growth of the colonies through the membrane versus directly on agar plates. The results showed that with longer incubation times, the CFUs obtained in both cases were similar. The experiments were repeated several times with consistent results.

Table 3.11 Log kills of *B. anthracis* spores.

Nanoparticle Formulation	Log Reduction *B.anthracis (delta sterne)*
NA-Al_2O_3/Cl_2	6.8
NA-Al_2O_3/Br_2	6.8
NA-Al_2O_3/ICl	6.8
NA-Al_2O_3/IBr	6.8
NA-Al_2O_3/ICl_3	6.8
NA-TiO_2/ICl	6.8
NA-TiO_2/IBr	6.8
NA-TiO_2/ICl_3	6.8

Further, Transmission Electron Microscope images were obtained to prove that the cells and spores were destroyed, rather than just prevented from reproduction.

Control images of *B. anthracis* Δ Sterne strain vegetative cells are shown in Figures 3.21-3.24. In Figures 3.23 and 3.24 the cell membrane is clearly seen, indicating a healthy cell with no cell membrane damage. It can also be observed that the cells are uniformly dense with no big holes.

The treated cells have been treated with NA-Al_2O_3/ICl_3 Plus and can be seen in Figures 3.25-3.28. Figure 3.26 shows a cell that is not completely destroyed, but that has a damaged cells membrane as compared to that in Figure 3.23 or 3.24. Figure 3.27 and 3.28 shows how the nanoparticles again have attached to the cells and then destroyed them.

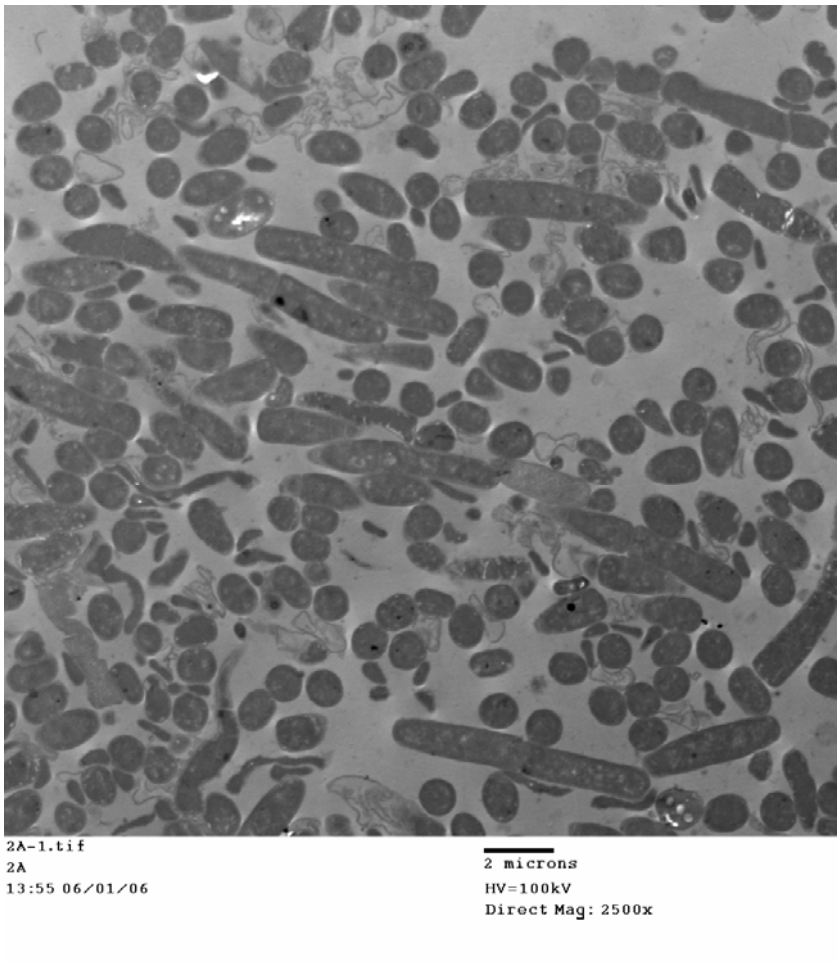

Figure 3.21 TEM micrograph of untreated *B. anthracis* cells – low magnification.

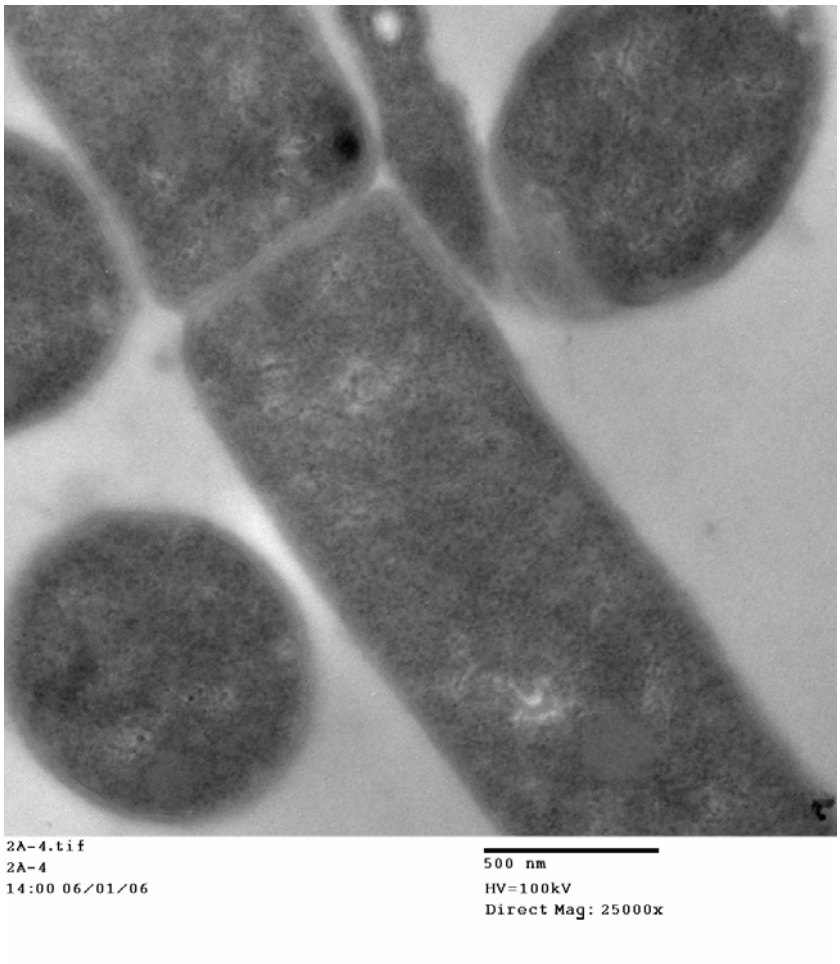

Figure 3.22 TEM micrograph of untreated *B. anthracis* cells – high magnification.

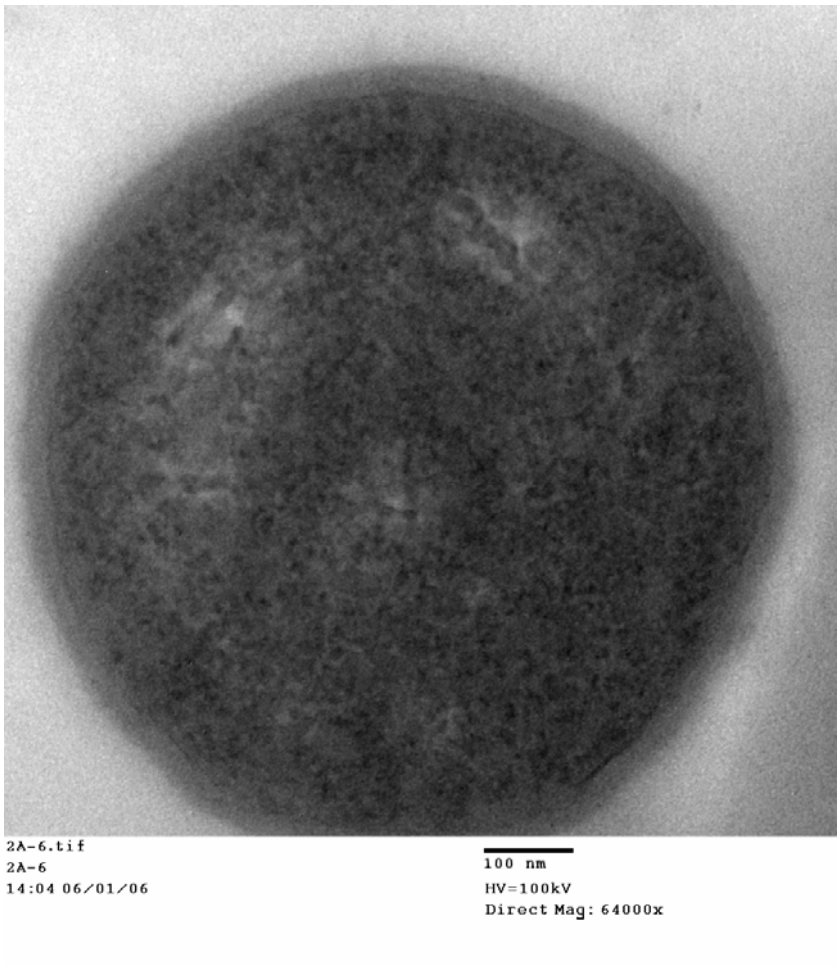

Figure 3.23 TEM micrograph of untreated *B. anthracis* cells – displaying one single cell.

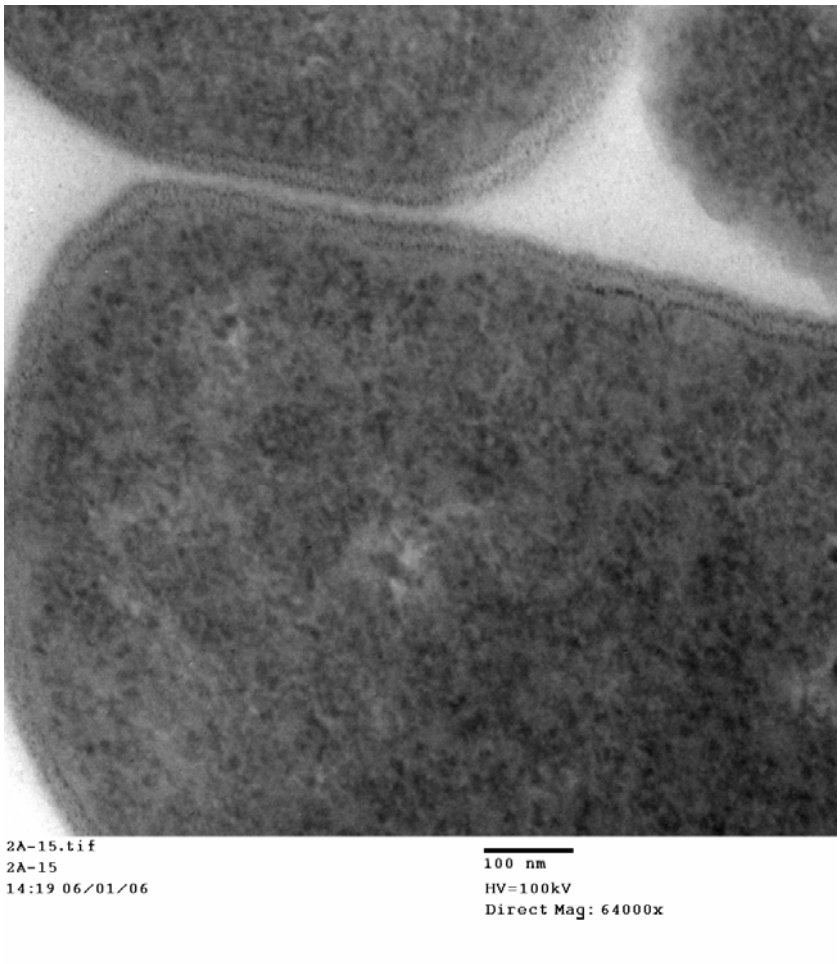

Figure 3.24 TEM micrograph of untreated *B. anthracis* cells – displaying the cell wall.

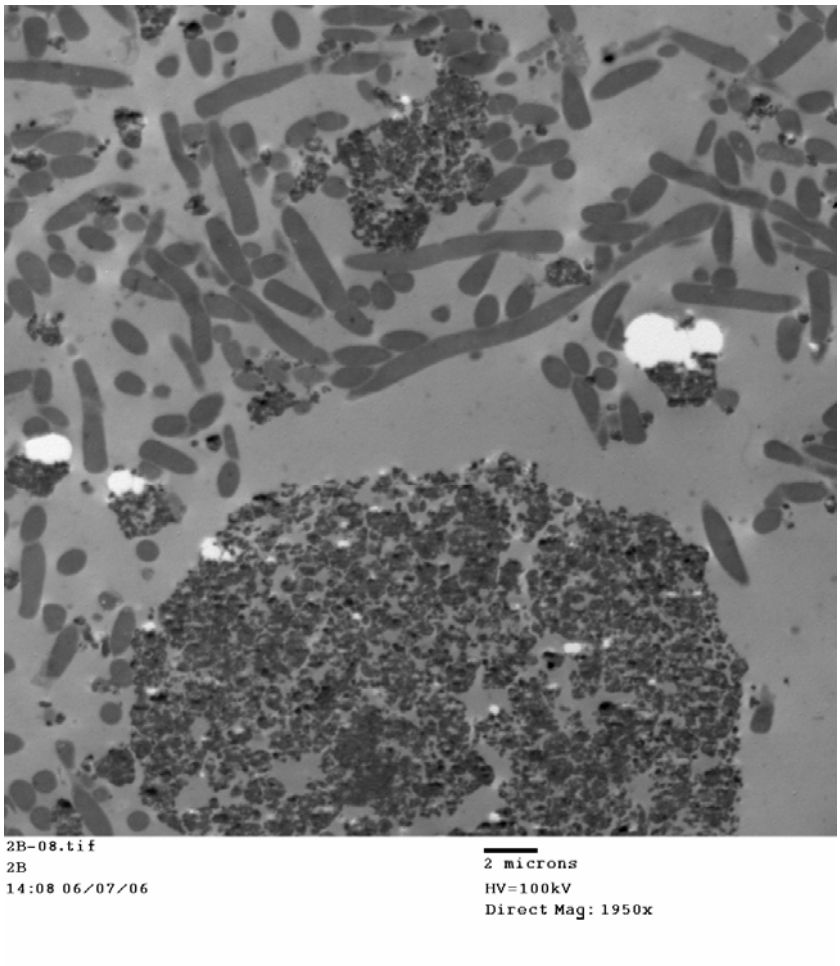

Figure 3.25 TEM micrograph of treated *B. anthracis* cells – low magnification.

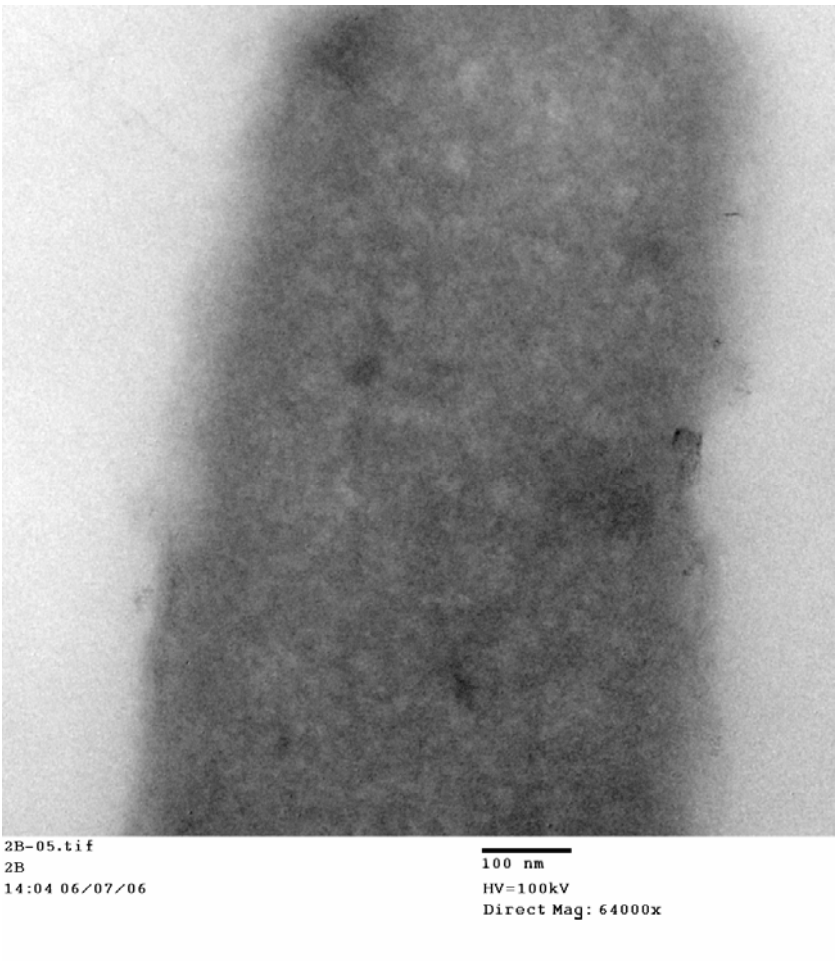

Figure 3.26 TEM micrograph of treated *B. anthracis* cells – displaying a damaged cell wall.

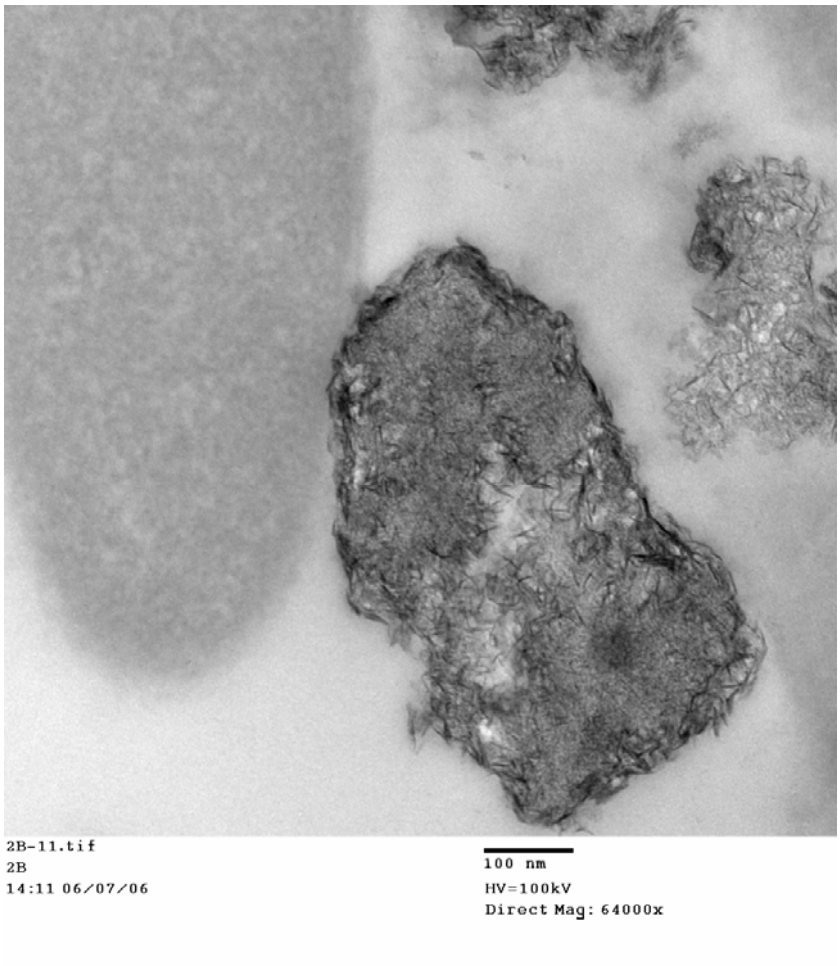

Figure 3.27 TEM micrograph of treated *B. anthracis* cells – displaying a damaged cell.

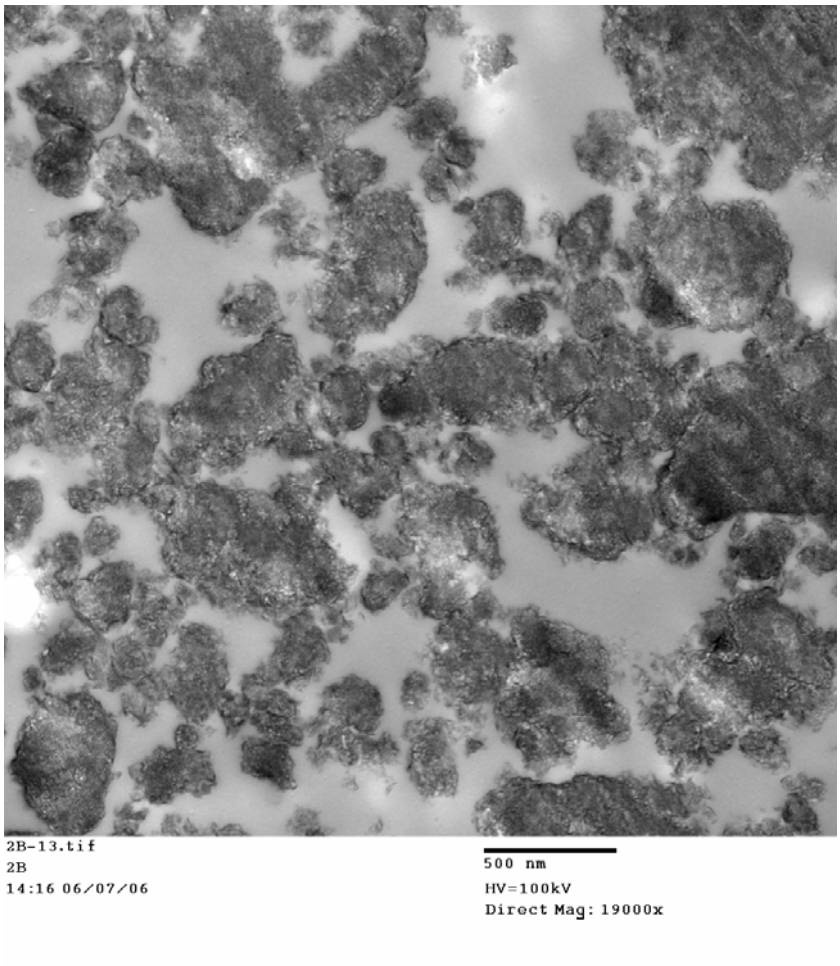

Figure 3.28 TEM micrograph of treated *B. anthracis* cells – displaying dead cell parts.

Electron micrographs of the prepared *B. anthracis* Δ Sterne strain spores are shown in Figures 3.29 and 3.30. The spores in Figure 3.29 are further stained with uranyl acetate to enhance the spores. Figure 3.30 shows one single healthy spore, displaying its very tough and thick protective coat. Each individual spore displays a diameter of approximately 500 nm.

The treated spores are shown in Figures 3.31 and 3.32. Figure 3.31 shows very well the believed mechanism in which the death occurs. The spore is not completely healthy anymore, but it can be seen how it is surrounded by metal oxide material. This picture represents the perfect 'intermediate' stage of the process in which the spores die. One step further is represented in Figure 3.32. Only DNA, proteins and parts of the spores remain.

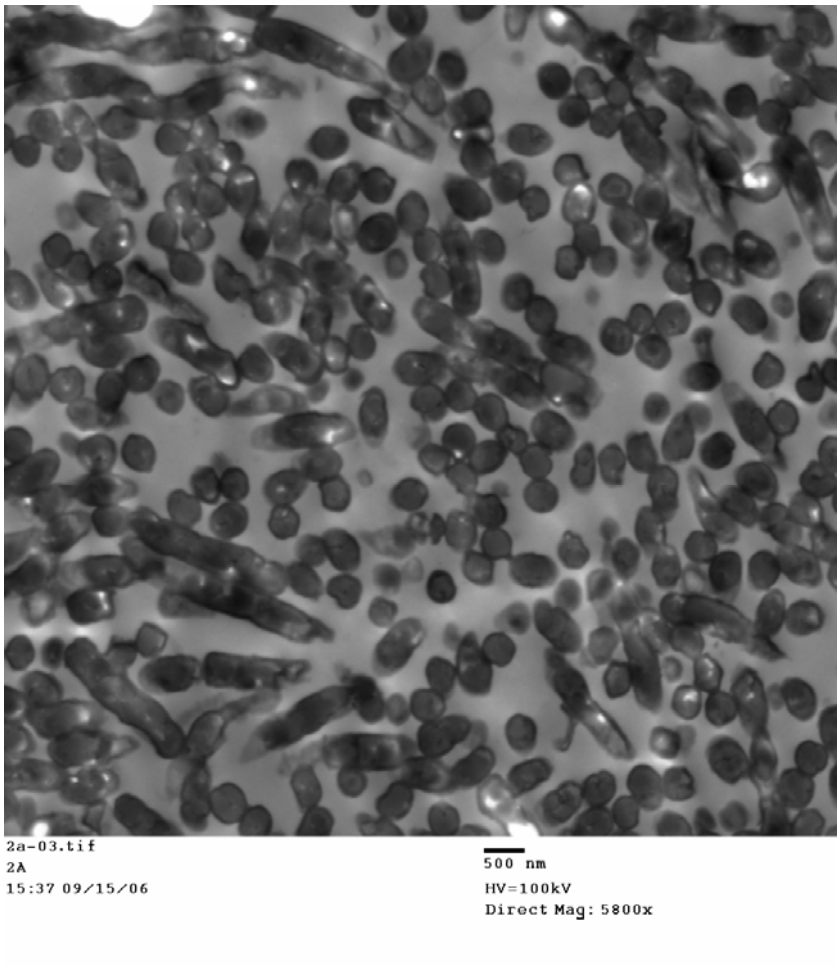

Figure 3.29 TEM micrograph of untreated *B. anthracis* spores – low magnification.

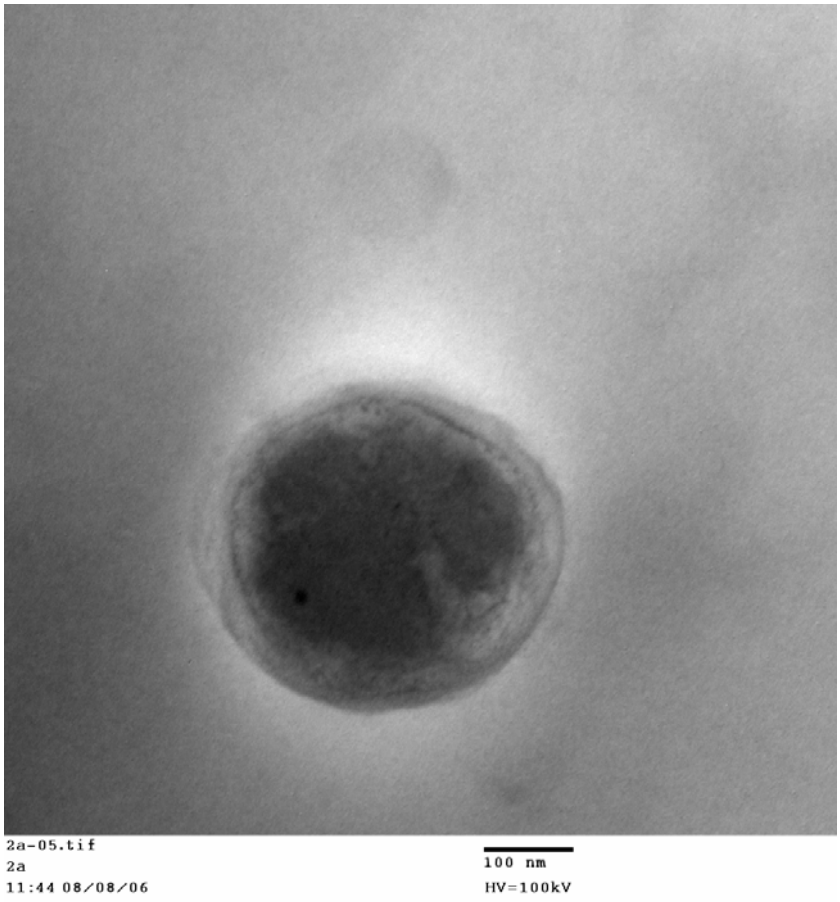

Figure 3.30 TEM micrograph of untreated *B. anthracis* spores – high magnification.

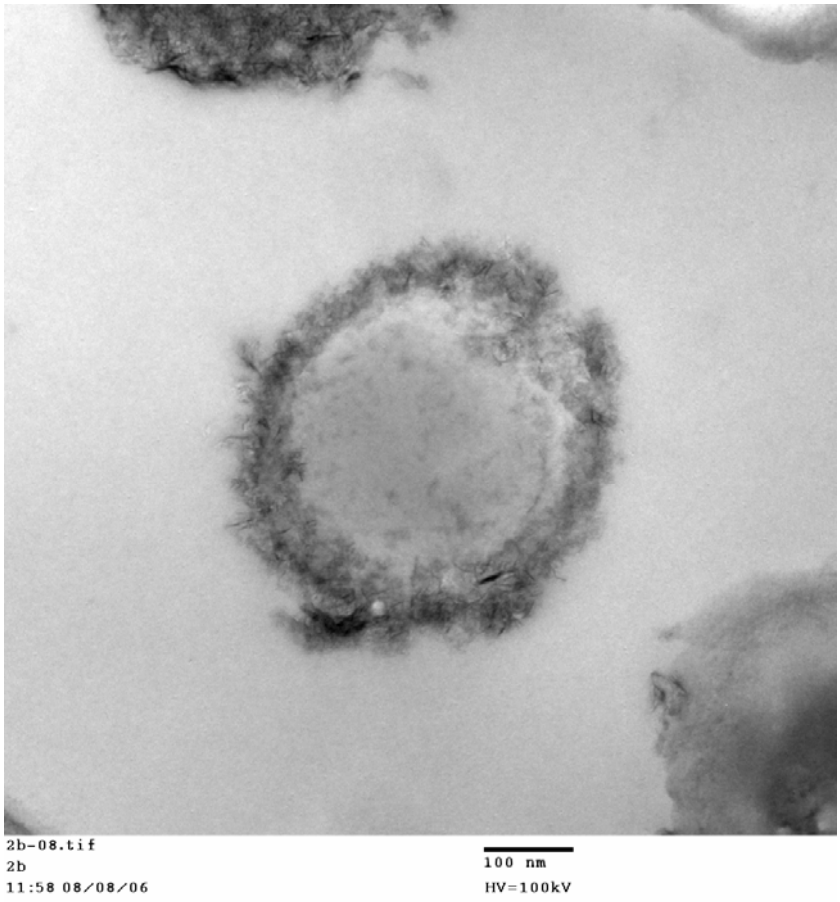

Figure 3.31 TEM micrograph of treated *B. anthracis* spores –displaying damaged spore.

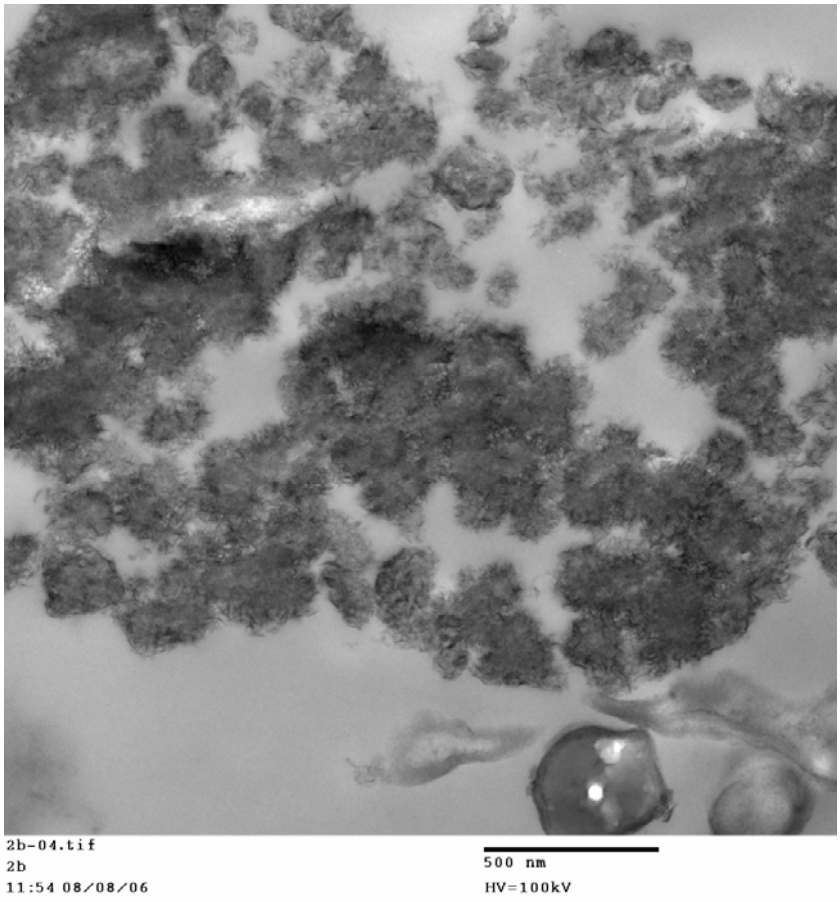

Figure 3.32 TEM micrograph of treated *B. anthracis* spores – displaying spore remains.

3.5 Conclusions

In order to kill spores, a material normally needs to have some functional group or chemical attached to it that is very aggressive and most often not environmentally friendly. The search for the ultimate environmentally safe biocide continues, but it is rather difficult to find a material that is completely environmentally friendly and at the same time kills several microorganisms, including vegetative cells and the more dormant spores.

It is noteworthy that most of these experiments were performed using the membrane method, which includes having a 'solid-solid' interaction. These results may have been even better if performed in a water suspension where the direct contact between cells/spores and nanoparticles might be better, leading to higher log kills. Although utilizing this 'solid-solid' interaction method, the results obtained were very satisfactory, including log kills of spores over 6 in several cases. The vegetative cells of *E. coli* and *B. anthracis* had little resistance against all of the halogenated and interhalogenated adducts, leading to complete kills of the high concentrations used during testing. It is also worth to note that the non-halogenated metal oxides had some biocidal activity against the *E. coli* cells, with log kill values over 5 in all of the metal oxides.

Reasons for the excellent biocidal and sporicidal activity of these nanomaterials include their abrasive character, caused by their high surface area and many corners, edges and defect sites, the oxidative power of the halogens/interhalogens and the electrostatic attraction, as seen in the TEM pictures, caused by the overall negative surface charge of most microorganisms and the overall positive surface charge of many metal oxides.

3.6 References

(1) Nishino, T.; Nakazawa, S. *Jap. J. Microbiol.* **1973**, *17*, 383-392.

(2) Williams, N. D.; Russell, A. D. *FEMS Microbiol. Lett.* **1993**, *106*, 183-186.

(3) Gorman, S. P.; Hutchinson, E. P.; Scott, E. M.; McDermott, L. M. *J. Appl. Bacteriol.* **1983**, *54*, 91-99.

(4) Newton, J. M.; Henderson, G.; Vickers, J. A. *J. Appl. Bacteriol.* **1967**, *30*, 484-487.

(5) Helander, I. M.; Alakomi, H-L.; Latva-Kala, K.; Mattila-Sandholm, T.; Pol, I.; Smid, E. J.; Gorris, L. G. M.; von Wright, A. *J. Agr. Food Chem.* **1998**, *46*, 3590-3595.

(6) Tennen, R.; Setlow, B.; Davis, K. L.; Loshon, C. A.; Setlow, P. *J. Appl. Microbiol.* **2000**, *89*, 330-338.

(7) Williams, N. D.; Russell, A. D. *FEMS Microbiol. Lett.* **1992**, *99*, 277-280.

(8) Foegeding, P. M.; Busta, F. F. *Appl. Environ. Microbiol.* **1983**, *45*, 1374-1379.

(9) Barker, C.; Park, S. F. *Appl. Environ. Microbiol.* **2001**, *67*, 1594-1600.

(10) Bloomfield, S. F.; Arthur, M. *Lett. Appl. Microbiol.* **2001**, *8*, 101-104.

(11) Bloomfield, S. F.; Arthur, M. *J. Appl. Microbiol.* **1992**, *72*, 166-172.

(12) Bloomfield, S. F.; Megid, R. *J. Appl. Microbiol.* **1994**, *76*, 492-499.

(13) Coates, D.; Death, J. E. *J. Clin. Pathol.* **1978**, *31*, 148-152.

(14) Cousins, C. M.; Allan, C. D. *J. Appl. Bacteriol.* **1967**, *30*, 168-174.

(15) Gorman, S. P.; Scott, E. M.; Hutchinson, E. P. *Int. J. Pharm.* **1983**, *17*, 291-298.

(16) Gorman, S. P.; Scott, E. M.; Hutchinson, E. P. *J. Appl. Bacteriol.* **1984**, *56*, 295-303.

(17) Gorman, S. P.; Scott, E. M.; Hutchinson, E. P. *J. Appl. Bacteriol.* **1985**, *59*, 99-105.

(18) Russell A. D. *Clin. Microbiol. Rev.* **1990**, *3*, 99-119.

(19) Wyatt, L. R.; Waites, W. M. *J. Gen. Microbiol.* **1975**, *89*, 337-344.

(20) Lim. D. *Microbiology*. Boston, MA. 2nd Ed. **1998**.

(21) http://www.cat.cc.md.us/courses/bio141/lecguide/unit1/prostruct/gpcw.html

(22) http://www.jochemnet.de/fiu/lab7.pdf

(23) Tennen, R.; Setlow, B.; Davis, K. L.; Loshon, C. A.; Setlow, P. *J. Appl. Microbiol.* **2000**, *89*, 330-338.

(24) Bloomfield, S. F.; Megid, R. *J. Appl. Bacteriol.* **1994**, *76*, 492-499.

CHAPTER 4 - VIRUCIDAL PROPERTIES OF METAL OXIDE NANOPARTICLES AND THEIR ADDUCTS

4.1 Introduction

This chapter will include using the prepared halogen and interhalogen adducts to see if they can be used successfully against different viruses, including MS2, φ-X174 and PRD1. Their characteristics will be explained in detail in **4.2**.

There is a very limited amount of data available on the use of nanomaterials against viruses. Koper et al.[1] described the use of chlorine and bromine adducts of nanosized and conventionally prepared MgO and CaO against MS2 virus. They varied the concentration of the materials along with the contact times and found that at a powder concentration of 10 mg/mL all formulations were very efficient. As the powder concentrations were decreased the virucidal activity also went down.

A patent[2] was released in 2004 in which the authors used a photocatalytic nano-crystalline TiO_2 thin film preparation in a reverse micelle solution to kill both bacteria and viruses. The organisms were destroyed using UV light in order to enhance the photocatalytic activity of the thin films.

Nanoparticles have also been used as drug carriers to perform antiviral activity in vitro. One example is the work done by Bender, et al.[3] that involved polyhexylcyanoacrylate nanoparticles loaded with the HIV protease inhibitor saquinavir. Results showed the inhibition of HIV type 1 antigen production. Nanoparticles have been used as carriers in an attempt to use a smaller dose and to minimize side effects and toxicity.

Hamouda and co-workers[4] reported on the use of a non-ionic surfactant nanoemulsion against enveloped viruses. The authors have previously reported on the use of different nanoemulsions as biocides. These emulsions are novel water-in-oil formulations, stabilized by small amounts of surfactants. Essentially they consist of a uniform population of droplets with a diameter of 400-800 nm. The nanoemulsion used in this study was named 8N8. They found that one percent of the 8N8 nanoemulsion was virucidal within 15 minutes and that the oil droplets fused with the viral envelopes.

Although not many nanomaterials have been used to destroy viruses there are many other materials that have been used. Sommer et al.[5] reported the use of a combination of ozone and hydrogen peroxide, to generate radicals and kill several viruses, including MS2, φ-X174 and PRD1. A 6-log kill was observed with all the three test viruses.

The need of finding methods to remove and/or destroy viruses is of big importance. Especially disinfection of wastewater is of big concern. Different methods have been used and many of them involve the filtration of organisms, rather than destroying them. The biggest concern regarding wastewater disinfections is the need for a material or method that is a broad spectrum biocide, that is, it needs to kill many different types of organisms, including Gram-positive and Gram-negative bacteria, as well as different viruses and perhaps even spores. Blatchley and co-workers[6] found that a combination of chlorination and dechlorination followed by UV irradiation provided only modest inactivation of phage and bacteria. Spores were not investigated.

Efforts were made by Pedahzur et al.[7] to increase the disinfection of water using a combination of Ag and H_2O_2, in hope that both bacteria and viruses could be killed. Bacteria were killed with great success, but the effect on the MS2 phage was very moderate.

A British patent[8] was released in 2002, in which they have used a dry mixture of an inorganic halide, such as potassium chloride, an oxidizing agent, such as a persulfate salt, and two surfactants to kill bacteria and viruses. The system generates hypohalite ions upon dissolution in water, which act as biocides. Sodium bicarbonate is another material that is known to be biocidal against certain bacteria and fungi, but its activity against viruses was not investigated until recently.[9] Special interest in sodium bicarbonate arise from its possible use to disinfect food contact surfaces which requires a non-corrosive and non-toxic disinfectant. A 5% concentration of sodium bicarbonate was found to have a 4-log reduction against the selected test virus, within 1 minute. A combination of sodium bicarbonate and either aldehyde or hydrogen peroxide further increased the virucidal efficiency.

One method to remove viruses instead of killing them include filtration using specially prepared membranes. The simplest filters used are plain filters with very small pore diameters (0.1 and 0.2 μm),[10] which is small enough to remove bacteria and some viruses. This method, however, is very time consuming since the flow rate is determined by the small pore diameter. One way to increase the flow rate is to use larger pore sizes and develop a filter media that itself is capable of either adsorbing or killing organisms. This has been done using nanoporous aluminum oxide[11] which adheres to the microorganisms by electrostatic interactions and hence removes them from the water. Tepper et al.[12] found that a filter media with an alumina (AlOOH) as the active component retained a log 6 amount of viruses and bacteria through electrostatic interactions. The AlOOH fibers were 2 nm in diameter and had a surface area of 350-500 m^2/g. Significantly large flow rates were still possible as compared to the filters that separated microorganisms from the water solely based on pore size.

Battigelli and co-workers reported on the use of UV light to inactivate several model viruses in water, including MS2 and Phi-X174.[13] They found that UV radiation of 254 nm in wavelength was efficient to inactivate bacteriophages in phosphate buffered water but only to a certain extent. MS2 exhibited the greatest resistance, showing less than a 1 $\log_{10}$ reduction. Phi-X174 however, showed a 7 log inactivation using less exposure. While this result seems promising, consideration must be taken to the fact that in waters of high turbidity, disinfection efficiency would be much lower.

Brion and co-workers studied the use of iodine for disinfection of MS2 phage suspended in buffered water.[14] Iodine has been of interest as a disinfectant because it is easy to apply and has stable chemical storage characteristics. Since iodine is a weaker oxidant than chlorine it has been of interest due to its lower corrosive character. Iodine was found to be very efficient against MS2 phage even at low concentrations of iodine. Little is known about the mechanism in which iodine and other halogens disinfect viruses. Speculations of how iodine acts on MS2 phage include disruption of the protein coat of the virus, and that iodine is acting upon sulfhydryl bonds in the protein coat.

The mechanism involved using either chlorine dioxide or iodine for the inactivation of poliovirus has been studied by Alvarez et al.[15] Poliovirus is very similar in physical characteristics to MS2 and MS2 is often used as a model virus for poliovirus. The authors found that chlorine dioxide damages the nucleic acids of the phage, whereas iodine reduced the ability of the virion to adsorb to the host cell. They also found that the reaction of hypoiodous acid (HIO) with the protein coat appeared to be oxidative, in similarity with how iodine has been reported to act on proteins and viruses by oxidation of the sulfhydryl groups.

There is an urgent need for a new material that can be used to kill viruses, and nanomaterials are a promising class of materials with much potential that are worth investigating. Just like anthrax, viruses could be weaponized and used as warfare agents and there is little or no equipment available for such a virus attack, which could cause a terrible situation. Not much work has been done to date involving this class of materials, and the main reason for this could be that bacteriophages (viruses that use bacteria as their host) are slightly difficult to work with and easily get contaminated. This chapter will describe in detail the work that we have done using our halogenated and interhalogenated nanoparticles against viruses.

4.2 Structure and Properties of Viruses

The word virus comes from the Latin language and means toxin or poison.[16] The name came from the fact that viruses are capable of infecting cells of biological organisms. The main difference between a bacteria and a virus is that the virus needs to infect a host cell before it is capable to reproduce, whereas a bacteria can reproduce independently through cell division.[16,17] One common form of viruses, commonly known as bacteriophage or phage, are those that infect bacteria. Bacteriophages infect only specific bacteria and the process includes binding to surface receptor molecules followed by entering the cell.[16] Almost immediately bacterial polymerase translates viral mRNA into protein, which then becomes either new virions within the cell, helper proteins, which assembles new virions, or become proteins involved in cell lysis.

A bacteriophage can exist in three major forms,[18] somewhat similar to the way a typical bacillus can exist either as a vegetative bacteria or a spore. The three states are: prophage, vegetative phage and mature phage. When the phage is metabolically inert, the phage exists

outside of the host cell in the mature form. As some of the phage particle penetrates the cell after adsorption it is referred to as in the vegetative state, caused by its almost unlimited reproductive capacity. A third state, prophage exists only in certain temperate phages in which the phage does not kill the host cell, but rather lives in a relationship with the bacteria.

The infective process consists primarily of four steps:[18] (1) adsorption of the phage to the host cell, (2) penetration of the phage to the host cell, (3) the intracellular multiplication of the virus, and (4) lysis of the host cell and release of phage progeny. The environmental conditions at which adsorption and infection occur are very important and it is not difficult to find conditions of temperature, pH, salt concentration or chemical composition at which host cells will multiply, but no lysis will occur. The adsorption stage is very specific and if a coliphage fails to attack a certain strain of *E. coli*, it is most likely due to the lack of adsorption of the host cell to the phage. The actual attachment to the cell is made to specific receptor substances on the cell surface, often parts of the cell wall. In addition to using the right strain of host cell (for example *E. coli* C3000 for MS2 phage), the environmental factors are also of major significance. Even with the correct strain there may be lack of adsorption due to lack of the right salt concentration, for example. Upon adsorption of phage particle to the cell certain reproductive components of the phage penetrate to the cell interior, thus the phage changes from the mature to the vegetative condition. The host cell then stops cell division and major cytological changes occur. At this point synthesis of phage protein and DNA (or RNA, depending upon what kind of phage) starts and phage multiplication has started. The number of infected particles in each cell increases until host cell lysis occurs.

The viruses studied herein are all phages that infect *E. coli* cells. Bacteriophages that infect *E. coli* are commonly referred to as coliphages. Since viruses need a host in order to

replicate themselves, it is commonly argued whether or not they are in fact living organisms.[16] Most virologists agree that since they do not meet all of the criteria of the definition of life, they are in fact non-living organisms.

Viruses are known to cause many common infectious human diseases, such as AIDS, common influenza and bird flu, to name a few. There are very few medicines that have any effect on the diseases, but it is rather better to prevent a viral infection with a vaccination. Although commonly believed, normal antibiotics have no effect on viral diseases.

All viruses have the same general structure:[17] their genetic material can be of either DNA or RNA and the genetic material is surrounded by a protein coat. Some viruses also have an additional outer membrane outside of the protein coat. The complete virus particle, including its nucleic acid and coat is often referred to as a virion. Another interesting and very characteristic aspect of viruses is that they are extremely small. Compared to bacteria, viruses are much smaller, in fact, most viruses are smaller than 200 nm and many even smaller than 100 nm. This makes them much more difficult to observe, which means an electron microscope is in need for its visualization.

In general, there are four different types of viruses: helical, polyhedral (often referred to as icosahedral), enveloped and complex (or binal) viruses.[16,17] These forms describe the overall shape of the virus. Helical viruses consist of subunits arranged together around a central axis,[16] forming a helical structure. The overall arrangement appears like a rod-shaped virion that can vary in size significantly. Polyhedral or icosahedral viruses appears as having a spherical symmetry at low magnification, but in fact looks similar to a soccer ball, which is not truly spherical on closer inspection. Enveloped viruses encompass a viral envelope, which can give the virus further protection against enzymes and certain chemicals. Complex, or binal, viruses

may possess extra structures, such as a tail or outer structures, and are not entirely helical or polyhedral.

The strandedness of a virus is irrespective to the nucleic acid (DNA or RNA) and may be single or double. A single-stranded virus consists of an unpaired nucleic acid, whereas a double-stranded virus consists of two complimentary paired nucleic acids.

4.3 Experimental Methods

4.3.1 Preparation of High Titer Lysates

To prepare high titer lysates of the three bacteriophages used (MS2, Phi-X174 and PRD1) the following procedure was used. 10 sterile tubes (10 mL) with caps were placed into a test tube rack in a 47-50 °C water bath. 2.5 mL of melted TYE soft agar was added to each tube, along with 0.1 mL of *E. coli* overnight culture and 0.1 mL of respective lysates. For MS2 the C3000 strain of *E. coli* was used, for Phi-X174 *E. coli* B strain and for PRD1 *E. coli* C strain was used. Each tube was swirled to mix thoroughly. Each tube was then poured onto a room temperature TYE agar plate and the plate was swirled to ensure that the overlay covered the entire surface of the agar plate. Cold plates could not be used as the soft agar overlay would solidify too quickly and not cover the entire agar surface. The overlay was allowed to solidify and then the plates were inverted and incubated at 37 °C for 24 hours (lysis should be evident after approximately 4 hours, if successful). After 24 hours a small amount of Benzer Dilution Fluid (BDF) was poured onto one plate and a hockey stick (bent glass rod) was used to carefully scrape off the soft agar overlay. The overlay was then poured into another of the lysed plates and this was continued until all of the soft agar had been collected in BDF. The BDF and agar was then collected in a

couple of centrifuge tubes and centrifuged at 1000 rpm for 25 minutes. The supernatants were collected and poured into a sterile bottle. A small amount of chloroform was added to prevent bacterial contamination and the lysate was stored at 4-8 °C in the refrigerator.

In order to determine the concentration of the prepared lysates serial dilutions were performed. The stock was expected to be approximately 10^{8}-10^{11} in concentration; therefore 10^{-5}, 10^{-6}, 10^{-7}, 10^{-8}, 10^{-9} and 10^{-10} dilutions were used in hope to give viable results. Three tubes were prepared for each dilution factor and in each tube 2.5 mL of melted soft agar and 0.1 mL *E. coli* was added. 0.1 mL of each dilution factor was added to each set of three tubes; the tubes were swirled and poured onto labeled agar plates. Once solidified, the plates were inverted and placed for 24 hours into the incubator at 37 °C. The plates were then removed, plaques were counted and the titer concentration determined.

4.3.2 Test Procedure

The *E. coli* host culture was prepared according to the following procedure: 100 µL of stock solution, 100 µL 1 M $CaCl_2$, 1 mL 10 % glucose and 100 µL 1 % thiamine were added to approximately 30 mL TYE media. The solution was allowed to grow over night and used the following day.

TYE Complete agar plates were prepared according to the following procedure: 1 g yeast extract, 8 g NaCl, 10 g tryptone and 15 g agar were dissolved in deionized water, with the final volume equal to 1 L. The mixture was then autoclaved at 121 °C for 20 min and slowly cooled down to 50-60 °C, when 10 mL of a 10 % glucose solution, 2 mL 1 M $CaCl_2$ solution, and 1 mL

1% thiamine solution were added to the solution. After mixing the solution was poured in Petri dishes and after solidification TYE Complete agar plates were obtained.

Soft agar was prepared according to the following procedure: 5 g NaCl, 7 g agar, and 10 g tryptone were dissolved in deionized water with the final volume equal to 1 L. The mixture was allowed to boil under stirring and later poured into 250 mL individual bottles and autoclaved at 121 °C for 20 min. Before use, the soft agar was micro waved for approximately 2-3 minutes until desired softness was reached and then kept at 47 °C in a water bath until further use.

Typical lysates used contained approximately 1 x 10^7 -10^{11} plaque forming units (PFUs) per mL. During each experiment, nanoparticles were added to phosphorous buffer solution (PBS) to a final concentration of either 10 mg/mL or 20 mg/mL.[1] 100 µL bacteriophage (MS2, φ-X174 or PRD1) was added to each solution and the mixture was vortexed. After 5 and 30 minutes reaction time, an aliquot of 100 µL was removed from the solution and added to the *E. coli* host culture solution kept at 47 °C, containing 100 µL *E. coli* in 2.5 mL TYE soft agar. This mixture was then plated on TYE Complete agar plates and incubated. Each sample was plated in duplicate and the experiment was repeated at least one more time. After 24 hrs of incubation at 37 °C plaque forming units were counted, compared to the control count and log kill values were calculated.

In order to exclude that there was a toxic effect of the nanoparticle supernatant to the host cells (which would lead to false good results, due to no host cells available for the phage to reproduce on); the following experiment was developed and performed. Nanoparticles were added to phosphorous buffer solution (PBS) to a final concentration of 20 mg/mL. The solution was vortexed and after 30 minutes reaction time, an aliquot of 100 µL was removed from the solution and added to the *E. coli* host culture solution kept at 47 °C, containing 100 µL *E. coli* in

2.5 mL TYE soft agar. This mixture was then plated on TYE Complete agar plates and incubated. If there was a severe toxic effect caused by the nanoparticle supernatant solution, the incubated plates would not show a lawn of bacteria growth. Several experiments were performed using different nanoparticles and no toxic effect was found.

4.3.3 Transmission Electron Microscopy (TEM)

TEM images were recorded on a Philips CM 100, operating at 100 kV.

In order to view the virus under the microscope, the following procedure was performed. The procedure included staining the virus solution with uranyl acetate, so called negative staining, in order to visualize the virus better. 20 μL of virus solution was put on parafilm in a Petri dish. If necessary, the virus solution was diluted in distilled water first. With a pair of tweezers, the 300 mesh copper Formvar/carbon grid was carefully floated on top of the drop for one minute. The grid was removed and the edge of the grid was then carefully touched against a filter paper, in order to remove excess virus solution. The grid was floated on top of a 20 μL drop of 2 % uranyl acetate for one minute, followed by removal of excess solution against a filter paper. The grid was then imaged under the microscope.

In order to visualize treated virus solutions under the microscope, 200 μL of the virus solution was allowed contact with less than 50 mg of NA-Al_2O_3/ICl_3 Plus. The mixture was vortexed and then allowed to interact for 10 minutes. The mixture was centrifuged for 5 minutes and 20 μL of the supernatant was imaged under the microscope, using the above described procedure.

4.4 Results and Discussion

4.4.1 MS2

For a long time it has been known that many of the common disease producing animal viruses, for example those that cause influenza and polio, contain RNA as their genetic material.[19] MS2 is one of the most common surrogates of human enterovirus[1] and it is a single stranded and linear RNA (ssRNA) virus that belongs to the Leviviridae family.[20,21] The complete RNA sequence of the phage was determined in 1976 by Walter Fiers.[21] It was the first genome to be discovered in scientific history. MS2 phage has been recommended in the past[20] as a model phage for chlorine, ozone and other disinfectant inactivation studies; however it has been found that the phage is sensitive to iodine already at low doses. MS2 is a coliphage, meaning that it uses *E. coli* as its host cell.[19] The molecular weight of MS2 is approximately 1 x 10^6 Da.

The experiments using the prepared halogen and interhalogen adducts described in Chapter 2 were tested against the different bacteriophages using a method described in the literature.[1] The results are discussed in groups of metal oxide used.

An initial concentration of 20 mg nanoparticles per mL of buffer solution was used to determine if the nanoparticles were at all efficient. The 'naked' metal oxides were tested as well, in hope that the more environmentally friendly nanoparticles were efficient. Table 4.1 shows the results using the different adducts of NA-Al_2O_3 Plus against the coliphage MS2. Only high concentrations of the phage was used, as it was of interest to distinguish between the possibly various activities of the different adducts (including adducts of NA-TiO_2 and NA-CeO_2). A complete kill of all the viruses present leads to a 7.11 Log Reduction, so it can be observed that all the prepared halogen and interhalogen adducts of NA-Al_2O_3 Plus displayed a complete kill (a

Log-7 kill) of the MS2 phage. The 'naked' alumina, however, did not have any measurable activity using these high concentrations. It should be noted though that if much lower concentrations had been used, some activity might have been observed. We chose however, to only look for the most active materials in this study. Standard deviation values were not calculated as all the halogenated and interhalogenated adducts displayed a complete kill of all the phage present.

Table 4.1 Log Reduction of MS2 virus by NA-Al_2O_3 Plus Adducts (20 mg/mL).

Nanoparticle Formulation	Contact Time [min]	
	5	30
NA-Al_2O_3-act.	t.n.t.c	t.n.t.c
NA-Al_2O_3/Cl_2	7.11	7.11
NA-Al_2O_3/Br_2	7.11	7.11
NA-Al_2O_3/I_2	7.11	7.11
NA-Al_2O_3/ICl	7.11	7.11
NA-Al_2O_3/IBr	7.11	7.11
NA-Al_2O_3/ICl_3	7.11	7.11

t.n.t.c = too numerous to count

Table 4.2 Log Reduction of MS2 virus by NA-Al_2O_3 Plus Adducts (10 mg/mL).

Nanoparticle Formulation	Contact Time [min]	
	5	30
NA-Al_2O_3-act.	t.n.t.c	t.n.t.c
NA-Al_2O_3/Cl_2	7.11	7.11
NA-Al_2O_3/Br_2	7.11	7.11
NA-Al_2O_3/I_2	7.11	7.11
NA-Al_2O_3/ICl	7.11	7.11
NA-Al_2O_3/IBr	7.11	7.11
NA-Al_2O_3/ICl_3	7.11	7.11

t.n.t.c = too numerous to count

Table 4.2 displays the results using a slightly lower nanoparticle concentration (10 mg/mL). It can be seen that again, a complete kill of all the phage present has occurred, even at this lower concentration of nanoparticles. These results are very promising since very high concentrations of the phage were used and very high log kills were obtained.

Table 4.3 displays the results using NA-CeO_2 and its adducts against MS2 (nanoparticle concentration = 20 mg/mL). The main difference between these adducts and those of NA-Al_2O_3 Plus is that the chlorinated adduct of NA-CeO_2 does not appear to have any activity, similar to the 'naked' metal oxides. This can possibly be explained by the low amount of chlorine present, compared to NA-Al_2O_3/Cl_2 Plus. When a lower concentration of nanoparticles is used (10 mg/mL), similar results are observed (Table 4.4); again the 'naked' cerium oxide and its chlorinated adduct are not active in the use against MS2 phage.

Table 4.3 Log Reduction of MS2 virus by NA-CeO_2 Adducts (20 mg/mL).

Nanoparticle Formulation	Contact Time [min]	
	5	30
NA-CeO_2-act.	t.n.t.c	t.n.t.c
NA-CeO_2/Cl_2	t.n.t.c	t.n.t.c
NA-CeO_2/Br_2	7.11	7.11
NA-CeO_2/I_2	7.11	7.11
NA-CeO_2/ICl	7.11	7.11
NA-CeO_2/IBr	7.11	7.11
NA-CeO_2/ICl_3	7.11	7.11

t.n.t.c = too numerous to count

Table 4.4 Log Reduction of MS2 virus by NA-CeO_2 Adducts (10 mg/mL).

Nanoparticle Formulation	Contact Time [min]	
	5	30
NA-CeO_2-act.	t.n.t.c	t.n.t.c
NA-CeO_2/Cl_2	t.n.t.c	t.n.t.c
NA-CeO_2/Br_2	7.11	7.11
NA-CeO_2/I_2	7.11	7.11
NA-CeO_2/ICl	7.11	7.11
NA-CeO_2/IBr	7.11	7.11
NA-CeO_2/ICl_3	7.11	7.11

t.n.t.c = too numerous to count

Table 4.5 displays the results obtained using NA-TiO_2 and its halogen and interhalogen adducts (20 mg/mL). In similarity with the NA-CeO_2 adducts, the chlorinated adduct was not efficient along with the 'naked' TiO_2. The other halogen and interhalogen adduct were, however, very efficient, displaying a complete kill of all the phage present. Even at a low nanoparticle concentration of 10 mg/mL, the same results were obtained with complete kills of all adducts with the exception of the chlorinated adduct (Table 4.6).

Table 4.5 Log Reduction of MS2 virus by NA-TiO_2 Adducts (20 mg/mL).

Nanoparticle Formulation	Contact Time [min]	
	5	30
NA-TiO_2-act.	t.n.t.c	t.n.t.c
NA-TiO_2/Cl_2	t.n.t.c	t.n.t.c
NA-TiO_2/Br_2	7.11	7.11
NA-TiO_2/I_2	7.11	7.11
NA-TiO_2/ICl	7.11	7.11
NA-TiO_2/IBr	7.11	7.11
NA-TiO_2/ICl_3	7.11	7.11

t.n.t.c = too numerous to count

Table 4.6 Log Reduction of MS2 virus by NA-TiO_2 Adducts (10 mg/mL).

Nanoparticle Formulation	Contact Time [min]	
	5	30
NA-TiO_2-act.	t.n.t.c	t.n.t.c
NA-TiO_2/Cl_2	t.n.t.c	t.n.t.c
NA-TiO_2/Br_2	7.11	7.11
NA-TiO_2/I_2	7.11	7.11
NA-TiO_2/ICl	7.11	7.11
NA-TiO_2/IBr	7.11	7.11
NA-TiO_2/ICl_3	7.11	7.11

t.n.t.c = too numerous to count

To summarize, almost all of the prepared halogen and interhalogen adducts displayed a complete kill of all the bacteriophage present (corresponding to more than a log-7 kill). MS2 phage is not a very resistant bacteriophage,[20] compared to the other two phages studied, but a log-7 kill already within 5 minutes is very impressive. The 'naked' metal oxide nanoparticles do not display any detectable activity against the phage in any of the three used metal oxides, indicating that the oxidizing role of the halogen/interhalogen is extremely important. The mechanism in which this damage takes place is not completely known but it is believed that the oxidative character of the different halogens and interhalogens play an important role.

TEM images of the MS2 virus can be seen in Figures 4.1-4.3. The virus is approximately 29 nm in size (Figure 4.3), which is fairly small for a virus. Microscopic measurement of size of virus particles is complicated by shrinkage and distortion of drying, but also by increase of size by shadowing with metals (such as uranyl acetate).[18] However, electron microscope is still the most informative method of size characterization. Images of MS2 virus treated with nanoparticles (NA-Al_2O_3/ICl_3 Plus) can be seen in Figures 4.4-4.7. It appears that the virus particle has been destroyed and only nucleic acids and proteins remain in random arrangements.

In Figures 4.4 and 4.6 it seems like the remaining proteins and nucleic acids of the former virus have agglomerated together into certain structures, whereas in Figures 4.5 and 4.7 is appears that very small parts of proteins and nucleic acids almost form an infinite network together. It can be clearly seen though, that there has been a definite change in the structure of the virus and it is no longer a healthy virus.

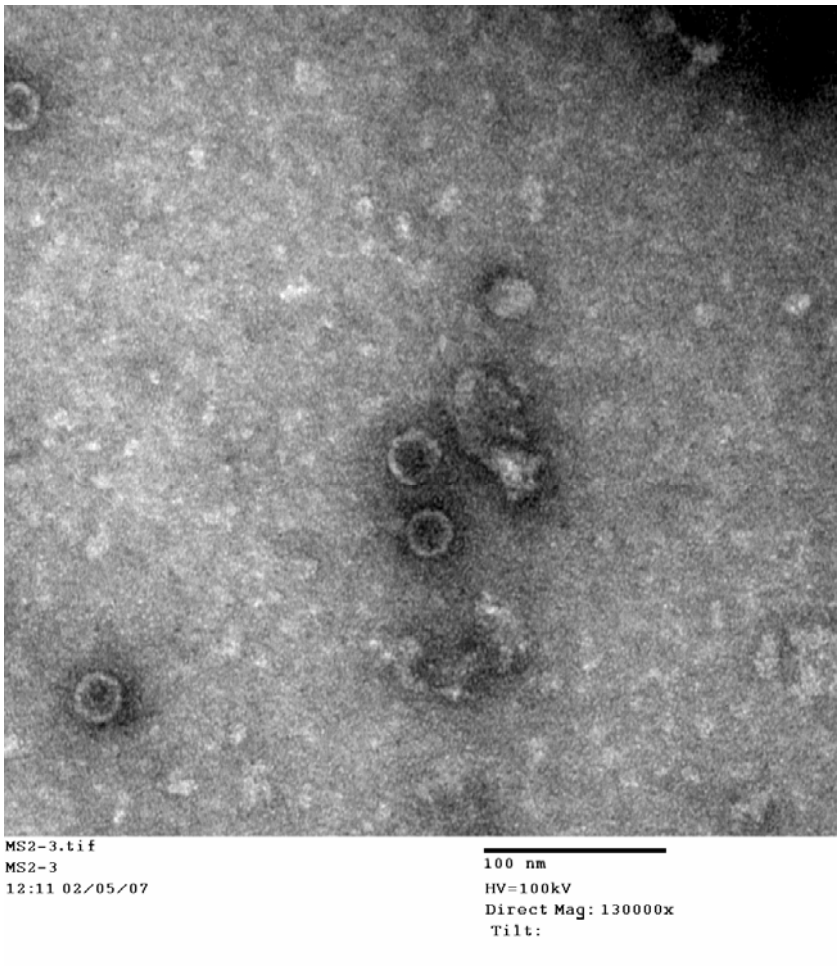

Figure 4.1 TEM image of untreated MS2 virus – low magnification.

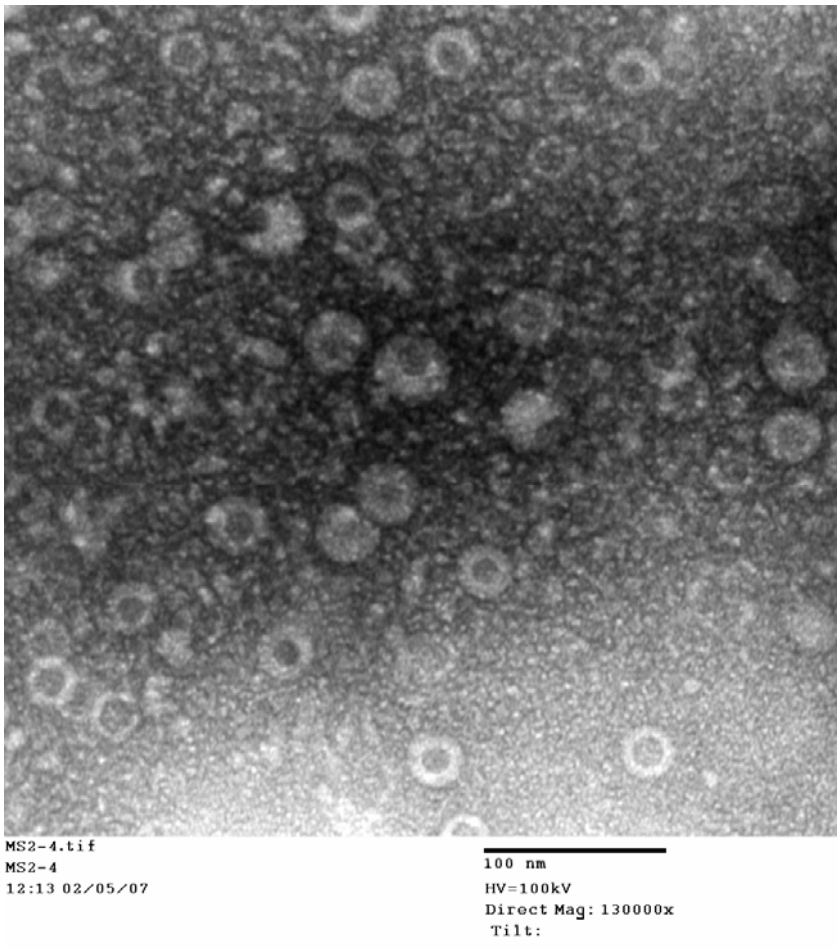

Figure 4.2 TEM image of untreated MS2 virus – displaying several viruses.

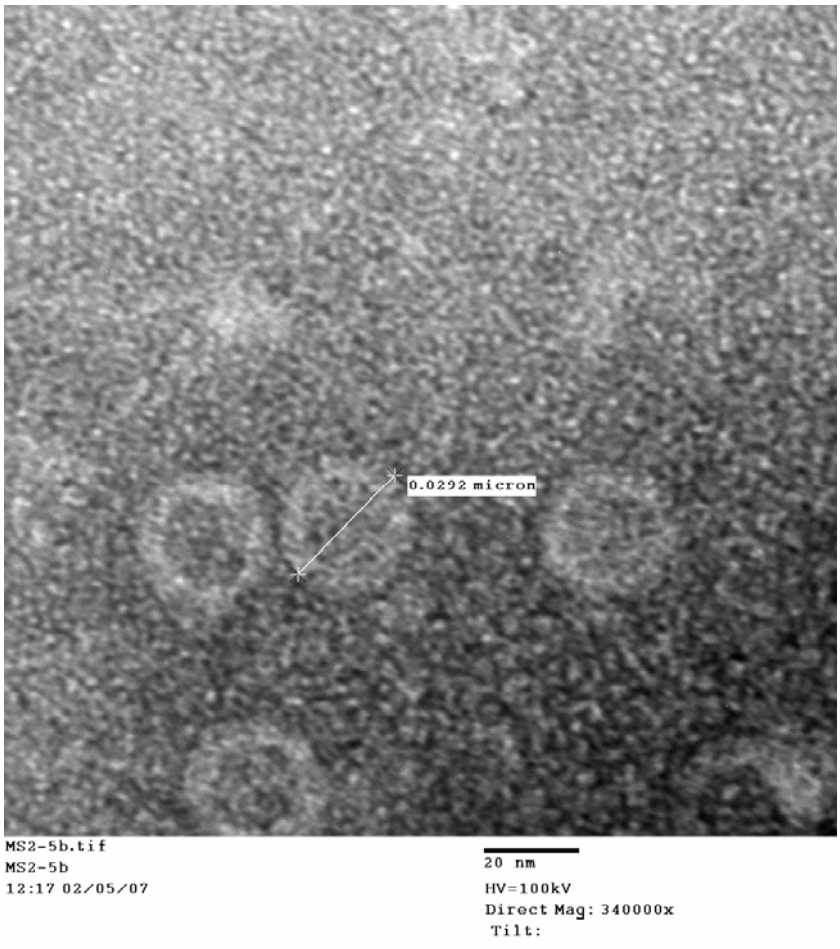

Figure 4.3 TEM image of untreated MS2 virus – high magnification.

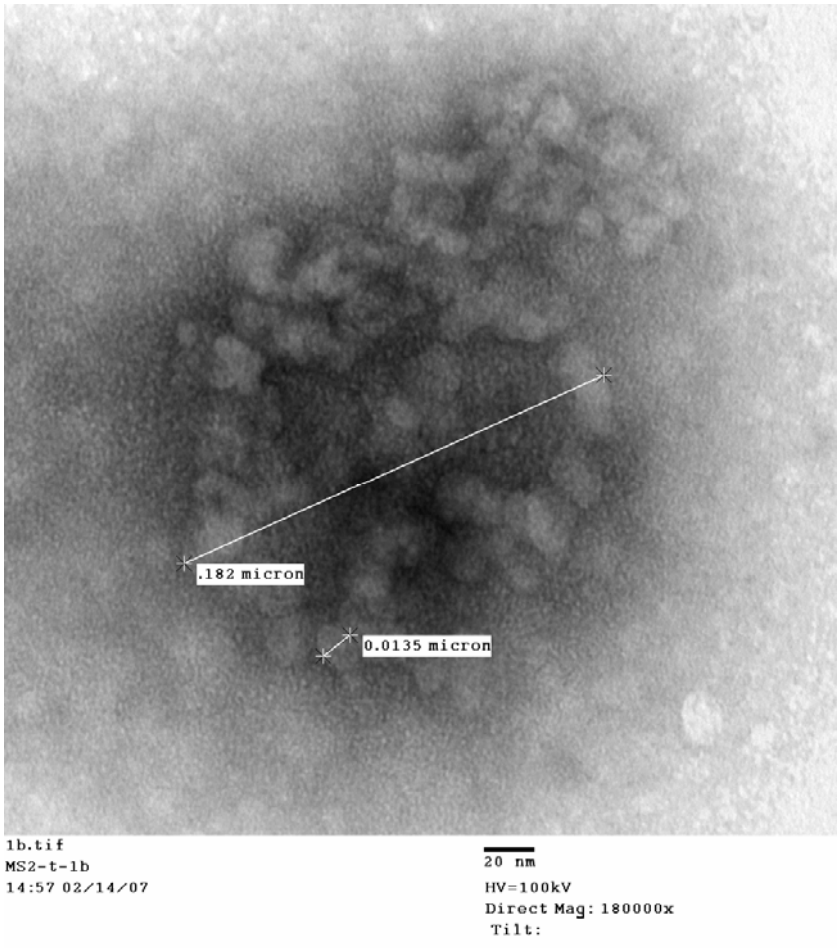

Figure 4.4 TEM image of treated MS2 virus – displaying remains.

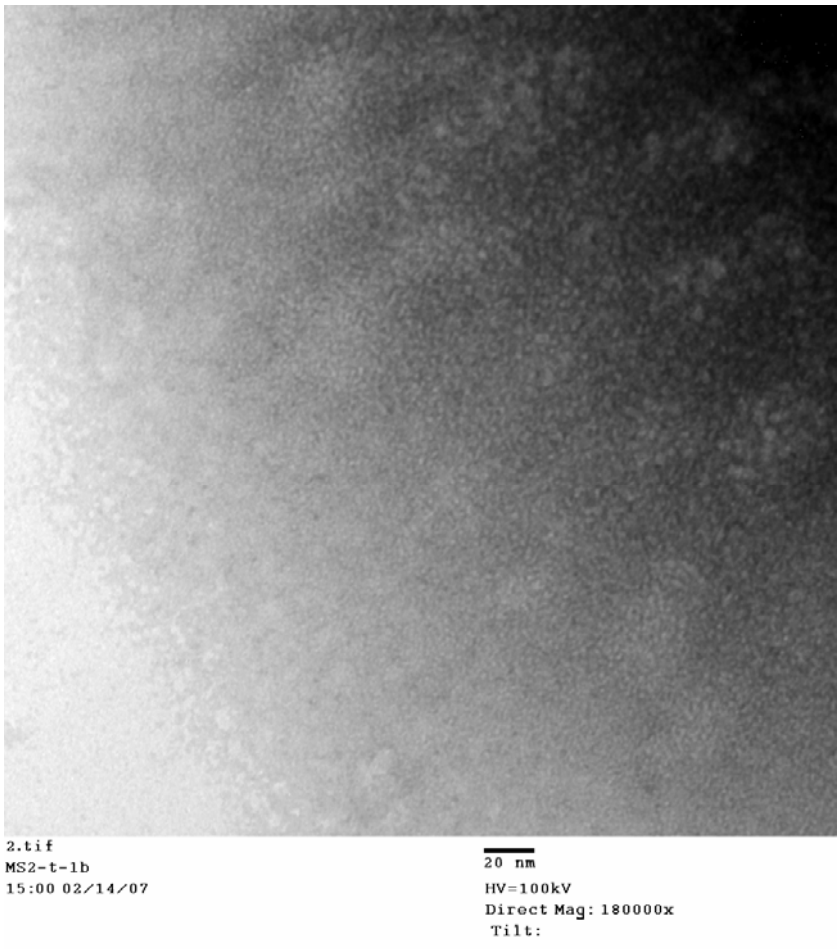

Figure 4.5 TEM image of treated MS2 virus – displaying virus remains.

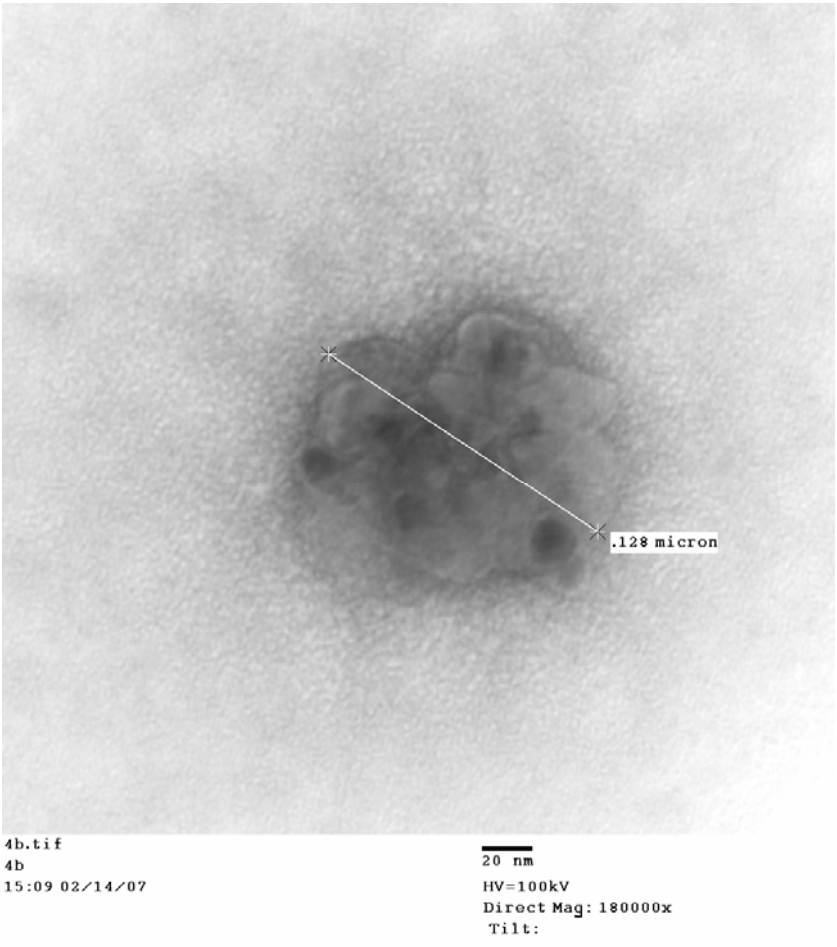

Figure 4.6 TEM image of treated MS2 virus – displaying virus remains.

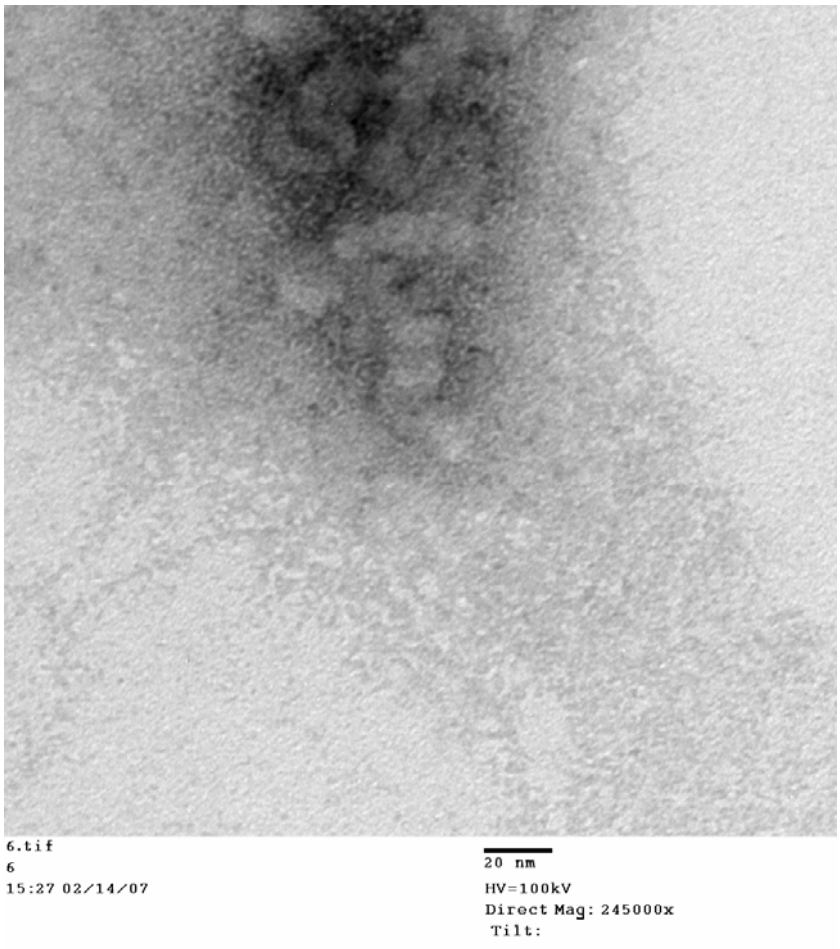

Figure 4.7 TEM image of treated MS2 virus – high magnification.

4.4.2 Phi-X174

Phi-X174, or φ-X174, belongs to the Microviridae family.[20] It is a single-stranded DNA virus (ssDNA)[20,22] whose nucleic acid sequence was determined in 1977 by Fred Sanger and his co-workers.[21] Together with MS2, these two viruses were the first to have their genomes determined in scientific history. The Phi-X174 phage has a very small amount of DNA, containing only 11 genes. The DNA of the Phi-X174 phage is circular, which was initially considered very strange and unusual.[19] The spherical phage Phi-X174 uses *E. coli* as its bacterial host and it is by far the most widely studied single stranded DNA phage. It is icosahedral in shape and has a molecular weight in the order of 1.6×10^6 Da.[19,23] The DNA contains of about 25 % adenine, 32 % thymine, 24 % guanine and 19 % cytosine. Infection with Phi-X174 is always lethal to the host cell (*E. coli*).

An initial concentration of 20 mg nanoparticles per mL of buffer solution was used to determine if the nanoparticles were efficient against Phi-X174. The initial results against MS2 virus were indeed very promising, but Phi-X174 has been reported to be slightly tougher against halogen treatment.[20] The 'naked' metal oxides were tested as well, although they were not efficient against MS2 coliphage. However, the slight differences between the viruses might make them sensitive against different kinds of treatments, making it worthwhile to test the 'naked' metal oxides as well. Table 4.7 shows the results using the different adducts of NA-Al_2O_3 Plus against the coliphage Phi-X174 using a nanoparticle concentration of 20 mg/mL. Only high concentrations of the phage was used, as it was of interest to distinguish between the perhaps various activities of the different adducts (including adducts of NA-TiO_2 and NA-CeO_2).

Immediately it can be seen that the chlorinated adduct of NA-Al_2O_3 Plus is no longer efficient, as it was against MS2 phage. The 'naked' alumina displays no activity either, not surprisingly. However, all of the other halogenated and interhalogenated adducts display a complete kill of the Phi-X174 phage, corresponding to a log kill of almost 8. Table 4.8 shows the results using a 10 mg/mL concentration of nanoparticles. Similar results are obtained: again the chlorinated and 'naked' metal oxides are not efficient, whereas the other adducts display excellent activities.

Table 4.7 Log Reduction of Phi-X174 virus by NA-Al_2O_3 Plus Adducts (20 mg/mL).

Nanoparticle Formulation	**Contact Time [min]**	
	5	**30**
NA-Al_2O_3-act.	t.n.t.c	t.n.t.c
NA-Al_2O_3/Cl_2	t.n.t.c	t.n.t.c
NA-Al_2O_3/Br_2	7.85	7.85
NA-Al_2O_3/I_2	7.85	7.85
NA-Al_2O_3/ICl	7.85	7.85
NA-Al_2O_3/IBr	7.85	7.85
NA-Al_2O_3/ICl_3	7.85	7.85

t.n.t.c = too numerous to count

Table 4.8 Log Reduction of Phi-X174 virus by NA-Al_2O_3 Plus Adducts (10 mg/mL).

Nanoparticle Formulation	Contact Time [min]	
	5	30
NA-Al_2O_3-act.	t.n.t.c	t.n.t.c
NA-Al_2O_3/Cl_2	t.n.t.c	t.n.t.c
NA-Al_2O_3/Br_2	7.85	7.85
NA-Al_2O_3/I_2	7.85	7.85
NA-Al_2O_3/ICl	7.85	7.85
NA-Al_2O_3/IBr	7.85	7.85
NA-Al_2O_3/ICl_3	7.85	7.85

t.n.t.c = too numerous to count

Table 4.9 displays the results using NA-CeO_2 and its adducts against Phi-X174 (20 mg/mL nanoparticle concentration). The difference between these adducts and those of NA-Al_2O_3 Plus is that in addition to that the chlorinated adduct does not have any activity, neither do the brominated and iodinated adducts of NA-CeO_2. This can possibly be explained by the relatively lower amounts of halogen present, as compared to the NA-Al_2O_3 Plus adducts. When a lower concentration of nanoparticles is used (10 mg/mL), even lower activities are observed (Table 4.10); both the ICl and the ICl_3 adducts no longer have a detectable effect, whereas the activity of NA-CeO_2/IBr has significantly decreased; now displaying log-kills less than 5. The standard deviation values obtained for NA-CeO_2/IBr using a 10 mg/mL concentration were both less than ±0.5. The other values could not be calculated since the adducts displayed a complete kill of the phage, or the plaques were too numerous to count at all.

Table 4.9 Log Reduction of Phi-X174 virus by NA-CeO_2 Adducts (20 mg/mL).

Nanoparticle Formulation	Contact Time [min]	
	5	30
NA-CeO_2-act.	t.n.t.c	t.n.t.c
NA-CeO_2/Cl_2	t.n.t.c	t.n.t.c
NA-CeO_2/Br_2	t.n.t.c	t.n.t.c
NA-CeO_2/I_2	t.n.t.c	t.n.t.c
NA-CeO_2/ICl	7.85	7.85
NA-CeO_2/IBr	7.85	7.85
NA-CeO_2/ICl_3	7.85	7.85

t.n.t.c = too numerous to count

Table 4.10 Log Reduction of Phi-X174 virus by NA-CeO_2 Adducts (10 mg/mL).

Nanoparticle Formulation	Contact Time [min]	
	5	30
NA-CeO_2-act.	t.n.t.c	t.n.t.c
NA-CeO_2/Cl_2	t.n.t.c	t.n.t.c
NA-CeO_2/Br_2	t.n.t.c	t.n.t.c
NA-CeO_2/I_2	t.n.t.c	t.n.t.c
NA-CeO_2/ICl	t.n.t.c	t.n.t.c
NA-CeO_2/IBr	4.21	4.93
NA-CeO_2/ICl_3	t.n.t.c	t.n.t.c

t.n.t.c = too numerous to count
Phage control was 7.85

Table 4.11 displays the results obtained using NA-TiO_2 and its halogen and interhalogen adducts (20 mg/mL). In similarity with both the NA-CeO_2 and NA-Al_2O_3 Plus adduct, the chlorinated adduct was not efficient along with the 'naked' TiO_2. The brominated adduct had a decreased efficiency and did not display a complete kill of the amount of phage used. The calculated log kill was strangely higher during a 5 minute interaction compared to the 30 minute

interaction. The experiment was repeated many times with the same results obtained. The other halogen and interhalogen adducts were, however, very efficient, displaying a complete kill of all the phage present. Even at a low nanoparticle concentration of 10 mg/mL, similar results were obtained with complete kills of all the interhalogen adducts and complete kill using the iodinated adduct (Table 4.12). In Tables 4.11 and 4.12 the standard deviation values for the NA-TiO_2/Br_2 adduct were calculated and were found to be less than ±0.5. The other values could not be calculated since the adducts displayed a complete kill of the phage, or the plaques were too numerous to be counted at all.

Table 4.11 Log Reduction of Phi-X174 virus by NA-TiO_2 Adducts (20 mg/mL).

Nanoparticle Formulation	**Contact Time [min]**	
	5	**30**
NA-TiO_2-act.	t.n.t.c	t.n.t.c
NA-TiO_2/Cl_2	t.n.t.c	t.n.t.c
NA-TiO_2/Br_2	6.25	5.32
NA-TiO_2/I_2	7.85	7.85
NA-TiO_2/ICl	7.85	7.85
NA-TiO_2/IBr	7.85	7.85
NA-TiO_2/ICl_3	7.85	7.85

t.n.t.c = too numerous to count

Table 4.12 Log Reduction of Phi-X174 virus by NA-TiO_2 Adducts (10 mg/mL).

Nanoparticle Formulation	Contact Time [min]	
	5	30
NA-TiO_2-act.	t.n.t.c	t.n.t.c
NA-TiO_2/Cl_2	t.n.t.c	t.n.t.c
NA-TiO_2/Br_2	5.57	4.56
NA-TiO_2/I_2	7.85	7.85
NA-TiO_2/ICl	7.85	7.85
NA-TiO_2/IBr	7.85	7.85
NA-TiO_2/ICl_3	7.85	7.85

t.n.t.c = too numerous to count

To summarize, we have seen a distinct difference in the use of the prepared nanoparticles against MS2 and Phi-X174, with the former being less resistant to nanoparticle treatment. A similar observation has been reported by literature, where iodinated resins were used against MS2, Phi-X174, PRD1 and GA virus.[20] Using the more resistant virus Phi-X174, we have been able to notice differences in the activities between the adducts prepared from different metal oxide nanoparticles. The adducts prepared from NA-Al_2O_3 Plus are noticeably better than the adducts prepared from NA-CeO_2 or NA-TiO_2. All the adducts prepared from NA-Al_2O_3 Plus except for the chlorinated adduct displayed a complete kill of the Phi-X174 phage, corresponding to a log kill of almost 8. The NA-TiO_2 adducts are also very active; however the brominated adduct did not display a complete kill of the phage used. The NA-CeO_2 adducts did not perform nearly as well as the already mentioned NA-Al_2O_3 Plus and NA-TiO_2 adducts. Only the interhalogen adducts performed somewhat well, with all of them displaying a complete kill at a 20 mg/mL nanoparticle concentration.

TEM images of the Phi-X174 virus can be seen in Figures 4.8-4.10. The virus is approximately 56 nm in size (Figure 4.9). Images of Phi-X174 virus treated with nanoparticles (NA-Al_2O_3/ICl_3 Plus) can be seen in Figures 4.11-4.15. It appears that the virus particle has been destroyed and only nucleic acids and proteins remain in random arrangements. In Figures 4.11-4.12 it appears that small parts of proteins and nucleic acids almost form infinite networks together. It can be clearly seen though, that there has been a definite change in the structure of the virus and it is no longer a healthy virus. In Figure 4.14 and 4.15 small dark spots, approximately 30 nm in size, can be observed. We believe these spots are due to halogen that has remained after the treatment. The spots are very electron dense and halogens would appear dark in a TEM image so this is the most likely explanation.

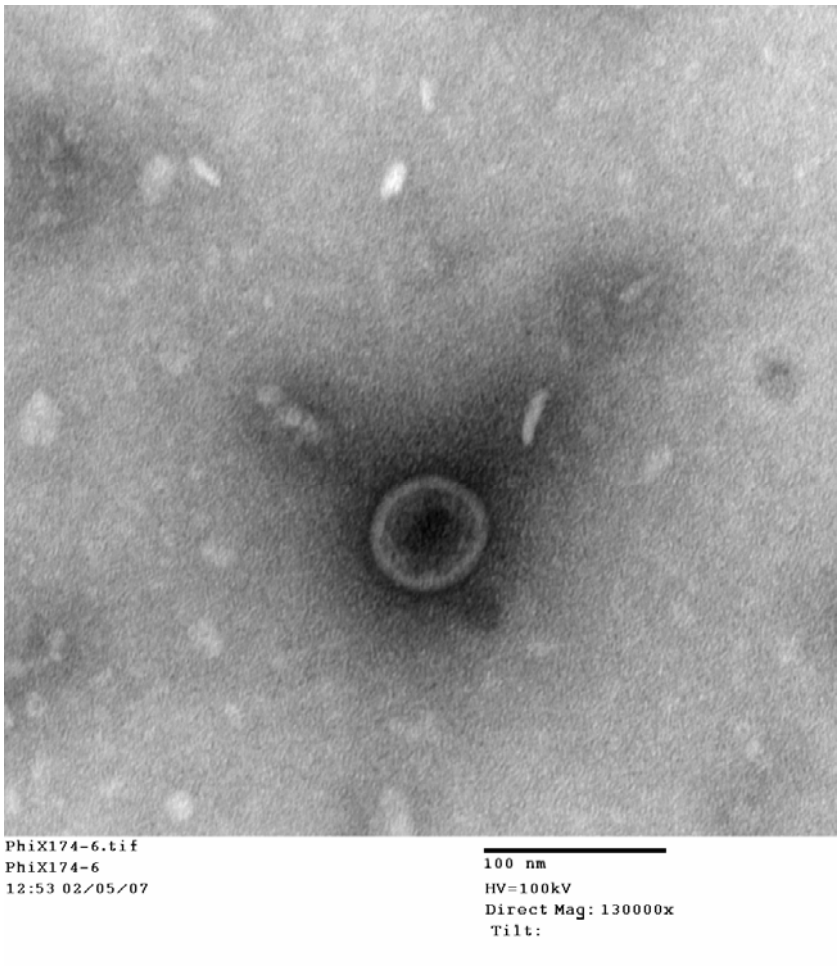

Figure 4.8 TEM image of untreated Phi-X174 virus – single virus.

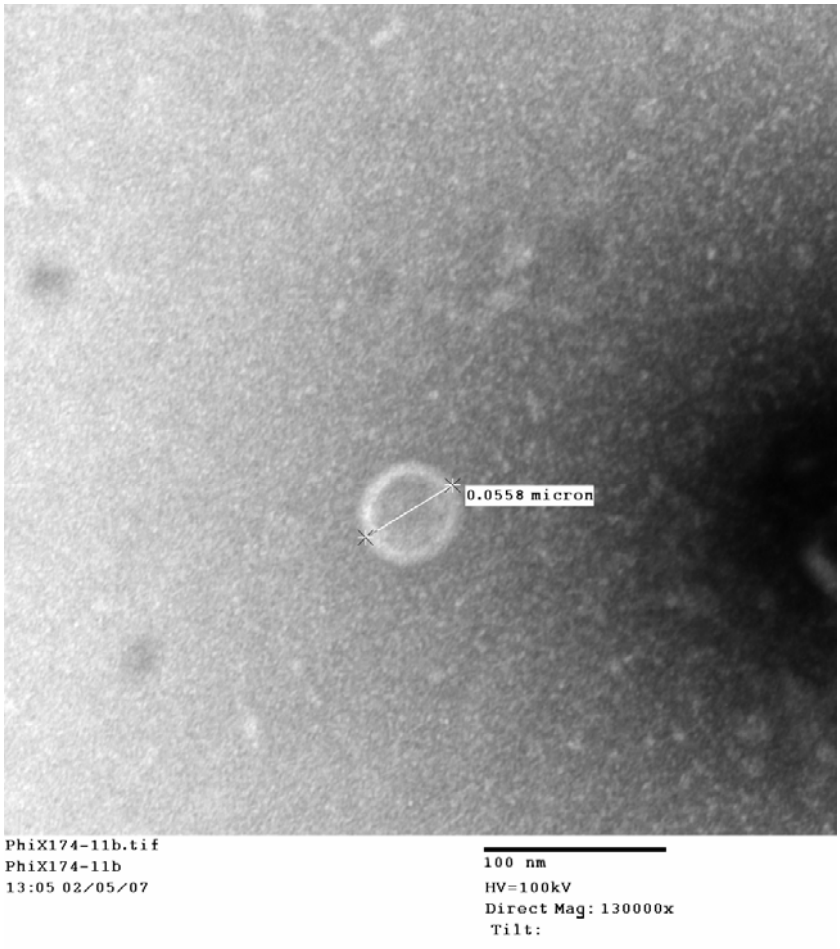

Figure 4.9 TEM image of untreated Phi-X174 virus – displaying size

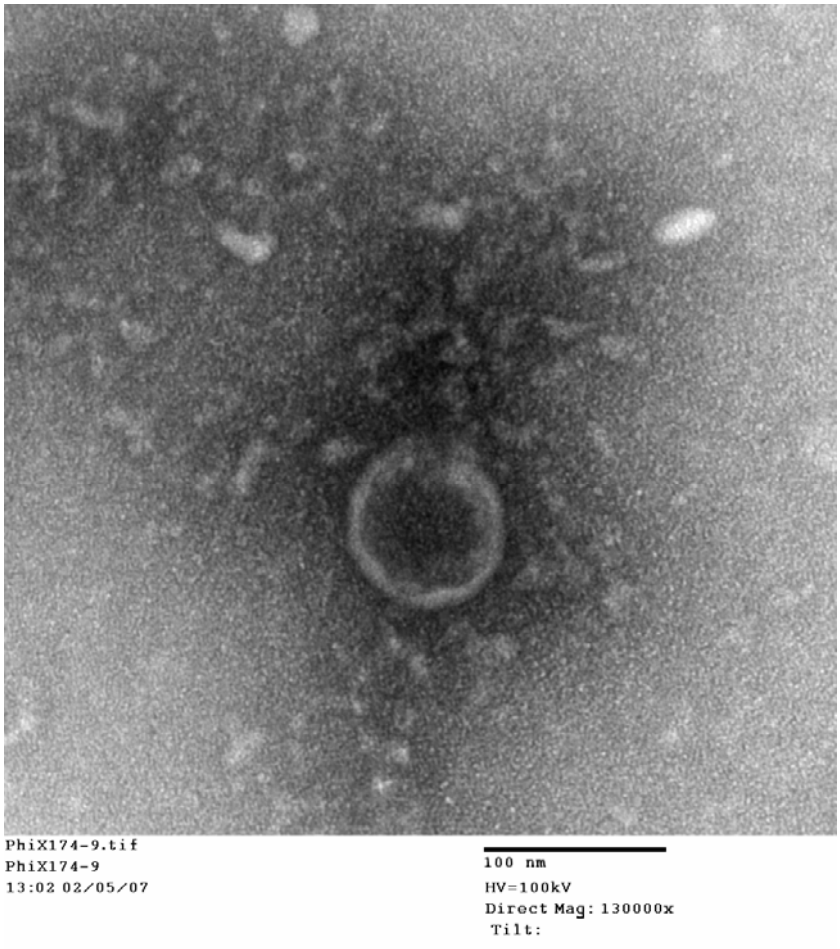

Figure 4.10 TEM image of untreated Phi-X174 virus – high magnification.

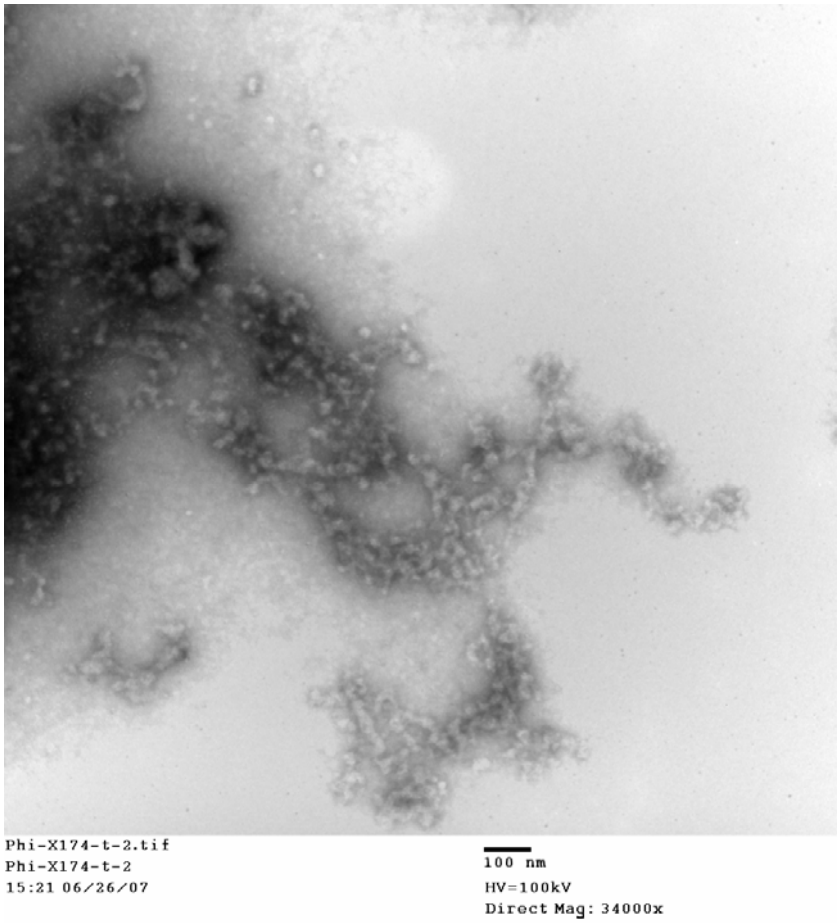

Figure 4.11 TEM image of treated Phi-X174 virus – displaying remains.

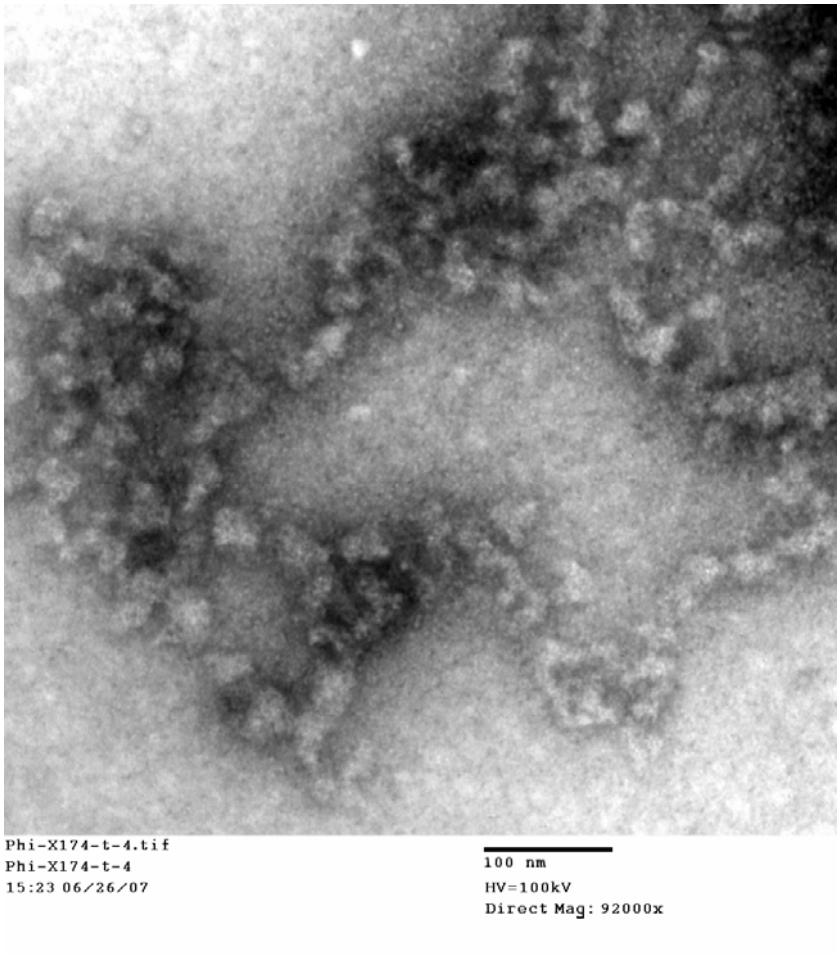

Figure 4.12 TEM image of treated Phi-X174 virus – displaying remains.

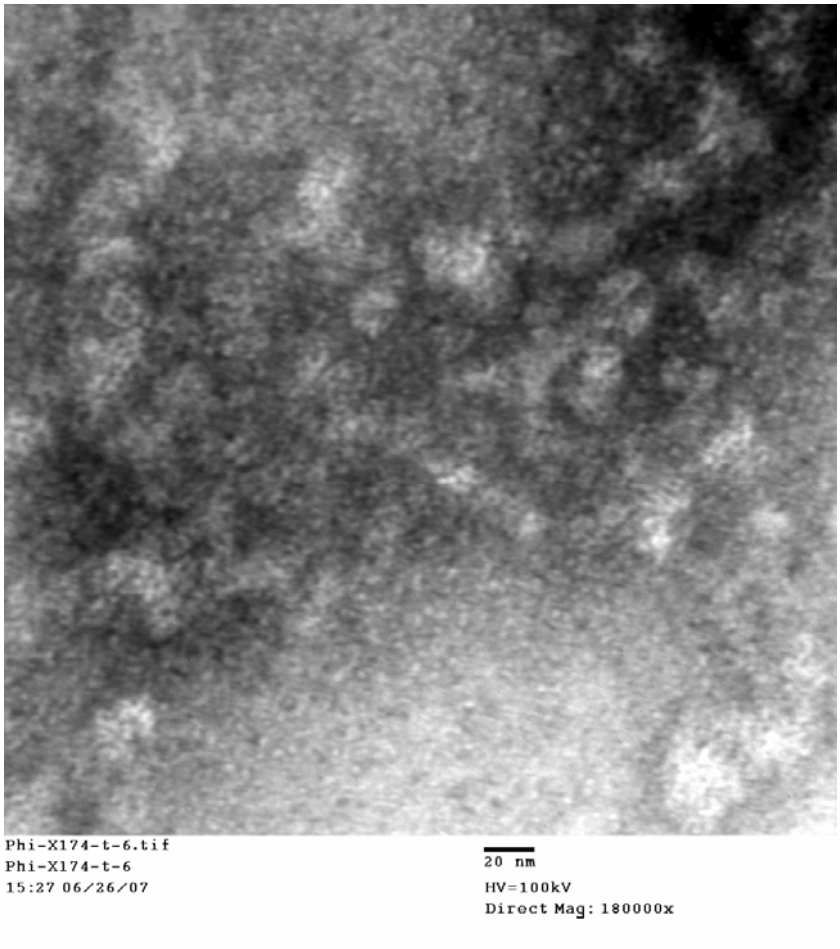

Figure 4.13 TEM image of treated Phi-X174 virus – high magnification.

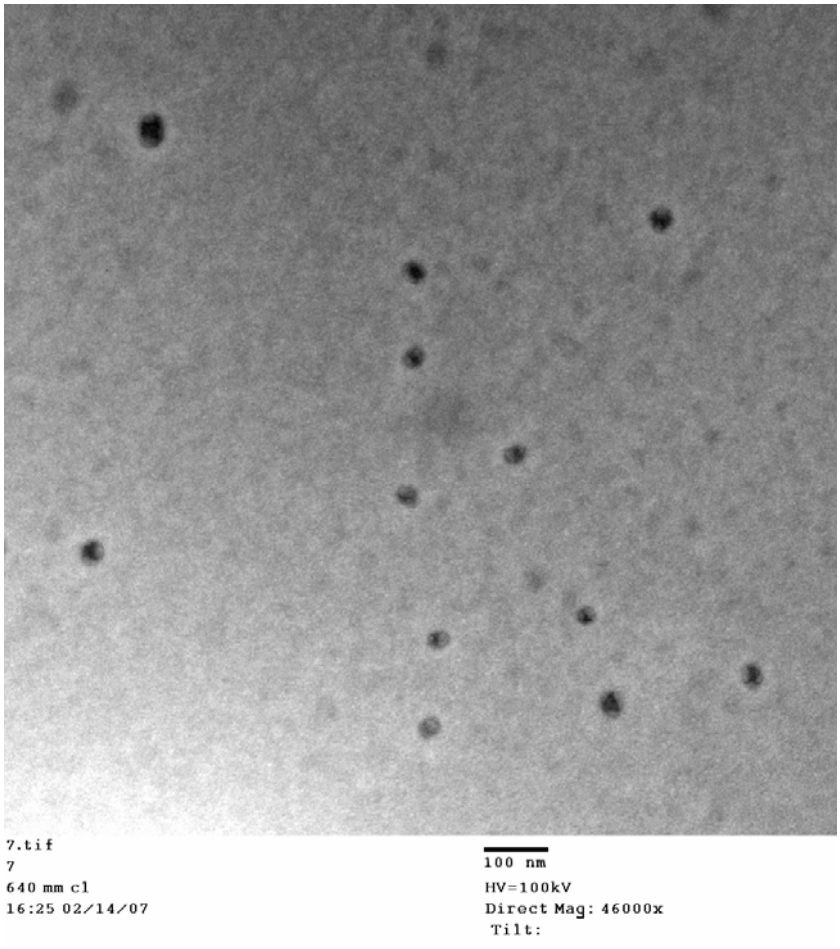

Figure 4.14 TEM image of treated Phi-X174 virus – unidentified remains.

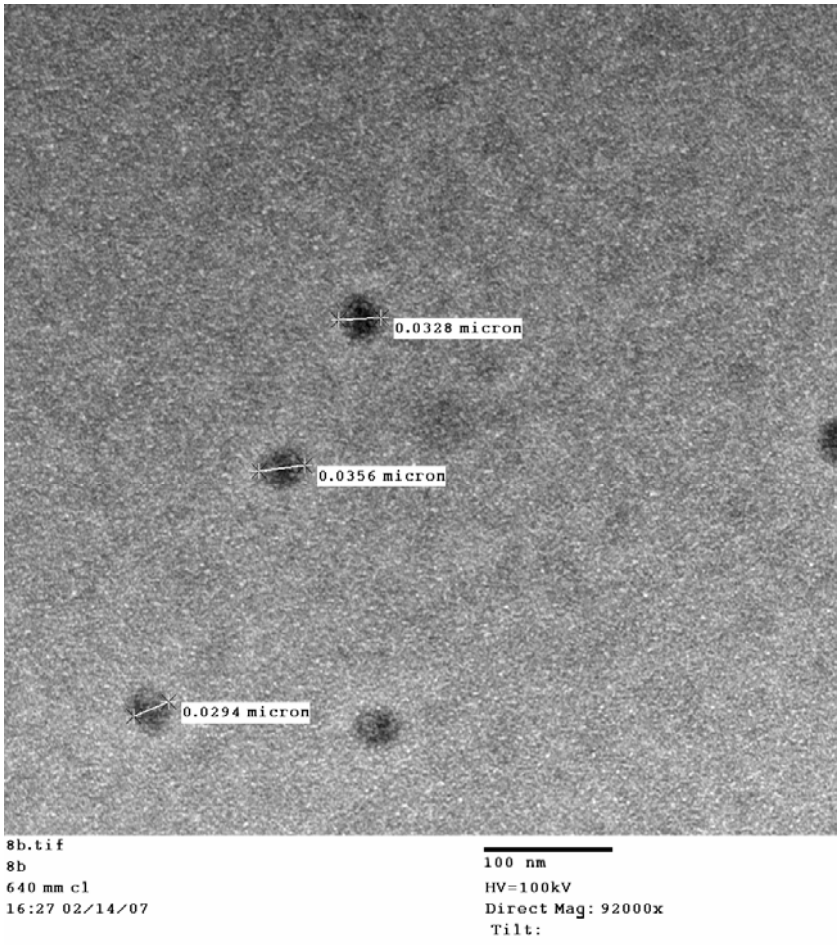

Figure 4.15 TEM image of treated Phi-X174 virus – displaying size.

4.4.3 PRD1

PRD1 belongs to the Tectiviridae family and is a lipid-containing virus.[20] It is a very complex membrane-containing double stranded DNA virus (ds-DNA), containing a lipid layer underneath the viral capsid.[24] The lipid layer consists of phosphatidylethanolamine, phosphatidylglycerol and cardiolipin. PRD1 has icosahedral protein capsid symmetry and infects Gram-negative bacteria such as *E. coli* and *Salmonella enterica*.[25] The capsid is approximately 70 nm in diameter. The mature virion has a molecular mass of about 66 x 10^6 Da.[26]

During the experiments performed it was noticed that it was more difficult to get reproducible data than in previous experiments using MS2 and Phi-X174. In some cases inconsistent results were obtained. After several sets of experiments performed and still some inconsistencies in the results we also noticed other problems with the phage, such as sudden low concentration, contamination, etc. Attempts were done in order to prepare new high titer lysates without contaminants, but with no success. After many tries we gave up and thus herein present the initial results obtained using PRD1. Some of these results should be studied with caution as some of the data was not reproducible. For these reasons the standard deviation values were not calculated for these experiments and have not been reported herein. Because of these problems with the phage TEM images were also not collected.

An initial concentration of 20 mg nanoparticles per mL of buffer solution was used to determine if the nanoparticles were at all efficient against PRD1. The initial results against MS2 and Phi-X174 were indeed very promising, but PRD1 has been reported to be very resistant against halogen treatment.[20] The 'naked' metal oxides were tested as well, although they were not efficient against neither MS2 or Phi-X174 coliphages. Table 4.13 shows the results using the

different adducts of NA-Al_2O_3 Plus against the coliphage PRD1 using a nanoparticle concentration of 20 mg/mL. Only high concentrations of the phage was used, as it was of interest to distinguish between the perhaps various activities of the different adducts (including adducts of NA-TiO_2 and NA-CeO_2). It can be seen that using a 20 mg/mL concentration of the nanoparticles lead to a complete destruction of the PRD1 phage during 30 minutes of interaction for all the interhalogenated adducts as well as for the brominated and iodinated adducts. The chlorinated adduct gave inconsistent results during the set of experiments performed. Table 4.14 displays the results using the lower nanoparticle concentration of 10 mg/mL and it was found that the brominated adduct was no longer active against the phage. The reason for the better results obtained using this lower nanoparticle concentration for the ICl and ICl_3 adduct during the 5 minute interaction is unknown, but could be due to the previously mentioned problems including fluctuations in the phage concentration.

Table 4.13 Log Reduction of PRD1 virus by NA-Al_2O_3 Plus Adducts (20 mg/mL).

Nanoparticle Formulation	Contact Time [min]	
	5	30
NA-Al_2O_3-act.	t.n.t.c	t.n.t.c
NA-Al_2O_3/Cl_2	n.c.r	n.c.r
NA-Al_2O_3/Br_2	10.39	10.39
NA-Al_2O_3/I_2	10.39	10.39
NA-Al_2O_3/ICl	t.n.t.c	10.39
NA-Al_2O_3/IBr	10.39	10.39
NA-Al_2O_3/ICl_3	6.86	10.39

t.n.t.c = too numerous to count
n.c.r = not consistent results
Phage control was 10.39

Table 4.14 Log Reduction of PRD1 virus by NA-Al_2O_3 Plus Adducts (10 mg/mL).

Nanoparticle Formulation	Contact Time [min]	
	5	30
NA-Al_2O_3-act.	t.n.t.c	t.n.t.c
NA-Al_2O_3/Cl_2	t.n.t.c	t.n.t.c
NA-Al_2O_3/Br_2	t.n.t.c	t.n.t.c
NA-Al_2O_3/I_2	10.39	10.39
NA-Al_2O_3/ICl	10.39	10.39
NA-Al_2O_3/IBr	10.39	10.39
NA-Al_2O_3/ICl_3	10.39	10.39

t.n.t.c = too numerous to count
Phage control was 10.39

Table 4.15 displays the results obtained using NA-CeO_2 against the PRD1 phage (20 mg/mL nanoparticle concentration). Immediately it can be noticed that the NA-CeO_2 adducts are not as efficient against this phage as the NA-Al_2O_3 Plus adducts. During a 5 minute contact time, only the IBr adducts showed some activity; however during the 30 minute interaction all of the interhalogenated adducts and the iodinated adduct had some activity. Only the I_2 and IBr adducts, however, displayed a complete inactivation of the PRD1 phage during 30 minutes of interaction. Table 4.16 displays the use of the same adduct, but using a lower concentration (10 mg/mL). The iodinated adduct was no longer efficient at this concentration but the IBr adducts was still the most efficient in the series, displaying a complete kill of the phage at 30 minutes (higher than log 10 reduction) and higher than a 7 log reduction after 5 minutes. The activated metal oxide itself does not appear to have any activity, as expected.

Table 4.15 Log Reduction of PRD1 virus by NA-CeO_2 Adducts (20 mg/mL).

Nanoparticle Formulation	Contact Time [min]	
	5	30
NA-CeO_2-act.	t.n.t.c	t.n.t.c
NA-CeO_2/Cl_2	t.n.t.c	t.n.t.c
NA-CeO_2/Br_2	t.n.t.c	t.n.t.c
NA-CeO_2/I_2	t.n.t.c	10.39
NA-CeO_2/ICl	t.n.t.c	8.04
NA-CeO_2/IBr	7.74	10.39
NA-CeO_2/ICl_3	t.n.t.c	8.47

t.n.t.c = too numerous to count
Phage control was 10.39

Table 4.16 Log Reduction of PRD1 virus by NA-CeO_2 Adducts (10 mg/mL).

Nanoparticle Formulation	Contact Time [min]	
	5	30
NA-CeO_2-act.	t.n.t.c	t.n.t.c
NA-CeO_2/Cl_2	t.n.t.c	t.n.t.c
NA-CeO_2/Br_2	t.n.t.c	t.n.t.c
NA-CeO_2/I_2	t.n.t.c	t.n.t.c
NA-CeO_2/ICl	t.n.t.c	8.39
NA-CeO_2/IBr	7.4	10.39
NA-CeO_2/ICl_3	t.n.t.c	t.n.t.c

t.n.t.c = too numerous to count
Phage control was 10.39

Table 4.17 shows the results using the different adducts of NA-TiO_2 against the coliphage PRD1 using a nanoparticle concentration of 20 mg/mL. The NA-TiO_2 adducts seem to have an overall better activity against the phage as compared to the NA-CeO_2 adducts. All the interhalogenated adducts and the iodinated adducts display some activity or a complete

inactivation of the phage already at 5 minutes of contact time. The Cl_2 and Br_2 adducts do not appear to be efficient even after 30 minutes of contact time using this concentration of 20 mg/mL. The same is true for the activated TiO_2. Table 4.18 displays the use of the same adducts at a 10 mg/ml concentration. The activities appear to be very similar to using a nanoparticle concentration of 20 mg/mL.

Table 4.17 Log Reduction of PRD1 virus by NA-TiO_2 Adducts (20 mg/mL).

Nanoparticle Formulation	Contact Time [min]	
	5	30
NA-TiO_2-act.	t.n.t.c	t.n.t.c
NA-TiO_2/Cl_2	t.n.t.c	t.n.t.c
NA-TiO_2/Br_2	t.n.t.c	t.n.t.c
NA-TiO_2/I_2	8.05	10.39
NA-TiO_2/ICl	10.39	10.39
NA-TiO_2/IBr	10.39	10.39
NA-TiO_2/ICl_3	10.39	10.39

t.n.t.c = too numerous to count
Phage control was 10.39

Table 4.18 Log Reduction of PRD1 virus by NA-TiO_2 Adducts (10 mg/mL).

Nanoparticle Formulation	Contact Time [min]	
	5	30
NA-TiO_2-act.	t.n.t.c	t.n.t.c
NA-TiO_2/Cl_2	t.n.t.c	t.n.t.c
NA-TiO_2/Br_2	t.n.t.c	t.n.t.c
NA-TiO_2/I_2	10.39	10.39
NA-TiO_2/ICl	8.49	10.39
NA-TiO_2/IBr	10.39	10.39
NA-TiO_2/ICl_3	7.82	10.39

t.n.t.c = too numerous to count
Phage control was 10.39

To summarize, the results obtained using the PRD1 phage clearly displayed some differences using the different metal oxide nanoparticles, although some results were difficult to reproduce. The adducts prepared from NA-Al_2O_3 Plus appear to be the most efficient overall. It can also be noticed that in all the prepared adducts, the chlorinated and brominated adducts are not very efficient (except for in the case of Br_2 adduct of NA-Al_2O_3 Plus), whereas the iodinated adducts are very efficient in several of the cases at both concentrations tested. Iodine has been studied quite extensively in the past as a disinfectant and good results have been obtained using iodinated resins against all of the three phages studied herein.[20] The adducts prepared from NA-CeO_2 appear to have the lowest activity against the PRD1 phage.

4.5 Conclusions

We have in this chapter showed that nanoparticles are promising in the use against different viruses, including the bacteriophages MS2, Phi-X174 and PRD1. Although not much

data exists in the literature involving the use of nanomaterials against viruses we have now found that very successful data can be obtained using halogenated and interhalogenated metal oxide nanoparticles.

As supported by the research performed by Brion et al.[20] we have also found that the order of resistance against halogen treatment increases in the order of MS2 < Phi-X174 < PRD1. PRD1 is lipid-containing, which further increases its resistance against chemical treatment. In general, we found that the interhalogenated adducts were the most promising candidates for virus inactivation, however, the iodine adducts also proved to be very efficient. The chlorinated adducts did not perform very well; only in the case of MS2 phage did the NA-Al_2O_3 Plus adduct have some activity. The brominated adducts performed slightly better, displaying activity against MS2 phage in all the prepared metal oxide adducts, and activity against the other two phages, Phi-X174 and PRD1 in some instances. This lower activity for the chlorinated and brominated adducts compared to the other halogen and interhalogen adducts is believed to be due to the lower amounts of halogen present in those cases. The activated nanoparticles themselves did not display any activity against any of the three phages studied.

Overall, the NA-Al_2O_3 Plus adducts were outstanding in performance and exceeded the performance of the NA-CeO_2 adducts to a large extent. The activities of the NA-TiO_2 adducts were close to those prepared of NA-Al_2O_3 Plus, or even better in a few cases. The generally lower activities of the NA-CeO_2 adducts can be explained by the lower amounts of halogens/interhalogens adsorbed on the surface and by the fact that cerium oxide is a very heavy metal oxide, leading to less contact with the virus in the solution, as the particles settle down to the bottom sooner as compared to TiO_2 and Al_2O_3, whose particles remain suspended in the solution for longer times, leading to more interaction with the phage.

The mechanism in which this process occurs is not completely known at this time, but reasons for the excellent activity of these nanomaterials could include their abrasive character, caused by their high surface area and many corners, edges and defect sites as well as the oxidative power of the halogens/interhalogens. Further studies, including resin-embedded TEM images may give more insight to the mechanism.

4.6 References

(1) Koper, O. B.; Klabunde, J. S.; Marchin, G. L.; Klabunde, K. J.; Stoimenov, P.; Bohra, L. *Curr. Microbiol.* **2002**, *44*, 49-55.

(2) Yu, C. J.; Lin, J. U.S Pat. Appl. Publ. **2004**, 10 pp.

(3) Bender, A. R.; Von Briesen, H.; Kreuter, J.; Duncan, I. B.; Rubsamen-Waigmann, H. *Antimicrob. Agents Chemother.* **1996**, *40*, 1467-1471.

(4) Hamouda, T.; Myc, A.; Donovan, B.; Shih, A. Y.; Reuter, J. D.; Baker, J. R. *Microbiol. Res.* **2001**, *156*, 1-7.

(5) Sommer, R.; Pribil, W.; Pfleger,S.; Haider, T.; Werderitsch, Gehringer, P. *Water Sci. Technology.* **2004**, *50*, 159-164.

(6) Blatchley, E. R.; Gong, W-L.; Alleman, J. E.; Rose, J. B.; Huffman, D. E.; Otaki, M.; Lisle, J. T. *Water Environ. Res.* **2007**, *79*, 81-92.

(7) Pedahzur, R.; Katzenelson, D.; Barnea, N.; Lev, O.; Shuval, H. I.; Fattal, B.; Ulizur, S. *Water Sci. Technol.* **2000**, *42*, 293-298.

(8) Chowdhary, N. A. Brit. UK Pat. **2002**, 7 pp.

(9) Malik, Y. S.; Goyal, S. M. *Int. J. Food Microbiol.* **2006**, *109*, 160-163.

(10) Otaki, M.; Yano, K.; Ohgaki, S. *Water Sci. Technol.* **1998**, *37*, 107-116.

(11) Lau, B. L. T.; Harrington, G. W.; Anderson, M. A.; Tejedor, I. *Water Sci. Technol.* **2004**, *50*, 223-228.

(12) Tepper, F.; Kaledin, L.; Hartmann, C. *Advances in Filtration & Separation Media*. **2004**, 110-123.

(13) Battigelli, D. A.; Sobsey, M. D.; Lobe, D. C. *Wat. Sci. Tech.* **1993**, *27*, 339-342.

(14) Brion, G. M.; Silverstein, J. *Wat. Res.* **1999**, *33*, 169-179.

(15) Alvarez, M. E.; O'Brien, R. T. *Appl. Environ. Microbiol.* **1982**, *44*, 1064-1071.

(16) http://en.wikipedia.org/wiki/Virus

(17) Lim. D. *Microbiology*. Boston, MA. 2nd Ed. **1998**.

(18) Adams, M. *Bacteriophages*. New York, NY. **1958**.

(19) Mathews, C. K. *Bacteriophage Biochemistry.* New York. NY. **1971**.

(20) Brion, G. M.; O'Banion, N. B.; Marchin, G. L. *J. Water and Health*. **2004**, *2*, 261-266.

(21) http://en.wikipedia.org/wiki/Bacteriophage_MS2

(22) http://www.fermentas.com/techinfo/nucleicacids/mapfx174.htm

(23) Hayes, W. *The Genetics of Bacteria and their Viruses.* New York, NY. **1964**.

(24) Huiskonen, J. T.; Butcher, S. J. *Curr. Opin. Struct. Biol.* **2007**, *17*, 229-236.

(25) Huiskonen, J. T.; Manole, V.; Butcher, S. J. *PNAS*, **2007**, *104*, 6666-6671.

(26) Fuller, S. *Structure*, **2005**, *13*, 1738-1739.

Appendix A - Thermogravimetric Analysis (TGA)

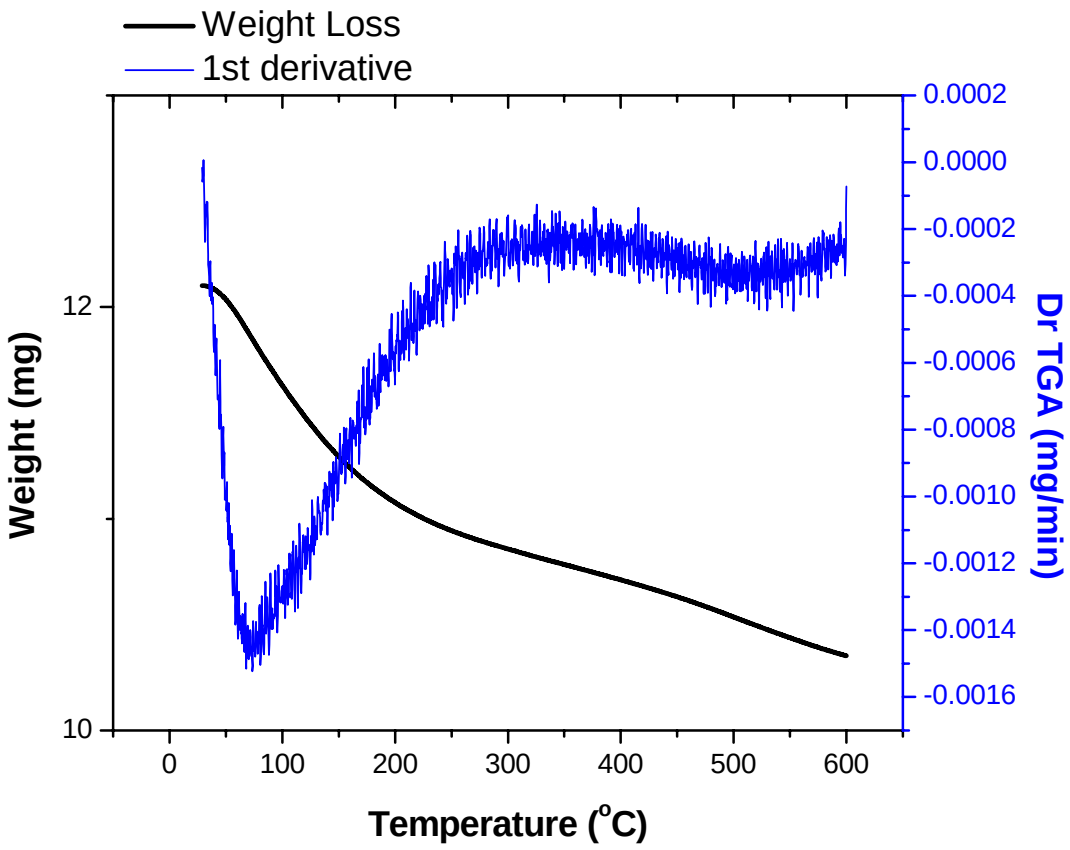

Figure A.1 TGA of NA-Al_2O_3/Cl_2 Plus.

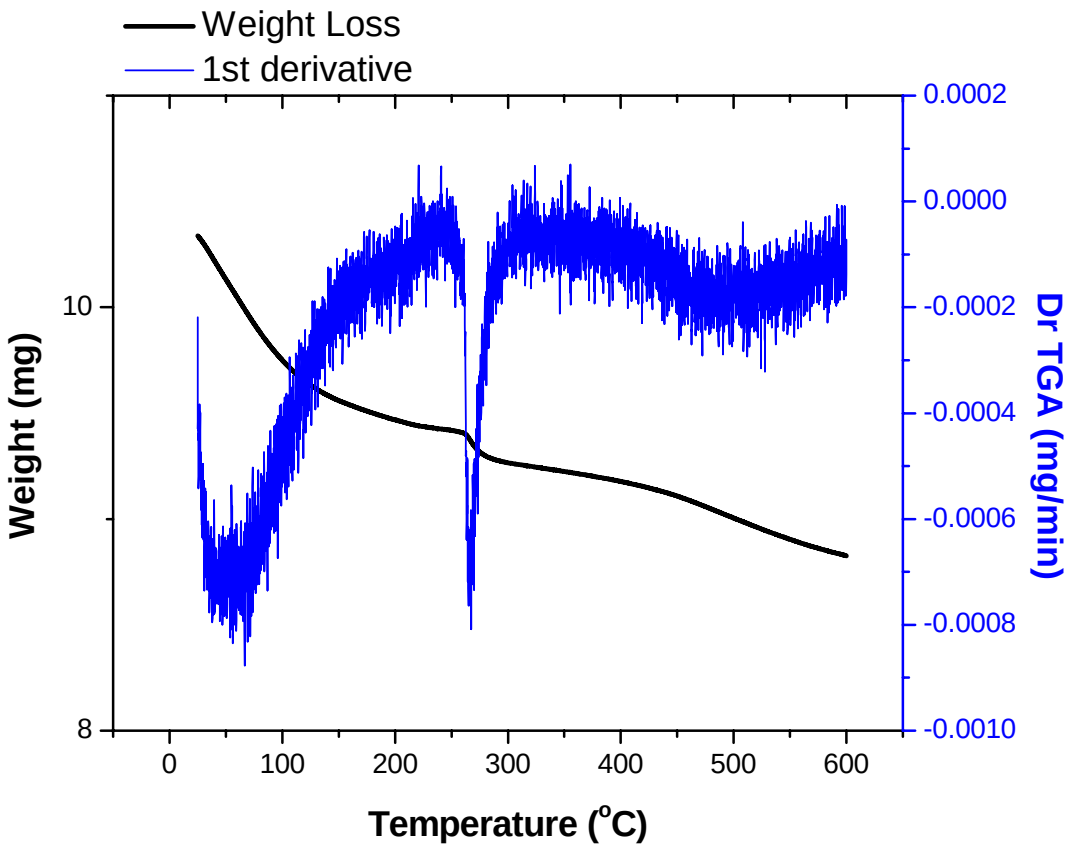

Figure A.2 TGA of NA-Al_2O_3/Br_2 Plus.

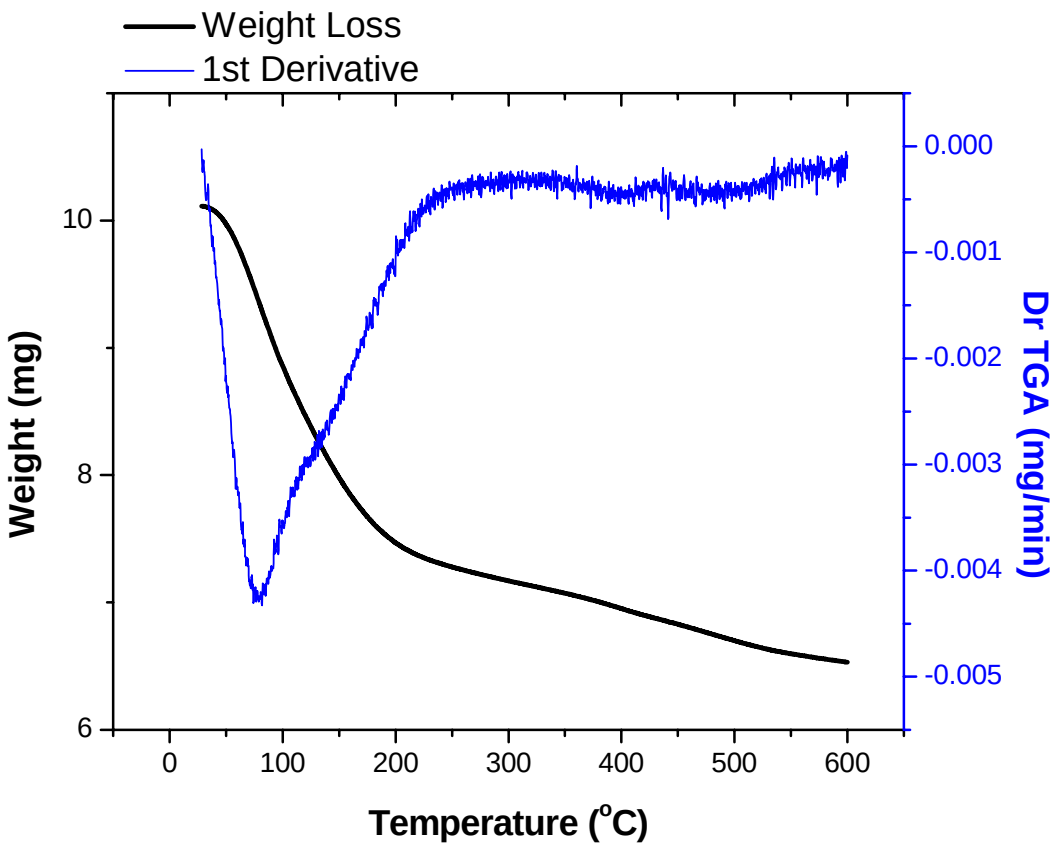

Figure A.3 TGA of NA-Al_2O_3/I_2 Plus.

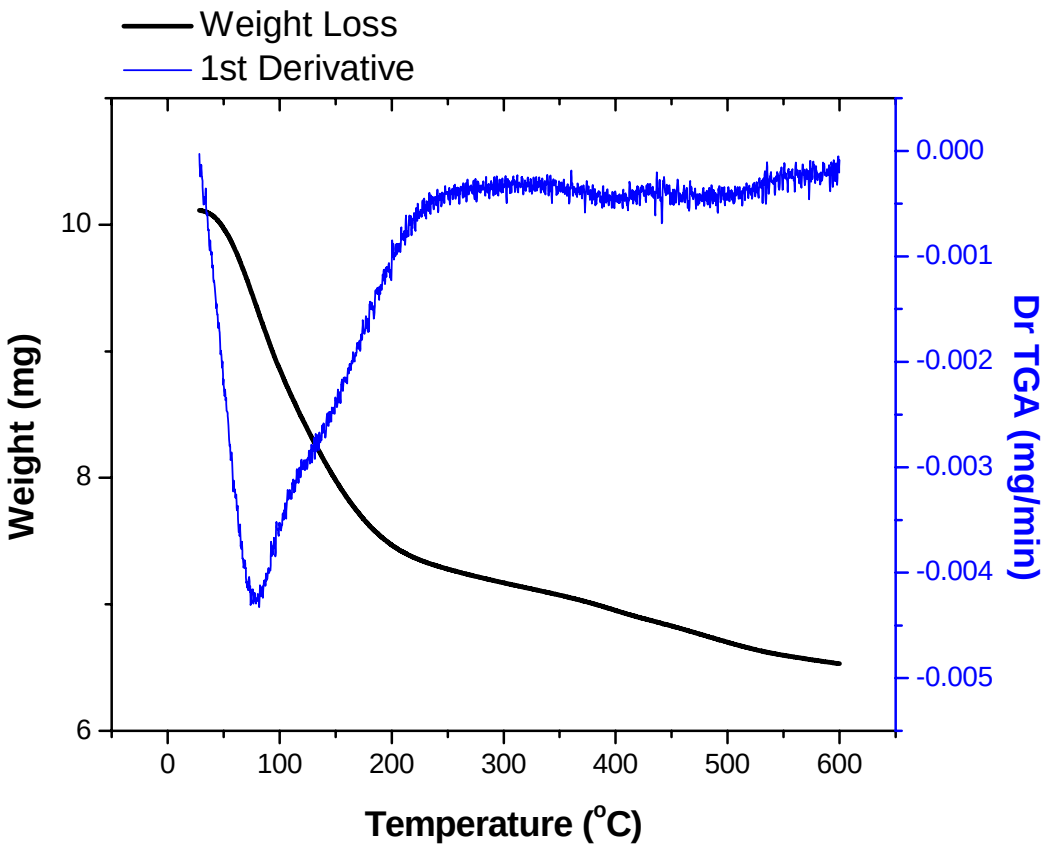

Figure A.4 TGA of NA-Al_2O_3/ICl Plus.

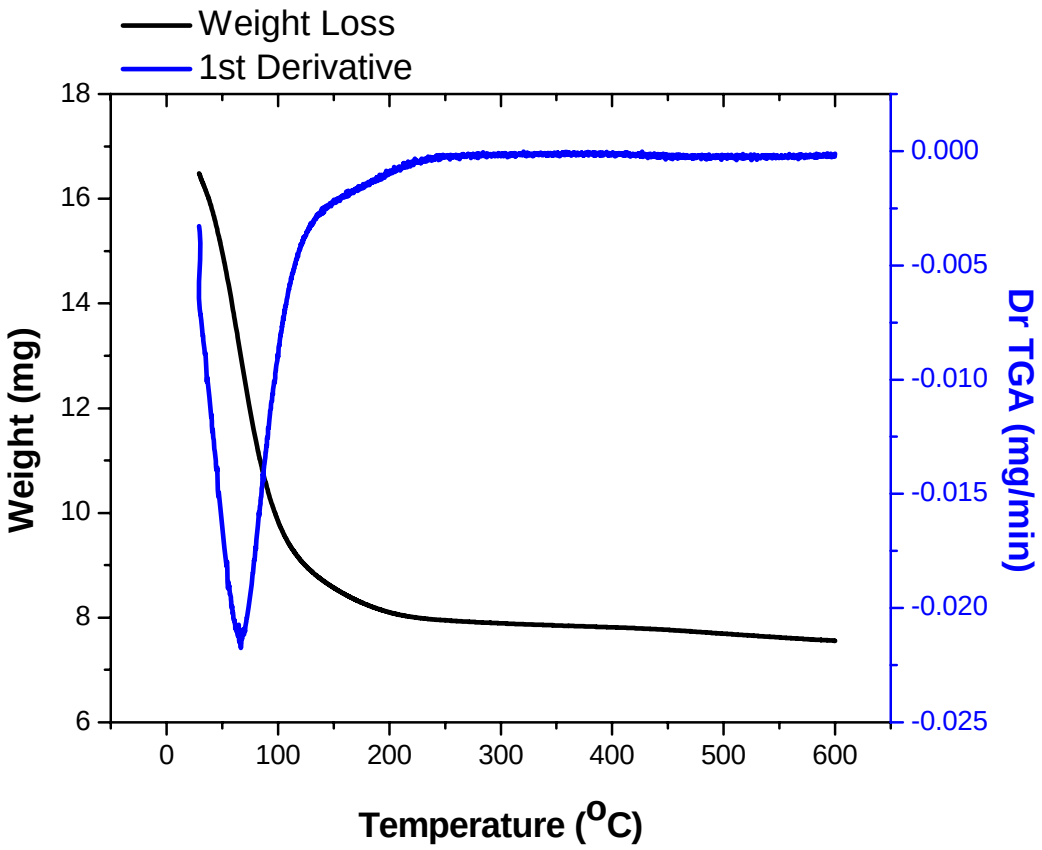

Figure A.5 TGA of NA-Al_2O_3/IBr Plus.

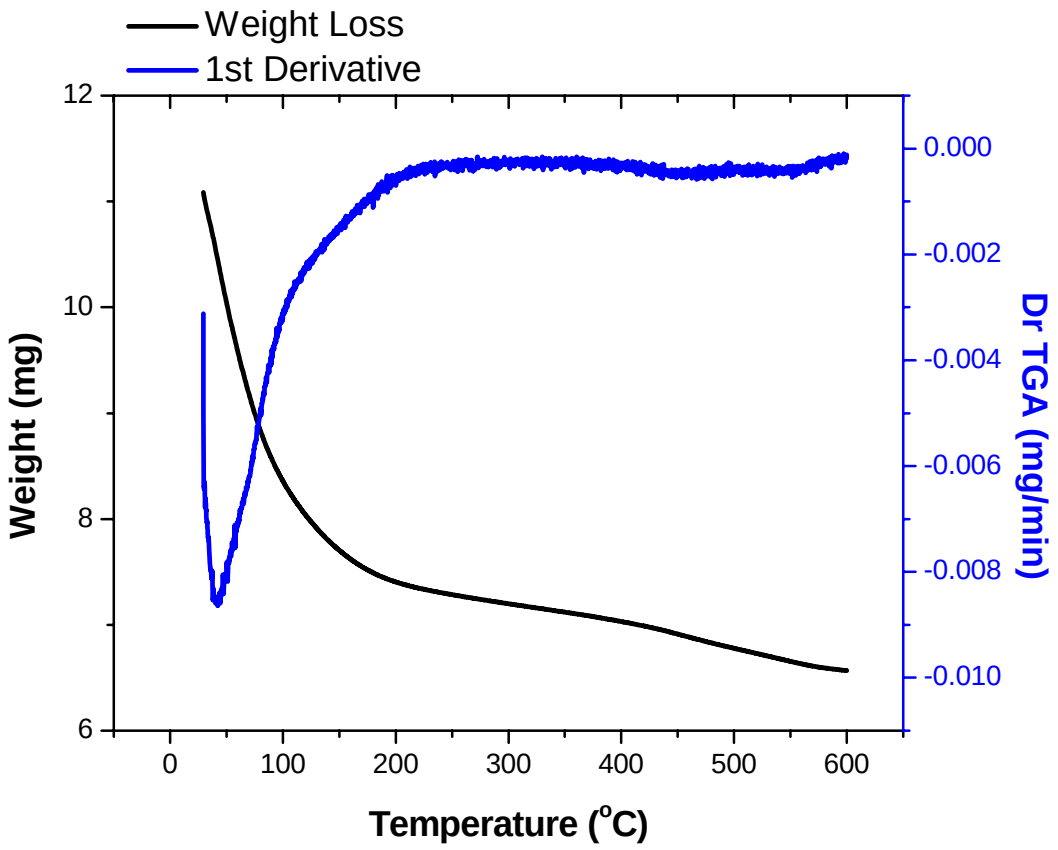

Figure A.6 TGA of NA-Al_2O_3/ICl_3 Plus.